CRAC channel related proteins in the pathogenesis of inborn errors of immunity

Laura Jane Rice

Submitted in accordance with the requirements for the degree of
Doctor of Philosophy

The University of Leeds
School of Medicine and Health

Under the supervision of

Rashida Anwar PhD and Sinisa Savic MD, PhD

June 2021

Publication statement

The candidate confirms that the work submitted is her own, except where work which has formed part of jointly-authored publications has been included. The contribution of the candidate and the other authors to this work has been explicitly indicated. The candidate confirms that appropriate credit has been given within the thesis where reference has been made to the work of others.

Acknowledgements

This work was funded by University of Leeds and CSL Behring (West Sussex, UK).

I would like to thank my supervisors for their continued support. Rashida Anwar for her scientific knowledge, detail driven questions and help during the writing of this thesis. Sinisa Savic for his encouragement and clinical and immunology expertise. The Anwar group and Level 9 WTBB PhD students made this experience enjoyable with coffee and gin.

I was fortunate to have collaborators with experience in CRAC channel research. The Gwack lab made the stable cell line work possible and I am so grateful for the opportunely to spend three months in LA. The McKeown group at the University of Leeds helped with the optimisation of calcium flux. The Clinical Immunology and Allergy Department at Leeds Teaching Hospitals provided patient data and expertise.

Lastly, I would like to thank Christopher and my greyhound Lucas for their moral support and cuddles.

Abstract

The aim of this project was to identify novel mutations in proteins causing immunodeficiency. This was achieved by confirming whole exome sequencing (WES) results of potential mutations and genes of interest through Sanger sequencing and allelic orientation of mutations. Functional experiments were then designed and performed on patient samples and stable cell lines expressing patient mutants. The experiments examined the known functions of the proteins of interest and cell types that appeared to be affected in the patient immunological profile.

The main topic of this thesis is centered around an index case who presented at age 17 with a life-long history of recurrent sinopulmonary infections and established bronchiectasis. Immunological investigations showed severe panhypogammaglobulinaema, marginally reduced CD4 count and reduced T cell proliferative responses.

WES identified potentially damaging mutations in Ca2+-release activated Ca2+ regulator 2A (CRACR2A): c.430 A>G (p.144R>G) and c.898 G>T (p.300E>*) which were inherited via the maternal line; c.834 G>T (p.278E>D) in the paternal allele. In primary patient samples, T cells had reduced calcium flux, cytokine production and p-JNK.

The two mutant patient alleles were expressed using retroviral transduction in the CRACR2A knock-out Jurkat cell line. Both alleles resulted in reduced calcium flux and IL-2 expression when compared to wild-type CRACR2A. The maternal mutant allele expression produced a truncated protein (resulting from the p.300E>* mutation), with abnormal localisation and significantly reduced p-JNK. This truncated protein was not seen in the primary cells, and so is not likely to be expressed in the patient.

The data suggests that biallelic mutations in CRACR2A can lead to primary immunodeficiency, which affects T cell related function. This is the first time CRACR2A has been linked to disease.

The identification of novel mutations in patient with primary immunodeficiency and using functional experiments to see their pathogenic effect in patient samples was also done in patients with STIM1 and STING mutations.

Table of Contents

CRAC channel related proteins in the pathogenesis of inborn errors of immunity ..... **i**
Publication statement ..... **ii**
Acknowledgements ..... **iii**
Abstract ..... **iv**
Table of Contents ..... **v**
List of Tables ..... **ix**
List of Figures ..... **x**
Abbreviations ..... **xii**
Chapter 1 Introduction **1**
1.1 Immune cell lineage 1
1.1.1 T cells 2
1.1.2 B cells 4
1.1.3 T and B cell interaction 6
1.1.4 Monocytes and macrophages 7
1.2 Primary immunodeficiency 8
1.2.1 Why study PID 9
1.2.2 Types of PID 10
1.2.3 Current Therapies for PID 13
1.2.4 Molecular screening of patients 14
1.3 The CRAC channel 15
1.3.1 CRAC channel 15
1.3.2 Role in the immune system 16
1.3.3 CRAC channel deficiencies 20
1.4 Aims 26
Chapter 2 Materials and Methods **27**
2.1 Materials 27
2.1.1 Cell lines 33
2.1.2 Patients and Healthy controls 35

2.2 Methods 36
2.2.1 Molecular Biology 36
2.2.2 Clinical Immunology 44
2.2.3 Blood work 44
2.2.4 Transient transfection methods 49
2.2.5 Generation of stable cell lines 52
2.2.6 Protein studies 57
2.2.7 T cell functional studies 60
2.2.8 Calcium flux 62
Chapter 3 CRACR2A and primary cell work 69
3.1 Introduction 69
3.1.1 STIM1 and Orai1 deficiency 69
3.1.2 CRACR2A 70
3.1.3 Case study 75
3.1.4 Aims 81
3.2 Materials and methods 82
3.2.1 Segregation of patient mutations when parental DNA was not available 82
3.3 Results 83
3.3.1 Genetic testing of patient 83
3.3.2 Protein expression in patient cells 95
3.3.3 Calcium flux in T cells 97
3.3.4 JNK signalling in T cells 106
3.3.5 Cytokine studies 106
3.4 Key Findings 108
3.5 Discussion 109
3.5.1 Whole Exome Sequencing 109
3.5.2 CRACR2A mutations 110
3.5.3 Use of primary samples 111
Chapter 4 CRACR2A cell line work 112
4.1 Introduction 112
4.1.1 Cell lines as a model for studying effects of mutations 112
4.1.2 Use of cell lines in CRACR2A research 114
4.1.3 Aims 115
4.2 Method Strategies 116

4.3 Results 117
4.3.1 CRAC channel proteins expression in Jurkat cells 117
4.3.2 Immunofluorescence to examine CRAC channel proteins 118
4.3.3 Transient expression models 119
4.3.4 Creating stable cell lines 126
4.3.5 CRACR2A function in stable transfected cell lines 136
4.4 Key findings 147
4.5 Discussion 148
4.5.1 Cell lines as a model for CRACR2A mutations 148
4.5.2 CRACR2A patient alleles 149
Chapter 5 CRAC channel related protein mutations 156
5.1 Introduction 156
5.1.1 STIM1 156
5.1.2 STING 159
5.1.3 Aims 162
5.2 Method strategies 163
5.2.1 Sequencing strategies 163
5.2.2 Publications about these specific patients 163
5.3 Results 164
5.3.1 STIM1 patients 164
5.3.2 STING patient 179
5.4 Key findings 186
5.5 Discussion 187
5.5.1 STIM1 phenotype 187
5.5.2 STIM2 overexpression 188
5.5.3 Measuring IFN levels 189
5.5.4 ISGs 189
Chapter 6 General discussion 192
6.1 Aims 192
6.1.1 Confirm potential mutations and their segregation in patients with PID. 192
6.1.2 Use primary samples and *in vitro models* to determine if mutations identified are pathogenic and causing of the patient's phenotype 193
6.2 Impact of work 194
6.2.1 Effect on patient treatment 194

6.2.2 Primary immunodeficiency field 195
6.2.3 The pathogenic effect of CRACR2A mutations 195
6.2.4 CRAC channel inhibitors as drug targets 197
6.3 Limitations 200
6.4 Future work 201
References 202

List of Tables

Table 1.3.1 Phenotypes associated with Orai1 and STIM1 deficiencies 21
Table 2.1.1 Oligonucleotides 28
Table 2.1.2 Plasmids 30
Table 2.1.3 Antibodies 31
Table 2.2.1 Cloning primer sequences 42
Table 2.2.2 Blood samples 45
Table 2.2.3 Comparison of Calcium methods used 64
Table 3.1.1 CRACR2A gene,1 mRNA and protein details 71
Table 3.1.2 Immunological clinical data 76
Table 3.1.3 T cell proliferation 79
Table 3.1.4 T cell populations activated after stimulation 80
Table 3.3.1 *DHRS4* mutation 85
Table 3.3.2. Mutations in *EFCAB4B* (protein CRACR2A). 88
Table 3.3.3 Summary of Patient sample responses on the Flex Station 100
Table 4.5.1 Primary and cell line functional data 150
Table 5.3.1 Lymphocyte and immunoglobulin counts and challenge response of P1 169
Table 5.3.2 T cell proliferation 170
Table 5.3.3 Gene panel for TaqMan experiment 182
Table 5.3.4 Significant results from ISGs experiment of STING patient 184
Table 6.2.1 CRACR2A Phenotypes 196
Table 6.2.2 CRAC channel inhibitor or modulator clinical trials 199

List of Figures

Figure 1.1.1 Immune cell lineages 1
Figure 1.1.2 T cells subtypes and functions 3
Figure 1.1.3 B cell subtypes and function 5
Figure 1.2.1 Prevalence of each IUIS category....11
Figure 1.3.1 The CRAC channel 17
Figure 1.3.2 Calcium and cytoskeleton response to TCR activation 20
Figure 2.2.1 Standard PCR reaction scheme....37
Figure 2.2.2 CRACR2A isoform sequences for cloning 40
Figure 2.2.3 pIRES2-EGFP plasmid map 41
Figure 2.2.4 qPCR reaction scheme 43
Figure 2.2.5 Method overview of B cell differentiation....48
Figure 2.2.6 B cell differentiation stages 49
Figure 2.2.7 siRNA CRACR2A binding location....51
Figure 2.2.8 FG11F plasmid map 52
Figure 2.2.9 psPAX2 map 53
Figure 2.2.10 pMD2.G map....54
Figure 2.2.11 LentiCRISPR (pXPR_001) 55
Figure 2.2.12 Calcium flux response to TG and TCR stimulation of Jurkat cells....61
Figure 3.1.1 CRACR2A functional regions. 72
Figure 3.1.2 *In vitro* B cell count and Immunoglobulin expression 78
Figure 3.1.3 T cell receptor specificities 80
Figure 3.3.1 Sanger sequencing of *DHRS4* exon 4 from patient genomic DNA 86
Figure 3.3.2 Sanger sequencing of *EFCAB4B* from genomic DNA of patient. 89
Figure 3.3.3. Sanger sequencing of patient cDNA and TA clone. 91
Figure 3.3.4 Sanger sequencing of maternal DNA. 92
Figure 3.3.5 Orientation of mutations in patient alleles. 93
Figure 3.3.6. Pedigree diagram for patient. 94
Figure 3.3.7 CRACR2A protein expression in PBMCs 96
Figure 3.3.8 CRACR2A protein in expanded T cell population 97
Figure 3.3.9 Calcium flux response to TG, CRACR2A patient T cells compared to HC....101
Figure 3.3.10 Intercellular signalling of HC T cells after expansion....104
Figure 3.3.11 Calcium flux of expanded HC and Patient T cells 105
Figure 3.3.12 p-JNK of expanded HC and Patient T cells....106
Figure 3.3.13 Cytokine expression of expanded HC and Patient T cells 107
Figure 4.2.1 Simplified viral transduction method 116
Figure 4.3.1 CRAC channel protein expression 118
Figure 4.3.2 siRNA KD test 120
Figure 4.3.3 Recommended protocols for Jurkat cells 122
Figure 4.3.4 Recommended protocols for HEK293 cells 123

Figure 4.3.5 Electroporation test 125
Figure 4.3.6 Optimising cell number per well for MTT assay 127
Figure 4.3.7 Puromycin kill curve 128
Figure 4.3.8 Trans-IT transfection test 130
Figure 4.3.9 Second puromycin selection treatment on KO CRACR2A Jurkat cells 131
Figure 4.3.10 Calcium flux response to TG with Jurkat KO cells 132
Figure 4.3.11 Stable cell line blotted with anti-CRACR2A Ab 134
Figure 4.3.12 Stable cell lines blotted with anti-FLAG Ab 135
Figure 4.3.13 Localisation of mutants using FLAG Ab 137
Figure 4.3.14 Localisation of mutants using CRACR2A Ab 138
Figure 4.3.15 IL2 expression for stable cell lines 141
Figure 4.3.16 Calcium flux of stable cell lines 143
Figure 4.3.17 p-JNK response of stable cell lines to TCR stimulation 144
Figure 4.3.18 IP of stable cell lines 146
Figure 5.1.1 STIM1 protein functional domains 157
Figure 5.1.2 STING protein functional domains 160
Figure 5.3.1 *STIM1* Sanger sequencing of P1 family 165
Figure 5.3.2 P1 family pedigree. 166
Figure 5.3.3 Amino acid sequence of STIM1. 171
Figure 5.3.4 qPCR of STIM1 in Patient 1 172
Figure 5.3.5 STIM1 WB with P1 sample 173
Figure 5.3.6 Range of STIM1 Antibodies with P1 and P2 175
Figure 5.3.7 STIM2 WB 176
Figure 5.3.8 Calcium flux of P1 T cells 177
Figure 5.3.9 qPCR of STIM1 patients basal Interferon levels 178
Figure 5.3.10 Sanger sequencing of *TMEM173* from patient genomic DNA 180
Figure 5.3.11 Structure of STING and pArg331 181
Figure 5.3.12 Interferon related gene expression in monocytes 183
Figure 5.3.13 IFN response of patient cells 185

Abbreviations

AD	Autosomal dominant
ADP	Adenosine diphosphate
AED	Anhidrotic ectodermal dysplasia
AICD	Amyloid precursor protein intracellular domain
AI	Amelogenesis imperfecta
AIHI	Autoimmune hemolytic anemia
AIRE	Autoimmune regulator
AR	Autosomal recessive
ASMA	Airway smooth muscle cells
CAD	CRAC activation domain
CaM	Calmodulin
CANT1	Calcium activated nucleotidase 1
CBD	C-di-GMP-binding domain
CD	Cluster of differentiation
CDI	Ca^{2+} dependent inactivation
CDNs	Cyclic dinucleotides
cGAS	cyclic GMP-AMP Synthase
CID	Combined immunodeficiency
co-IP	Co-immunoprecipitation
CRAC	Ca^{2+}-release activated Ca^{2+}
CRISPR	Clustered regularly interspaced short palindromic repeats
CTLA	Cytotoxic T-lymphocyte-associated protein
CTT	C-terminal tail
CVID	Common Variable Immunodeficiency
CXCL10	C-X-C Motif Chemokine Ligand 10
DAG	Diacylglycerol
DBQD	Desbuquois dysplasia
DC	Dendritic cells
DHRS	Dehydrogenase/reductase
DM	Double mutant
ds	Double-stranded
EAE	Experimental autoimmune encephalomyelitis
ED	Ectodermal dysplasia
EDA-ID	Anhidrotic ectodermal dysplasia with immunodeficiency
ER	Endoplasmic reticulum
FcRs	Fc receptors
Foxp3	Forkhead box P3
GCs	Germinal centres
GDP	Guanosine diphosphate
GFP	Green fluorescent protein
GoF	Gain-of-function

GTPase	Rab guanine triphosphatase
HC	Healthy control
HSCT	Hematopoietic stem cell transplantation
HUVEC	Human umbilical vein endothelial cells
ICOS	Inducible T-cell costimulatory
IFNs	Type 1 interferons
Ig	Immunoglobulin
IL	Interleukin
IP3	Inositol trisphosphate
IRF3	Interferon regulatory factor 3
ISGs	IFN-stimulated genes
IS	Immunological synapse
ITP	Immune thrombocytopenic purpura
IUIS	International Union of Immunological Societies
JAK	Janus kinase
JNK	Jun N-terminal kinase
KD	Knock-down
KO	Knock-out
LoF	Loss of function
MAPK	Mitogen-activated protein kinase
MEFs	Mouse embryonic fibroblasts
MHC	Major histocompatibility complex
MOC	Microtubule organizing centre
NADPH	Nicotinamide adenine dinucleotide phosphate
NFAT	Nuclear factor of activated T cells
NFκB	Nuclear factor-κB
NGS	Next generation sequencing
NK	Natural killer
NLR	NOD-like receptors
Orai	Calcium release-activated calcium channel protein
OX40	Tumor necrosis factor receptor superfamily, member 4
P	Patient
PBMCs	Peripheral blood mononuclear cell
PD-1	Programmed cell death protein 1
PID	Primary immunodeficiency
PIDDs	Primary immunodeficiency diseases
PIP2	Phosphatidylinositol 4,5-bisphosphate
PLC	Phospholipase C
PMCAs	PM Ca^{2+} ATPases
PRRs	Pattern recognition receptors
RA	Retinoic acid
ROS	Reactive oxygen species
SAID	Systemic autoinflammatory diseases
SAM	Sterile α motif
SARAF	Store-operated calcium entry-associated regulatory factor

SAVI	STING-associated vasculopathy with onset in infancy
SCID	Severe combined immunodeficiency
SCR	Scramble
SDR	Short-chain dehydrogenase/reductase
SD	Standard deviation
SERCA	Sarcoplasmic/ER Ca^{2+} ATPases
SLO	Secondary lymphoid organs
SOCE	Store-operated calcium entry
SR	Sarcoplasmic-reticulum
STAT	Signal transducer and activator of transcription
STING	Stimulator of interferon genes
TBK1	TANK-binding kinase 1
TCR	T cell receptor
TLR	Toll-like receptors
TM	Transmembrane protein
TRP	Transient receptor potential
UDP	Uridine diphosphate
UTP	Uridine triphosphate
WAS	Wiskott-Aldrich syndrome
WB	Western blot
WES	Whole exome sequencing
WGS	Whole genome sequencing
WPBs	Weibel-Palade bodies
WT	Wild type

Chapter 1 Introduction

1.1 Immune cell lineage

The immune system is split into two main categories; the innate and adaptive response. The innate immune system provides the initial response to infection and consists of granulocytes and monocytes. The main subtypes of this system can be seen in Figure 1.1.1. Adaptive immune response is the focus of this thesis The main cells of this system are lymphoid cells, such as T and B cells. Both of these cell types produce memory cells that allow for a rapid secondary response to the same foreign invasion.

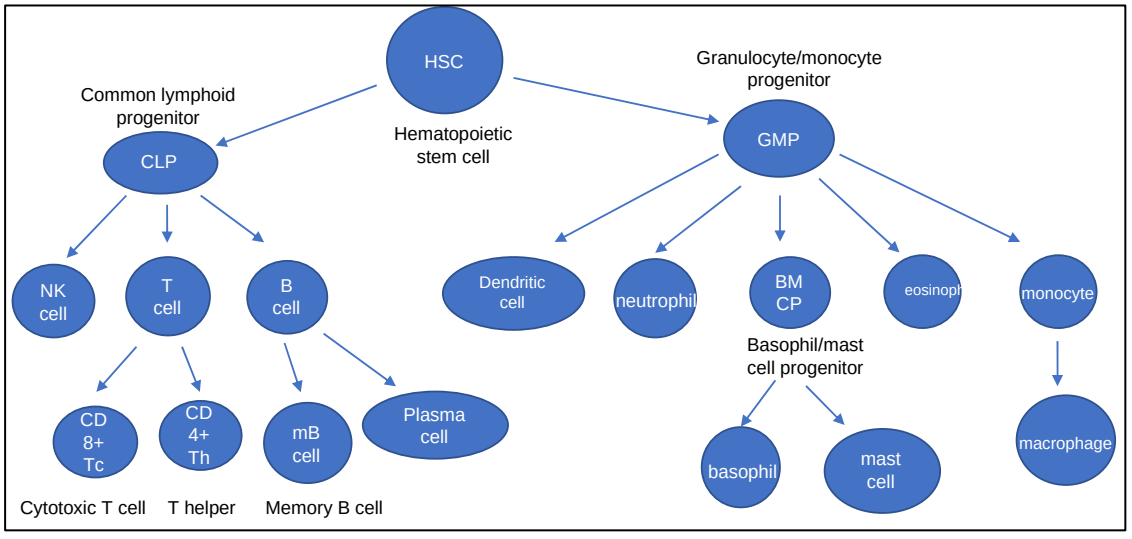

Figure 1.1.1 Immune cell lineages
General information regarding lineages visualised (Janeway CA Jr, Travers P, Walport M, 2001; LaRosa and Orange, 2008).

1.1.1 T cells

T cells are part of the adaptive immune response. T cells mature in the thymus and express T cell receptor (TCR), and either cluster of differentiation (CD)8 or CD4 glycoproteins on their surface. CD8+ cells (Tc) are cytotoxic and are involved in the viral and tumour immune responses. CD4+ cells are helper T cells (Th) that differentiate into different subsets as shown in Figure 1.1.2 and are characterised by different cytokine profiles (Romagnani, 2000; Geginat, Lanzavecchia and Sallusto, 2003; Raphael *et al.*, 2015; Golubovskaya and Wu, 2016). Th cells have different functions in the immune system depending on the cytokines they express, such as pro-inflammatory or regulatory. All Th cells express interleukin (IL)-2, which induces proliferation of all T cell subtypes, which then creates a positive feedback loop during an immune response. Different subsets work to balance the immune response, for example Th17 are proinflammatory and when not regulated can cause autoimmunity and break immune tolerance. However, regulatory T cells (Tregs) are able to supress and moderate Th17 cells and so maintain immune tolerance and lymphocyte homeostasis.

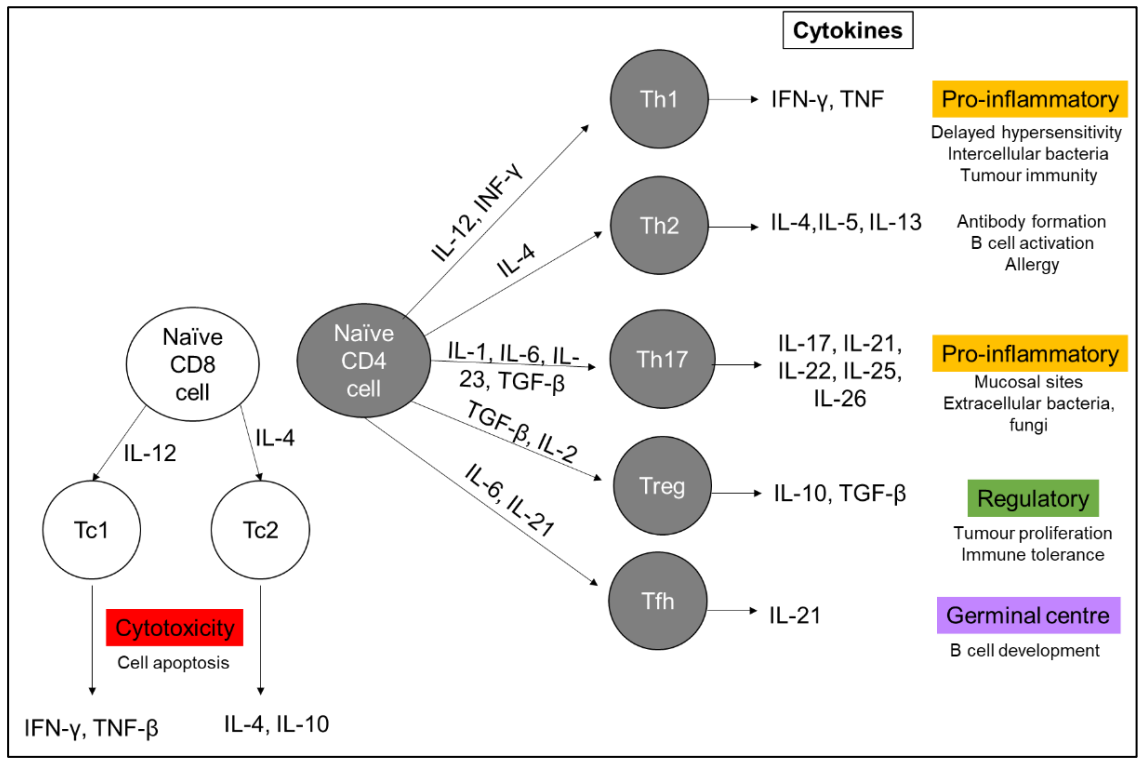

Figure 1.1.2 T cells subtypes and functions

Figure taken and adapted with permission from Golubovskaya and Wu, 2016 licenced under CC BY (Janeway CA Jr, Travers P, Walport M, 2001; Golubovskaya and Wu, 2016; Kwun et al., 2017).

1.1.1.1 T cell development

As part of the adaptive immune response T cells need to be able to distinguish between self and non-self, this is controlled by positive and negative selection in the thymus. Immature T cells progress through multiple developmental stages and undergo somatic recombination to generate individual T cell clones expressing unique TCRs. These TCRs bind and recognize different antigens. In general, this antigen recognition process occurs when the TCR binds to antigen being presented by other cells on major histocompatibility complex (MHC) proteins. MHC class I interact with CD8+ T cells and MHC class II with CD4+ T cells. During positive selection the T cells are selected on their ability to bind to MHC complexes. Apoptosis is induced in cells that cannot bind, while positively selected cells receive survival signals, determination of whether the cells will be CD8+ or CD4+ is also determined at this stage by which type of MHC complex they bind most effectively. Negative selection allows for the removal of T cells that bind too strongly to self-antigens. The autoimmune regulator (AIRE) protein in thymus induces the expression of proteins from other tissues and cell types not normally found in the thymus, to allow for selection against most self-antigens (Klein *et al.*, 2014).

1.1.2 B cells

B cells link the innate and adaptive immune responses. They have the ability to respond rapidly to damage-associated molecular patterns and antigenic stimuli, but also form long-lived serologic memory. B cells perform diverse functions, such as antibody secretion, cytokine production and antigen presentation. They interact with both innate cells and T cells, and therefore shape the outcome of the immune response toward immunity or tolerance (Hoffman, Lakkis and Chalasani, 2016).

B cells express clonally diverse cell surface immunoglobulin (Ig) receptors recognising specific antigenic epitopes. As shown in Figure 1.1.1, B cells differentiate into plasma cells. Plasma cells are big lymphocytes with large amounts of endoplasmic reticulum (ER), which produce antibodies to specific antigens. They respond to signals from T cells (Figure 1.1.2) during infection and continue to produce antibodies to the required antigen until the infection is controlled. Plasma cells are often found within chronic infection and inflammation (Janeway CA Jr, Travers P, Walport M, 2001).

1.1.2.1 B cell Development

Once differentiated in the primary lymphoid organ, the bone marrow, the B cells migrate and reside in the follicles of the spleen.

B cell subtypes and their functions can be seen in Figure 1.1.3.

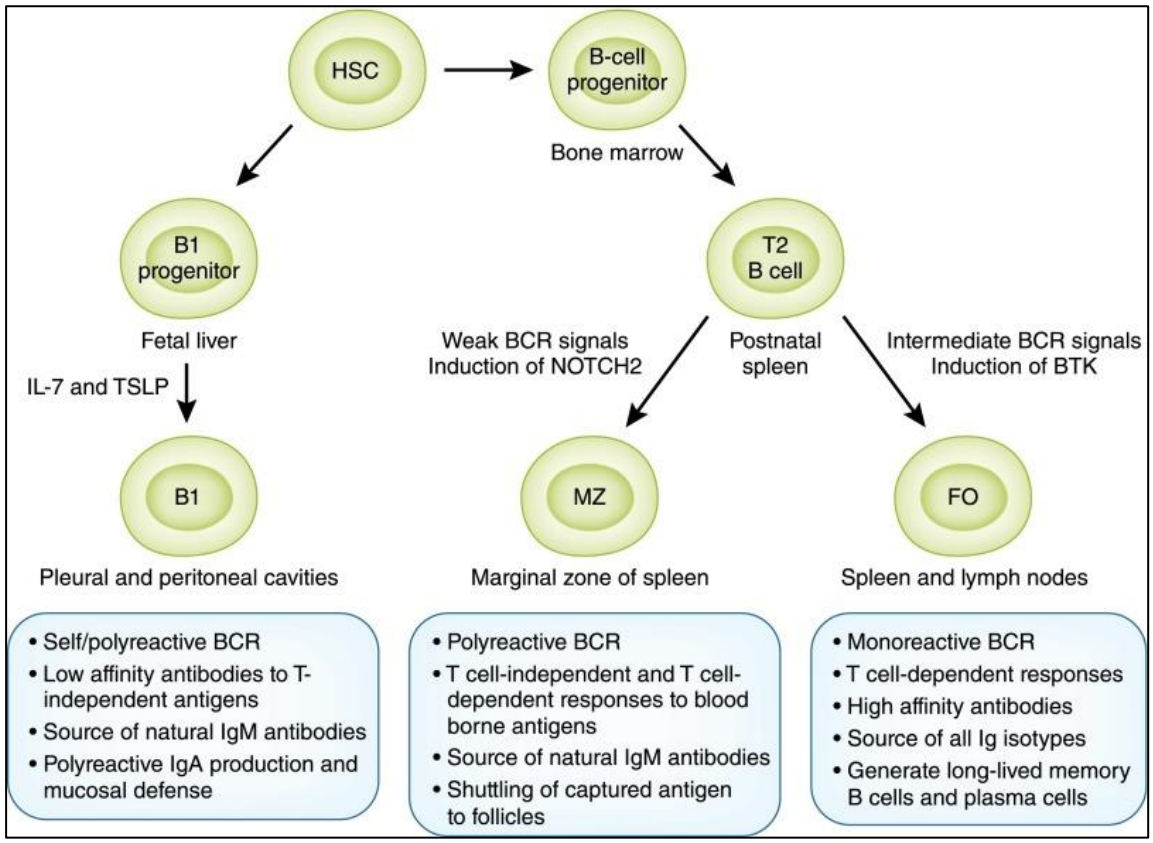

Figure 1.1.3 B cell subtypes and function

Republished with permission of American Society of Nephrology, from B Cells, Antibodies, and More., Hoffman, William; Lakkis, Fadi G; Chalasani, Geetha, volume 11, issue 1, 2016]; permission conveyed through Copyright Clearance Center, Inc. (Hoffman, Lakkis and Chalasani, 2016).

1.1.3 T and B cell interaction

A successful immune system is characterised through interactions between distinct cell types.

1.1.3.1 T cell influence on B cells

T cells play a role in the maturation of B cells in the follicles of secondary lymphoid organs (SLO), such as the lymph nodes and the spleen, this subset of T cells is called follicular helper T cells (Tfh). Tfh , B cells, and IL-21 drive B cells to proliferate and differentiate into plasma cells, leading to antibody production. SLO are organised into T and B cell zones. Tfh reside in B cells zones and form germinal centres (GCs) during an ongoing immune response. B cells within GCs undergo rapid proliferation, differentiation into plasma cells and antibody diversification (Kwun *et al.*, 2017).

The interaction between Th cells and B cells can occur outside of SLOs and is essential for the production of antibodies and the autoimmune response. The T cell dependent response of B cells results in optimal affinity-matured antibody responses that are required for host defence, including rapid neutralization of bacterial toxins and blockade of viral cell entry (Petersone *et al.*, 2018).

Costimulatory molecules are essential for T and B cell interaction, such as CD28, CD40, cytotoxic T-lymphocyte-associated protein (CTLA)-4. CTLA-4-mediated regulation of CD28 signalling controls the engagement of secondary costimulatory pathways such as inducible T-cell costimulatory (ICOS) and OX40, and profoundly influences the capacity of T cells to provide B cell help.

Most B cells require interaction with T cells in order to produce antibodies, except for a small number found within specialised sites such as the spleen and peritoneum. They are particularly important for dealing with encapsulated bacteria, which often have a polysaccharide outer layer as opposed to proteins, which allows them to evade T cells. T-independent B cells are able to recognise these layers and produce antibodies without T cell interaction (Hoffman, Lakkis and Chalasani, 2016).

1.1.3.2 B cell influence on T cells

B cells have cellular functions that can affect T cells, through presentation of antigens, costimulatory factions or cytokines. T cell activation and the production of memory cells can be stimulated by antigen presentation on MHC molecules on B cell

surface, through CD40 and CD40L interaction and IL-6 signalling. B cells can also inhibit T cells by expressing IL-10, which reduces T cell activation and increases differentiation into Tregs. (Hoffman, Lakkis and Chalasani, 2016)

1.1.4 Monocytes and macrophages

Monocytes and macrophages are a component of innate immunity, through the mononuclear phagocyte system. Monocytes are derived in the bone marrow and circulate in the blood and spleen. They are the first line of host defence and can recognize danger signals or infection-associated pathogen-associated molecular patterns via pattern recognition receptors (PRRs), such as toll-like and nucleotide oligomerization domain (NOD)-like receptors (TLR and NLR) (Takeuchi and Akira, 2010; Varga and Foell, 2018). Monocytes can phagocytose, present antigens, secrete chemokines, and proliferate in response to infection and injury. Monocytes also differentiate into macrophages and dendritic cells. Macrophages are terminally differentiated cells that phagocytose pathogens and toxins, secrete chemokines to recruit other immune cells, and migrate to local lymph nodes (Chiu and Bharat, 2016).

1.1.4.1 Interferon response

Macrophages and dendritic cells produce type 1 interferons (IFNs) after sensing pathogen components via their PRRs. IFNs are polypeptides that are secreted by infected cells. They induce antimicrobial states that limit the spread of viral pathogens, promote antigen presentation and natural killer (NK cell function, inhibit cytokine production and activate antigen-specific T and B cell responses and immunological memory (Trinchieri, 2010; Ivashkiv and Donlin, 2014). Canonical type I IFN signalling activates the Janus kinase (JAK)–signal transducer and activator of transcription (STAT) pathway, leading to transcription of IFN-stimulated genes (ISGs).

The expression of IFNs and pro-inflammatory cytokines following the detection of foreign DNA species, such as cyclic dinucleotides (CDNs), can be controlled by stimulator of interferon genes (STING). This protein is ubiquitously expressed on the membrane of ER, and can be activated by ER stress. Upon activation they can activate the downstream signalling cascades for the production of cytokines and chemokines (Ishikawa, Ma and Barber, 2009; Motwani, Pesiridis and Fitzgerald, 2019).

1.2 Primary immunodeficiency

Primary immunodeficiency (PID) and primary immunodeficiency diseases (PIDDs) are a group of disorders which result in a compromised immune system. The definition has continued to expand and now encompasses not only susceptibilities to infections but also dysregulated inflammation and tolerance toward endogenous and exogenous antigens. Over 340 of the recognised 350 PIDDs are associated with a single gene. Monogenetic mutations make up 80% of all rare Mendelian diseases (Wright, FitzPatrick and Firth, 2018; Rahit and Tarailo-Graovac, 2020). The disorders are varied resulting in a large range of phenotypes and severities. The inborn errors cause part of the immune system to be missing or not function correctly (Bousfiha *et al.*, 2018; Picard *et al.*, 2018; Chinn *et al.*, 2020). To help better understand and diagnose patient PIDs are classified into categories. It is thought that PIDs are more common than reported and epidemiologic studies would be one of the only ways to fully grasp the prevalence of these diseases . PID can present at any age, 1 in 2000 people may have a PID of some form though the most severe forms of PID are normally found in the first few months of life (Bousfiha *et al.*, 2013).

PID covers three distinct but often overlapping types of disease: immunodeficiency, autoimmunity and autoinflammatory. Immunodeficiency is characterised by the susceptibilities to infections and will be the main topic of discussion in this project (Todoric *et al.*, 2013).

Autoimmunity is when the immune system attacks self. The susceptibility to autoimmune disease is often influenced by a large number of polymorphic genes, rather than a single gene as seen in immunodeficiency. The adaptive immune response targets self-antigens and can affect either a specific organ (Grave's and multiple sclerosis) or lead to a more general inflammatory condition (systemic lupus erythematous). Autoimmunity is associated with relapses and flares of disease (Truedsson, Bengtsson and Sturfelt, 2007; Todoric *et al.*, 2013).

Autoinflammatory diseases are defined as self-directed inflammation. These systemic diseases may affect any organ or system, are considered rare and encompass a wide variety of diseases and syndromes. Innate immune cells, including macrophages and neutrophils, are activated in these diseases. Chronic or recurrent episodes of inflammation occur in the absence of normal stimuli, such as high titre autoantibodies or autoreactive lymphocytes (Alsharief *et al.*, 2020).

Autoimmunity and autoinflammation can manifest in immunodeficiency diseases. Common Variable Immunodeficiency (CVID), for example, can result in inflammatory bowel disease, haemolytic anaemia and rheumatoid arthritis as well as the characteristic recurrent chronic infections (Goyal *et al.*, 2009).

1.2.1 Why study PID

PIDs are rare diseases, with a reported prevalence of between 1:16 000 and 1:50 000 (O'Shea, 2018). These small numbers provide challenges to effective diagnosis, clinical care and research. The number of patients being diagnosed with PID is increasing, the United Kingdom Primary Immunodeficiency (UKPID) Registry increased from 2229 patients to 4758 between 2013 to 2018 (Shillitoe *et al.*, 2018). This expansion has allowed for improved molecular diagnostics, an increased number of identified genes and increased collaboration between clinicians/researchers. However, as at 2018 less than 22% of patients had a proven genetic defect underlying their PID (Shillitoe *et al.*, 2018).

Being able to identify the genetic cause of a patient's disease can improve the diagnosis and treatment options available to the patient. More informed and quicker decisions are possible to the clinicians and scientists who contribute to this process, if it is a known gene associated with PID. Personalised medicine or gene therapies may be available depending on the genetic cause. It can also identify family members at risk. In addition to improving patient care, identifying the genetic cause of disease can improve the PID field and immunology in general. As it can lead to broader or more detailed phenotype data and a better understanding of the immune system as well as protein function. PID potential can lead to the identification of novel genes essential for the normal immune response, which would normally be identified in knock-down (KD) cell culture studies, where potential genes of interest are KD and the affect analysed. It allows for understanding of important mechanisms and pathways for immune cells. Potential novel genes or mutations could also lead to potential therapeutic targets of interest for other diseases, such as cancer. Immunotherapy can improve treatment efficacy in cancer (Robert, 2020). Checkpoint inhibitor antibodies are used to block the binding of co-stimulatory molecules on T cells, such as CTLA-4, programmed cell death protein 1 (PD-1) and programmed death-ligand 1 (PD-L1), from binding to their protein partners. This allows for the activation of cytotoxic T cells which can kill cancer cells (Rosenberg, Yang and Restifo, 2004; Robert, 2020).

1.2.2 Types of PID

PIDs have been categorised into 9 broad sections by the International Union of Immunological Societies (IUIS) Expert Committee of PID. However, an important point to remember is that this classification is very general and other considerations should be taken into account (Al-Herz and Notarangelo, 2012). Between the 9 sections there are some deficiencies that fall into multiple categories and ones that have yet to be identified may require a new section altogether. Casanova et al. 2008 shows 3 different factors which need to be considered for each new case of PID to gain a better understand of the disease: epidemiological (frequency and age of onset), phenotype (clinical and cellular) and genotype (mode of inheritance and mutations). Another factor that can complicate classifying a PID is genotype versus phenotype. Mutations can give rise to diverse phenotypic presentations in different individuals due to a range of genetic and environmental differences. (Lawrence *et al.*, 2005; Boisson, Quartier and Casanova, 2015; Dadak *et al.*, 2017; Bousfiha *et al.*, 2020).

1.2.2.1 Categories

The 9 main categories, shown in Figure 1.2.1 represent the most profound phenotype associated with each identified gene (Casanova *et al.*, 2014; Picard *et al.*, 2015; Bousfiha *et al.*, 2020; Tangye *et al.*, 2020). The Online Mendelian Inheritance in Man (OMIM) reference is included for each defect as they recognise the wide phenotypic variability associated with each gene, due to the different mutations in the same gene, environmental and host factors. The patients discussed in this thesis fall into 3 of these categories.

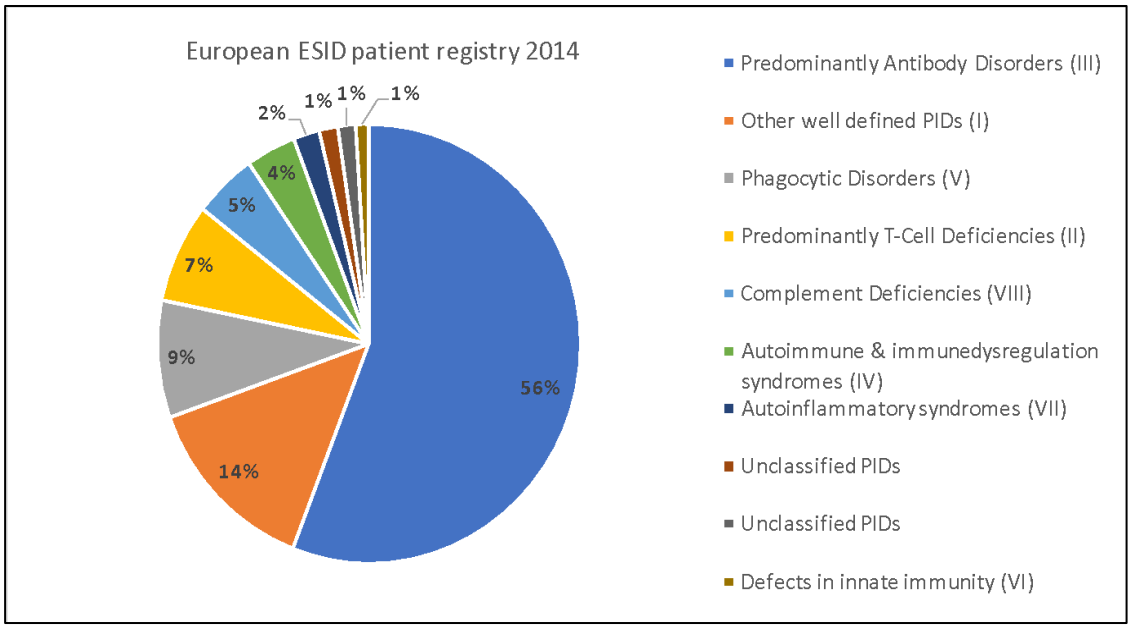

Figure 1.2.1 Prevalence of each IUIS category

Data taken from the ESID for the patient population in 2014. Antibody disorders (III) are the most common making up more than half of the population. PIDs affecting cellular and humoral immunity affect (I) 14% of this population and around 70% of those cases are SCID. Data taken from http://esid.org/Working-Parties/Registry/ESID-Database-Statistics

1.2.2.1.1 Immunodeficiency affecting cellular and humoral immunity (I)

The two main branches for this category are severe combined immunodeficiency (SCID) and combined immunodeficiency (CID), distinguished by lymphopenia and normal white cell count respectively. SCID is a group of different PIDs, where the main clinical symptom is severe infection, often more serious than that of a healthy child and possibly life threatening. Infections that are not normally harmful to children can cause devastating effects to those with SCID. SCID can be fatal and is normally diagnosed in infancy. Along with severe recurrent infection, SCID is also associated with chronic diarrhoea and a failure to thrive . There is often a low total lymphocyte count due to the characteristic defect in T cell function but in some types of SCID,

natural killer (NK) cells and B cells can also be affected. Autoimmune manifestations can occur due to alterations in the central and peripheral tolerance which filters out self-reactive lymphocytes (Giardino *et al.*, 2016; Pai, 2019).

X-linked SCID is the result of a mutation in the IL-2 receptor subunit gamma (*IL-2RG)* gene critical for lymphocyte development and function and accounts for about half of SCID cases. T and NK cells are normally absent while B cells are non-functional. Male infants with this disease have chronic diarrhoea, thrush, severe bacterial infections, skin rashes and an absence of tonsils and lymph nodes. A bone marrow transplant or gene therapy is required to repair the immune system as the disease can be fatal within the first two years of life (Allenspach, Rawlings and Scharenberg, 1993).

1.2.2.1.2 Combined immunodeficiency with associated or syndromic features (II)

This category contains deficiencies with a well-defined set of signs and symptoms that appear together to define the disease. The PIDs are generally associated with T cell immunodeficiency. Many in this category have some form of growth or developmental abnormities and reduced function or number of a specific T cell subtype. Wiskott-Aldrich syndrome (WAS) is characterised by thrombocytopenia, eczema, and recurrent bacterial infection. Thrombocytopenia is a lack of platelet cells and so is associated with abnormal bleeding. It is an X-linked disease associated with WAS protein which is expressed only in the hematopoietic cells. The protein functions in the cell cytoskeleton, regulating actin polymerization (Bompard and Caron, 2004; Boisson, Quartier and Casanova, 2015; Giardino *et al.*, 2016).

Calcium release-activated calcium channel protein 1 (Orai1) deficiency is another disease with a unique clinical phenotype and the complete loss of function of Orai1 can cause SCID. It is associated with severe infections early in life due to defects in the development or activation of T cells, immunodeficiency, anhidrotic ectodermal dysplasia (AED) and congenital myopathy, a muscle disorder present at birth. AED is the reduced ability to sweat, reducing the body's ability to modulate temperature as well as sparse scalp and body hair. ORAI1 is involved in calcium transport through the formation of Ca^{2+}-release activated Ca^{2+} (CRAC) channels in the plasma membrane. Calcium influx is essential for T cell activation, proliferation and cytokine production and important for nuclear factor of activated T cells (NFAT) and nuclear factor-κB (NFκB) pathways. (Feske, Picard and Fischer, 2010)

1.2.2.1.3 Predominantly antibody deficiencies (III)

Predominantly antibody deficiencies are the most common type of PID as seen in Figure 1.2.1, with selective IgA deficiency and CVID being the most prevalent respectively. Most PIDs in this category are associated with recurrent bacterial infections and are categorised according to the specific immunoglobulin deficiency (IgG, IgA, and IgM) and the B cell numbers. CVID is a heterogeneous group of disorders which have a serum Ig characterised by low IgG and IgA with or without low IgM. The phenotype can vary but most cases present with recurrent infections, cytopenia, enlarged lymph nodes, poor antibody response to vaccines and low switched memory B cells. 25% of patients develop autoimmune complications (Giardino *et al.*, 2016; IPOPI, 2016).

1.2.3 Current Therapies for PID

The main treatment for SCID or severe disease is allogeneic hematopoietic stem cell transplantation (HSCT). This HSCT requires a stem cell match, and may require chemotherapy prior to transplant. It has a good survival rate, but normally antibody production is not regained so immunoglobulin therapy is required (Bousfiha *et al.*, 2015; Pai, 2019). Recently, new born screening for SCID has allowed for early diagnosis and treatment, which has improved the survival rate of this therapy (Bucciol and Meyts, 2020).

Immunoglobulin replacement therapy allows antibodies to be infused into patients with antibody deficiencies. The infusions are given every 3 to 4 weeks and normally continue for the patient's lifetime. Like Ig infusions more targeted therapies are available such as cytokines, cytokine inhibitors and small molecules, to control symptoms. Rituximab (anti-CD20) for examples is used to treat autoimmune phenotypes and selective inhibition of IL-6R is used with tocilizumab (Bousfiha *et al.*, 2015; Bucciol and Meyts, 2020).

Gene therapy has been used in the treatment of X linked SCID and WAS. It involves inserting a normal copy of the gene into the immune cells of the patient (Bousfiha *et al.*, 2015; Bucciol and Meyts, 2020).

1.2.4 Molecular screening of patients

In PID 340 genes have been identified, but there are still many cases where the affected gene is unknown. There is a push in the research community to discover more of these targets, to add to gene panels for mutation screening, which can ultimately lead to better treatment for patients.

Gene panels screen patients for known mutations that cause disease, these panels can be specified to the patient phenotype. For example, a patient with antibody deficiency can be screened for known mutations and genes of interest that have previously been shown to be pathogenic, such CD40 ligand which caused immunodeficiency with hyper-IgM (Bousfiha *et al.*, 2015).A next generation sequencing (NGS) PID panel of 242 genes has been reported (Rae *et al.*, 2018). It was tested on twenty-seven participants, and identified 15 reportable variants in 48% of the participants. The panel results had implications for treatment in 37% of the patients. In patients with mutations not identified by gene panels, whole exome sequencing is available (WES).

WES is a powerful technique that allows the sequencing of specific DNA that makes up 2 % of the total genome. The exome makes up the coding regions of genes, which accounts for 85 % of known disease related variants. WES has many advantages as a genetic platform for identifying novel genes and mutations associated with PID. It is high-yield and more cost-efficient than whole genome sequencing (WGS). It is an unbiased technique and it has wide utility due to its use in both commercial and research facilities. The main limitations are that 50-70 % of patients do not receive a diagnosis after WES and not all patient exomes have 100 % coverage (Choi *et al.*, 2009; Y. Yang *et al.*, 2013; 1000 Genomes Project Consortium *et al.*, 2015; Warr *et al.*, 2015; Meyts *et al.*, 2016; Chinn *et al.*, 2020).

1.3 The CRAC channel

The CRAC channel has an important role in non-excitable cells, due to the more passive nature of the channel. Calcium moves into the cell due to the gradient created by low internal calcium concentration maintained in cells. Excitable cells such as nerves and muscles, rely more heavily on voltage gated channels (Lewis, 2001; Jairaman and Prakriya, 2013).

The movement of calcium is essential for many cellular functions, due to this pronounced gradient maintained in cells, as calcium spikes are sufficient to deliver non-encoded messages unlike K^+ and Na^+. Calcium can induce large conformational changes in receptors and proteins with EF hand domains, due to its divalent charge. These interactions have a high affinity and specificity, making calcium an excellent secondary massager for cellular signalling (Carrasco and Meyer, 2010; Jairaman and Prakriya, 2013).

1.3.1 CRAC channel

Calcium release-activated calcium channel protein (Orai1) is a 32.7 kDa glycoprotein comprising of four transmembrane α helices anchored in the plasma membrane (PM), which forms the pore of the CRAC channel. Stromal Interaction molecule 1 (STIM1) STIM1 is a 77 kDa single-pass transmembrane protein located in the ER, a calcium sensor protein which activates the formation of CRAC channels when the ER stores are depleted (Srikanth and Gwack, 2012; Joseph, Reicher and Barda-Saad, 2014). The resting and active states of the channel are shown in Figure 1.3.1. During TCR activation multiple CRAC channels form at the immunological synapse (IS) and form puncta, this allow for large effector functional changes to take place within the cells (Barr *et al.*, 2008, 2009; Srikanth and Gwack, 2012).

Regulation of the CRAC channel occurs predominantly through STIM1 (Prakriya, 2009). At low Ca^{2+} concentrations of the ER, CRAC channel activation is initiated through the EF hand domain of STIM1. Regulation can also occur due to Ca^{2+} concentration levels in the cytosol. Cytosolic Ca^{2+} can inactivate CRAC channels through two spatially and temporally distinct mechanisms, called fast and slow inactivation, through Ca^{2+} dependent inactivation (CDI). Ca^{2+} −dependent fast inactivation develops over milliseconds and reflects build-up of Ca^{2+} close to the channel pore and slow inactivation develops over tens of

seconds and requires a rise in global Ca^{2+}. It is regulated by mitochondria and the ER-resident protein, store-operated calcium entry-associated regulatory factor (SARAF) (Srikanth, Ribalet and Gwack, 2013). Additional regulation can occur through calmodulin (CaM) which is able to bind the N terminus of Orai1 at elevated Ca^{2+} concentration and cause CDI. In contrast, calcium release activated channel regulator 2A (CRACR2A) is able to stabilise the CRAC channel complex and promotes the channel formation (Srikanth, Jung, Kim, *et al.*, 2010; Srikanth, Ribalet and Gwack, 2013; Parekh, 2017). This protein is also able to respond to changes in cytosolic Ca^{2+} through its EF hand domains. More details about the protein CRACR2A are provided in Chapter 3.

In its resting state STIM1 has recently been found to have another role, binding to STING in the ER, which keeps STING inactive and unable to play its role in interferon expression. STING plays a key role in the viral immune response in the cGAS pathway, which is activated by single stranded DNA. More details about STING are provided in Chapter 5. (Ishikawa, Ma and Barber, 2009; Motwani, Pesiridis and Fitzgerald, 2019; Rice *et al.*, 2019; Srikanth *et al.*, 2019)

1.3.2 Role in the immune system

Lymphocytes are electrically non-excitable cells, so the majority of calcium influx is mediated by store-operated calcium entry (SOCE). CRAC channels are predominately made up of two proteins; Orai1 and STIM1.

At rest lymphocytes maintain low levels of calcium. Regulated oscillations in cytosolic and organellar Ca^{2+} concentrations control effector functions such as metabolism, proliferation, differentiation, antibody and cytokine secretion and cytotoxicity. As an essential secondary messenger, unregulated Ca^{2+} changes in lymphocytes can lead to various autoimmune, inflammatory and immunodeficiency syndromes (Lewis, 2001; Jairaman and Prakriya, 2013; Christo *et al.*, 2015; Trebak and Kinet, 2019). The CRAC channel was originally defined in T cells and mast cells (Hoth and Penner, 1992; Zweifach and Lewis, 1993).

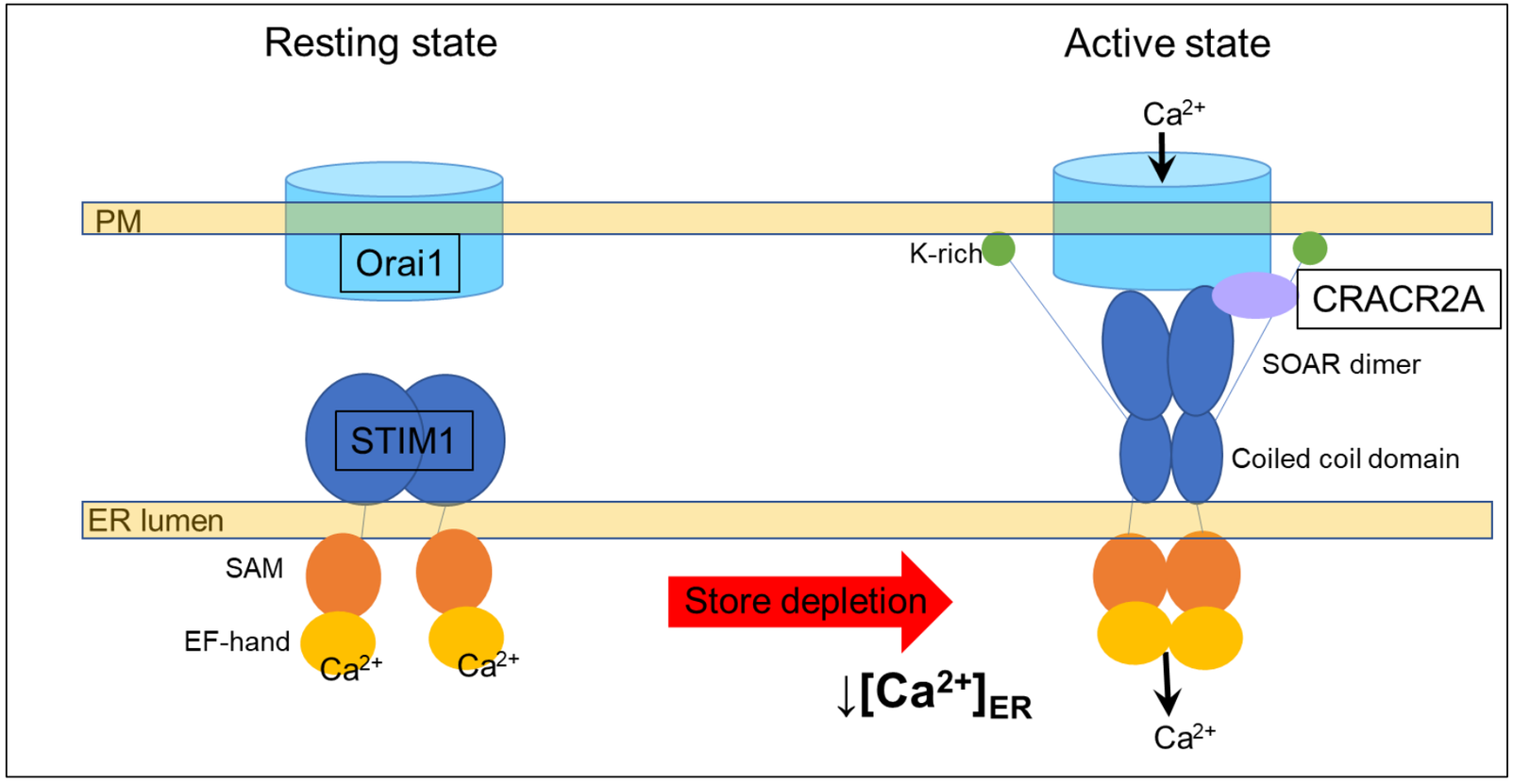

Figure 1.3.1 The CRAC channel

Key components of the CRAC channel, Orai1 pore complex and STIM1 translocate to ER- PM junctions during store depletion of the ER, the proteins oligermise to form puncta made up of many CRAC channel complexes. Figure modified with permission and licenced under CC BY 4.0 (Zhou *et al.*, 2015).

1.3.2.1 Calcium in T cells and pathways

Calcium flux is especially important in T cells for activation, proliferation, cytokine production and NFAT and NFκB signalling. Ca^{2+} influx and efflux across the PM of T cells occurs via several types of Ca^{2+}-permeable channels and transporters, including SOCE. SOCE or calcium influx after store depletion is essential for T cell function, such as TCR activation and acute release of cytotoxic granules by CD8 + T cells within minutes of stimulation (Oh-hora and Rao, 2008). Different T cell subsets have varied sensitivity to calcium flux. Th1 and Th17 cell function is inhibited by moderate suppression of SOCE, whereas Tfh, Treg, and CD8 + T cells are relatively unaffected by suppression of the CRAC channel function (Vaeth, Kahlfuss and Feske, 2020). T cells also have voltage channels such as the PM Ca^{2+} ATPases (PMCAs) and sarcoplasmic/ER Ca^{2+} ATPases (SERCAs) which pump Ca^{2+} from the cytosol to the extracellular space and the ER, respectively. They pump Ca^{2+} ions against the electrochemical gradient, thus requiring energy in the form of ATP (Kozak and Putney, 2017). The function of these channels in immune cells is not as profound as in nerves and muscles.

1.3.2.2 T cell receptor activation

When the TCR is activated, phospholipase C (PLC) $_{\gamma}$1 hydrolyses phosphatidylinositol 4,5-bisphosphate (PIP2) into inositol trisphosphate (IP3) and diacylglycerol (DAG). IP3 binds to its receptor in the ER and the calcium stores are released. The STIM1 molecule can sense the depletion of the calcium stores due to the EF hand domains. When the T cells are in a resting state the EF domains are bound by calcium but as the store is depleted, the calcium dissociates from causing a conformational change, multimerization and the translocation to areas of the ER membrane in close proximity to the PM. Orai1 interacts with the STIM1 forming the CRAC channel which allows calcium to enter into the ER store, by SOCE. When the store is replenished calcium binds to STIM1 causing it to dissociate from Orai1. The calcium flux in T cells is heavily controlled which causes oscillating calcium concentrations. These oscillations of calcium rhythms are thought to be an additional regulation of downstream T cell effector function, as specific rhythms can cause particular gene transcription patterns through the NFAT and NFκB. The oscillations also sensitise the T cells to changes in calcium flux (Barr *et al.*, 2008; Christo *et al.*, 2015; Woo *et al.*, 2018; Trebak and Kinet, 2019).

Rapid cytoskeletal rearrangements and the increase of intracellular calcium concentration downstream of TCR activation allow for T cell effector functions and organisation of an immunological synapse. Formation of the IS facilitates redistribution of receptors, signalling molecules and organelles towards the T cell–APC interface. These two systems form a positive feedback loop and are able to respond rapidly to T cell activation, as shown in Figure 1.3.2.

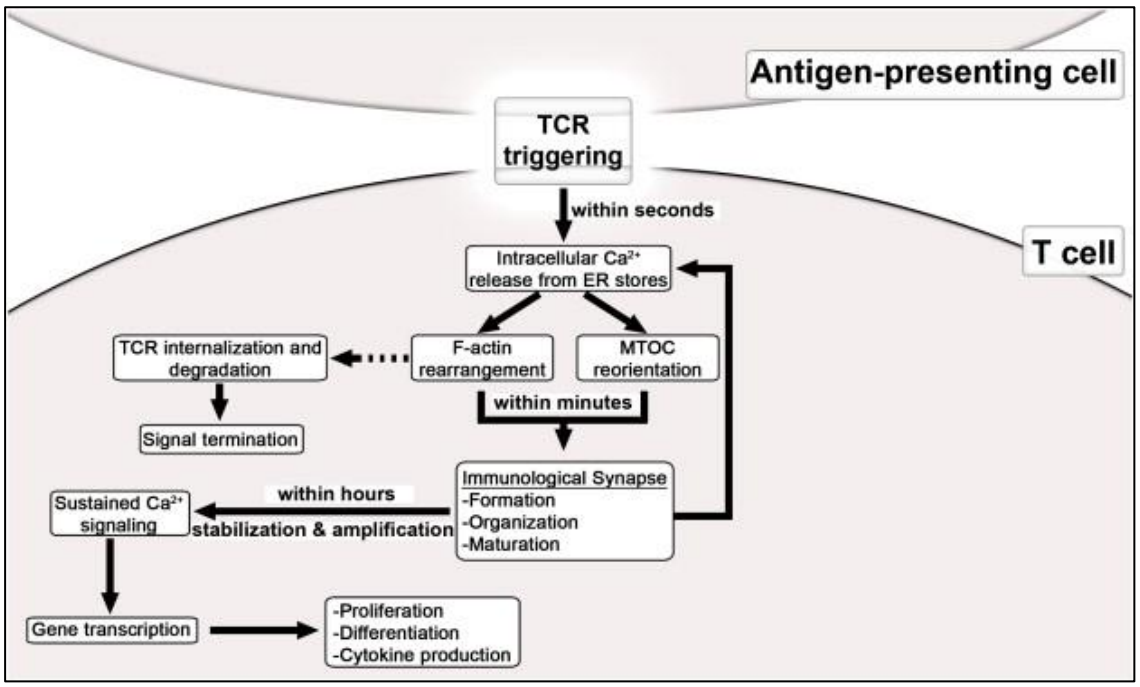

Figure 1.3.2 Calcium and cytoskeleton response to TCR activation

Reprinted from The calcium feedback loop and T cell activation: Biochimica et Biophysica Acta (BBA) - Biomembranes, 1838 edition 2, Noah Joseph,Barak Reicher,Mira Barda-Saad, How cytoskeleton networks control intracellular calcium flux, Pages No. 557-568, Copyright (2014), with permission from Elsevier (Joseph, Reicher and Barda-Saad, 2014).

1.3.3 CRAC channel deficiencies

CRAC channel deficiencies were briefly mentioned in Section 1.2.2.1.2, as they fit under the PID category II. Deficiency of Orai1 or STIM1 can result in SCID which presents with severe infections, immunodeficiency, AED and congenital myopathy, a muscle disorder present at birth. SCID can be fatal and is normally diagnosed in infancy. The syndromic features of these deficiencies are shown in Table 1.3.1. The severe infections are a result of impaired T cell activation and development. T cells are sensitive to mutations in CRAC channel proteins. There is 4 fold more STIM1 expressed and they do not express the homologs Orai2/3 and STIM2/3 (Picard *et al.*, 2009; Feske, Picard and Fischer, 2010; Feske, 2011).

Table 1.3.1 Phenotypes associated with Orai1 and STIM1 deficiencies

Deficiency	**Orai1**		**STIM1**	
Host	**Human**	**Mouse**	**Human**	**Mouse**
Survival limited by	Immunodeficiency	Perinatal lethality	Immunodeficiency	Perinatal lethality
Immune dysfunction	Infections T cell activation defect Mitochondria-mediated cell death pathways ↓	T cell defect Mast cell defect	Infections T cell activation defect Treg numbers ↓	T cell defect Mast cell defect Macrophage defect
Autoimmunity	Neutropenia Thrombocytopenia	No	Splenomegaly lymphadenopathy AIHA thrombocytopenia	AIHA ITP
Muscular dysfunction	Myopathy - congenital, global Respiratory muscle insufficiency Atrophy of type II muscle fibres	Myopathy	Myopathy - congenital, global	Myotube dysfunction Mitochondriopathy Muscular hypotenia
ED like phenotype	Dental enamel defect (amelogenesis imperfecta type III) Anhydrosis Dry and exfoliate skin Sparse/thin/brittle hair	Alopecia	Dental enamel defect Anhydrosis	Anhydrosis Enamel hypoplasia Demititis
Thrombocyte function	No bleeding diathesis	Platelet activation ↓ Thrombus formation ↓	No bleeding diathesis Thrombocytopenia (autoimmune)	Platelet activation ↓ Thrombus formation ↓

Autoimmune hemolytic anemia (AIHA), Ectodermal dysplasia (ED), Immune thrombocytopenic purpura (ITP)
(Feske, 2010; Kim *et al.*, 2011; Eckstein and Lacruz, 2018; Rice *et al.*, 2019)

1.3.3.1 Immune cell phenotype

CRAC channel deficiency can result in T cell dysregulation. As previously mentioned, SOCE is essential for many T cell functions. The T cell phenotype often has a normal number of total T cells, but the Treg and Th numbers are reduced. T cells have reduced proliferation responses and reduced cytokine production (Feske, 2011; Rice *et al.*, 2019).

Myeloid lineage cells, such as mast cells, macrophages, and dendritic cells, express Fc receptors (FcRs), which activate phospholipase C and subsequently induces Ca^{2+} depletion from the ER. In mast cells, SOCE and STIM1 have a critical role in degranulation. The initial release of Ca^{2+} from the ER stores and the final fusion step with the plasma membrane of mast cell degranulation requires calcium, after the initial granular translocation and docking. STIM1-dependent Ca^{2+} influx positively regulates the activation of both NF-κB and NFAT in mast cells. NF-κB promotes the expression of IL-6 and TNF and NFAT enhances the production of IL-13 and TNF. Impaired NF-κB and NFAT activation in STIM1 deficiency may contribute to the insufficient production of these cytokines (Blank and Rivera, 2004; Baba *et al.*, 2008).

In B cells, SOCE also plays an important signalling function. Deficiency in either STIM or Orai proteins show a defect in SOCE and proliferation response to BCR activation. B cell development and antibody responses remain normal. B cells from B-dKO mice fail to produce an anti-inflammatory cytokine, IL-10. The deficiency of CRAC channel proteins does not seem to have as profound an effect in B cells as in T cells (Scharenberg, Humphries and Rawlings, 2007; Gwack et al., 2008; Matsumoto et al., 2011).

1.3.3.1.1 Nervous system

In CRAC channel deficiencies, neuronal phenotypes are normally limited to developmental delays and seizures. Neurological phenotypes linked to CRAC channel deficiency are rare (Feske, 2010, 2011; Bollimuntha, Pani and Singh, 2017; Kozak and Putney, 2017).

1.3.3.2 Muscle phenotype

SOC is important for the regulation of muscle function, which is highlighted by muscular hypotonia, or decreased muscle tone, in patients with both STIM1 and Orai1 deficiency (McCarl *et al.*, 2009; Picard *et al.*, 2009; Feske, Picard and Fischer, 2010;

Bousfiha *et al.*, 2015; Rice *et al.*, 2019). STIM1 was found to be expressed at high levels in skeletal muscle controlling muscle function and properties. Calcium drives NFAT-dependent morphogenetic remodeling and sarcoplasmic-reticulum (SR) Ca^{2+}-store filling. Orai1 loss of function mutations can result in myopathies. SOCE deficient phenotypes include abnormal muscle development, differentiation and function due to the reduced NFAT signalling, and reduced expression of SERCA channels and MHC proteins (Kiviluoto *et al.*, 2011; Li *et al.*, 2012).

1.3.3.3 Ectodermal dysplasia like phenotype

Ectodermal dysplasia (ED) are a group of disorders in which two or more of the ectodermally derived structures develop abnormally such as the skin, sweat glands, hair, nails, teeth and mucous membranes. 90 % of cases are linked to mutations in four genes: *EDA1*, *EDAR*, *EDARAAD* and *WNT10A.* CRAC channel deficiency is not associated with ED, because even though the same tissues are affected and the phenotypes look similar, the underlying mechanisms of disease differ. There is no evidence that Orai1 or STIM1 are involved in the development of these tissues, but rather in their function and maintenance. The enamel develops normally but has mineralization defects, which is linked to the upregulation of STIM1 and ORAI1 during maturation at the mineralization stage (Eckstein and Lacruz, 2018).

CRAC proteins have important roles in eccrine sweat glands, ORAI1 allows for stimulation of chloride channels necessary for fluid secretion and STIM1/2 enables sustainable levels of Ca^{2+} transport in ameloblasts to cause proper enamel mineralization. The enamel defects are present in deciduous and permanent teeth, the teeth can appear discoloured, have increased wear, hypoplasia (thinning of enamel) and chipping. ED like symptoms vary and are not always present in patients (Feske, Picard and Fischer, 2010; Concepcion *et al.*, 2016; Eckstein and Lacruz, 2018).

1.3.3.4 Neurons phenotype

Calcium and SOCE are important for neurosecretion, exocytosis, neuronal growth and differentiation, and the maintenance of neural circuits. In neurons, the main channel responsible for store-operated calcium entry are transient receptor potential (TRP) channels. In general, altered calcium signalling can lead to reactive oxygen species (ROS) production, abnormal protein synthesis, ER stress and mitochondria dysfunction. These have been linked to bipolar disorder, HIV-induced dementia,

Huntingtons and muscular dystrophy. As stated above neuronal phenotypes are rare in CRAC channel deficiencies. STIM2 is thought to compensate during STIM1 deficiency (Feske, 2011; Bollimuntha, Pani and Singh, 2017; Kozak and Putney, 2017).

1.3.3.5 Mice phenotype

As described in Table 1.3.1, mice phenotypes of Orai1 and STIM1 deficiency are similar to those shown in humans. Complete deficiency of these genes can lead to fatality 24 h postpartum. Cytokine production by CD4+ and CD8+ T cells are dramatically impaired, including that of IFNγ, TNF, IL-2, IL-4, IL-10 and IL-17 (Trebak and Kinet, 2019).

1.3.3.5.1 Orai1 deficiency

Orai1 deficient mice are small in size, with eyelid irritation and sporadic hair loss. T and B cells develop normally, but have impaired function due to reduced SOCE and cytokine production. B cells have a decreased Ca^{2+} influx and cell proliferation in response to B-cell receptor stimulation (Gwack *et al.*, 2008).

T cell-specific Orai1-knockout mice show no signs of experimental autoimmune encephalomyelitis (EAE) and have reduced Th1 cell-dependent and Th17 cell-dependent cytokine production, including IL-17A and IFNγ (Ma *et al.*, 2010). ORAI1 deficiency renders T cells resistant to death upon long-term TCR activation, due to the reduction in nuclear import of NFAT. This can be restored by expression of either ORAI1 or constitutively active NFAT. The mice have no developmental defects in T cells, but have increased memory and effector T cells. The mice have splenomegaly and lymphadenopathy phenotypes (Trebak and Kinet, 2019).

SOCE seems to be involved in neuronal functions, but not development. In Orai1 deficient mice, no abnormal structures in the brain were found (Kozak and Putney, 2017).

1.3.3.5.2 STIM1 deficiency

STIM1 deficient mice have 70 % lethality due to cardiopulmonary defects. The surviving animals have retarded growth, shortened life spans (4-6 weeks), reduced thymocytes numbers by 2-fold, but with normal ratios of CD4+ to CD8+ T cells. The

Ca^{2+} store-refilling rate in smooth muscle cells and activation of multiple signal transduction cascades associated with growth signalling (calcineurin, AKT, and ERK1/2) are reduced, which results in impaired neonatal muscle growth (Beyersdorf *et al.*, 2009; Li *et al.*, 2012).

Mice lacking STIM1/2 in T cells (T-dKO mice) developed sever autoimmune disease (Oh-hora et al., 2008). SOCE is essential for the development and function of Tregs, which express Forkhead box P3 (Foxp3) as a master transcription factor. Tregs in these mice had a decreased expression of inhibitory surface molecules such as CTLA-4 and TIGIT. B cells were present at normal levels, but had increased turnover (ki-67 expression). The B cells were constitutively active, with continuous plasma cell differentiation and a 10-fold increase of Igs in sera compared to WT mice (Kozak and Putney, 2017).

CD4+ T cell-specific STIM1 deficiency have reduced SOCE in response to anti-CD3 stimulation. The cells failed to sustain NFAT nuclear translocation and produce IL-2 on TCR activation (Trebak and Kinet, 2019).

STIM1 and Orai1-knockout mouse embryonic fibroblasts (MEFs) are more susceptible than wildtype cells to oxidative stress. STIM1 deficiency in particular was shown to be involved in regulation of mitochondrial shape, bioenergetics and in oxidative stress (Henke *et al.*, 2012; Kozak and Putney, 2017).

1.4 Aims

The overall aim of this thesis tis to investigate potential novel genes or mutations that could be causing the patient's PID phenotype. For each case study there are two main directions used to investigate this where possible which are broken down below.

First, by looking at the genetic and molecular data, to see if the mutations are present and the possible functional effects of these mutations using existing research, databases and computational models. This can help rule out mutations unlikely to be pathogenic and therefore allow for more in depth functional studies on likely candidates, as seen in the second section.

1. Confirm potential mutations and their segregation in patient with PID.
    - Research genes and mutations identified by WES or gene panels
    - Identify mutations that could be pathogenic by finding potential links between protein function and patient phenotype
    - Confirm mutations by Sanger sequencing
    - Identify segregation of mutations by sequencing parental DNA or through cloning

The second avenue is taking the potential candidate and looking in more detail at the cell types, pathways and functions associated, to see the pathogenic affect. This was done both in primary patient cells and in cell line models expressing the mutations. This was done to amass data on whether these mutations are affecting function and therefore causing the patient phenotype.

2. Use primary samples and *in vitro models* to determine if mutations identified are pathogenic and causing of the patient phenotype
    - Develop functional assays specific to the mutations confirmed in the patient
    - Perform functional experiments in patient and HC samples
    - Develop cell lines with the genes of interest knocked out
    - Express patient mutants in cell lines for functional analysis

Chapter 2 Materials and Methods

2.1 Materials

The oligonucleotides used for this project were purchased from Sigma and are shown in Table 2.1.1. The vectors and antibodies used in this project can be found in Table 2.1.2 and Table 2.1.3.

Table 2.1.1 Oligonucleotides

Code	Name	Sequence	Tm (˚C)	Ta (˚C)	Application
A	DHSR4_ex4_F	GGAACCCACTCTAACTCCTCA	62.1	65	PCR and sequencing of gDNA. Amplicon 299 bp (Chapter 3)
B	DHSR4_ex4_R	TCCATAGCAGCCTTCAGTCC	64.3		
C	EFCAB4B_ex6_F	ATGATTCCTGGCAGGTGAGA	64.7		PCR and sequencing of gDNA. Amplicon 380 bp (Chapter 3)
D	EFCAB4B_ex6_R	ATTCCAGTGCAGGGACCAG	65.2		
E	EFCAB4B_ex9_F	GGCCCTGATGTTGAGTAGGT	62.9		PCR and sequencing of gDNA. Amplicon 279 bp (Chapter 3)
F	EFCAB4B_ex9_R	GTGAATGGCAGGGAAAGTGG	66.6		
G	EFCAB4B_ex10_F	AAACAAGGTGAGGCCAGGG	66.3		PCR and sequencing of gDNA. Amplicon 384 bp (Chapter 3)
H	EFCAB4B_ex10_R	AGCCCAAATCCTCTTTTCACAG	65.3		
I	EFCAB4B-var1_F	TGTTTGATGCCCTGGATGCT	67.8	67	PCR and sequencing of cDNA. Amplicon 234 bp (Chapter 3)
J	EFCAB4B-var1_R	GGGCTCCAAGTCTGTCCATC	66		
K	EFCAB4B-var2/3_F	GTTTCAAGCCCGCAGTCAAG	67		PCR and sequencing of cDNA. Amplicon 232 bp (Chapter 3)
L	EFCAB4B-var2/3_R	GCTTTCCAACTGCTGCTGAG	65.2		
M	sR2A_D230A_F	GATGGACAGACTTGGAGCCC	66		PCR and sequencing of cDNA. Amplicon 305 bp (Chapter 3)
N	sR2A_D230A_R	CTTGACTGCGGGCTTGAAAC	67		
O	mtR2A_D230A_F	GCTGCTTATGCTGAAGAAATCC	63.9	58	Mutagenesis (Chapter 3)
P	mtR2A_D230A_R	AATTTTCCTTTTTAGGGCAC	58.6		
Q	mtR2A_Q131*_F	TGCAGGTGAATAGGTGGCCCA	71.8	67	Mutagenesis (Chapter 3)
R	mtR2A_Q131*_R	TCTTCCTGACTTGGGTTATTCTGG	66.1		
S	Mt_R144G_F	AGGTGTATCTGTCCGGAGGGGATGAGGATC	77.1	72	Mutagenesis (Chapter 4)
T	Mt_R144G_R	GATCCTCATCCCCTCCGGACAGATACACCT	77.1		
U	Mt_E278D_F	AGCAGGAGCTGGATCAGCTCACCCAGAAGC	80	72	Mutagenesis (Chapter 4)
V	Mt_E278D_R	GCTTCTGGGTGAGCTGATCCAGCTCCTGCT	80		
X	Mt_E300*_F	ATCATGACAAGCATTAGACCAAGGCTGAGA	73	72	Mutagenesis (Chapter 4)
Y	Mt_E300*_R	TCTCAGCCTTGGTCTAATGCTTGTCATGAT	73		
Z	STIM1_ex4 F	TGTGGTAAATATTAAGGTCAGCATGA	64.1	63.8	PCR and sequencing of gDNA. Amplicon 289 bp (Chapter 5)
A1	STIM1_ex4 R	TCACTTAACTGGCCAGAGCA	63.4		
B1	CANT1_ex2 F	CGGGGTCTAAGGACAGGTG	64.5	65	PCR and sequencing of gDNA. Amplicon 379 bp (Chapter 5)
C1	CANT1_ex2 R	GAGGCAAATGCAGGAGGAAG	66		

Code	Name	Sequence	Tm (˚C)	Ta (˚C)	Application
D1	**TMEM173_ex5F**	TCCCAGCAAGTTCTCTAGGT	60.5	63	PCR and sequencing of gDNA. Amplicon 347 bp (Chapter 5)
E1	**TMEM173_ex5R**	TTCAGCCACTGAAGAGAGCC	64.7		
F1	**h36B4 F&R**	F- CAACGTGGGCTCCAAGCAGAT, R - GGTCCTCCTTGGTGAACA	N/A	N/A	SYBR green qPCR (Chapter 5)
G1	**hSTIM1 F&R**	F- TCCCTTGTCCATGCAGTCCC, R- GGAATGGGTCAAATCCCTCT	N/A	N/A	SYBR green qPCR (Chapter 5)
H1	**hIFNa F&R**	F- TAGACAAATTCTGCACCGAAC, R- AGATGGAGTCCGCATTACTC	N/A	N/A	SYBR green qPCR (Chapter 5)
I1	**hIFNB F&R**	F - TGCTCTGGCACAACAGGTAG, R - AGCCTCCCATTCAATTGCCA	N/A	N/A	SYBR green qPCR (Chapter 5)

F- forward, R- reverse, Tm – Melting temperature, Ta - annealing temperature used in experiments, red bases are ones that are mutated from WT. All primers were checked by Sigma design tool (https://www.sigmaaldrich.com/pc/ui/tube-home/standard) and SNP check (https://genetools.org/SNPCheck/snpcheck.htm).

Table 2.1.2 Plasmids

Name	Insert	Features of interest	Application	Supplier	Vector Map
pC2.1	-	TA cloning site, easy insertion	TA cloning	TA cloning kit (Invitrogen, K202040)	N/A
pIRES2_EGFP	CRACR2A WT , CRACR2A R144G, CRACR2A E278D, CRACR2A E300*	EGFP in same open reading frame as insert (bicistronic), to track expression of recombinant proteins	Electroporation of CRACR2A into Jurkat cell lines	Gifted from Gina Doodey	Figure 2.2.3
pMAX GFP	N/A	Small size, easy to transfect	Electroporation high efficiency plasmids	Nucleofection kit (Lonza, VACA-1003)	N/A
FG11F	empty contains GMP, CRACR2A WT, CRACR2A R144G, CRACR2A E278D, CRACR2A E300*, CRACR2A DM, CRACR2A Q131*, CRACR2A D230A	Stable and transient expression, self-inactivating 3' long terminal repeat (LTR)	Electroporation and stable cell lines, expression of CRACR2A mutants	Gifted by Gwack Lab	Figure 2.2.8
Mo70	CRACR2A WT, CRACR2A E278D, CRACR2A DM	High transfection efficiency in HEK293 cells. Does not express in Jurak cells.-	High efficiency HEK293 test	Gifted by Gwack Lab	N/A
CRISPR-shR2A	sh CRACR2A	LentiCRISPR lentiviral CRISPR/Cas9 and single guide RNA system by GeCKO	CRACR2A KO	Gifted by Gwack Lab	Figure 2.2.11
pMD2.G	VSV-G expressing envelope plasmid	Packaging vector	Viral transduction	Gifted by Gwack Lab	Figure 2.2.10
psPAX2	gag, pol, rev, tat	Packaging vector	Viral transduction	Gifted by Gwack Lab	Figure 2.2.10

Table 2.1.3 Antibodies

All antibodies are selective to human.

Name	Target	Host	Supplier	Application	Conditions	Other
hCD3	-	E.coli	Invitrogen, #16-0037-81	Cytokine study, calcium flux (Flex Station), culturing	-	(All chapters)
hCD28	-	E.coli	Invitrogen, 14-0289-80	Cytokine study, calcium flux (Flex Station), culturing	-	(All chapters)
Anti-GAPDH	GAPDH	Rb	Genetex GTX10018	WB of PBMCs and cell lines	1:10000 in 5 % milk	(All chapters)
Anti-CD4-FITC	CD4	ms	Invitrogen, #11-0042-82	FACS (T cells)	5 µL/ sample	FITC (Chapter 3)
Anti-CD8-PE	CD8	ms	Invitrogen, MHCD0804	FACS (T cells)	5 µL/ sample	PE (Chapter 3)
Anti-CD56-eFluor 450	CD56	ms	Invitrogen, #48-0566-42	FACS (NKT cells-CD4-CD56+)	5 µL/ sample	eFluor 450 (Chapter 3)
Recombinant Human IL-2	-	E.coli	PeproTech, #200-02	T cell expansion	-	Purity ≥ 98 %, specific activity of ≥ 1 x 10^7 units/mg (Chapter 3)
Anti-hIL4-APC	IL-4 monoclonal	ms	eBioscience, Clone 8D4-8	Flow cytometry	5 µL/ sample	(Chapter 3)
Anti-hIFNγ-PE	IFNγ monoclonal	ms	Invitrogen, Clone 45B3	Flow cytometry	5 µL/ sample	(Chapter 3)
Anti-CRACR2A	CRACR2A	Rb	ProteinTech, Cat LOT	WB of PBMCs and cell lines	1:800 in 5 % milk	(Chapters 3&4)
Anti-CRACR2A (Gwack)	CRACR2A	Rb	Made in house by Gwack lab	WB of PBMCs and cell lines	IF - 1:2000, WB - 1:5000 5 % milk	(Chapters 3 & 4)

Name	Target	Host	Supplier	Application	Conditions	Other
Anti-β actin	β actin	ms	Santa Cruze, SC47778, Lot J1518	WB of PBMCs and cell lines	1:2000 in 5 % BSA	(Chapters 3 & 4)
Phalloidin	F actin	-	Life Tech, Lot 1246066	IF	1:40 / sample	Alexa Fluor 488 (Chapter 4)
Anti-Vav1	Vav1			IP		(Chapter 4)
anti- hIL-2-PE	IL-2 monoclonal	Rat	eBioscience, MQ117H17	Flow cytometry	5 µL / sample	(Chapter 4)
Donkey anti-Mouse IgG Secondary Antibody	ms IgG	Donkey	Invitrogen, A10037	IF secondary	1:500 / sample	Alexa Fluor 568 (Chapter 4)
Donkey anti-Rabbit IgG Secondary	Rb IgG	Donkey	Invitrogen,	IF secondary	1:500 / sample	Alexa Fluor 568 (Chapter 4)
Anti-FLAG	FLAG	ms	Millipore, F7425	WB of cell lines	IF - 1:500, WB - 1:5000 in 5 % BSA	(Chapter 4)
Anti-Orai1	Orai1	Rb	Sigma, O8264	WB of cell lines	1 in 100	(Chapter 4)
IFN α 2A	-	Xeno-Free	Merk millipore GF416	Monocyte stimulation	EC50 0.1-0.4 ng/mL	Human Recombinant, purity > 95 % (Chapter 5)
Anti-STIM1	STIM1	Rb	Sigma, HA161	WB of PBMCs and cell lines	1:250 in 5 % milk	Raised against full length protein (Chapter 5)
Anti-STIM1 D88E10	STIM1	Rb	CST #5668	WB of PBMCs	1:5000 in 5 % milk	Raised against C-terminal (Chapter 5)
Anti-GOK/STIM1	STIM1	ms	BD #610954	WB of PBMCs	1:500 in 5 % milk	Raised against N-terminal (Chapter 5)
Anti-STIM2	STIM2	Rb	CST #4917	WB of PBMCs	1:1000 in 5 % milk	(Chapter 5)

2.1.1 Cell lines

2.1.1.1 Reagents

Dulbecco's Modified Eagle Medium (DMEM) - Gibco

Fetal Calf Serum (FCS) – Sigma (St. Louis, USA), F7524

Freeze media for all cell lines and PBMCs – FCS and 10 % DMSO (Sigma)

G418 disulfate salt solution or Geneticin – Sigma, G8168

Hanks' Balanced Salt solution (HBSS) – Sigma, 55021C

L-Glutamine (200 mM) – Thermo, 25030081

MEM non- essential amino acid (NEAA) (100X) – Sigma, M7145

Penicillin-Streptomycin (Pen/Strep) - Gibco™ (USA), 15070

Roswell Park Memorial Institute (RPMI) 1640 Medium - Gibco

Sodium Pyruvate (100 mM) –Thermo, 11360070

Trypsin (10 x) - Life Technologies, Carlsbad, (USA), 15400

X-Gal – Invitrogen, B1690

LB broth – Sigma

2.1.1.2 Cell lines

2.1.1.2.1 DH5α cells

Subcloning efficiency DH5α competent cells (Invitrogen, Cat:18265017) are chemically derived competent cells with a transformation efficiency of >1x10^6 cfu/μg plasmid DNA. They contains l*ac*ZΔM15 for blue/white screening with X-gal. The cells are cultured at 37 ˚C either on LB agar plates or on an orbital shaker in LB Broth. Both the solid and liquid media were made as per manufacturer's instructions. These cells were used for subcloning, TA cloning and transformation.

2.1.1.3 HEK293

HEK293 (ATCC- CRL-1573) were cultured at 37 ˚C with 5 % CO_2, in complete DMEM medium with 1 % Pen-Strep and 10 % FCS. Cell lysates from this line were used as a control in western blots.

2.1.1.4 HEK293T

HEK293T(ATCC- CRL-11268) are human embryonic kidney cells that were derived from HEK293 cells to contain a SV40 large T antigen and have high transfectability. Cells were cultured in the same way as the parent HEK293 line.

These cells were mainly used for retroviral transduction. They were transfected with a virus and their supernatant was added to 'difficult to transfect cells', in this case Jurkat cells. They were also used as a control in a range of experiments as they are a well-documented cell line that is easy to grow and to transfect. Gifted by the Gwack group (UCLA).

2.1.1.5 HEK293FT

These cells are a fast growing variant of HEK293T cells, specifically optimised for lentiviral transduction. They require a more complex media than other HEK293 cells: DMEM media with 10 % FBS, 0.1 mM NEAA, 6 mM L-glutamine, 1 mM MEM sodium pyruvate and 500 µg Geneticin. Gifted by Julie Burns (University of Leeds).

2.1.1.6 Jurkat cell line

Jurkat cells (ATCC: TIB-152) were derived from peripheral blood of a 14-year-old boy with acute T cell leukaemia. They are able to produce IL-2 after stimulation with phorbol esters and lectins or antibodies against the T3 antigen and provide a readout on the survival and signalling mechanisms of cells. The cells were cultured at 37 ˚C with 5 % CO_2, in complete RPMI 1640 medium with 1 % Pen-Strep and 10 % FCS. Gifted by Dr Gina Doody (University of Leeds).

This cell line was used as a T cell model, serving as a control due to its uniform response, in calcium flux experiments, western blots and qPCR. Assay for primary T cells were developed using Jurkat cells. Jurkat cells were also used to make stable cell lines to examine the effects of mutations in T cell related disease.

2.1.2 Patients and Healthy controls

The work in this project is covered by ethical approval granted for a study entitled ‘Molecular genetic investigations of autosomal recessive conditions’, which was approved by the South Yorkshire Research Ethics Committee on 18th February 2011 (REC ref. number 11/H1310/1). NHS Permission for Research at Leeds Teaching Hospitals NHS Trust was granted on 29th April 2011 (LTHT R&D number CG11/9764).

All patients who participated in this study consented to whole exome sequencing (WES) and further research testing with ethical approval. Patient samples were made available by Dr Sinisa Savic and the Department of Clinical Immunology and Allergy at St James’s University Hospital (Leeds, UK).

2.2 Methods

During this project multiple methods and reagents were used in similar experiments, as they were performed in different laboratories. This is because the same reagents were not available in all locations. During the secondment in LA, the Gwack Labs standard protocols and reagents were used rather than ones previously optimised in University of Leeds. The protocol used is specified in the legends to all figures and tables.

2.2.1 Molecular Biology

2.2.1.1 Whole exome sequencing (WES)

Whole blood DNA was prepared for exome sequencing using SureSelectXT with All Exon v5 capture library and sequenced on Illumina HiSeq 3000 for 2 × 150-bp paired-end sequencing. Reads were aligned with BWA-MEM to GRCh37/hg19 and variant calling was performed according to GATK-best practices.

2.2.1.2 Selection of potentially pathogenic mutations from WES data

Once the mutations are identified the frequency in the population is located. In general, if it is rare in a population (<0.0001) it is likely to cause disease. Next the genes associated with these rare mutations are compared to the patient phenotype to see if the gene function is similar or has previously been linked to other disease states. Before any further experiments are run it is essential to confirm the mutations of interest by Sanger sequencing. WES is a very powerful technique but artefacts can appear. In Sanger sequencing a much smaller and specific section of the genomic DNA are analysed and which provides more confidence in the results.

Filtering and prediction of functional consequences was performed using Variant Effect Predictor (VEP) (http://www.ensembl.org/info/docs/tools/vep/index.html), Exome Variant Server (http://evs.gs.washington.edu/EVS/), the Single Nucleotide Polymorphism database (https://www.ncbi.nlm.nih.gov/projects/SNP/) and ClinVar https://www.ncbi.nlm.nih.gov/ clinvar/), the Exome Aggregation Consortium and the Genome Aggregation Database

(http://gnomAD.broadinstitute.org). Filtering of common variations and annotation was performed using vcfhacks (https://github.com/gantzgraf/vcfhacks) and in-house scripts. Candidate variants were required to pass the following filtering conditions: frequency (count/coverage) between 20-100%, according to VEP-annotation at least one canonical transcript is affected with one of the following consequence: variants of the coding sequence, frameshift, missense, protein altering, splice acceptor, splice donor, or splice region; an in frame insertion or deletion; a start lost, stop gained, or stop retained, or according to VEP an ExAC frequency unknown, <=0.01, or with clinical significance 'path'.

2.2.1.3 Polymerase chain reaction (PCR)

PCR was used for the amplification of specific regions of single stranded DNA from 5′ to 3′ using synthetic primers seen Table 2.1.1. All standard PCRs were performed with 1x PCR Master Mix HotShot Diamond (Clent Life Science HS002) , 20 µM Primer (forward and reverse) and genomic DNA at 20-21 ng in a final volume of 10 µL, following the reaction scheme in Figure 2.2.1.

1. 95ºC 5 minutes
2. 94ºC 30 seconds
3. 65ºC 30 seconds (variable, Tm dependent
4. 72ºC 45 seconds (variable timing, 30 sec/500bp)
5. Go to step 2 for 44 times
6. 72ºC 5 minutes
7. Keep at 15ºC

Figure 2.2.1 Standard PCR reaction scheme

As a negative control for all PCR experiments, a reaction mix was set up without DNA, to check for contamination of the primer stocks and reaction mixes.

2.2.1.4 Sanger sequencing

PCRs were generated using the standard protocol and primers. Free nucleotides were removed by ExoSAP-IT (Affymetric) before a sequencing reaction was performed using the BigDye Terminator v3 Cycle Sequencing Kit (Thermo, 4337455) as per manufacturer’s instructions. The reaction used a single primer, normally one of two primers originally used to generate the PCR product, or one located within the PCR product. The products generated were ethanol precipitated and the DNA

resuspended in Hi-Di Formamide (Thermo, 4311320) for analysis on the ABI3130xl Genetic Analyzer, which used capillary electrophoresis to separate DNA by size.

Sanger sequencing was performed in house, except for sequencing performed at UCLA which was outsourced to Laragen (CA, USA). When confirming mutations, two PCRs were generated for each patient and sequenced with the forward and reverse primers.

2.2.1.5 Gel electrophoresis

PCR products were run on 1.5 % agarose gels to check the quality of the PCR product and to ensure that they were the expected molecular weight. Initially ethidium bromide (EtBr) was used to visualise the DNA, but later in the project a safer gel dye was used in the form of Gel Red.

2.2.1.5.1 Reagents

1.5 % agarose gel – 1.5 % SeaKem LE Agarose (Lonza), 1 x TAE in water with EtBr (Thermofisher) or GelRed (Biotium)
6X DNA Loading Dye – Thermofisher, R0611
100 bp Marker – NEB, N3231L
50x TAE, pH 8.5 – 0.04 M Tris base, 0.002 M Disodium EDTA, 0.02 M acetic acid (all reagents from Fisher Scientific)

2.2.1.6 cDNA generation

RNA was isolated from PBMCs using the QIAamp RNA Blood Mini Kit (QIAGEN, 52304), following manufacturer's instructions. Reverse transcription was performed on 1 µg total RNA using GoScript Reverse Transcription System using both random primers and Primer dT, or using High capacity RNA kit, which uses Random primers only. The switch to the high capacity kit was due to the use of an established protocol for cDNA isolation from monocytes in a 96 well plate for TaqMan qPCR (Srikanth *et al.*, 2019).

2.2.1.7 TA cloning

To determine the orientation of mutations, on a single allele, cDNA was isolated and amplified as detailed in Section 2.2.1.6. TA Cloning Kit with CR2.1 Vector (Invitrogen, K202040, Table 2.1.2) and subcloning efficiency DH5α competent cells were used to perform TA cloning of this PCR product. Following transformation, positive cells were selected with Ampicillin (100 µg/mL final concentration) and identified using X-Gal (20 µg/mL). Colony PCR, which includes an additional 10 minute step at 95 $^{\circ}$C before the standard PCR reaction scheme (Figure 2.2.1), was used to identify colonies with the vector and insert, on an agarose gel. GenElute™ Plasmid Miniprep Kit (Sigma) was then used to purify DNA from these positive colonies. Sanger sequencing was finally used to confirm the mutations.

2.2.1.8 CRACR2A cloning and site directed mutagenesis

A variety of cloning protocols were performed on the cDNA sequence of CRACR2A. Figure 2.2.2 shows the sequences of the short and long isoforms of the protein with codons of interest highlighted. The two isoforms of CRACR2A share the first 1119 nucleotides.

S-CRACR2A_WT, 1188 bp

ATGGCTGCCCCTGACGGGAGGGTAGTCTCCAGACCCCAGAGACTTGGTCAGGGGTCTGGCCAGGGGCCAAAGGGGAGTGG
AGCCTGCCTGCATCCCCTGGACAGCCTGGAGCAGAAGGAGACTCAGGAGCAAACGTCGGGCCAGCTAGTCATGCTGAGGAA
GGCACAGGAGTTCTTTCAGACCTGTGATGCTGAAGGCAAGGGCTTCATCGCCAGGAAGGATATGCAGAGGCTGCATAAGGAG
CTACCGCTCAGCCTGGAGGAACTGGAGGATGTGTTTGATGCCCTGGATGCTGATGGCAATGGCTATCTGACCCCACAGGAGT
TCACTACTGGATTTAGTCATTTCTTCTTCAGCCAGAATAACCCAAGTCAGGAAGATGTAGGTGAACAGGTGGCCCAGCGCCAT
GAAGAGAAGGTGTATCTGTCCAGAGGGGATGAGGATCTGGGCGACATGGGCAAAGATGAGGAAGCCCAGTTCCGGATGCTG
ATGGACAGACTTGGAGCCCAAAAGGTGTTGGAAGATGAAAGTGATGTCAAGCAGCTCTGGTTGCAGCTGAAGAAGGAGGAAC
CTCATTTACTGTCCAACTTTGAAGACTTCCTGACCAGAATCATCTCCCAGCTCCAAGAAGCCCATGAGGAGAAGAATGAACTGG
AGTGTGCCCTAAAAAGGAAAATTGCTGCTTATGATGAAGAAATCCAGCATCTCTATGAGGAGATGGAACAACAAATCAAAAGTG
AGAAGGAGCAGTTTCTCCTGAAGGACACAGAGAGGTTTCAAGCCCGCAGTCAAGAGCTGGAGCAGAAACTGTTATGTAAGGA
GCAGGAGCTGGAGCAGCTCACCCAGAAGCAGAAAAGGCTGGAAGGTCAGTGCACAGCCCTGCATCATGACAAGCATGAGAC
CAAGGCTGAGAATACCAAGCTGAAACTCACTAACCAGGAGCTGGCCCGGGAGCTGGAGCGGACTTCCTGGGAGCTCCAGGA
TGCTCAGCAGCAGTTGGAAAGCCTCCAGCAAGAGGCCTGCAAACTCCACCAAGAGAAGGAGATGGAAGTGTACCGTGTGACG
GAGAGTCTACAGCGTGAGAAGGCCGGGCTCCTCAAGCAGCTGGATTTCCTAAGGTGCGTCGGTGGGCACTGGCCTGTGCTG
AGAGCACCTCCCAGAAGCCTGGGGTCGGAAGGACCAGTCTAA

L-CRACR2A_WT, 2199 bp

ATGGCTGCCCCTGACGGGAGGGTAGTCTCCAGACCCCAGAGACTTGGTCAGGGGTCTGGCCAGGGGCCAAAGGGGAGTGG
AGCCTGCCTGCATCCCCTGGACAGCCTGGAGCAGAAGGAGACTCAGGAGCAAACGTCGGGCCAGCTAGTCATGCTGAGGAA
GGCACAGGAGTTCTTTCAGACCTGTGATGCTGAAGGCAAGGGCTTCATCGCCAGGAAGGATATGCAGAGGCTGCATAAGGAG
CTACCGCTCAGCCTGGAGGAACTGGAGGATGTGTTTGATGCCCTGGATGCTGATGGCAATGGCTATCTGACCCCACAGGAGT
TCACTACTGGATTTAGTCACTTCTTCTTCAGCCAGAATAACCCAAGTCAGGAAGATGCAGGTGAACAGGTGGCCCAGCGCCAT
GAAGAGAAGGTGTATCTGTCCAGAGGGGATGAGGATCTGGGCGACATGGGCGAAGATGAGGAAGCCCAGTTCCGGATGCTG
ATGGACAGACTTGGAGCCCAAAAGGTGTTGGAAGATGAAAGTGATGTCAAGCAGCTCTGGTTGCAGCTGAAGAAGGAGGAAC
CTCATTTACTGTCCAACTTTGAAGACTTCCTGACCAGAATCATCTCCCAGCTCCAAGAAGCCCATGAGGAGAAGAATGAACTGG
AGTGTGCCCTAAAAAGGAAAATTGCTGCTTATGATGAAGAAATCCAGCATCTCTATGAGGAGATGGAACAACAAATCAAAAGTG
AGAAGGAGCAGTTTCTCCTGAAGGACACAGAGAGGTTTCAAGCCCGCAGTCAAGAGCTGGAGCAGAAACTGTTATGTAAGGA
GCAGGAGCTGGAGCAGCTCACCCAGAAGCAGAAAAGGCTGGAAGGTCAGTGCACAGCCCTGCATCATGACAAGCATGAGAC
CAAGGCTGAGAATACCAAGCTGAAACTCACTAACCAGGAGCTGGCCCGGGAGCTGGAGCGGACTTCCTGGGAGCTCCAGGA
TGCTCAGCAGCAGTTGGAAAGCCTCCAGCAAGAGGCCTGCAAACTCCACCAAGAGAAGGAGATGGAAGTGTACCGTGTGACG
GAGAGTCTACAGCGTGAGAAGGCCGGGCTCCTCAAGCAGCTGGATTTCCTAAGGGAAAGGAACAAGCACCTTCGGGATGAAC
GGGACATATGTTTTCAGAAAAATAAGGCAGCCAAGGCAAACACAGCTGCTTCCAGGGCAAGTTGGAAAAAGAGATCTGGCTCT
GTGATAGGCAAATATGTGGACAGCAGAGGGATTCTTAGGAGCCAGTCAGAGGAGGAGGAGGAGGTGTTTGGCATCCCAAGGA
GAAGCTCCCTGGGCCTGAGTGGATATCCCCTAACAGAAGAGGAGCCAGGAACCGGGGAGCCAGGGCCTGGGGGTCCGTACC
CCCGGCCGCTCCGCAGAATCATCTCCGTTGAAGAAGACCCCCTGCCCCAGCTCCTGGATGGTGGCTTTGAGCAACCCCTGAG
CAAATGCTCAGAAGAGGAAGAGGTCTCTGACCAGGGGGTACAGGGACAAATCCCGGAGGCCCCACCCTTGAAACTCACCCCC
ACATCCCCCCGAGGGCAGCCTGTTGGAAAAGAAGCCCTGTGTAAGGAGGAAAGCTCTCCCTCTGCCCCTGACCGGCTCTTCA
AGATTGTGTTCGTGGGCAATTCCGCGGTGGGGAAGACATCCTTCCTGAGGAGATTCTGTGAGGACCGGTTCTCCCCAGGCAT
GGCGGCCACTGTGGGCATTGATTACCGTGTGAAGACGTTGAATGTGGACAACTCTCAGGTGGCCCTGCAGCTGTGGGACACG
GCTGGGCAGGAGAGGTACCGGTGCATCACCCAGCAGTTCTTCAGAAAGGCAGATGGTGTCATCGTCATGTACGATCTCACAG
ACAAGCAGTCGTTCCTGTCGGTCCGGCGGTGGCTGAGCAGCGTGGAGGAAGCTGTGGGAGACCGGGTGCCTGTTCTTCTGC
TGGGTAATAAGCTTGACAACGAGAAGGAGCGGGAAGTCCCCCGGGGCCTCGGAGAGCAGCTTGCCACGGAGAACAATCTGA
TCTTCTATGAATGCAGCGCCTACTCTGGTCACAACACCAAAGAGTCCCTGCTCCATCTGGCCAGGTTCCTCAAGGAGCAAGAA
GACACAGTGAGAGAGGACACCATTCAGGTCGGCCACCCTGCTAAGAAGAAATCCTGCTGTGGCTGATAG

Figure 2.2.2 CRACR2A isoform sequences for cloning

The two isoforms of CRACR2A share the first 1119 nucleotides. The donor plasmids gifted by Lynn McKeown (University of Leeds) contain the cDNA sequences for the long and short isoforms of CRACR2A. The sequence of both isoforms was confirmed by Sanger sequencing in-house. ATG – Start codon, TAA and TAG - Stop codons, NNN – codon containing main patient mutations described in Chapter 3, the base in red is the point mutation location.

2.2.1.8.1 PCR cloning

The basic protocol for plasmid cloning by PCR was forced cloning performed by restriction with XhoI+EcoR1. The recipient plasmid used in this project was pIRES2-EGFP (Figure 2.2.3) a bicistronic vector designed for the simultaneous expression of a green fluorescent protein and a protein of interest (CRACR2A) from the same transcript in transfected mammalian cells. This vector contains an internal ribosome entry site (IRES2). When a gene of interest is inserted into the multiple cloning site (MCS)

located upstream of the IRES, both the gene of interest and the EGFP coding region are transcribed into, and then translated from a single bicistronic mRNA.

The sequence of the primers used for cloning are in Table 2.2.1 The PCR cloning adds additional bases so predicted sizes of the short and long amplicons increased to 1218 bp and 2239 bp respectively.

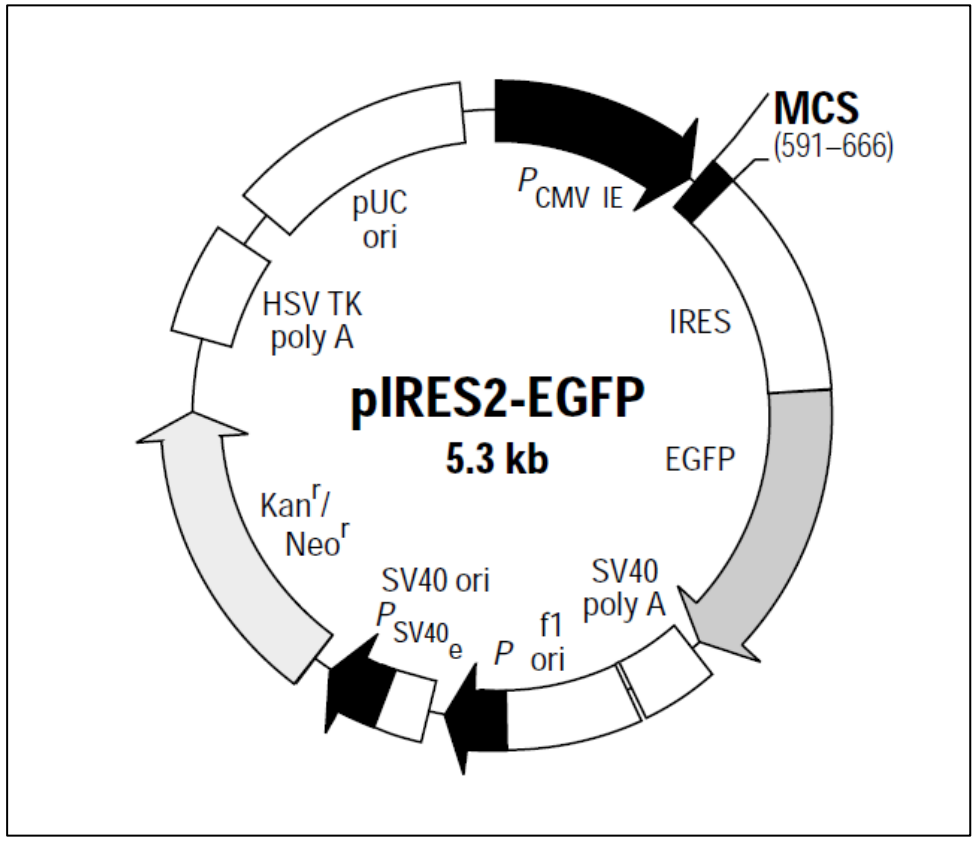

Figure 2.2.3 pIRES2-EGFP plasmid map

Map taken from BDbioscience, PT3267-5, #6029-1.

pIRES2-EGFP contains the internal ribosome entry site (IRES) of the encephalomyocarditis virus (ECMV) between the multiple cloning site (MCS) and the enhanced green fluorescent protein (EGFP) coding region.

Table 2.2.1 Cloning primer sequences

Primer Name	RE	Sequence
Cloning_F1	XhoI	tagatcCTCGAGGCCACCATGGCTGCCCCTGACGGGAGGGT A
Cloning_R_short	EcoR1	tagatcGAATTCTTAGACTGGTCCTTCCGA
Cloning_R_long	EcoR1	tagatcGAATTCCTATCAGCCACAGCAGGATTT

Primers were made by Sigma. The Tm of all primers was above 70 ˚C at 90.6, 71.2 and 74.7 ˚C respectively. All PCR reactions used a temperature of 70 ˚C for annealing. Lower case is the leader sequence, CTCGAG - XhoI at 5' end, GAATTC - EcoRI at 3' end after stop codon, GCCACC - KOZAK , ATG – Start codon, TTA and CTA - Stop codon in reverse orientation.

The cloning PCR primers contain three key elements. A leader sequence of 3-6 bp at the 5' end of the primer to assist with restriction enzyme digestion. A restriction site, that is present in the MCS of the recipient plasmid and not present in the sequence of interest, in this case XhoI and EcoR1 were used: A hybridization sequence, which binds to the donor plasmid and allows amplification to occur, usually this is 18-21 bp, and should be checked against the rest of the donor plasmid for sequence identity. The forward primer contains an additional element of the KOZAK sequence, which provides an effective translational start.

Phusion Hot start flex 2x master mix (Biolabs, M05365) was used as per manufacturer's instructions for the 2 step PCR, due to the high Tm of the primers. The reactions were performed with and without DMSO, and both produced bands at the predicted sizes for the long and short isoform when run on a 1.5 % agarose gel.

The restriction digests of the PCR cloning product and the recipient plasmid were performed as per the Promega protocol for a single step double digest in buffer D with XhoI (Promega, R6161) and EcoR1 (Promega, R6011) for 4 hours at 37 ˚C. The cutting efficiency in this buffer was 75 % for EcoR1 and 100 % for XhoI.

The RE digestion products were run on a 1 % agarose gel and the cDNA inserts and digested vector, the DNA bands of interest, were cut out and gel extraction performed with QIAquick Gel Extraction Kit (Qiagen, 28115) as per manufacturer's instructions.

The purified vector and PCR products were then ligated and inserted into the cells by transformation, done using the TA cloning kit reagents and protocol. Recombinant vectors were checked as for TA cloning. The ligation, transformation, colony PCR, miniprep and Sanger sequencing method details are the same as those used in the TA cloning (Section 2.2.1.7).

2.2.1.8.2 Mutagenesis

Mutagenesis was performed using primers described in Table 2.1.1 on the CRACR2A containing vectors, pIRES2_EGFP and FG11F (Table 2.1.2), to induce the point mutations seen in the CRACR2A patients described in Chapter 3. The mutagenesis was performed with the Q5 kit as per manufacturer's instructions. The full cDNA sequence in the resulting plasmids was checked for accuracy prior to their use in experiments.

2.2.1.9 qPCR

Both SYBR green and TaqMan probe protocols use the same reaction scheme as can be seen in Figure 2.2.4. Both were run on Applied Biosystem machines, QuantStudio™ 5 System 96-well and QuantStudio™ 7 Flex Real-Time PCR System, 384-well respectively.

Figure 2.2.4 qPCR reaction scheme
Taken from 96 well ABI instrument, but same conditions were used for all protocols.

2.2.1.9.1 TaqMan protocol

Applied Biosystems TaqMan MGB (minor groove binder) probes are dual-labelled probes with a 5' fluorescent reporter dye and a 3' nonfluorescent quencher (NFQ). The NFQ offers the advantage of lower background signal, which results in better precision in quantitation.

This method, used for the STING patient monocytes TaqMan experiment, was taken from Srikanth *et al.*, 2019. In summary, monocyte stimulation was performed on negatively selected monocytes (Section 2.2.3.4 for details). Half the cell were stimulated for 20 hours with 100 units/mL IFN alpha 2A (Table 2.1.3). cDNA was generated (Section 2.2.1.6) and real-time qPCR was performed using TaqMan Universal PCR Master Mix (ThermoFisher, #4304437) using FAM-MGB probes for detection of the following: *MX1* (Hs00895608_m1), *IFI44* (Hs00951349), *IFI44* (Hs00915292_m1), *IFI27* (Hs01086370_m1), *ISG15* (Hs00192713_m1), *CXCL10* (Hs01124251_g1), *RSAD2* (Hs01057264_m1), *IFIT1* (Hs01675197_m1), *IFI6* (Hs00242571_m1), *OAS1* (Hs00973635_m1), *IL6* (Hs00985639_m1), and *HPRT1* (Hs99999909_m1).

The relative abundance of each transcript was normalized to the expression level of *HPRT1* to obtain ΔC_T and further normalized to the values obtained for healthy controls to obtain $\Delta\Delta C_T$.

2.2.2 Clinical Immunology

All tests described in this section were performed by the Leeds Clinical Department at St James's University Hospital (SJUH) and results supplied by Clive Carter. All tests were performed following standard protocols and standard operating procedures (SOP) of the clinical lab. More details can be found at https://www.leedsth.nhs.uk/a-z-of-services/pathology/.Tests run by this service include:

- Cell counts
- T cell expansions
- Immunoglobulin (Ig) counts
- HLA-DR levels
- T cell spectratyping

2.2.3 Blood work

Patient and healthy control blood was used to obtain DNA, cDNA, protein and whole cells from PBMCs for further testing. The average amounts of each obtained from 1 mL of healthy control peripheral blood are detailed in Table 2.2.2

Table 2.2.2 Blood samples

Sample	Average yield from 1 mL human whole blood	Method details
DNA	40 µg	QIAamp DNA Blood Maxi Kit (QIAGEN, 51192) used on ETDA whole blood samples as per manufactures instructions
RNA	3 µg	See Section 2.2.1.6
Protein	30 µg	See Sections 2.2.6.1.2 and 2.2.6.2.2
PBMC cells	5,000,000 cells	See Section 2.2.3.1
Serum	500 µL	See Section 2.2.3.2

Predicted amount of cell/blood component gained from 1 mL of healthy control whole blood, using the experimental methods listed.

2.2.3.1 Isolation and storage of PBMC

Peripheral blood was collected by venepuncture in heparin or EDTA tubes and PBMCs were isolated by density gradient (lymphoprep, STEMCELL technologies) as per manufacturer's instructions. Cells were counted and then either used in functional studies or stored. For functional studies the cells were cultured in RPMI or underwent additional isolation processes as detailed in Section 2.2.3.3. The cells were otherwise stored as follows:

- As protein - 5-10x10^6 cells lysed in NP40 lysis buffer (VWR, J60766) with cOmplete Protease Inhibitor Cocktail (Roche)
- As cells - 5-10x10^6 cells frozen at -80 ˚C in heat inactivated foetal calf serum with 10 % DMSO

For calcium flux experiments using the Flex station, SepMate (STEMCELL technologies) tubes were used to speed up isolation of lymphocytes to allow time for further processing.

2.2.3.2 Plasma preparation from whole blood

Blood collected in serum tubes was spun for 10 minutes at 1500 x g at 4 ˚C. Plasma was then removed and stored in 500 µL aliquots at -80 ˚C.

2.2.3.3 Isolation of specific cell types

PBMCs isolated by gradient separation contain many different subtypes of immune cells (StemCell, 2019).

2.2.3.3.1 T cells

T cells were isolated from patients and healthy controls for functional studies. Different methods for cell selection were used based on the exact experimental requirement as well as for optimisation.

The cell isolation and separation techniques that provide the highest purity and specificity are antibody binding passed techniques, such as fluorescence-activated cell sorting (FACS) and bead-based cell sorting (Andrä *et al.*, 2020). In this project, FACS was initially used to isolate CD4+ and CD8+ T cells when calcium flux was being measured by flow cytometry. When using this method many of the cells became activated due to the physical manipulation of the cells. This meant that the baseline calcium flux of the cells was very high and the cells did not respond well to further activation. Letting the cells rest after FACS did not always improve the baseline readings and so FACS was determined to be unsuitable for function based experiments.

Bead based separation also uses antibodies so has high specificity but has the added benefit of negative selection. In this method, all cells are bound to the column except for the cells of interest, which have therefore been manipulated as little as possible.

2.2.3.3.2 Negative selection columns

T Pan isolation kit (MACS Miltenyi Biotec, 130-096-535) with LS columns was used on PBMCs as per manufacturer's instructions (Section 2.2.3.1).

2.2.3.3.3 Culturing

Culturing PBMCs for extended period of time in the presence of specific stimuli can result in the proliferation and expansion of a specific cell type (Bulent Arman Aksoy, Pinar Aksoy, Megan Wyatt, Chrystal Paulos, 2018). This technique is useful if only a

limited number of cells are available, but it can result in a biased population, which does not fully represent the distribution of cells in the original blood sample. This is a result of different subpopulations responding and proliferating better to specific stimuli (Geginat, Lanzavecchia and Sallusto, 2003; Pennock *et al.*, 2013).

Cells were cultured under high (anti-CD3 10 µg/mL and anti-CD28 10 µg/mL) or low (anti-CD3 2 µg/mL and anti-CD28 5 µg/mL) stimulation conditions with 20 U/mL IL-2 (see Table 2.1.3 for details). CRACR2A patient cells described in Chapter 3 could only be cultured using low stimulation due to the phenotype of the cells.

Procedure:

Day 1 - PBMCs($14x10^6$ cells) that had been stored at -80 ˚C in freeze media for at least 72 hrs were thawed and then cultured in RPMI+10 % FBS for 24 hrs.
Day 2 and 3 - Cells transferred to anti-CD3 coated plates with soluble anti-CD28
Day 4-8 – Cells added to anti-CD3 coated plates, with -anti-CD28 and IL-2 in the media
Day 9 + – Cells were frozen or used in function studies

2.2.3.4 Monocytes

Monocytes were used in the TaqMan experiment (Section 2.2.1.9.1), following published protocols (Srikanth *et al.*, 2019). PBMC were isolated by gradient separation (Section 2.2.3.1). Monocytes were purified from PBMCs using the Monocytes separation kit II (Miltenyi Biotec, 130-091-153,), which uses negative selection. This isolation leaves 3 types of sample available for testing: normal PBMCs, monocytes and the PBMCs without monocytes or non-monocytes (NM), the cells that bound to the negative selection column and was eluted as per the manufacturer's instructions.

2.2.3.5 *In vitro* B cell differentiation

PBMCs were isolated from peripheral blood via density gradient centrifugation (Lymphoprep, Allere Ltd.) and incubated with antibody cocktail from memory B-cell isolation kit (Miltenyi, negative selection) and then anti-biotin microbeads.

B-cell purity was assessed by flow cytometry and the cells cultured in IMDM + 10% HIFBS, Lipid Mixture 1 and MEM amino acids solution. The B-cells were stimulated with CD40L and F(ab')2 anti-IgG/M and cultured sequentially with cytokines essential for differentiation, as shown in Figure 2.2.5 and Figure 2.2.6.

Enzyme-linked immunosorbent assay (ELISA) for immunoglobulin IgM and IgG detection were performed with Human IgM ELISA Quantitation Set (E80-100) or Human IgM ELISA Quantitation Set (E80-104) (Bethyl Laboratories Inc, USA) according to the manufacturer's instructions.

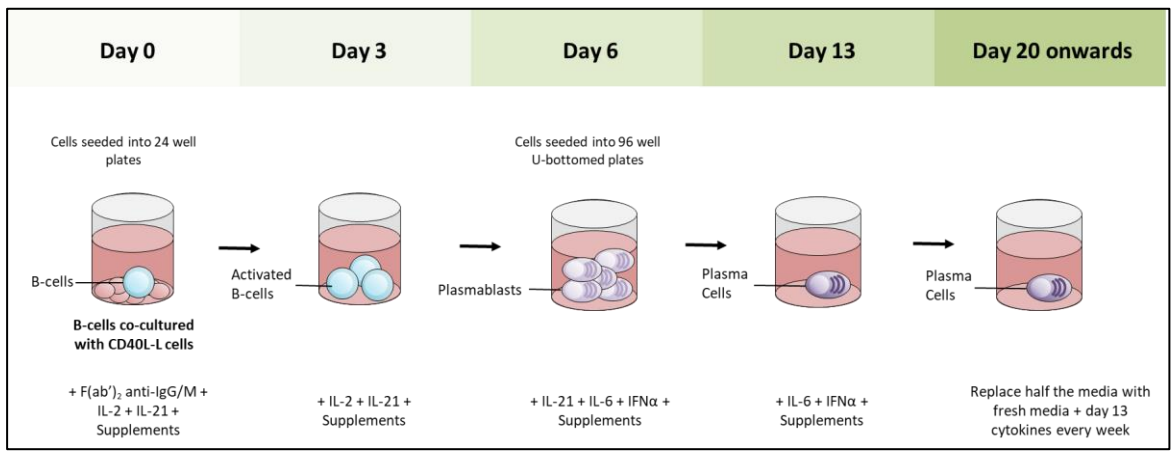

Figure 2.2.5 Method overview of B cell differentiation

Day 0-3: hIL-2 (20 U/mL), hIL-21 (50 ng/mL) and F(ab')$_2$ goat anti-human IgM and IgG (10 µg/mL). **Day 3-6:** hIL-2 (20 U/mL) and hIL-21 (50 ng/mL).
Day 6-9: hIL-6 (10 ng/mL), hIL-21 (50 ng/mL), IFN-α (100 U/mL. **Day 13 +:** hIL6 + IFN-α.

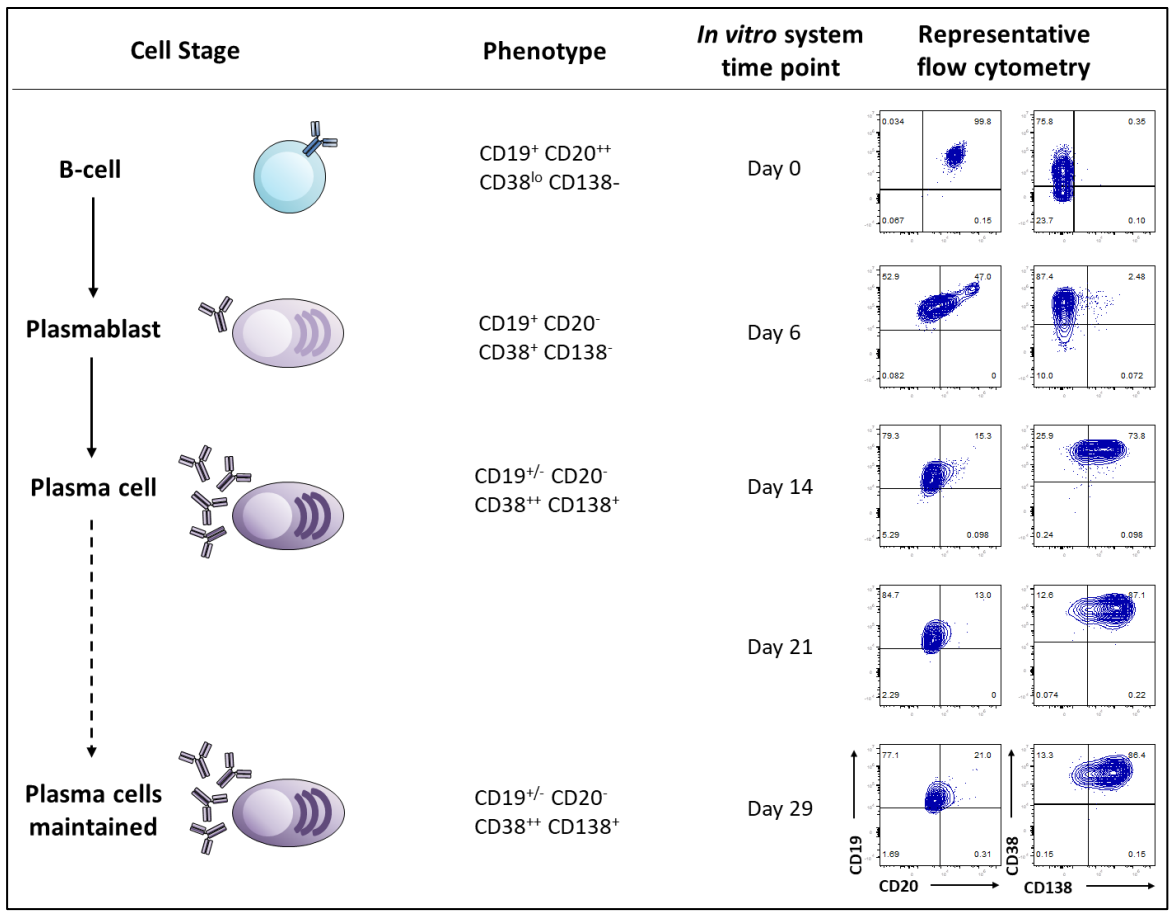

Figure 2.2.6 B cell differentiation stages

Cells were stained with hCD19, hCD20, hCD27, hCD38 and h7-AAD for analysis with flow cytometry

2.2.4 Transient transfection methods

2.2.4.1 Nucleofection

Nucleofector Kit V (Lonza, VACA-1003) was used with the corresponding Nucleofector 2b Device, a single cuvette electroporation device, due to its high transfection efficiency reported with Jurkat cells. The kit was used as per manufacturer's instructions using both the Jurkat and HEK293 recommended protocols.

2.2.4.1.1 siRNA

Transient gene silencing using RNA interference was done using siRNA. The dsRNA has a two nucleotide overhang at the 3' end that activates RNAi, leading to the degradation of mRNAs in a sequence-specific manner dependent upon complementary binding of the target mRNA (Keefe, 2013).

The siRNA was selected on the recommendation of Dr Lynn McKeown (University of Leeds), due to optimisation experiments performed in their lab using HUVEC and HEK293 cells. The siRNA (ThermoFisher, siRNA ID n341045) binds to the promotor region of the human *EFCAB4B* gene which encodes for CRCAR2A. The sequence details are not available in the genomic map provided by the company, which only shows where it binds in relation to the coding region of the protein as shown in Figure 2.2.7.

For optimisation of siRNA experiments, transfection efficiency was tested using pmaxGFP Vector. The GFP expression was visualised using Zeiss, AxioImager.Z1 fluorescence microscope, with a x20 objective lens and exposure 120 m/s.

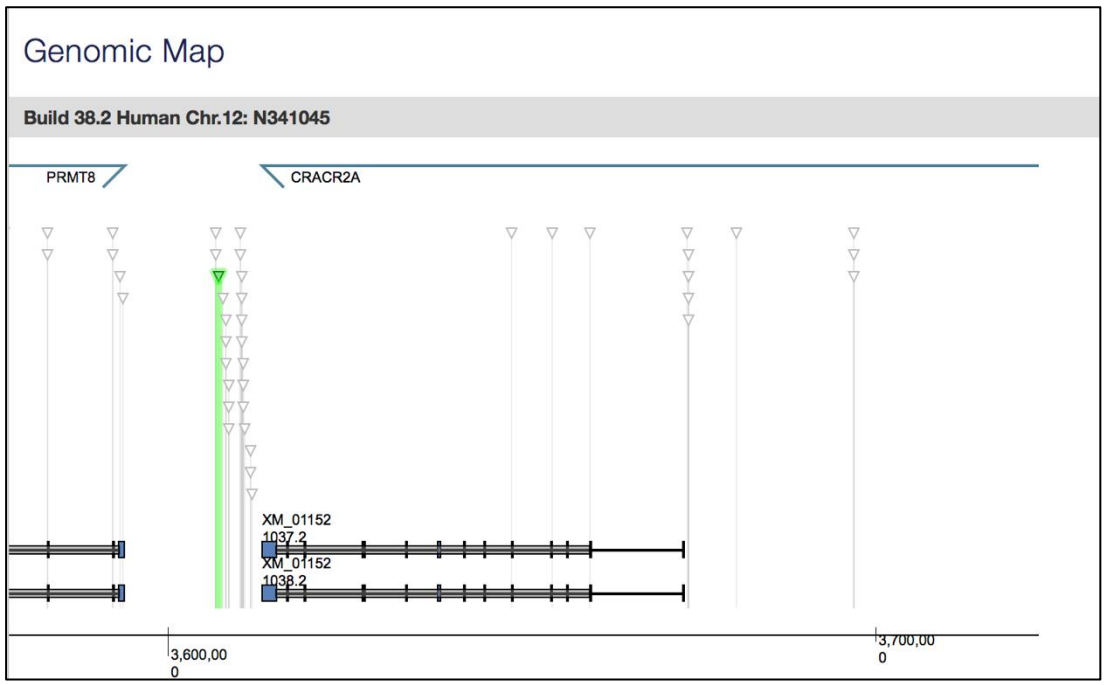

Figure 2.2.7 siRNA CRACR2A binding location

This image was provided by ThermoFisher.. The XM_01152 region is the CRACR2A transcript on the human chromosome. The siRNA ID n341045, highlighted in green, binds to the promotor of this gene.

As a negative control, to check transfection efficiency and the effect of siRNA delivery to the cell, Silencer Negative Control #1 siRNA (Invitrogen, AM4611) was used.

2.2.4.2 Electroporation

Electroporation was performed using 15 µg plasmid of interest and 5 µg FG11F with EGFP (Figure 2.2.8) in each cuvette. The collected cells were resuspend in 10 mL of OPTI-MEM (Gibco, 31985062), counted, spun and resuspended with $3x10^6$ Jurkat cells in 400 µL OPTI-MEM per cuvette. The cells and DNA were added to the cuvette, and incubated at RT for 15 minutes, before being mixed and pulsed (210 V for 40 ms), then rested for 15 minute at RT in the cuvette. The cells were then resuspended in 2.5 mL of prewarmed media and cultured for 24 hrs. The GFP expression was checked and the cells pelleted for WB.

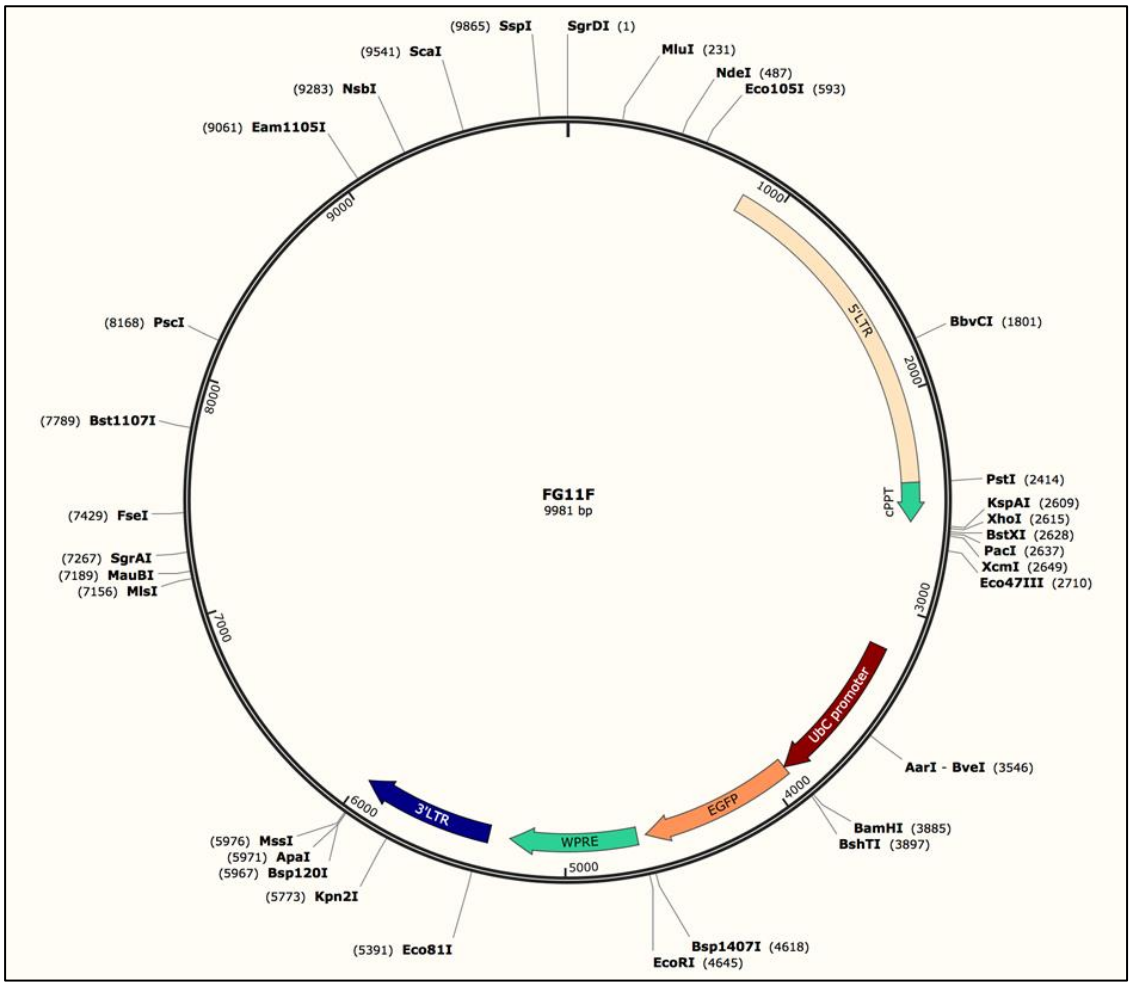

Figure 2.2.8 FG11F plasmid map

The map and plasmid were gifted by Gwack lab (UCLA). Cloning involved removal of the EGFP and insertion of the N-FLAG CRACR2A mutants.

2.2.5 Generation of stable cell lines

Viral transduction was used to create knockout (KO) Jurkat cell lines, and to stably express mutant CRACR2A. A 2nd generation lentiviral system was used, gifted by the Gwack lab (Srikanth *et al.*, 2016; Woo *et al.*, 2018).

All viral work at Leeds University was done in compliance with generic Class 2 risk assessment Ref-GM559/99.3. The lentivirus was made by calcium phosphate or TransIT transfection, of the plasmids into donor cells (HEK293T or 293FT cells respectively). The lentivirus containing FG11F or pLKO.1 plasmids was secreted into the supernatant which was added to target cells (Jurkat cells) and removed completely after 24 hrs. The donor cells were disposed by autoclaving, after a 30 minute

incubation in 10 % Virusolse+ solution, and the target cell kept from regular culture labs until sufficient passages had taken place to ensure all virus is removed.

The mutant expression vectors FG11F (Figure 2.2.8) had a N-terminal FLAG tag at the 5’ end of CRACR2A full length sequence. The gene was integrated and expression activated by the UbC promoter. However, expression can also occur without integration of the sequence in a transient manner as seen when the FG11F plasmid was used in electroporation experiments. No selection was used for the expression of CRACR2A mutants. Inappropriate genetic transfer was guarded against as the packaging and envelope proteins needed for viral production were encoded on separate plasmids (Figure 2.2.9, Figure 2.2.10) and only the region between the viral LTRs of the transfer vector was packaged within the viral capsid.

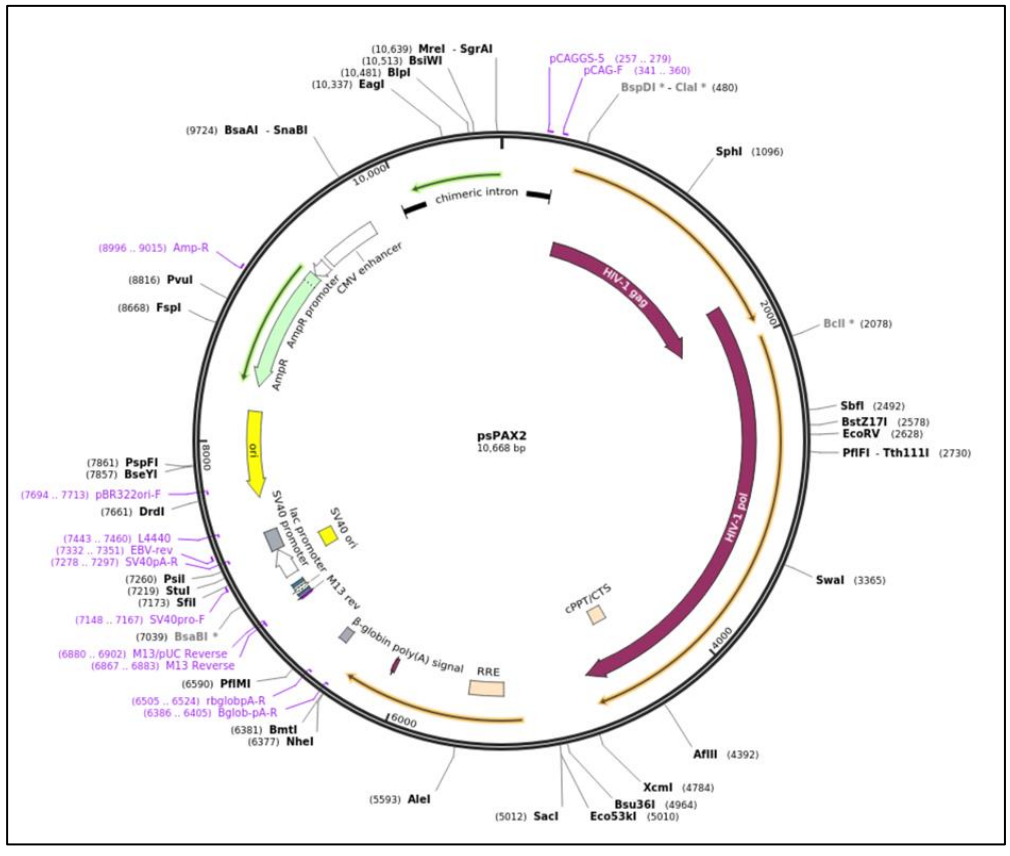

Figure 2.2.9 psPAX2 map

psPAX2 and pMD2.G were gifted by the Gwack lab and amplified by QIAGEN plasmid mini and maxi prep kits as per manufactures instruction. Risk of reactivation was significantly reduced by the viral components being encoded on separate plasmids (pMD2.G – VSV-G expressing envelope plasmid, psPAX2 – gag, pol, rev, tat), with wild-type virulence and replication genes deleted and the lentiviral transfer vector (FG11F) containing a modified, self-inactivating 3' long terminal repeat (LTR) which renders the resulting lentiviral particles replication incompetent.

psPAX2 was a gift from Didier Trono (Addgene plasmid # 12260 ; http://n2t.net/addgene:12260 ; RRID:Addgene_12260)

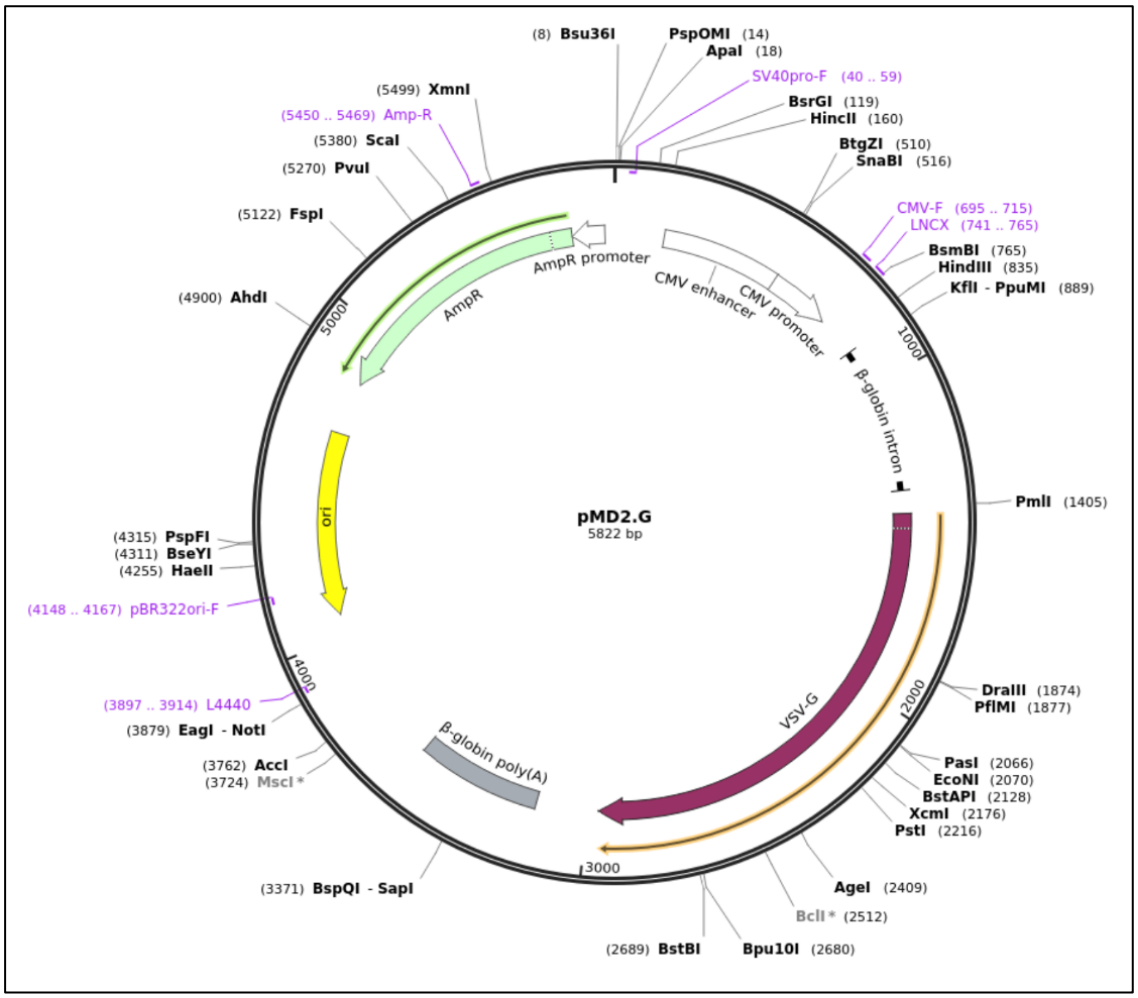

Figure 2.2.10 pMD2.G map

See Figure 2.2.9 for description. pMD2.G was a gift from Didier Trono (Addgene plasmid # 12259 ; http://n2t.net/addgene:12259 ; RRID:Addgene_12259)

2.2.5.1 Generating KO CRACR2A cells

Clustered Regularly Interspaced Short Palindromic Repeats (CRISPR) was used to generate KO CRACR2A cells. The guide RNA was designed and optimised by the Gwack lab, using the LentiCRISPR lentiviral CRISPR/Cas9 and single guide RNA system by GeCKO (Figure 2.2.11). The one vector system, contains two expression cassettes, hSpCas9 and the chimeric guide RNA. The guide RNA binds to a specific region thought to be important for expression of a specific gene. The cas9 enzyme is then able to cleave the target DNA strand and DNA repair mechanisms in the cell repair the cleavage by removing the remaining complementary sequence in this region, therefore, allowing genome editing.

The method used for making KO cell lines was the same as for expressing CRACR2A mutants (Sections 2.2.5.2, 2.2.5.3 and 2.2.5.4), but with different vectors and the additional step of 4 µg/mL puromycin (Sigma, P8833) selection 48 hrs after first addition of virus.

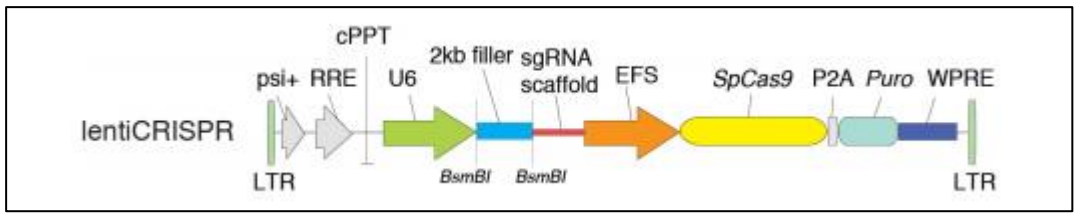

Figure 2.2.11 LentiCRISPR (pXPR_001)

The plasmid contains two expression cassettes, hSpCas9 and the chimeric guide RNA. The vector can be digested using BsmBI, and a pair of annealed oligos can be cloned into the single guide RNA scaffold. The oligos are designed based on the target site sequence (20 bp) and needs to be flanked on the 3' end by a 3 bp NGG PAM sequence.
The CRACR2A shRNA sequence used was TTTCAGCTTGGTATTCTCAGC, referenced as hCRACR2A_shRNA2 (mature antisense) in Woo *et al.*, 2018, which binds in exon 7, in the region coding for amino acids 303-307. This region is found in the coiled coil domain that exists in both the long and short isoform of CRACR2A.

2.2.5.2 Calcium Phosphate transfection

Calcium phosphate transfections were performed on HEK293T cells that were at 60-70 % density in a 10 cm cell culturing plates. 8 µg plasmid of interest (FG11F, pLKO.1 scramble or pLKO.1 shRNA) and 4 µg each of packaging vectors (pMD2G, psPAX2) were mixed with 420 µL dH_2O and 260 mM $CaCl_2$ (Sigma, C1016). This mixture was added dropwise to 500 µL 2x HBS while vortexing. The solution was then incubated at RT for 1-1.5 hours and then added dropwise to the HEK293T donor cells. The cells were incubated overnight and transfection efficiency checked, using the FGF11 empty plasmid that expresses GFP, using a florescence microscope. The media was replaced with fresh media (less media was added, to make a more concentrated viral supernatant) and incubated for a further 24 hours, before collecting the supernatant containing the virus, by centrifugation at 4000 rpm for 20 minutes at RT. The supernatant could be collected for an additional day. The supernatant could be stored at 4 ˚C for 24 hours, or at -20 ˚C for long term storage. However, the virus is most active when fresh.

2.2.5.3 Trans IT

70 % confluent 293FT cells in T25 flasks were used for TransIT transfections. 1 µg plasmid of interest (FG11F, pLKO.1 scramble or pLKO.1 shRNA) and 1 µg each of packaging vectors (pMD2G, psPAX2) were added to 750 µL OPTI-MEM (Gibco,

31985062), with 8 µL TransIT x2 (Mirus, MIR 6003), which was then incubated at RT for 15-30 minutes, before being added dropwise to cells. The cells were incubated at 37 ˚C, 5 % CO_2 for 12-15 hours, before replacing the media.

All the supernatant from the cells was collected for the next 2 days, by centrifugation at 4000 rpm for 20 minutes at RT, and the media replaced.

2.2.5.4 Transduction

The fresh supernatant of donor cells was generated using either calcium phosphate or TransIT protocols. 2 mL of supernatant containing 2nd generation lentivirus was added to Jurkat cells. 1 hour before the addition of the supernatant, Jurkat cells were plated at 0.5-1 million cells per well (in a 6 well plate) in 2 mL of Jurkat media, with additional 5 µg/mL of polybrene (Sigma, TR-1003) and 10 mM HEPES (Sigma, H0887). With the addition of the supernatant, each well contained 4 mL of media. This was then spun at 2000 rpm at 25-32 ˚C for 1 hour and incubated overnight at 37 ˚C (spinfection). The transduction was repeated the next day if transfection efficiency was low, without the addition of polybrene.

2.2.5.5 MTT assay,

MTT, a yellow tetrazole, is reduced to purple formazan in living cells. This change can be read by a plate reader and so the proliferation or death of cells can be monitored. In this project MTT assays were performed during the process of generating a puromycin kill curve, in order to determine how much puromycin would kill all cells.

All MTT assays were performed with 3 controls, media only wells for background readings, cells only for positive/no death and 50 % DMSO for complete death. All conditions were performed in triplicate.

Day 1 - Cells are added to a 96 well plate. 50,000 Jurkat cells per well or 20,000 HEK293 cells

Day 2 – Drug of interest added at range of concentrations.

Day 3 or 4 – 20 µL MTT reagent (Sigma, M5655) was added to cells at 5 mg/mL for 4 hrs at 37 ˚C, while protected from light. The plates were spun at 1000 x g for 5 minutes and the liquid removed. The plates were either stored at -20 ˚C or 50 µL DMSO

was added immediately, the plate shook for 15 minutes to resuspend the formazan precipitate and the fluorescence read at 560 nm.

2.2.6 Protein studies

2.2.6.1 Western Blot (Method A)

Method used at the University of Leeds.

2.2.6.1.1 Reagents

Blocking buffer - 5 % NFDM (dried milk powder[Marvel]) in PBS

Lysis buffer - NP40 lysis buffer (VWR, 18C1456418) and c0mplete tablets (Roche, 17113900).

PBS - PBS (Invitrogen, 003002) tablets in denoised water

Ponceau stain – 0.1 % (w/v) Ponceau S (Sigma-Aldrich, P3504) in 5 % acetic acid (Sigma-Aldrich, 338826)

Transfer buffer – 1 x Bolt transfer buffer (20x Invitrogen, BT0006), 10 % Methanol (ThermoFisher) and deionised water, protected from light and kept at 4 ˚C until used.

Wash buffer – 0.1 % Tween 20 (Sigma-Aldrich, P9416) in PBS

2.2.6.1.2 Cell lysis

The cell pellets were washed in PBS twice to remove media and then were resuspended in the lysis buffer for 10 minutes on ice and then centrifuged at 4 ˚C at 12000 x g for 10 minutes. They were then stored at -80 ˚C or the protein concentration measured immediately using a Pierce BCA Protein Assay Kit (Thermo Scientific, 23225) following manufacturer's instructions.

2.2.6.1.3 Protocol

Samples were prepared so that 20 µg of protein was added to each well, using the BCA results. The cell lysate and 4x Bolt® LDS Sample Buffer (Invitrogen, B0007) were mixed and the volume made up with fresh lysis buffer. The samples were heated for 10 minutes at 65 ˚C and spun down before use.

Bolt™ 4 to 12 %, Bis-Tris, 1.0 mM, Mini Protein Gel, 10 or 15 well gels (Invitrogen, NW04120BOX or NW04125BOX) were loaded, with protein ladder (Color-coded Prestained Protein Marker, Broad Range 11-250 kDa [Cell Signalling Technologies, 14208]) and run for 30 minutes at 60 V and 1.5 hours 120 V in Bolt® MOPS SDS Running Buffer (20x, Invitrogen, B0001). The electrophoresed proteins were transferred onto Polyvinylidene Difluoride membrane (PVDF) membranes (0.4 5 µm, Roche, 03010040001) using the wet sandwich method and cold transfer buffer at 20 V for 2 hours.

After transfer the total protein transfer was checked using ponceau stain. The membrane was then washed twice for 10 minutes each on a shaking platform before blocking for 1 hour while shaking. The primary antibody was added as required and incubated overnight at 4 ˚C. The washing procedure above was then performed 3 times and the secondary antibody with a HRP tag (see Table 2.1.3) was added for 2 hours at RT.

For visualisation the SuperSignal West Pico PLUS Chemiluminescent Substrate (Thermo Scientific, 34579) kit was used as per manufacturer's instructions, together with the ChemiDoc MP Imaging System (Bio-rad).

2.2.6.2 Western Blot (Method B)

Western blot method used during UCLA secondment.

2.2.6.2.1 Reagents

40 % Acrylamide (Sigma, A7168)

10 % ammonium persulfate - APS (Sigma, A36376) in water

RIPA buffer - RIPA buffer (R0278) with 1 in 2000 Leupeptin (L2884), 1 in 2000 Aprotinin (A1153), and 1 in 100 Phenylmethanesulfonyl fluoride (PMSF, P7626) all from Sigma

2x SDS Loading Dye with Beta-Mercaptoethanol – 4x Tris-Cl/ SDS (pH 6.8), 200 mL/L Glycerol, 40 g/L SDS, 20 mL/L of Beta-Mercaptoethanol, 10 mg/L Bromophenol Blue

10x SDS PAGE Running Buffer - 30.3 g/L Tris Base (Calbiochem, 643310), 144 g/L Glycine (Calbiochem, 4840), 10 g/L SDS (Promega, H5114)

10x Transfer buffer – 30.4 g/L Tris Base (Calbiochem, 643310), 144.2 g/L Glycine (Calbiochem, 4840)

Tetramethylethylenediamine (TEMED, Sigma, T9281)

Tris-buffered saline-Tween (TBST) buffer – 20x TBS (VWR, J640), 20mL/L Tween 20 (Sigma, P1379)

4x Tris SDS - 182 g/L Tris Base (Calbiochem, 643310), 4 g/L SDS (Promega, H5114), pH adjusted with HCl to pH 8.8 or 6.8

Unmasking Buffer – 2 % w/v SDS, 62.5mM Tris-HCl, 0 mM BME (final concentration of 6 µL/mL)

The recipe for 10 % SDS PAGE gels is shown below. Reagents are listed in the order of addition. TEMED was added last.

Reagent	Resolving gel (mL)	Stacking gel (mL)
Water	9.78	2.55
40 % Acrylamide	5	0.4
4x Tris SDS	5 (pH 8.8)	1 (pH 6.8)
10 % APS	0.2	0.05
TEMED	0.02	0.005

2.2.6.2.2 Cell lysis

Lysate was made from 4-5 million Jurkat cells either in RIPA buffer or by sonication. The cell pellet was washed once in PBS before lysis. For RIPA buffer, the cells were kept on ice for 30 minutes and vortexed every 10 minutes, then spun at 4 ˚C at 14000 x g for 10 minutes, then mixed at 1:1 ratio with 2x loading dye and heated for 10 minutes at 65 ˚C, before being spun down and loaded into the SDS gel. For sonication, loading dye was added directly to the washed cell pellet. The cells underwent ultrasonication for 2 minutes, with 10 second pulse and 10 second rests 6 times, before being heated in the same way as the RIPA buffer lysate.

2.2.6.2.3 Protocol

10 % SDS PAGE gel , with 15 wells was run. 20 µL of each lysate was added per lane, and the molecular weight marker used was Precision Plus Protein Dual colour standard (Biorad, 1610374). Gels were run at 40 V for 30 minutes and then at 100 V for 2 hours. Protein transfer onto PVDF 0.2 µm membrane (Thermo Scientific, 88520) was conducted at 300 mA for 1 hour in cold transfer buffer. All membranes were checked with Ponceau S staining after transfer.

The membrane was washed 3 times for 10 minutes each in TBST, blocked in 5 % milk at RT for 1 hour with the liquid changed once during that time. Then the membrane was incubated overnight at 4 ˚C with the primary Abs. If the Ab was diluted in 5 % BSA instead of milk, additional wash steps were performed before incubation, with water, then TBST.

For visualisation, the membrane was rinsed in running water before being washed 3 times for 10 minutes in TBST. It was then incubated for 1-3 hours at RT with the secondary Ab at 1:5000. Washing was repeated and the membrane was finally covered in 1 ml of Immobilon Forte Western HRP substrate (Millipore, WBLUF0500) and imaged at a range of exposure times.

If the WB needed to undergo unmasking, this was done by rinsing the membrane in water before adding 10 mL of the unmasking buffer for 10 minutes, while shaking at 2 minute intervals, before again rinsing in water. The membrane was then washed 5 times with water for 1 minute each, then in TBST for 20 minutes, before re-blocking for 1-3 hours before adding the new primary Ab.

2.2.6.3 Protein localisation

IF was performed using an established protocol used by the Gwack lab, to investigate CRACR2A mutant localisation in stable cell lines. IF was performed in Nunc Glass Bottom Dishes (Thermo Scientific, 150680). Poly-L-lysine solution (Sigma, 8920) was coated on the dishes for 15 minutes at RT, before being washed with water 3 times and left to dry at 37 ˚C for 45 minutes. The cells were resuspended in Ringers solution (2 mM Ca^{2+}, 116 mM NaCl, 9 mM KCl, 5.0 mM HEPES, pH 7.2) and incubated for 20 minutes before being washed with Ringers solution. The cells were then fixed with 4 % PFA (Polysciences, 04018) at RT for 20 minutes and washed with PBS. To permeabilise the cells PBS with 0.5 % NP40 was used to the cells for 30 minutes at RT. Blocking was performed with PBS with 0.5 % NP40 and 1 % FBS at RT for 30 minutes. Before incubation with the primary Ab in blocking solution for 1 hour at RT or overnight at 4 ˚C, the cells were rinsed in blocking buffer, before adding the secondary Ab for 30 minutes at RT. Phalloidin (Table 2.1.3) was used to stain the F-actin, this was done with a 1:40 dilution in PBS for 30 minutes at RT, followed by 2 PBS washes. The cells were stored at 4 ˚C in PBS.

2.2.7 T cell functional studies

2.2.7.1 Calcium flux

2.2.7.1.1 Flow cytometry

To measure the calcium flux using flow cytometry a calcium sensor dye Indo-1 AM is used, it binds to calcium in the cell. As Indo-1 enters the cell the acetoxymethyl ester (AM) group is cleaved off by endogenous enzymes, leaving the calcium sensor trapped within the cell. When Indo-1 is excited by ultraviolet (UV) light, it emits light at different wavelengths depending on if calcium is unbound or bound (485 nm or 405 nm). Using a ratio of the fluorescence obtained at the 2 wavelengths, the calcium

flux can be monitored. Thapsigargin (TG), ionomycin (I) and T cell receptor stimulation were used to induce calcium influx. TG induces sustained calcium influx, ionomycin causes the maximal response and TCR stimulation induces normal physiological influx. BTP2 is a specific CRAC channel inhibitor, which was used as a negative control.

Peripheral blood mononuclear cells (PBMCs) isolated by Lymphoprep and incubated for 24 hrs prior to processing with or without 100 nM BTP2 were used. In later experiments, the cells were sorted using Fluorescence-activated cell sorting (FACS) before the 24 hr incubation to isolate the T cells. Cells resuspended in supplemented HBSS (1 mM $CaCl_2$, 1 mM $MgCl_2$ and 1 % FBS) and Indo-1 added at 6 µg/ml and incubated at 37 °C protected from light for 40 minutes. After being washed twice, antibodies for gating on T cells were added (CD3 or CD4 and CD8). The cells were then resuspended in supplemented HBSS and run on the LSRII 4 flow cytometer. At 50 seconds the first treatment was added of anti-CD3 and CD28 anti-Biotin MACSiBead Particles (1:1 ratio), Thapsigargin (1 µM) or Ionomycin (0.5 µM). If the beads were the first treatment, then a second treatment of Thapsigargin (1 µM) was added at 7 minutes. Data was analysed using FlowJo version 10.

2.2.7.1.2 Flex Station

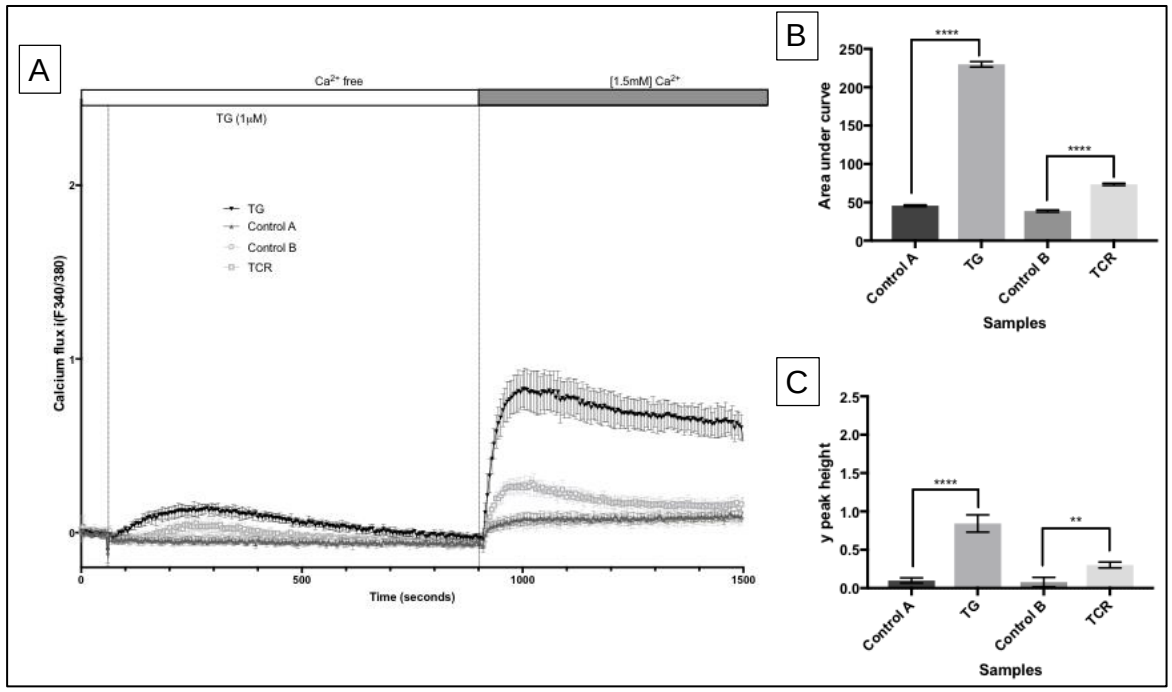

Figure 2.2.12 Calcium flux response to TG and TCR stimulation of Jurkat cells
Performed using protocol in Section 2.2.7.1.2 for the Flex station, all conditions were performed in duplicate with n=4. To compare the results, Prism was used with Ordinary One way ANOVA for multiple comparisons.

T cells were incubated for 1 hour at 37 ˚C in 0 % CO_2 with 2 µM fura-2 AM in standard bath solution (SBS) with 0.01 % pluronic acid (Invitrogen). Cells were seeded at $5x10^5$ cells/well. T cells were stimulated for 90 seconds by either Thapsigargin (TG) at 1 µM or the TCR was activated by soluble CD3 at 1 µg/mL (Clone OKT3). For TCR stimulation the plate was coated with anti-CD28 (1µg/mL, Clone CD28.2). Fura-2 was excited at 340 nm and 380 nm and emission was collected at 510 nm. Measurements were taken on a 96-well fluorescence plate reader (FlexStation III, Molecular Devices). Optimisation was performed using Jurkat cells, testing different stimulations and cell numbers. The optimal conditions mentioned above were used in Figure 2.2.12.

2.2.7.1.3 Single cell imaging

This was performed as detailed in Srikanth *et al.*, 2016.

2.2.8 Calcium flux

Gaining meaningful and reproducible calcium flux data from primary patient samples was one of the main challenges in this project. In the literature, many different ways have been reported to measure calcium flux and three methods were tested: flow cytometry, plate reader and single cell imaging.

2.2.8.1 Comparison of different techniques

Flow cytometry was used to identify issues in calcium flux by our group previously, by monitoring NK cells and T cell response to different stimuli (Parry *et al.*, 2016). Flow cytometry is a quantitative technique. The main benefit to flow cytometry is its ability to monitor a large population of cells such as PBMC and with a range of cell surface markers, and so multiple cell population responses can be investigated in a single experiment. However, during the optimisation flow experiments performed as part of this study it became apparent that using PBMCs and gating on the CD4+CD8+ cell was providing low cell numbers, which led to fluctuating calcium responses. As a result, cell sorting was used to isolate T cells. Due to this change in protocol the benefits of flow cytometry were minimised, though the calcium response of different T cells could still be analysed, such as

CD4+ T helper cells, CD8+ cytotoxic T cells and with the addition of CD45RA marker, naive T cells. As described in this chapter, flow cytometry was eventually abandoned due to the high cell number needed for patient and HC cells.

The main technique for monitoring the calcium flux used other than flow cytometry is confocal microscopy (Srikanth, Jung, Kim, *et al.*, 2010; Srikanth, Jung, Ribalet, *et al.*, 2010; Christo *et al.*, 2015; Srikanth *et al.*, 2016). Real time analysis of an individual cell can be monitored using a calcium sensor dye, Fura-2 AM which works in a similar way to Indo-1, where a ratio of bound and unbound calcium is measured to give the calcium flux in response to stimuli. The individual calcium flux results can be pooled to give the cell population response. Confocal microscopy is sensitive enough to measure the oscillations of calcium concentrations, as images are taken at regular intervals and the ratio calculated for each image (Christo *et al.*, 2015). This technique was not used initially as only small, uncharacterised population of cells can be observed in a single experiment. However, when flow cytometry was identified as unsuitable the reduced cell numbers and large data output made this technique very beneficial to this project.

Plate readers can be used to measure calcium flux, using calcium sensor dyes as well (Wilson *et al.*, 2015; Miteva *et al.*, 2019). Similarly to confocal microscopy, a small population of cells is used and characterising of the cell subpopulations is not possible in real time. This technique requires less specialised equipment and training, but is not as sensitive and doesn't allow for individual cell readings. As a result, it is most useful for cell lines, where only a single cell population is present.

Whole patch clamp measures the electrophysiological currents of a single cell. Using this method the intracellular calcium concentration of the cell can be measured and ER calcium stores depleted by dialysis of the cells, and this stimulates SOCE, which can be measured through changes in voltage (Hoover, Lewis and Aldrich, no date; Srikanth, Jung, Ribalet, *et al.*, 2010; Mcnally *et al.*, 2012). The main disadvantages of this technique are that the entire cells voltage is monitored, so any subtle changes in calcium flux may be missed and that a physiological stimulus cannot be used to induce calcium influx.

For more subtle changes in the channel function to be detectable, cell lines are needed. As the channel of interest can be over expressed or even tagged with green fluorescent protein (GFP) so the channel can be identified for analysis. This means that this type of analysis could not be run on patient primary cells (Mcnally *et al.*, 2012).

The main comparisons of methodologies used in this project are summarised in Table 2.2.3.

Table 2.2.3 Comparison of Calcium methods used

	Flow cytometry	**Plate reader (Flex Station)**	**Single cell imaging**
Main limitations	High cell number needed One sample run at a time	No selection of cell possible Conditions (16 wells) per experiment	Highly skilled training and equipment needed Only frozen samples were available One sample ran at a time
Main benefit	Selection of populations	Low cell number needed Multiple samples run at once	Single cell analysis allows for the selection of responding cells
Cell used	Fresh, PBMC FACS sorted T cells	Fresh, negatively selected T cells	Frozen, expanded T cells
Calcium sensor dye	Indo-1	Fura-2	Fura-2
Cell populations	Total PBMCs measured. Cell types could be separated using markers	Total T cells only No visibility of cell types or responses	Individual cells, but no sub-population available Selection of single cells so non responders can be excluded
Minimum cells per sample	10,000,000	500,000	10,000
Sensitive	Medium	Low	High
Reproducible	No	No	Yes
Main use	Population studies when high cell number is available	Single cell populations (cell lines)	Single cell analysis

The final and most reliable data produced with patient samples was by using single cell imaging. The other two methods required high cell numbers to produce calcium flux data, these high numbers were not obtainable from the patient. The patient phenotype includes low T cell numbers, which made getting the cell numbers needed even more challenging than it was from HC samples. The cell numbers required by flow cytometry in particular were very high, which meant no cell type or population calcium data was collected. Exploring the effect of CRACR2A in different cell types including NK cells, could provide more insight into its function. Looking at different subtypes could be performed by cell sorting patient samples prior to single cell imaging or through the use of mouse models, due to larger cell numbers.

This inability to distinguish between different cell sub-populations is the main limitation of single cell imaging. Only frozen, expanded T cells were available from the patient and HC. The patient phenotype showsTable 3.1.2, Table 3.1.3 and Table 3.1.4, shows a reduced T cell number, a reduced proliferation response and a greater expansion of the CD8+ T cells compared to HC. CD8+ T cells are less responsive to calcium than CD4+ cells (Arrol *et al.*, 2008), and this could be the reason for the reduced calcium flux seen in the patient T cells compared to HC. If these experiments were to be repeated, performing flow cytometry subtyping after single cell imaging would confirm the cell populations and distribution in the samples. Cell sorting could also be performed prior to imaging, after expansion by FACS or selection columns, though it is suspected that cell numbers would be low and may result in cell death, particularly in the patient cells due to their reduced proliferation seen in culture. In order to explore further if the reduced calcium flux was a result of the CRACR2A mutations alone or the different distributions of T cell types, cell line studies were performed due to their single population, as described in Chapter 4.

2.2.8.2 Comparison of calcium flux stimulation

Thapsigargin was used for sustaining calcium influx through passive store depletion (Srikanth *et al.*, 2016) by inhibiting the SERCA ATPase calcium transport into the ER. TG induces an extreme calcium influx as the cell tries to restore calcium to the depleted ER when the main channel for this is inhibited. TG is also used in ER stress tests (Beriault and Werstuck, 2013), so can place a lot of strain on the cell with extended use. This stimuli was not used in the final calcium flux experiments using single cell imaging as minimal samples were available, meaning it was more beneficial to use multiple stimuli on the same sample. Sustained calcium flux was later measured induced by TG in cell lines as shown in Chapter 4.

TCR stimulation is the best representation of the physiological calcium influx and is more likely to show the subtle response expected from mutations in CRACR2A as it is a regulator of the CRAC channel rather than one of the core proteins. As a result, it was used in all calcium flux experiments. As shown in Figure 3.3.11, TCR stimulation was followed by ionomycin stimulation. This is the most extreme stimulus used, as it causes the maximal response and so can be used to check the Indo-1 loading. This stimuli can cause cell death and cell stress at high concentrations. This stimulus is also used in cell culture to induce cytokine production

YM58483 or BTP2 is a specific CRAC channel inhibitor in human T cell which was used as a negative control, in flow cytometry experiments that were not shown here (Zitt *et al.*, 2004; Yoshino *et al.*, 2007; Tian *et al.*, 2016). Through the CRAC channel it can inhibit cytokine production and proliferation in T cells (Ohga *et al.*, 2008). If the calcium flux experiment were to be designed again a different drug for inhibition might be used as BTP2 can reduce the response to both TG and CD3 induced calcium influx. This means that any reduction in calcium response seen might have been due to the reduced response to stimuli rather than the loss of CRAC channel function. A possible alternative is DPB162-AE which is a very potent and selective inhibitor. It acts directly to disrupt the binding of STIM1 and Orai1 and so has no effect on the stimulation of calcium influx (Hendron *et al.*, 2014; Tian *et al.*, 2016). However, the drugt does cause the ER calcium stores to leak, causing depletion of the store at concentrations required for SOCE inhibition (Bittremieux *et al.*, 2017). This leakage from the ER could result in higher Indo-1 ratio readouts as the calcium sensor is contained in the cytosol. The overall calcium influx should still be less than the uninhibited samples.

In summary, although a mildly reduced calcium flux could be observed in primary cells the small numbers of T cells that could be isolated and expanded from the patient prohibited studies that could provide an insight into how the mutations identified may have given rise to the phenotype observed. *In vitro* studies undertaken in regard to this are described in the next chapter.

2.2.8.3 JNK signalling

This was performed as per Srikanth *et al.,* 2016, in both primary T cells and Jurkat cells.

2.2.8.4 Co-immunoprecipitation

Co-immunoprecipitation was performed as described in Srikanth *et al.,* 2016.

2.2.8.5 IL-2 expression

$1x10^6$ Jurkat cells were used per condition in a 12 well plate with a final volume of 1 mL per well. The cell were stimulated for 16 hours, with the addition of BFA (1 in 1000) to all wells, including resting cells, for the last 2 hours. The conditions used were:

- (Rest) Media only
- (High) PMA (80nM) + I (1 µM)
- (Low) PMA (20nM) + I (0.5 µM)

All centrifuge steps were performed at 2000 rpm at 4˚C for 5 mins. After stimulation the cells were transferred to FACS tubes with an additional 3 mL of PBS, centrifuged and washed with 4 mL PBS and all liquid removed by centrifugation. The cells were fixed in 4 % PFA for 15 minutes at RT, on a rocker, before being washed as before. Saponin buffer (0.5 % Saponin [Sigma S7900], 1 % FCS, 0.1 % sodium azide in PBS) was added with the hIL-2-PE (eBioscience MQ117H17) antibody for 45 minutes, protected from light on the rocker at RT. The cells were washed a final time before being resuspended in 350 µL of PBS.

2.2.8.6 Intracellular cytokine staining

$1\text{-}3x10^6$ primary T cells (in 1 mL media per well in a 12 well plate) were rested the day before stimulation. In fresh media, the cells were stimulated for 6 hours with 40 nM PMA and 1 µM ionomycin or 1 µg each of anti-CD3/CD28. 10 µg/mL of BFA was added for the last 2 hours. The cells were then harvested directly into a FACS tube and washed twice with 2 mL of 1 % FBS in PBS. The cells were then resuspended in 100 µL PBS with hCD4 FITC [eBioscience OKT4] and incubated on ice for 30 minutes and kept in the dark. The washing process was repeated and the cells were then fixed in 100 µL of 2 % PFA in PBS at RT for 10 minutes, being protected from light. The cells were washed again and resuspended in 100 µL of Saponin buffer with INFy

[PE Invitrogen,Clone 4563, Lot 1929458] and IL4 [APC,eBioscience, Clone 8D4-8, Lot E07369-1631]) and incubated for 45 minutes to an hour. Cells were washed and resuspend in 350 µL PBS and analysed by flow cytometry.

Chapter 3 CRACR2A and primary cell work

3.1 Introduction

This chapter presents a patient who fits into both primary immunodeficiency (PID) categories II and III, due to the his antibody deficiency (category III) but also T cell deficiency (category II), because of reduced T cell proliferation responses and abnormal distributions of subtype populations.

3.1.1 STIM1 and Orai1 deficiency

Deficiency of calcium release-activated calcium channel protein 1 (Orai-1) or stromal Interaction molecule 1 (STIM1) can result in severe combined immunodeficiency (SCID). Which presents with severe infections, immunodeficiency, anhidrotic ectodermal dysplasia (AED) and congenital myopathy. SCID can be fatal and is normally diagnosed in infancy. The severe infections are a result of impaired T cell activation and development. T cells are sensitive to mutations in Ca^{2+}-release activated Ca^{2+} (CRAC) channel proteins as they do not express the homologs Orai2/3 and STIM2/3. Calcium is an essential secondary messenger in T cells for cytokine production, proliferation and nuclear factor of activated T cells (NFAT) and nuclear factor-κB (NFκB) signalling (Feske, Picard and Fischer, 2010).

Our group previously identified a STIM1 mutation that broadened the phenotype of CRAC channel deficiencies (Parry *et al.*, 2016). The mutation caused impaired calcium flux, but no clinical immunodeficiency. The family had normal T cell function but impaired (natural killer) NK cell effector function, which deviated from normal STIM1 deficiency and results in impaired T cells.

3.1.2 CRACR2A

Calcium release activated channel regulator 2A (CRACR2A) protein, encoded on the gene EF-hand calcium-binding domain-containing protein 4B *(EFCAB4B)*, was isolated by affinity protein purification and identified as a modulator of Orai1 and STIM1. CRACR2A interacts directly with Orai1 and STIM1, forming a ternary complex that dissociates at elevated Ca^{2+} concentrations. siRNA knockdown showed that CRACR2A is important for clustering of Orai1 and STIM1 upon store depletion (Srikanth, Jung, Kim, *et al.*, 2010).

3.1.2.1 CRACR2A gene, mRNA and protein

Human *EFCAB4B* is located on the reverse strand of Chromosome 12, details about the gene, mRNA and protein are highlighted in Table 3.1.1. The details of three protein encoding transcripts are described, only the long and short transcripts have been confirmed by western blots in cells and so only these two transcripts are discussed further here (Srikanth, Jung, Kim, *et al.*, 2010; Srikanth *et al.*, 2016; *The Human Protein Atlas*, 2020). Figure 3.1.1 shows the functional domains of the long isoform of CRACR2A, the short isoform shares the first 373 amino acids. No confirmed 3 dimensional structure is available for the full length protein. Recently the EF hand domain pair structure was published (residues 47-121), as determined by x-ray diffraction (Dominguez, R., Lee, 2020). The CRACR2A protein has not previously been linked to disease.

Table 3.1.1 CRACR2A gene,1 mRNA and protein details

Name	Transcript	Transcript (bp)	Exons	Coding exons	Protein (residues)	Protein (kDa)	Biotype	UniProt	Domains
CRACR2A-Long	ENST00000440314.7	2704	20	17	731	83.21	Protein coding	Q9BSW2-2	EF hand, Small GTP-binding protein domain
CRACR2A-Short	ENST00000252322.1	2186	11	8	395	54.86	Protein coding	Q9BSW2-1	EF hand
CRACR2A-205	ENST00000535292.1	630	5	5	118	13.87	Protein coding	H0YFI5	EF hand

Gene location Chromosome 12: 3,715,799-3,873,985, reverse strand. Transcript details taken from http://asia.ensembl.org/index.html (accession date 10DEC2020). The cDNA sequences of the long and short transcripts can be found in Figure 2.2.2.

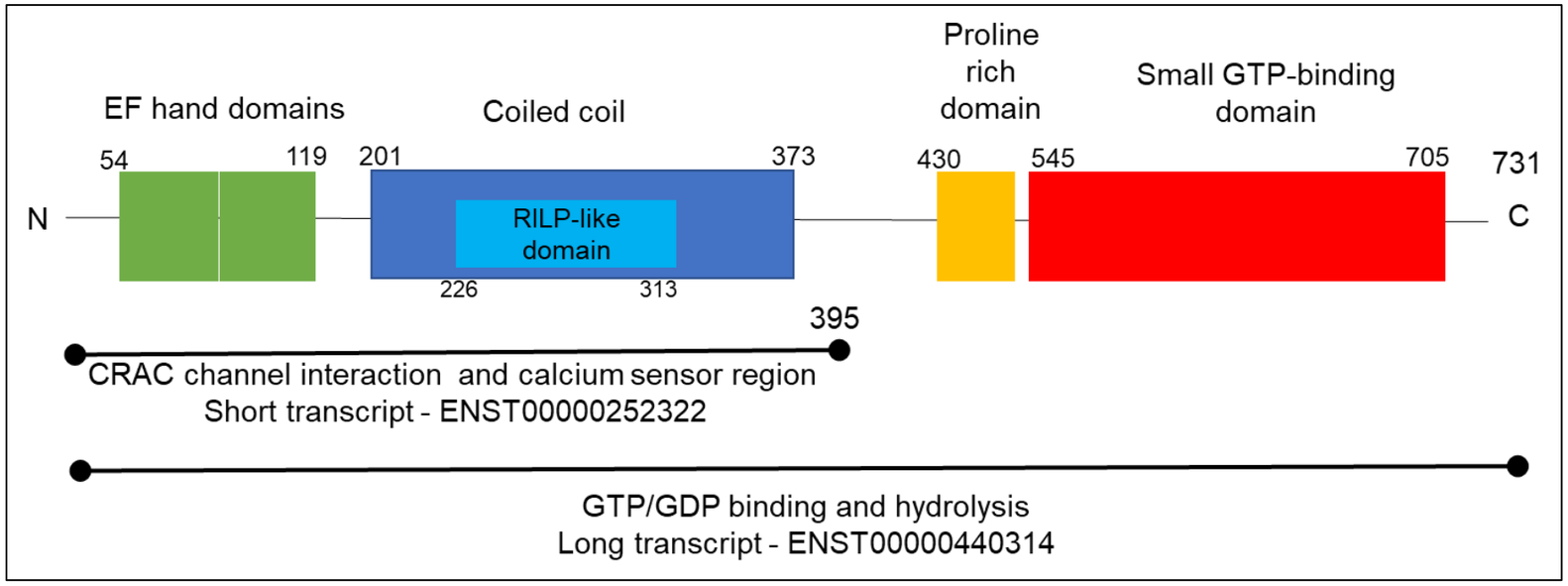

Figure 3.1.1 CRACR2A functional regions.

CRACR2A has two main transcripts. The short transcript containing the calcium function (amino acid 1-395) and the long transcript containing the additional GTP activity (amino acid 395-731). The Rab interacting lysosomal protein (RILP) homology domain functions as a novel effector domain for small GTPase. Figure was taken and adapted, with permission, from Srikanth et al., 2016.

3.1.2.2 CRACR2A in the CRAC channel

CRACR2A is a regulator of the interaction between Orai1 and STIM1 as it interacts directly with the cytoplasmic domains of both proteins, forming a ternary complex. It binds to a highly conserved region of Orai1, at amino acids 64-93. CRACR2A and STIM1 bind to Orai1, their binding partially overlaps and as a result when CRACR2A dissociates from the complex the CRAC channel disassembles, as the interaction between STIM1 and Orai1 are weakened. CRACR2A contains two EF hand domains that can bind calcium. When the cytoplasmic calcium concentration increases, calcium binds to the second EF domain which causes a conformational change, which weakens the tertiary CRAC channel complex. In this way, CRACR2A acts as a cytoplasmic calcium sensor which can stabilise the CRAC channel or promote disassembly. In 2010, CRACR2A was identified as a novel EF-hand protein that regulates the CRAC channel. In this paper, a lot of work was done in Jurkat cells to learn more about the function of the CRACR2A protein (Srikanth, Jung, Kim, *et al.*, 2010). Jurkat cells are an immortalised cell line of human T cells as described in Section 2.1.1.6. The Gwack lab showed that siRNA knockdown of CRACR2A caused a reduction in calcium flux by 50 % and impaired the production of IL-2, an important cytokine of the immune system. They produced a EF hand mutant which could no longer bind calcium, so no longer stabilised the CRAC channel in a calcium sensitive manner. This caused increased STIM1 clustering and an increase in cytoplasmic calcium which resulted in cell death. This paper also identified the homolog CRACR2B, with an overall protein sequence identity of 36 % to CRACR2A and conserved EF-hand motifs and coiled coil domain. The main difference observed between the two homologs is their expression levels in different cell types. CRACR2A is present at a higher amount in primary T cells, whereas CRACR2B is more abundant in fibroblasts.

3.1.2.3 CRACR2A's Rab GTPase related function

The C terminal end of CRACR2A has Rab guanine triphosphatase (GTPase) related function. Rabs regulate protein transport along the endocytic and exocytic pathways in and participate in vesicle budding, membrane fusion, and interactions with the cytoskeleton (Wandinger-Ness and Zerial, 2014). Not much is known about the function of this specific domain of CRACR2A domain, but it has recently been linked to Jun N-terminal kinase (JNK) signalling, transport and vesicles, as described in more detail below.

3.1.2.3.1 JNK signalling

The GTP/ guanosine diphosphate (GDP) binding and hydrolysis domain of CRACR2A had been shown to affect JNK signalling. JNKs have a range of functions including signalling events underlying tumorigenesis, tumour progression and regulation of cell proliferation, invasive migration, therapy resistance, and cell death. JNKs also have a wide range of functions within apoptotic mechanisms, including those of necroptosis, ferroptosis, pyroptosis, and autophagy, through the expression of specific genes and modulating the activities of pro- and anti-apoptotic proteins by phosphorylation. JNKs are activated by stress, growth factors and inflammatory cytokines. JNK-mediated signalling involves a three-tier kinase signalling relay upstream of the JNK, such as mitogen-activated protein kinase (MAPK), MAP3K and MAP2K. JNK is activated by the phosphorylation of the threonine (T) and tyrosine (Y)-residues of the TXY motif of JNKs. JNK-regulated pathways play a crucial role in both cell proliferation and cell death (Dhanasekaran and Reddy, 2017).

3.1.2.3.2 Dynein adaptor protein

CRACR2A binds to dynein in the presence of calcium, making the interaction calcium dependent due to the EF domains of CRACR2A. CRACR2A functions as a activating dynein adaptor and as such can stabilise and activate dynein-dynactin complexes into a processive motor, allowing the movement of specific cargo along toward the minus end of microtubules (Wang *et al.*, 2019). CRACR2A has been shown to localise to the golgi apparatus, near the minus end of microtubules, when not part of the immune synapse with Orai1 and STIM1 (Srikanth *et al.*, 2016). CRACR2A is a large protein compared to classical Rab proteins and combines the dynein-activation and cargo recruitment function into a single protein (Wang *et al.*, 2019).

3.1.2.3.3 Weibel-Palade bodies

CRACR2A dependent differential trafficking has been shown in P-selectin-negative Weibel-Palade bodies (WPBs). Endothelial cells selectively release cargo stored in WPBs to regulate vascular function. Histamine causes the release of the proinflammatory ligand, P-selectin, while diverting WPBs carrying non-inflammatory cargo away from the plasma membrane to the microtubule organizing centre (MOC). After acute stimulation of the histidine (H) receptor, CRACR2A induces dynein-

dependent retrograde transport of WPBs along microtubules. Continued histamine stimulation causes the dispersal of WPBs from the MOC by increasing intercellular calcium which can be sensed by the EF-hand domains of CRACR2A (Miteva *et al.*, 2019).

3.1.3 Case study

The patient this chapter focuses on is an East Asian male who was diagnosed with common variable immunodeficiency (CVID) at age 17. There is no family history of immune system disorders or PID.

3.1.3.1 Patient immunological profile

The patient is a 33 year old South Asian male who was diagnosed with common variable immunodeficiency (CVID) at age 17. He presented initially with chronic diarrhea, profound panhypogammaglobulineamia (low levels of all immunoglobulins), reduced CD4 count and a low T cell activation response, as seen in Table 3.1.2. A detailed CT scan of his chest showed cylindrical bronchiectasis of the left lower lobe, lingua and R middle lobe. This appearance remains unchanged 11 years later in 2016. He is currently being treated with regular intravenous immunoglobulin (IVIG) replacement therapy. His clinical progress since the diagnosis has been uncomplicated and the treatment with IVIG has resulted in excellent control of respiratory infections.

CVID is the most common PID and is predominantly an antibody deficiency. It is a heterogeneous group of disorders which have a serum Ig characterised by low IgG and IgA with or without low IgM. The phenotype can vary but most cases present with recurrent infections, cytopenia, enlarged lymph nodes, poor antibody response to vaccines and low switched memory B cells. 25 % of patients develop autoimmune complications (Giardino et al. 2016). The patient had immunological features of the associated with CVID, including low Ig, CD4 numbers below 200 cells/µl (Table 3.1.2, 2017 and 2019) and naive CD4 below 20 % (Ameratunga *et al.*, 2014; Wong and Huissoon, 2016).

Table 3.1.2 Immunological clinical data

Year		2005	2011	2017	2019	Ref
Lymphocytes	Total (cells/µL)	2880	990	1201	1572	1000-2800
CD3+	Total (cells/µL)	2505	733	891	990	700-1200
CD3+ CD4+	Total (cells/µL)	216	235	148	165	300-1400
	CD27+ CD45RA+ (naïve)%			20.92	12.65	37-97
	CD27+ CD45RA- (memory)%			42.34	47.04	13-76
	CD27-CD45RA- (memory effector)%			36.01	37.67	0.49-25
	CD25+CD127- (Treg)%			0.73	1.6	1-5
CD3+ CD8+	Total (cells/µL)	2080	475	738	840	200-900
	CD27+ CD45RA+ (naïve) %				17.69	20-95
	CD27+ CD45RA- (memory) %				25.16	0.4-18
	CD27- CD45RA- (memory effector) %				16.09	4-100
	CD27- CD45RA+ (effector) %				41.07	9-65
CD19+	Total (cells/µL)	245	102	73	77	100-500
	CD27- IgM+ IgD+ (naïve) %			63.1	89.18	65.0*
	CD24hi CD38hi (Transitional) %			6.7	10.3	6.2*
	CD27+ IgM+ IgD+ (non-switched) %			15.4	3.69	12.5*
	CD27+ IgM- IgD- (switched memory) %			14.7	7.15	16.4*
	Plasmablasts %			0.2	0.4	
CD56+ CD16+	NK cells Total (cells/µL)	144	139	290	486	90-600
T lymphocyte proliferation test	PHA	↓		↓	↓	
	Anti CD3	↓		↓	↓	
Immunoglobulin profile	IgG	1.4	8.4	10.3	8.3	6-16 g/L
	IgA	<0.06	<0.06	<0.06	<0.06	0.8-4 g/L
	IgM	<0.06	<0.06	<0.06	<0.06	0.5-2 g/L
	IgE				<0.2	1-120 ku/L

Patient clinical data from first attendance at clinic (2005) and at later follow ups. Data generated by Leeds Clinical Department and supplied by Clive Carter (SJUH). Results above (red text) or below (blue text) the normal reference ranges are colour coded. * indicated values from single HC. No data was available for the greyed out boxes.

The patient clinical immunological workup included cell type and subpopulation analysis. The results from these tests are detailed in Table 3.1.2, from 2005 when the patient first presented to the clinic up to late 2019. The most immunological test that showed the largest deviation from HC reference results were the immunoglobulin results. All immunoglobulin types were low and these severely low levels were maintained throughout the four tests performed over 14 years. As a result, the patient was placed on immunoglobulin therapy and was suspected of having a B cell defect. However, the B cell counts of the patient (CD19+ in Table 3.1.2) were initially found to be in normal numbers until the 2017 and 2019 readings, where they dropped slightly below the normal range (100-500 cells/ µL) to 73 and 77 cells/ µL respectively. In contrast, The patient T cell numbers appear to be affected in the earlier testing but fall within normal ranges later on. In 2005, the total T cells (CD3+) and the cytotoxic T cells (CD8+) have high cell numbers compared to normal ranges. The T helper cell (CD4+) numbers are below the normal reference ranges. The CD3+ and CD8+ counts return to normal ranges during all further tests, but the low CD4+ numbers persist. The ratio between CD4+ and CD8+ cells in healthy individuals normally leans towards a larger number of CD4+ cell, and these are the T cells that expand more readily in response to TCR stimulation. In the patient under study, this ratio is shifted. The patient T cells also showed a reduced proliferation response to PHA and CD3, this diminished response was observed throughout the 14 years.

This patient fits into both categories II and III, due to the antibody deficiency (III) but also into the T cell deficiency (II) due to T cell proliferation and abnormal populations.

3.1.3.2 B cell differentiation

The severely low level of all immunoglobulin and normal to slightly low B cell numbers seen in the patient (Table 3.1.2) meant a potential B cell defect could exist. The patient and HC B cells were taken into a T cell independent assay, to investigate their development and immunoglobulin expression.

The assay showed normal development of patient B cells compared to HC. This was monitored by flow cytometry using key surface markers as described in Section 2.2.3.5, with the characteristic loss of CD20 expression during differentiation and CD38 and CD138 upregulated as the cells transition from plasma blasts (CD38+CD138-) to plasma cells (CD38+ CD138+). CD27 was also upregulated during development as is seen in normal individuals.

The cell number and expression of IgG and IgM was also found to be comparable to healthy control in ELISAs, as seen in Figure 3.1.2. This normal response of the patient B cells in the *in vitro* assay suggested that the B cells were not directly responsible for the patient phenotype as they are able to produce normal levels of immunoglobulins and develop normally into plasma cells. Instead, the patient might have disruption to the signalling needed to stimulate the B cells. The T helper cells play an important role in B cell development. This cell population was reduced in the patient (Table 3.1.2) and as such the function of the patient T cells was investigated.

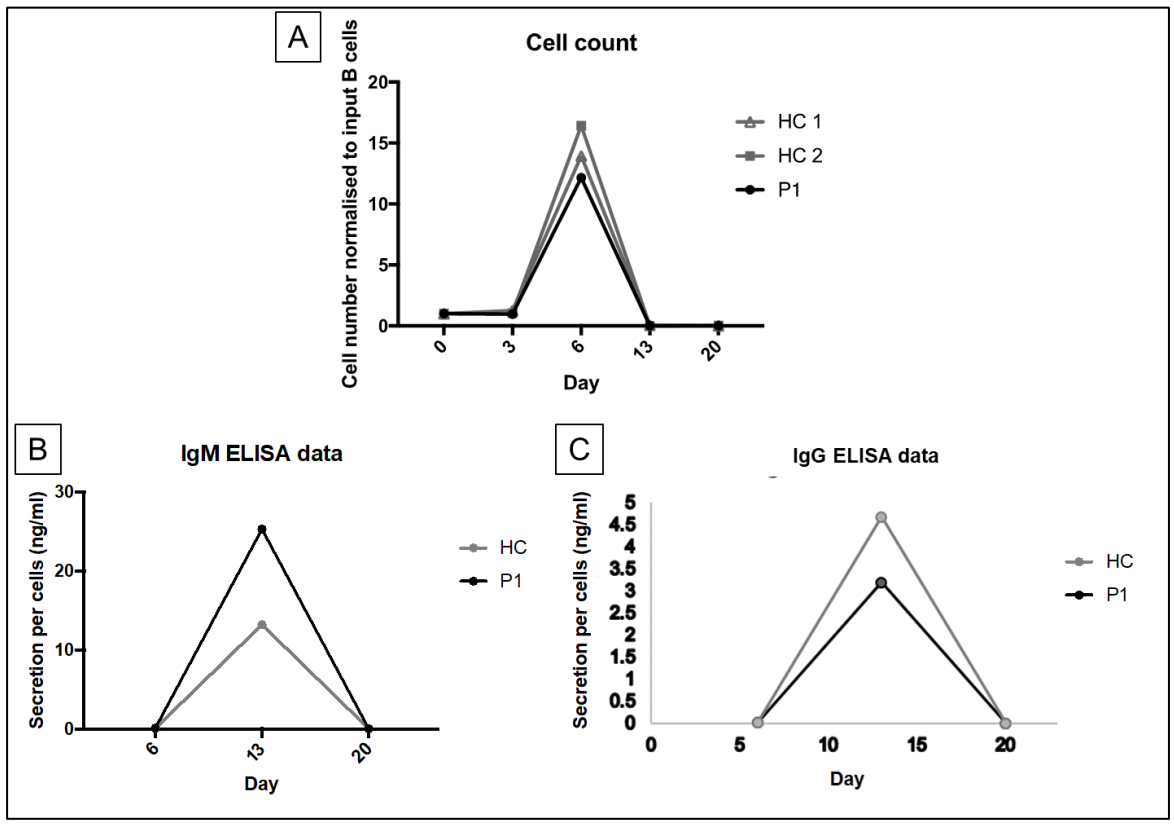

Figure 3.1.2 *In vitro* B cell count and Immunoglobulin expression
Data generated by Jennifer Shrimpton (University of Leeds). Method details are in Section 2.2.3.5.

3.1.3.3 T cell specific clinical tests

The reduced proliferation response reported over multiple visits in patient T cells (Table 3.1.3), and the normal B cell development *in vitro,* meant that the T cells were a likely candidate responsible for the patient phenotype. As a result additional T cell tests were performed during the 2017 check-up.

The T cell proliferation was shown to be reduced in response to both PHA and CD3 stimulation. With both stimulations the reduced proliferation response becomes more profound at the higher levels of stimulation. It appears that the patient cells can respond in a more comparable manner at rest and under lower stimulation conditions. At higher stimulation conditions a more dramatic difference can be seen in patient and HC, with the patient having lower number of cells, due to the reduced proliferation.

Table 3.1.3 T cell proliferation

PHA (µg/mL)	**0**	**5**	**10**	**100**
HC	654	119112	152745	150043
Patient	24	91642	85564	31095
CD3 (x10^5 cells/mL)	**0**	**2**	**1**	**0.5**
HC	654	123376	161025	179969
Patient	28	110415	45778	24462

Data generated by Leeds Clinical Department and supplied by Clive Carter (SJUH). Results above (red) or below (blue) the HC values are colour coded. The data is displayed in weakest to strongest for both stimulations. For PHA the dose was increased and the number of initial cells per condition stayed the same. For CD3 a standard amount of CD3 was coated on plates and the initial number of cells added was reduced, therefore increasing the amount of available CD3 per cell.

Normally when T cells proliferate the CD4+ population expands faster than the CD8+ cells. The opposite seems to occur in the patient, as the CD4:CD8 ratio is shifted compared to HC, both at rest and when stimulated with PHA, as seen in Table 3.1.4. This was measured by examining HLA-DR expression in T cells, which is a marker of activated T cells. The CD8+ expansion and low naïve T cells number (Table 3.1.2) are markers of CVID and can contribute to T cell exhaustion (Wong and Huissoon, 2016).

The diversity and development of T cells was further investigated by looking at the β chain of the TCR in the patient, Figure 3.1.3. Only two specificities were outside normal ranges, Vb5.2 was elevated in the patient and Vb7.2 reduced. This suggested that the expression and rearrangement of the β chain is comparable to HC.

Table 3.1.4 T cell populations activated after stimulation

		% CD4	% CD8
HC	-	1.26	0.84
	+	37.56	7.73
Patient	-	0.7	8.41
	+	17.8	40.72

Data generated by Leeds Clinical Department and supplied by Clive Carter (SJUH). Results above (red) or below (blue) the HC values are colour coded. PBMCs were stimulated with PHA at 2 µg/mL or at rest for 72 hours at 37 ˚C. Flow cytometry was performed to determine the levels of HLA-DR expressed on the surface of CD4+ and CD8+ populations.

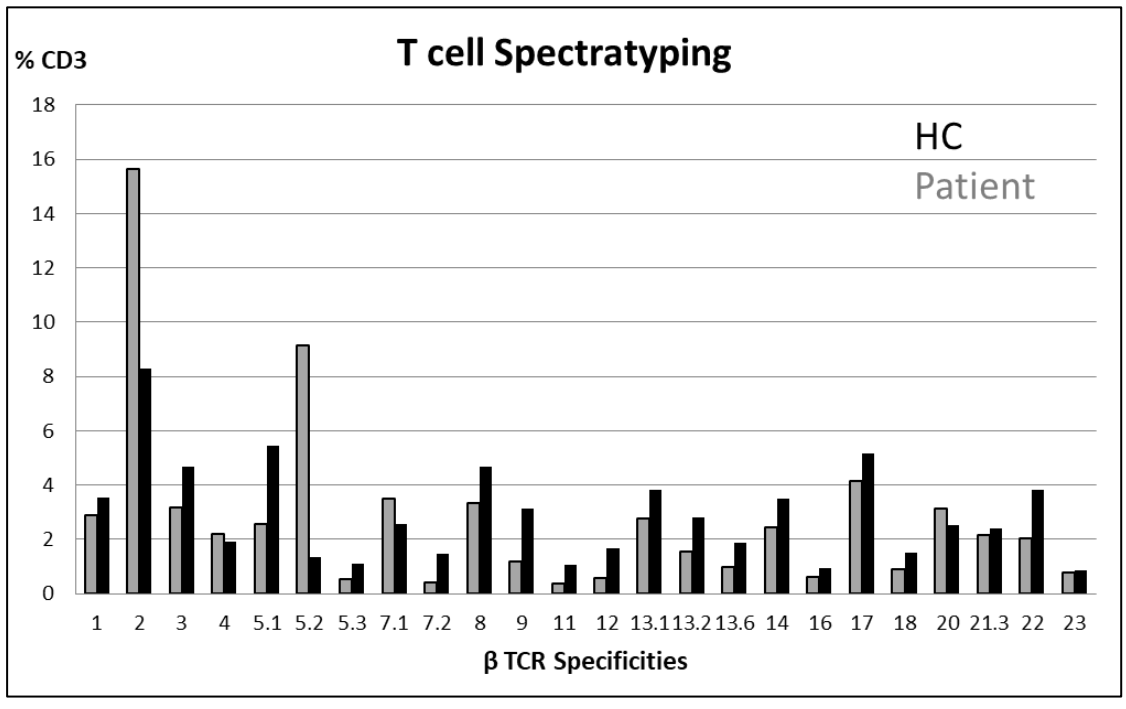

Figure 3.1.3 T cell receptor specificities

Data generated by Leeds Clinical Department and supplied by Clive Carter (SJUH). Flow cytometry was used to spectratype T cells of patient and HC.

3.1.4 Aims

For this case study standard clinical data was initially available that showed the patient had low levels of all immunoglobulins and reduced T cell functions with a shift towards CD8 T cell proliferation. B cell differentiation studies showed that their B cells were able to produce IgG and IgM *In vitro* and so suggested that the patient phenotype was T cell related. In order to investigate the possible cause of this, WES was performed and no known genes previously linked to PID were identified. As a result, further study was needed on the potential gene candidates identified. Knowing the cause of the patient phenotype can lead can potentially lead to better treatment and understanding of their disease.

In order to identify the potential candidates, the below steps were taken and the findings are detailed in this chapter:

- Confirm potential mutations and their segregation in patient with PID
- Use primary samples to determine if those mutations are pathogenic and causing of the patient phenotype, by looking at protein specific function.

3.2 Materials and methods

The method strategies and patient information are described in this chapter. For full method details see Chapter 2.

3.2.1 Segregation of patient mutations when parental DNA was not available

A polymerase chain reaction (PCR) was performed on patient cDNA to amplify a region that contained all mutations of interest. The TA cloning protocol was then done, to isolate a single amplicon per colony within the TA cloning plasmid. The plasmid was then purified by GenElute™ Plasmid Miniprep Kit (Sigma) and sequenced to determine which mutations were on the same allele.

3.3 Results

The results in this chapter focus on a single patient with primary immunodeficiency (PID). Whole Exome Sequencing (WES) did not identify any known mutations or genes previously linked to PID.

3.3.1 Genetic testing of patient

WES and the filtering strategy described in Section 2.2.1.1 was performed by Dylan Lawless (University of Leeds). This identified mutations in two potential genes of interest: EF-hand calcium-binding domain-containing protein 4B (*EFCAB4B*, protein CRACR2A) and dehydrogenase/reductase 4 (*DHRS4)*.

These two genes had previously been linked to the function of the immune system but had not been linked to PID. As a result further functional testing was needed to determine if the mutations identified by WES could be affecting the protein function and therefore be responsible for the patient's novel phenotype.

3.3.1.1 Confirming mutations in *DHRS4* gene

The *DHRS4* gene encodes for an enzyme in the short-chain dehydrogenase/reductase (SDR) family. It has nicotinamide adenine dinucleotide phosphate (NADPH)-dependent carbonyl-reductase activity on a broad set of substrates. It's role in retinol metabolism is of particular interest due to its association with the immune system. Dehydrogenase/reductase 4 reversibly converts retinol or Vitamin A to retinaldehyde which is then irreversibly converted into the biologically active, retinoic acid (RA). RA can inhibit the generation of B cells and the differentiation of dendritic cells (DC) which activate naïve T cells (Chen, Welner and Kincade, 2009; Raverdeau and Mills, 2014). Gain or loss of function mutations in dehydrogenase/reductase 4 could disrupt the metabolism of Vitamin A which could result in a PID with compromised B and T cells, as presented in the patient under study here.

WES was performed and identified a homozygous point mutation at cDNA position c.475 Cga>Tga, which would result in a premature stop codon at amino acid R158* (see Table 3.3.1). This residue is highly conserved throughout evolution (https://genome.ucsc.edu/) and the mutation was not listed in databases of healthy individuals (gnomAD). As with all enzymes the structure of the protein is highly specific and so the function can be easily affected by small changes. In this case, the point mutation results in a large change and a potentially truncated protein, reducing the polypeptide chain from 278 residues to 158. This truncated protein would not contain the two main residues of action, amino acid 169 which is a substrate binding site and residue 182 which is a proton acceptor active site. This means the truncated form of the protein is unlikely to function like the wild type protein. The premature stop codon could result in the mRNA being sent for nonsense mediated decay. The nonsense mediated pathway is a surveillance mechanism to detect and eliminate mRNA transcripts that contain premature stop codons, in order to halt the translation of these transcripts.

PCR was performed to amplify the *DHRS4* exon of interest, exon 4, using patient genomic DNA. Sanger sequencing of this PCR product showed the mutation to be in heterozygous form (Figure 3.3.1) instead of homozygous as had been identified in the WES. As a result, this mutation was considered less likely to be pathogenic and so was not pursued further.

Table 3.3.1 *DHRS4* mutation

Gene	**Mutation**	**Type**	**Exon**	**Codon change**	**Amino acid change**	**gnomAD**	**ExAC**
DHRS4	Homozygous	Stop gained	4/7	c.475 Cga>Tga	p.158 R>*	Not in gnomAD	Not on ExAC

Resources used for exome and genome sequencing data :https://gnomAD.broadinstitute.org/ and http://exac.broadinstitute.org/

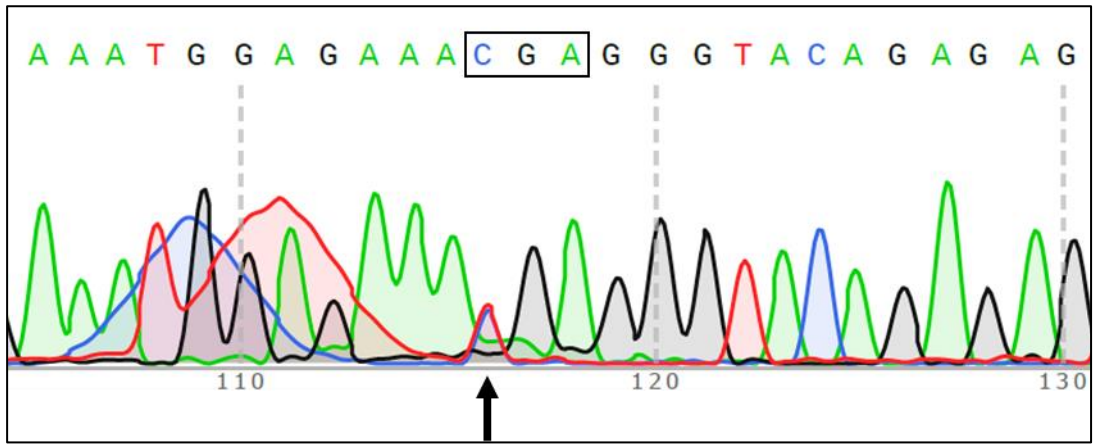

Figure 3.3.1 Sanger sequencing of *DHRS4* exon 4 from patient genomic DNA

Genomic DNA isolation from patient whole blood, PCR and Sanger sequencing were performed as per Sections 2.2.1.3 and 2.2.1.4.The primers used are shown in Table 2.1.1 (primers A+B). The PCR product was amplified in duplicate and run on a 1.5 % agarose gel. The band was found to be about the same size as the predicted amplicon of 299 base pairs. They were then directly sequenced using both the forward and reverse primer, and only the forward, A, is shown. The black arrow indicates the point mutation C>T and the affected codon is highlighted by a box.

3.3.1.2 Confirming mutations in *EFCAB4B* (CRACR2A protein) gene

The two main functional regions of the full length, long isoform of CRACR2A protein are the CRAC channel interaction region (amino acids 1-395) and the GDP functional domain (amino acids 395-731) are shown in Figure 3.1.1. All three of the mutations identified in this gene by WES fall within the CRAC interaction region and are also present in the shorter isoform of the CRACR2A protein. The latter is 395 amino acids long and shares its first 373 amino acids (1119 nucleotides of mRNA) with the long isoform.

The details of the three mutations, all heterozygous, are summarised in Table 3.3.2. Two of the mutations result in an amino acid change. The mutation at position 144 is from arginine to a glycine, changing the residue from a large positively charged side chain to a small non-polar sidechain. This could affect the protein conformation. Residue 144 is conserved throughout evolution and this mutation has not been found to date in the gnomAD database of normal population. This could mean that this residue is important to the structure or function of the protein. The other missense mutation is at position 278, and results in a conservative change from glutamic acid to aspartic acid. As both amino acids have small negatively charged side chains, a smaller effect on function may be predicted compared to if it was a non-conservative amino acid change. This mutation is present in the gnomAD database, but only in the heterozygous state and at a rare allele frequency of 0.00014. The frequency is slightly higher in the East Asian population, at 0.00092, which is still considered rare (<0.005). The last heterozygous mutation

resulted in a premature stop codon at amino acid 300, which is normally glutamic acid. This residue is highly conserved throughout evolution, and no mutations were recorded in gnomAD. The premature stop codon, could lead to a truncated protein, without the end of the coiled coil domain of the short isoform and without any GTP functional region in the long isoform. The mRNA may be sent for nonsense mediated decay.

Sanger sequencing was performed on the patient genomic DNA and confirmed all three mutations in *EFCAB4B*, c.430 A>G, c.834 G>T and c.898 G>T, that were identified by WES, all of which were heterozygous, as seen in Figure 3.3.2. The orientation of these mutations needed to be confirmed to see if they were all present on the same allele, or if they were compound heterozygous, without any wild type (WT) allele being present, and therefore increasing the likelihood of the mutations being pathogenic.

Table 3.3.2. Mutations in *EFCAB4B* (protein CRACR2A).

Exon	Mutation	Amino acid change	Type	gnomAD	ExAC
6/20	c.430 Aga>Gga Heterozygous	p.144 R>G	Missense variant	Not in gnomAD. Heterozygous R144S and R144I reported at frequency 0.000008 & 0.000004	Not on ExAC, Heterozygous R144S and R144I reported at frequency 0.000008 & 0.00002
9/20	c.834 gaG>gaT Heterozygous	p.278 E>D	Missense variant	Heterozygous present 0.00014, 0.00085 East Asian	Heterozygous present 0.00016, East Asian 0.00092
10/20	c.898 Gag>Tag Heterozygous	p.300 E>*	Stop gained	Not in gnomAD	Not on ExAC

Transcript ENST00000440314.7, of the long isoform. Resources of exome and genome sequencing data :https://gnomAD.broadinstitute.org/ (accession data 03JAN2021) and http://exac.broadinstitute.org/ (accession date 01JUN2018)

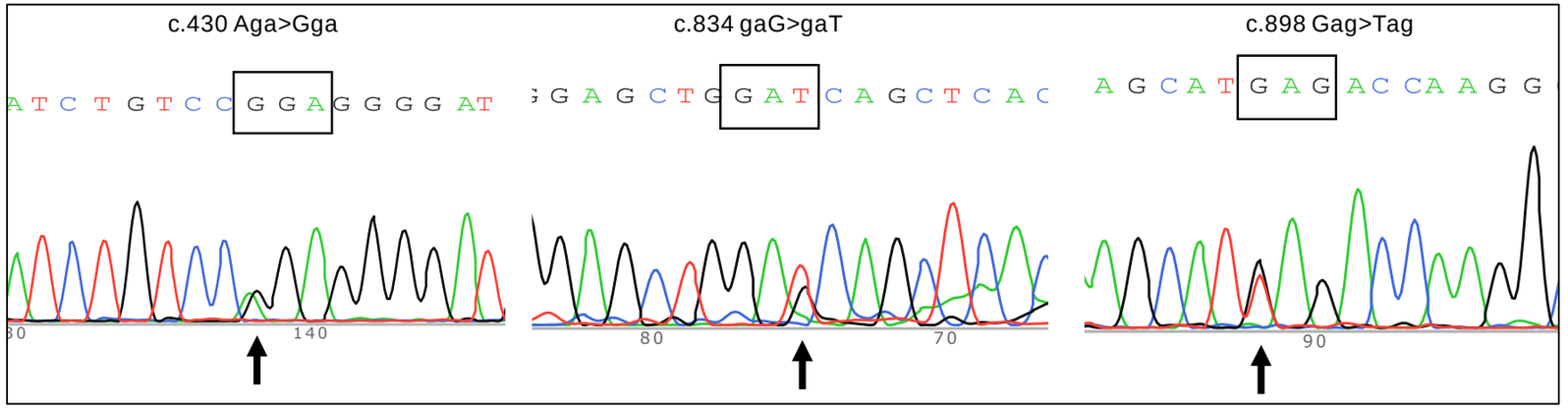

Figure 3.3.2 Sanger sequencing of *EFCAB4B* from genomic DNA of patient.

Genomic DNA isolation from patient whole blood, PCR and Sanger sequencing were performed as per Sections 2.2.1.3 and 2.2.1.4. Primer pairs C+D, E+F, and G+H were used to generate PCR products that were then sequenced directly using the corresponding forward primer C, E and G (Table 2.1.1). The PCR products was amplified in duplicate and run on a 1.5 % agarose gel, to confirm the predicted sizes. They were then directly sequenced using both the forward and reverse primers defined above. The black arrow indicates the point mutation and the affected codon is highlighted by a box

3.3.1.3 Mode of inheritance

After the three heterozygous mutations found (c.430 A>G, c.834 G>T and c.898 G>T) by WES were confirmed by Sanger sequencing, their orientation needed to be identified to determine if a WT allele could be present or if the mutations were compound heterozygous. This could normally be determined by sequencing genomic DNA from the parents of the proband, to create a family pedigree, which would show segregation of the affected alleles. Unfortunately, initially no parental DNA was available. Instead cloning was performed on the patient cDNA to separate the maternal and paternal alleles.

RNA was extracted from the patient PBMCs, and reverse transcription was performed using random primers and oligo dT primers, to form the stable cDNA. PCR was performed on the cDNA, to amplify the region that contained all three mutations within a single 731 base pairs long amplicon. The PCR product was sequenced before cloning and showed the heterozygous mutations at all three locations (Figure 3.3.3A), although the chromatogram showed some peaks to be present at higher concentrations (c.430A [WT], c.834T and c.898G [WT]). When TA cloning and transformations were done on the amplicons, ten colonies were selected and checked for the presence of CRACR2A using colony PCR. Of the ten selected, eight showed bands at the expected size on an agarose gel. These colonies were miniprepped and sequenced at all three mutation locations. All of the colonies contained the same sequence at the three mutations loci, c.430A [WT], c.834T and c.898G [WT], a representation of which is shown in Figure 3.3.3B. None of the colonies showed the c.430G and c.898T mutations, this was potentially as they were present at a lower concentration, as seen in the initial cDNA sequencing. This concentration discrepancy could have been a result of the cDNA generation, or more likely due to the presence of the premature stop codon caused by the mutation at position c.898T, which can result in mRNA being sent for nonsense mediated decay and so being present in the cell at a lower level than mRNA from the other allele.

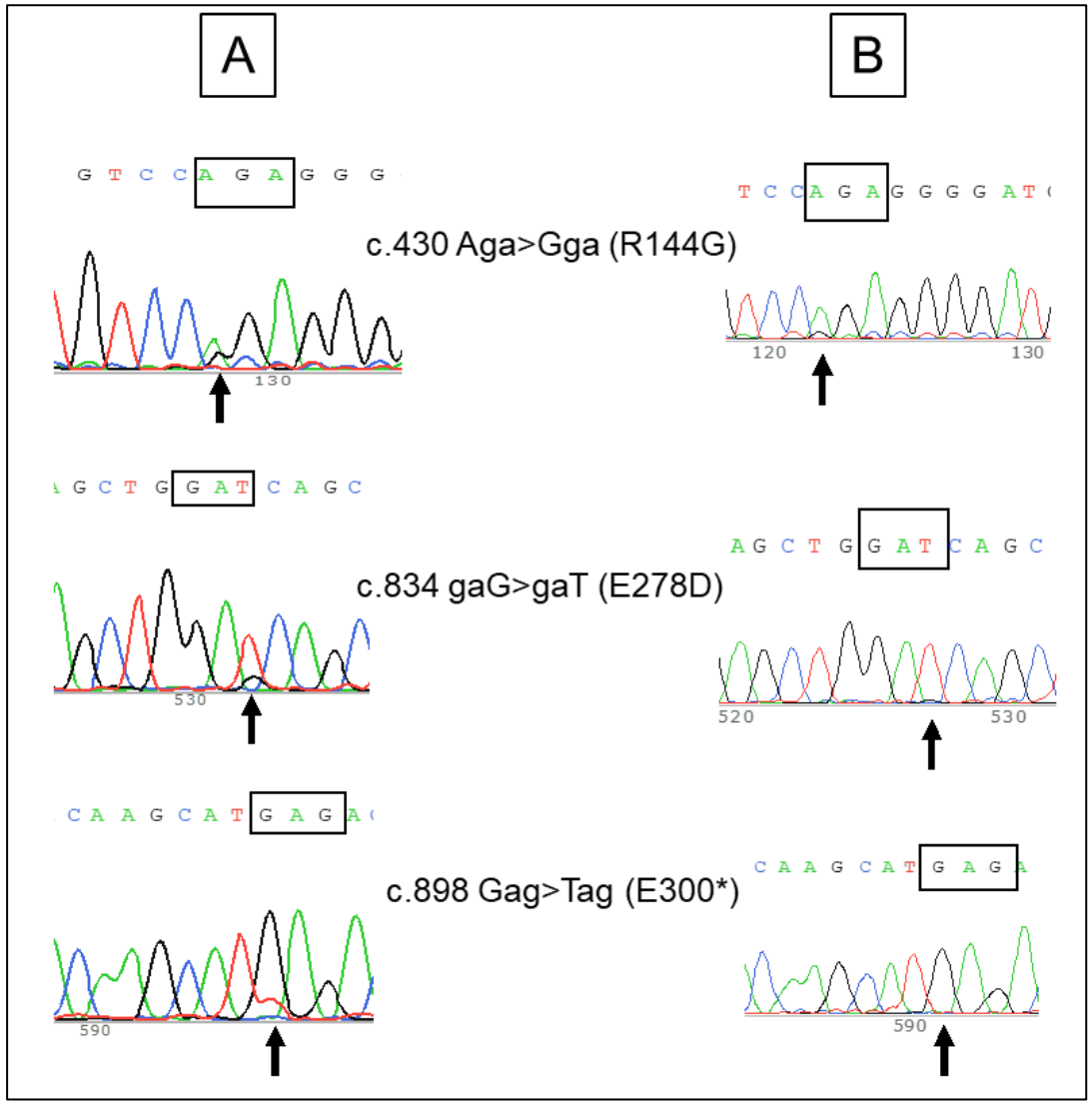

Figure 3.3.3. Sanger sequencing of patient cDNA and TA clone.
The 731 bp amplicon was created using I and L primers from Table 2.1.1 (located in exon 3 and exon 10, Ta – 66 ˚C). The 731 bp amplicon was generated from the patients cDNA and cloned using the TA cloning kit. Sequenced directly using the forward primer I. A) sequencing of original PCR product from patient cDNA and B) sequencing of representative clones

The cDNA cloning and sequence analysis suggested that the mutation c.834 G>T was present on its own in one allele. This would imply that the other two mutations, c.430 A>G and c.898 G>T, were present on the second allele. Hence, the patient had compound heterozygous mutations in the *EFCAB4B* gene. This increases the likelihood of the mutations identified as being pathogenic.

Later in the project, samples from the Mother and maternal Grandmother became available for Sanger sequence analysis. gDNA was extracted from whole blood and sequenced at all three mutation locations. Only the chromatograms for the Mother

are shown in Figure 3.3.4 as both individuals showed the same mutations at each location. The sequencing data clearly showed that the heterozygous mutations were present at positions c.430 A>G and c.898 G>T, but wildtype at position c.834 G>T. This information, with the original cDNA and TA cloning data analysis confirms that the patient mutations are compound heterozygous, as summarised in Figure 3.3.5.

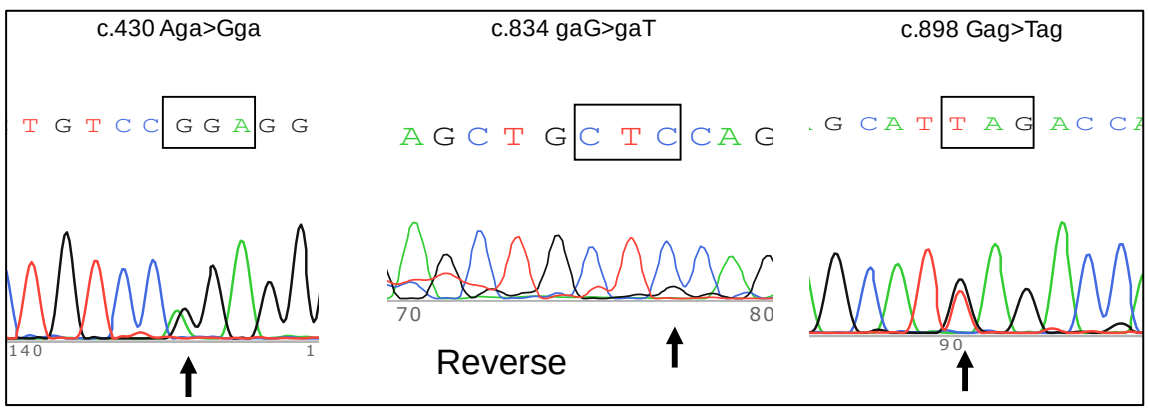

Figure 3.3.4 Sanger sequencing of maternal DNA.
The results from mother's genomic DNA from whole blood are shown here. Experiments were performed as described in Figure 3.3.2. For c.834 the reverse primer sequence is shown.

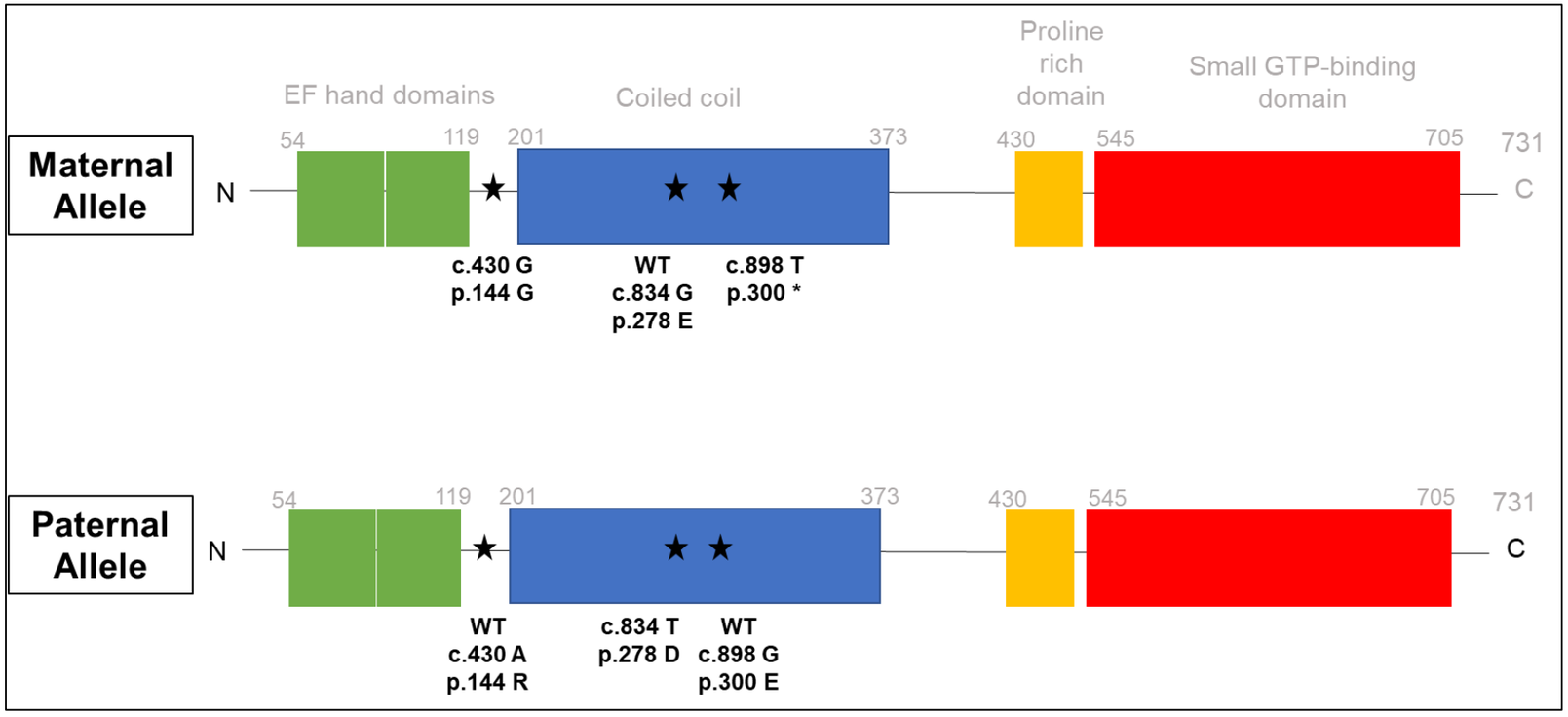

Figure 3.3.5 Orientation of mutations in patient alleles.

Stars indicate the locations of the mutations on the polypeptide, where these bases are WT this is indicated in the image. Maternal allele mutations confirmed by Sanger sequencing as shown in Figure 3.3.4. Paternal allele isolated by TA cloning as shown in Figure 3.3.3.

A pedigree for the proband was also produced from results of the sequencing of the maternal gDNA of the patient, as seen in Figure 3.3.6. As no paternal DNA was available for sequencing, the paternal alleles cannot be confirmed directly. However, segregation of the heterozygous c.834 G>T can be inferred from the patient cDNA cloning data, and clear absence of this mutation in the maternal line. The presence of this mutation on gnomAD as heterozygous at a very low allele frequency of 0.00014 or 0.00095 in the East Asian population further suggests that the c.834 G>T mutation was more likely to be inherited through the paternal line instead of arising spontaneously in the patient.

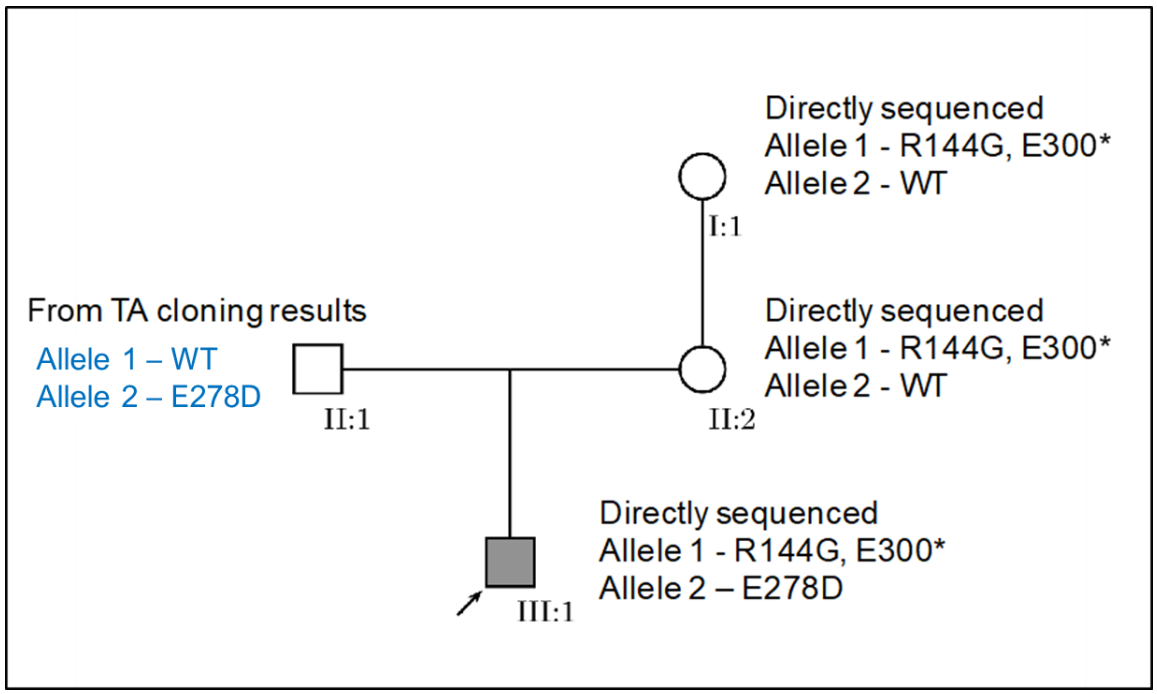

Figure 3.3.6. Pedigree diagram for patient.
The pedigree diagram was generated using the software available at http://www.pedigree.varphi.com/cgi-bin/pedigree.cgi. All alleles in black text were determined through experimentation and those inferred are in blue text.

3.3.2 Protein expression in patient cells

Once the orientation and the compound heterozygous nature of the CRACR2A mutations was confirmed, the expression of the protein in a healthy control (HC) and patient PBMCs was compared using western blots. A range of CRACR2A antibodies were tested in Jurkat cells and with HC PBMCs with varying results. The bulk of the repeats were performed with a Proteintech Ab in Table 2.1.3. When it came to western blotting using protein lysates from patient cells, there were a range of issues that presented themselves. There was limited sample available and the majority was used for calcium flux experiments. Thus, for some western blots the samples were from the flow though of the negative selection T cell columns, so both experiments could be performed from a single blood sample, as seen in Figure 3.3.7. This limited the amount of T cells in the PBMCs which was already low due to the patient phenotype. Low T cells were a problem, since these cells are known to have the highest level of expression of CRACR2A in PBMCs (Srikanth, Jung, Kim, *et al.*, 2010). The patient had a lower total protein concentration compared to HCs, as determined by BCA assay and total protein staining of the WB membrane by ponceau S staining. As a result, for every WB run with patient sample the maximum amount of patient lysate was loaded, which often appeared to be less than the target of 20 µg per well, as seen in the loading controls.

An example of the western blots produced with fresh patient cells and HC is presented in Figure 3.3.7. The loading control GAPDH is low for the patient compared to the HC. The long full length isoform of CRCRA2A (90 kDa) appears to be present at a comparable density to HC. The short isoform of CRACR2A

(45 kDa) was only present faintly or not detected in the patient cells when compared to HC. No band was seen at the predicted size of 34.5 kDa for the E300* truncated protein in the patient sample.

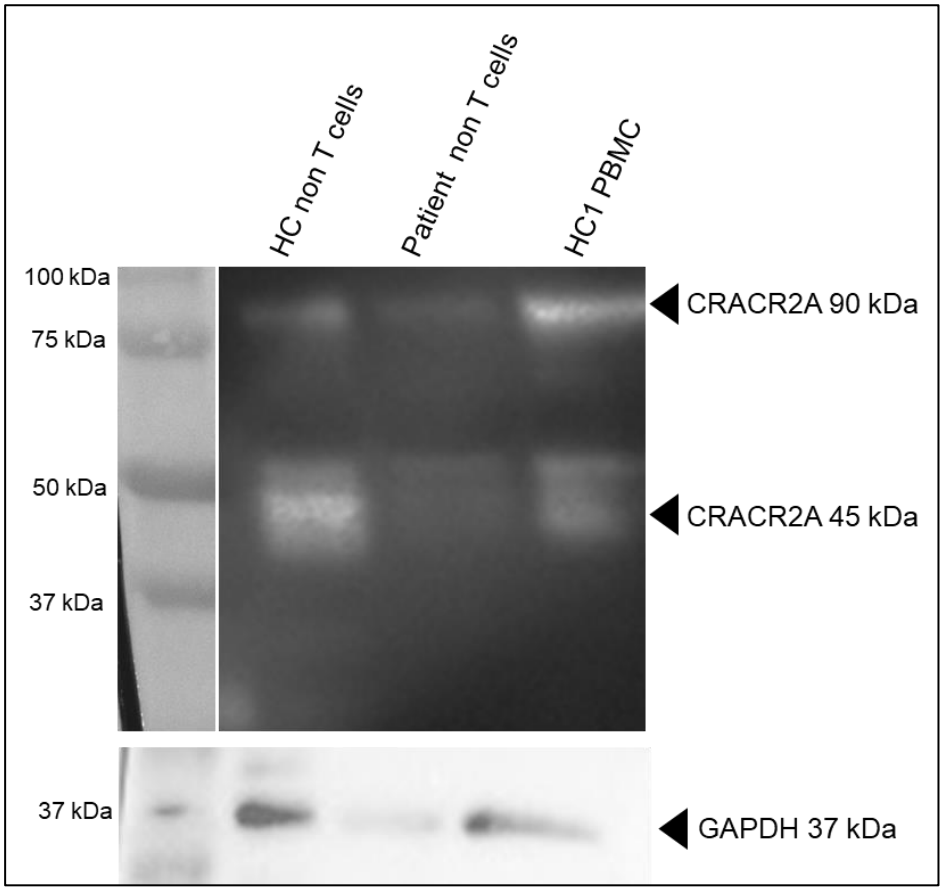

Figure 3.3.7 CRACR2A protein expression in PBMCs
Lysate for the non T cells samples was the flow through of the negative section T cell column, using methods in Sections 2.2.3.3.2. Lysate made in NP40 buffer and 20 µg loaded per well, or maximal loading for the patient, into 4-15 % BioRad gradient gels. Protein was blotted with primary antibodies CRACR2A (ProteinTech) 1:800 and GAPDH at 1:10000. More details can be found in Section 2.2.6.1.

The western blots were repeated in cultured and expanded T cells for the patient and HC (Figure 3.3.8). The same outcomes were seen in these cells, with regard to comparable full length protein, less short isoform and no truncated CRACR2A.

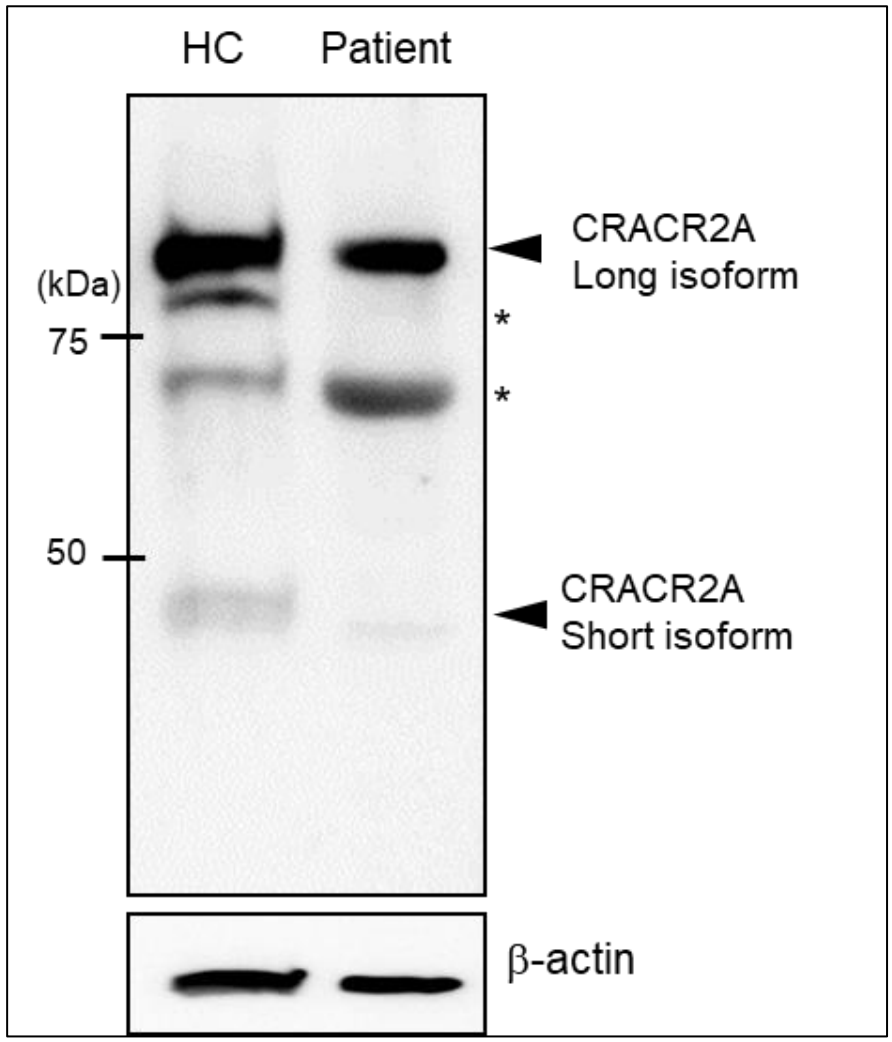

Figure 3.3.8 CRACR2A protein in expanded T cell population

This WB data was generated by Sonal Srikanth (UCLA). PBMCs were cultured and the T cells expanded before lysate was made by sonication. All method details can be found in Section 2.2.6.2.

* represent nonspecific bands. These bands are thought to be unspecific as no cleavage sites are seen in the protein which would give these theoretical sizes. Due to the small amount of sample available antibody dilutions or no primary controls were not performed at this time, but could be run in the future to see if the bands are non-specific.

3.3.3 Calcium flux in T cells

The reduced proliferation response in patient T cells and the normal B cell development observed *in vitro,* meant that the T cells were a likely candidate for the patient phenotype. This was enforced by CRACR2A role in the CRAC channel which is essential for T cell function such as cytokine production and proliferation. T cells are particularly sensitive to changes in calcium concentration fluctuations (Christo *et al.*, 2015).

In order to determine if the compound heterozygous mutations identified in CRACR2A were pathogenic, the calcium flux response was measured in the patient T cells and compared to a healthy control. Measuring calcium flux in T cells can be done using a range of techniques using calcium sensor dyes. The dyes are retained in the cells and fluoresce at different wavelengths depending on whether calcium is bound or unbound. The change in florescence can be measured at the two wavelengths and the ratio calculated (bound : unbound calcium). A higher ratio means more calcium is bound to the dye, and so shows that more calcium is present in the cell.

The techniques used to measure calcium flux in the patient T cells included:

- Flow cytometry
- Florescent plate readers
- Live cell imaging

3.3.3.1 Calcium flux using flow cytometry

Flow cytometry is a powerful technique as it allows for the grouping of cell types in a mixed population of cells. The markers used to separate the different populations can be either internal or external proteins, using specific antibodies with fluorophores attached that absorb and emit at different wavelengths. Flow cytometry had been used to compare the calcium flux response in STIM1 patient T and NK cells with healthy control in our lab previously (Parry *et al.*, 2016).

Using flow cytometry to compare the calcium flux response of HC and patient T cells was not feasible. Multiple protocols and parameters were tested using both the Jurkat cell line and HC PBMCs. The main limitation of this method was small cell numbers isolated from PBMCs. This meant there was only a small number of repeats and conditions that could to be tested with each blood sample. The low cell numbers also meant no data was gained from subpopulations of T cells such as T helper cells and the high baseline measurements due to manipulation and agitation of the cells. The many limitations of this method meant an alternative was needed.

3.3.3.2 Calcium flux using plate readers

Due to the issues with low cell numbers during flow cytometry experiments, the Flex Station was a possible alternative method of measuring calcium flux in patient and HC T cells. The Flex Station is a fluorescent plate reader that takes multiple readings over time. Fura-2 was the calcium sensor dye used with this method. As a plate reader is used, the same cells are measured over the length of the experiment, which reduces the cell numbers required compared to flow cytometry, which uses a stream of cells. Previously, this techniques has been used to monitor the effect of CRAC channel changes in adherent cell lines, and so some method development was needed for suspension cells. Jurkat cells were used to work up the protocol and drug stimulations before using HC or Patient T cells, both isolated using the negative selection columns.

The experiments differ from the flow cytometry protocol, as more flexibility was available. Instead of having the cell in calcium and stimulating them with TG or TCR activation, the cells start in calcium free media. This means that when the cells are stimulated the initial response is from the emptying of the calcium stores. In the human primary T cells, not much changes in the calcium ratio at this stage. This could be due to the small calcium stores of T cells or because the stores are depleted due to processing. Jurkat cells in the initial optimisation showed an emptying of these stores at this time in the experiment and the flux response returned to baseline by 900 seconds. At this point calcium is added back into the cells, the stores are replenished and the effect of the stimulation is shown. The calcium add back experiments provide additional data points and measurements. Patient sample became available for five Flex Station experiments. For the last two of the experiments, a single well of Jurkat cells was run as a system check, and both experiments had comparable Jurkat responses to those seen when optimising the protocol. Jurkat cells were introduced as an additional control, as well as the HC, because on the 2018-02-12 neither HC or patient T cells responded to stimuli or calcium being added back into the system.

The calcium flux experiments run using patient T cells are summarised in Table 3.3.3. For all of these experiments HC was run at the same time as the patient samples. HC gave a response to TG and TCR in most experiments, though there was a lot of variability in the maximal calcium influx. This may be because the same HC individual was not available for blood donation for all of these experiments.

Table 3.3.3 Summary of Patient sample responses on the Flex Station

Date	Jurkat control	HC response	Patient response
2017 10 27	x	HC with duplicate wells, good response	Low cell number, single well only, low/no response
2017 11 22	x	Had abnormal response	2 samples isolated separately for patient, low/no response
2018 02 12	x	No response, not added to Figure 3.3.9	No response, not added to Figure 3.3.9
2018 03 14	√	Had good response with TG and TCR stimulations	Patient unable to attend
2018 03 16	√	Had good response	Peak response comparable to HC, reduced sustained response
2019 04 13	√	Cell number too low, not added to Figure 3.3.9	Cell number too low, not added to Figure 3.3.9

The patient T cells gave little to no response in most cases. However, during the 2018-03-16 experiment there was a response seen in the patient cells, as seen in Figure 3.3.9. The initial add back response appeared to be comparable to the highest HC response, this calcium influx was not sustained, but instead drops off over time which had not been seen in any HCs, giving a similar profile as that seen in the Jurkat cell line (Figure 2.2.12) rather than the HCs.

The Flex Station produced more reliable data than that produced by flow cytometry. However, there were still limitations. There was still a higher number of cells needed, only eight wells could be run at one time, no population or single cell calcium data was possible and varied responses were seen from the patient sample. Hence, it was hard to fully trust the calcium flux data produced using this technique. So, a collaboration was established with the Gwack laboratory (UCLA) to gain access to expertise and new, more sensitive and reliable techniques for measuring calcium flux in patient T cells.

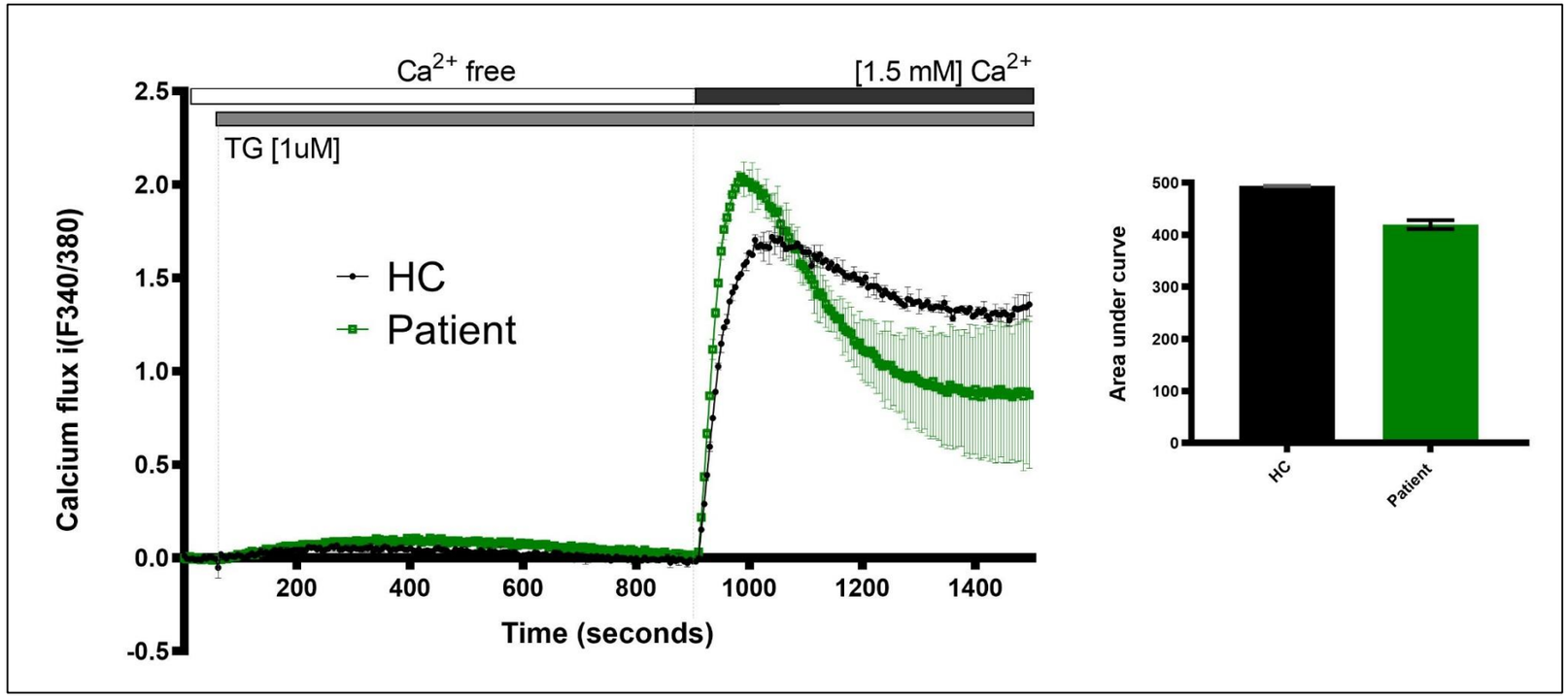

Figure 3.3.9 Calcium flux response to TG, CRACR2A patient T cells compared to HC

Data from patient and HC displayed from 2018-03-16 (Table 3.3.3). For all these samples a DMSO control was run at the same time and showed a reduced calcium influx. No significant difference was seen between patient and HC for Area under the curve, but the patient cells do not seem to have an as sustained calcium add back response.

3.3.3.3 Calcium flux using single cell imaging

The Gwack lab used single cell imaging to measure calcium flux in cell lines and primary T cells. This is a sensitive and established method and it too uses Fura-2 as the calcium sensor dye. Cells are adhered to a coverslip and solutions can be passed over the cells, allowing for changes in calcium concentration and stimulation of the cells with drugs. The cells are imaged in real time, with a fluorescent microscope, therefore allowing for a Fura-2 ratio to be generated. Once the experiment is complete, the calcium flux of individual cells can be observed over time. The system allows for the filtration of non-responding cells during analysis. For each sample, fifty cells were randomly selected for further data collection from the total population captured on the coverslip.

3.3.3.3.1 Culture of T cells from frozen

Due to the nature of the international collaboration, fresh primary samples could not be available for the experiment using patient cells. Instead the patient PBMCs were isolated and frozen at -80 ˚C in Leeds, before being shipped on dry ice to UCLA. A T cell culturing and proliferation protocol needed to be developed to expand the T cell population of the patient samples available, as freeze/thawing results in a decrease in the viable cell number.

Before using the patient sample, the experimental approach was tested and optimised using a HC sample. HC PBMCs ($14x10^6$ cells) were stored at -80 ˚C with 10 % DMSO for 72 hrs and then cultured in RPMI+10 % FBS for 24 hrs to rest the cells. The cells were stimulated with anti-CD3 10 µg/mL, anti-CD28 10 µg/mL and 20 U/mL IL-2 for 4 days, before being frozen, revived and rested (2^{nd} Defrost) or kept at rest for 38 hrs (1^{st} Defrost). In order to test the function of the expanded T cells, cytokines were measured by flow cytometry after PMA and ionomycin stimulation. The CD4+ population was gated on and the expression of IFNγ and IL4 measured.

The cytokines measured were chosen as they are produced by different subpopulations of T helper cells. Th1 cells produce IFNγ and are essential for the establishment of cellular immune responses. Th2 cells produce IL4 and facilitate immunoglobulin E synthesis by B cells and immunoregulation (Torres, Dutra and Gollob, 2004; Raphael *et al.*, 2015).

The culturing and freeze thawing of the HC T cells did not negatively affect the function of the cells as seen in Figure 3.3.10. The CD4+ population was still present and the cytokines IFNγ and IL4 were both produced, meaning that the both Th1 and Th2 populations expanded.

This culturing scheme was performed on the patient and HC PBMCs stored in parallel. The patient cells did not expand to the same extent as the HC, as was seen in the clinical tests presented in Table 3.1.4. The cell populations did expand sufficiently well for functional tests to be performed. However, the CD8 population expanded to a greater extent in the patient than the CD4 cells, meaning the patients CD4:CD8 ratio was even more in favour of the CD8 cells then what had been observed in a fresh sample. This shift in the ratio of T cell populations is part of the patient phenotype, as seen in Table 3.1.4, but may be exaggerated in the expanded cells.

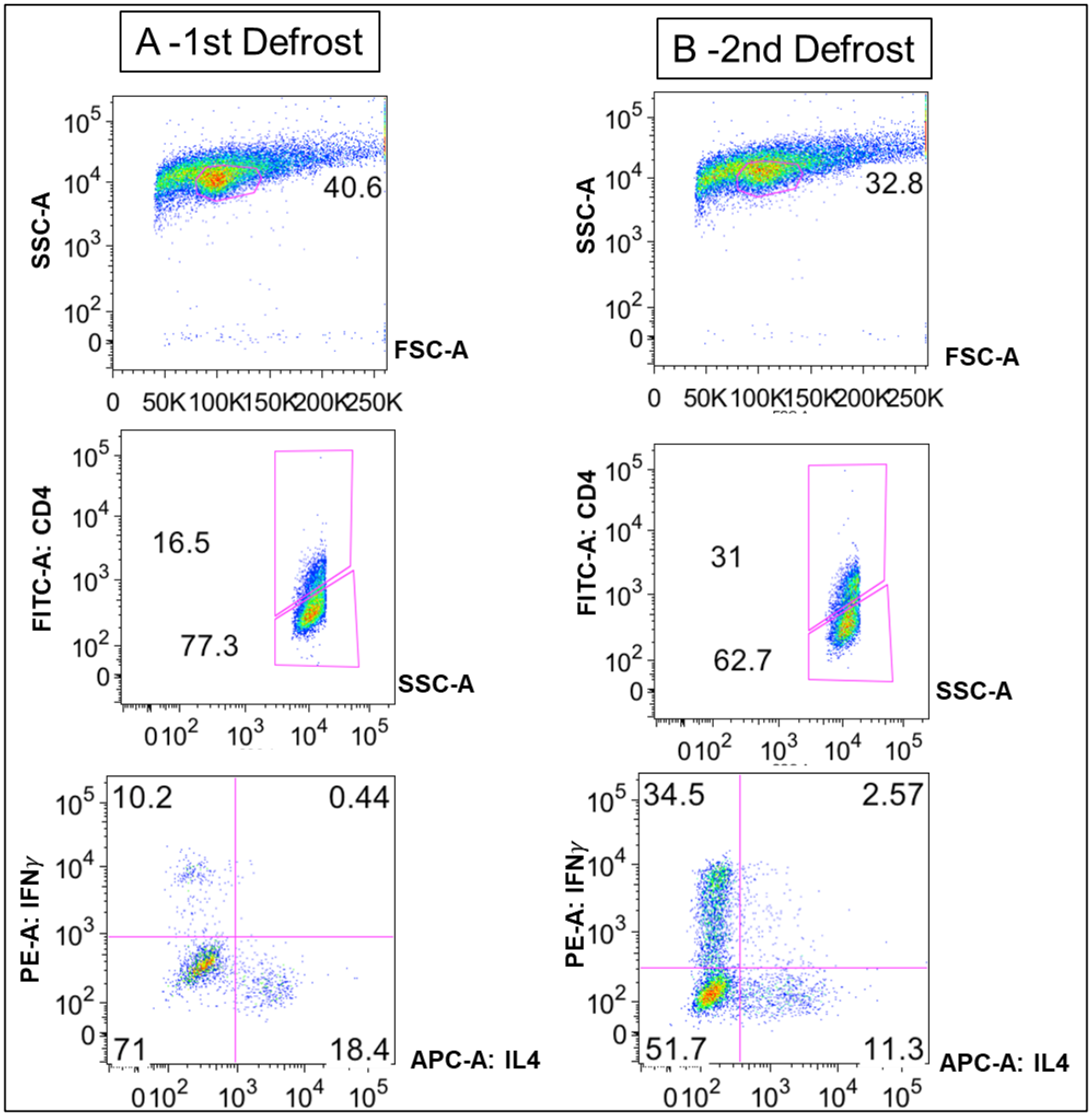

Figure 3.3.10 Intercellular signalling of HC T cells after expansion
Culturing and flow cytometry protocols can be found in Sections 2.2.3.3.3 and 2.2.8.6.

3.3.3.3.2 Calcium flux of patient T cells

The calcium flux for expanded T cells for the patient and HC was performed using single cell imaging (Figure 3.3.11). The cells were kept in calcium containing solution during the experiment and were stimulated with CD3 x-link for a physiological relevant response and with ionomycin to show the maximal response of the cells. Figure 3.3.11B shows the zoomed in response of the patient and HC cells with TCR activation. The patient shows a reduced calcium flux response compared to HC, though there is a slight increase in calcium influx, which would not be seen in STIM1 deficient patients (Rice *et al.*, 2019). In panel A, the

ionomycin response can also be seen, the maximal response of the patient is not as high as that seen in the HC. The cells seem to take longer to reach the maximum calcium influx and there is more variability between the cells, compared to the tight groupings seen in the HC.

In summary, in order to understand if the patient compound heterozygous mutations in CRACR2A were pathogenic, the calcium flux response was measured in the patient T cells and was found to be reduced compared to HC, whether using single cell imaging or the plate reader method. Although the calcium flux was reduced, this was not to the same extent as seen in patients with deficiency of STIM1 or Orai1.

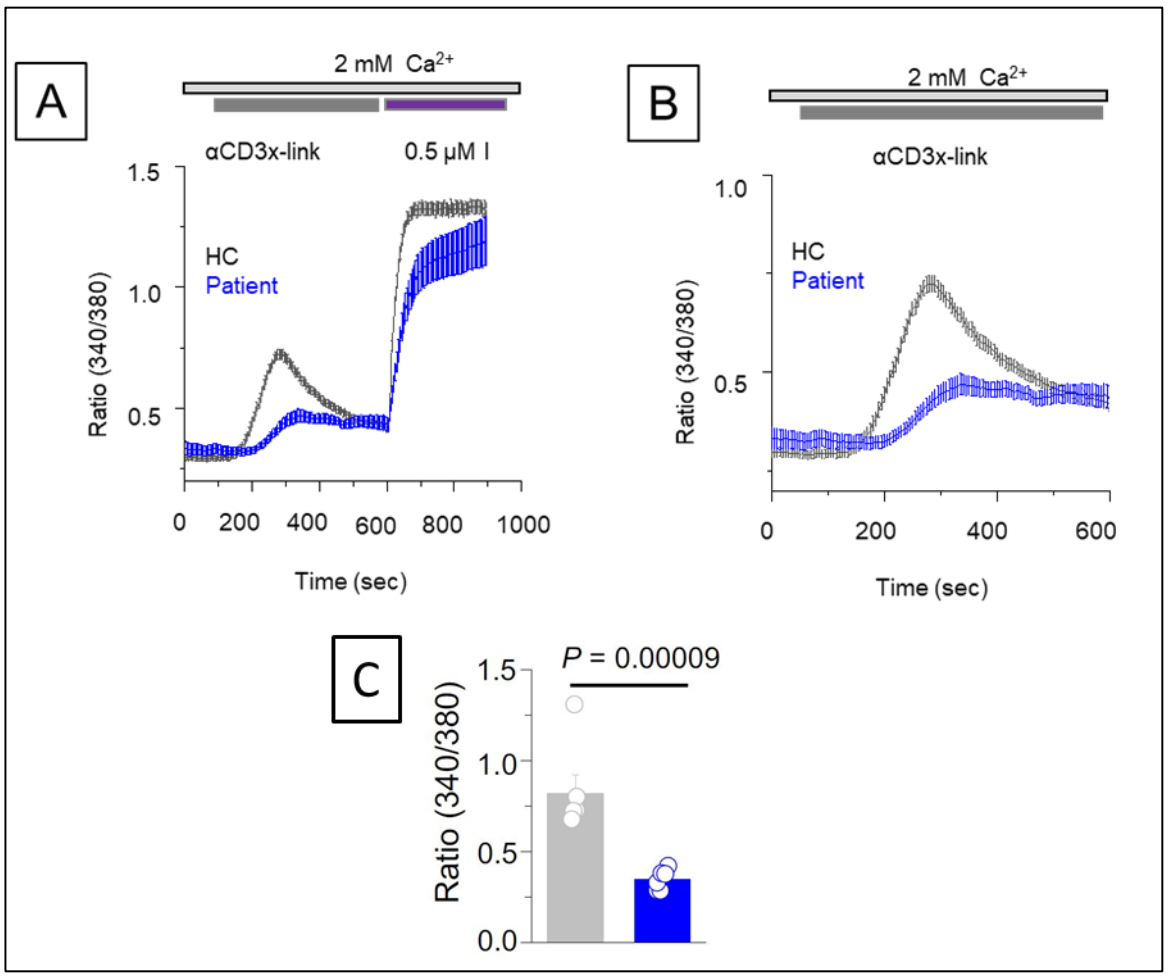

Figure 3.3.11 Calcium flux of expanded HC and Patient T cells

Data generated in collaboration with the Gwack lab (UCLA). Each sample represents 50 cells. For method details see Section 2.2.7.1.3. A) CD3 and ionomycin response of HC and patient T cells. B) zoomed in on the CD3 response, displaying the same data as in A).C) Averaged (± SEM) SOCE responses of B) from six independent experiments.

For this data the author developed the expansion method for these cells and performed the initial isolation of the PBMCs from the HC and patient blood, see methods in Sections 2.2.3.1 and 2.2.3.3.3. During the initial test the author observed these experiments, but was not able to participate due to the extensive training needed for this technique.

3.3.4 JNK signalling in T cells

The compound heterozygous mutations in CRACR2A appeared to have reduced the calcium flux response in patient T cells compared to HC. Another function of the protein is within JNK signalling due to the GTP/GDP binding and hydrolysis domain. The p-JNK signalling was measured in the expanded T cell populations for the patient and HC. Compared to HC, the JNK signalling was significantly reduced in the patient CD4+ cells when the TCR was activated (Figure 3.3.12). The patient cells did not increase the p-JNK levels upon stimulation and remained at baseline levels.

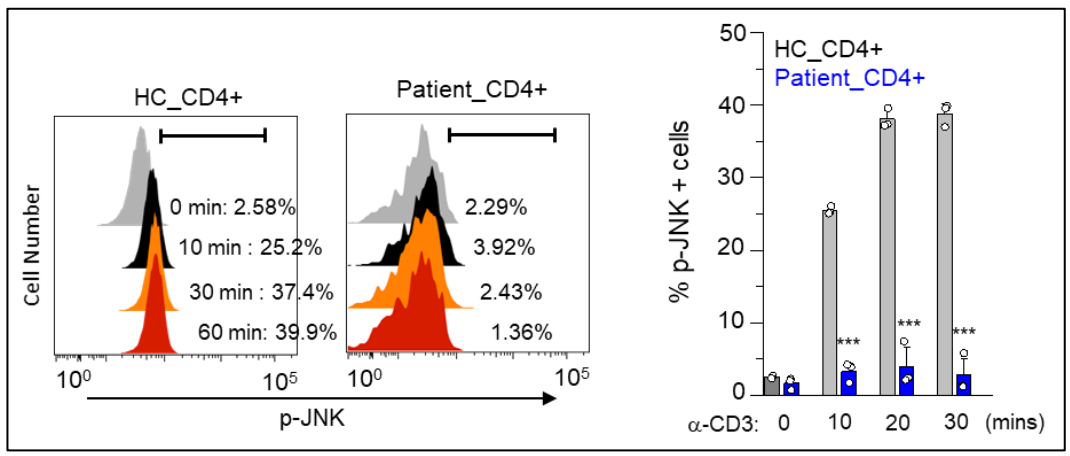

Figure 3.3.12 p-JNK of expanded HC and Patient T cells

Data generated in collaboration with the Gwack lab (UCLA). Method details are given in Section 2.2.8.3.
For this data the author developed the expansion method for these cells and performed the initial isolation of the PBMCs from the HC and patient blood, see methods in Sections 2.2.3.1 and 2.2.3.3.3.

3.3.5 Cytokine studies

An additional functional test performed on the expanded T cell population of the patient and HC was to look at the cytokine expression in response to PMA and ionomycin stimulation. The CD4+ population was gated on and the expression of IFNγ and IL-4 was measured by flow cytometry, as seen in Figure 3.3.13.

The patient cytokine profile shows a shift towards Th2 cells with the high expression of IL-4. These cells facilitate immunoglobulin E synthesis by B cells and immunoregulation and are normally present at a lower level than Th1 cells, which are involved in establishment of cellular immune responses.

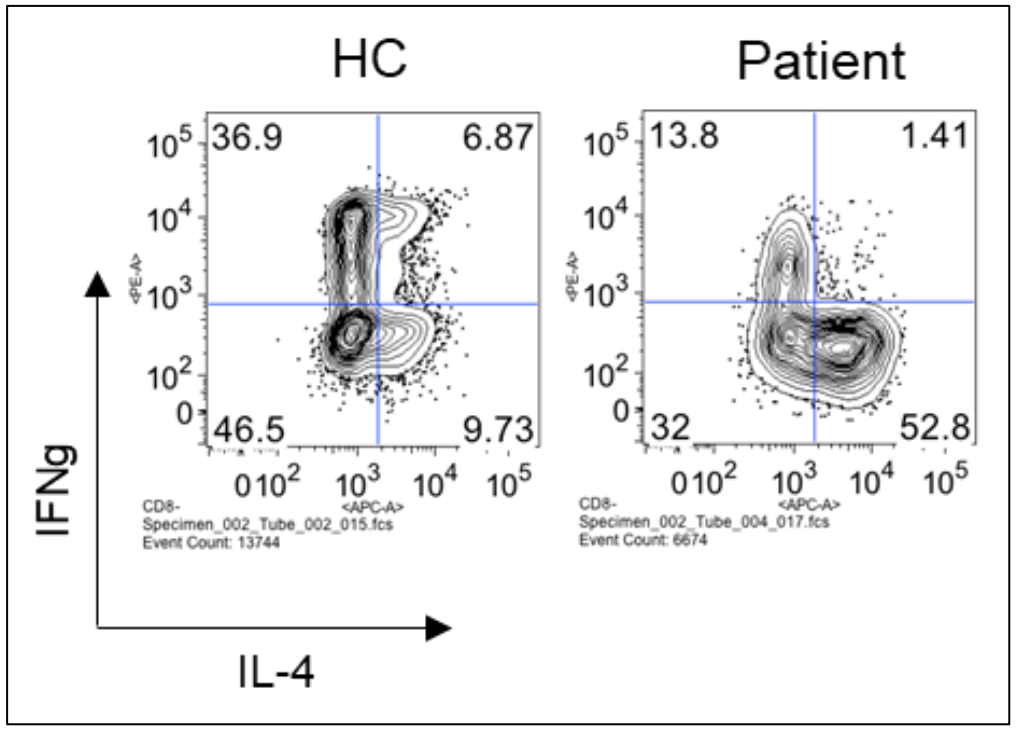

Figure 3.3.13 Cytokine expression of expanded HC and Patient T cells

Data generated in collaboration with the Gwack (UCLA). Culturing and flow cytometry protocols can be found in Sections 2.2.3.3.3 and 2.2.8.6.

For this data the author developed the expansion method for these cells and performed the initial isolation of the PBMCs from the HC and patient blood, see methods in Sections 2.2.3.1 and 2.2.3.3.3.

3.4 Key Findings

In this chapter, a range of tests were performed on primary samples of a single patient to further understand the cause of their disease. WES identified two potential genes of interest *DHSR4* and *EFCAB4B*.

- The mutation, c.373 Cga>Tga (p.125 R>*), in *DHSR4* was considered unlikely to be pathogenic as it was a heterozygous mutation, with a WT allele being present in the patient.
- The mutations in CRACR2A , R144G, E278D and E300*, were confirmed to be compound heterozygous mutations, through cloning of the patient cDNA and sequence analysis of maternal genomic DNA
- Functional studies on patient primary cells showed:
    - Patient B cells function normally *in vitro* (T cell independent assay)
    - Mildly reduced calcium flux in patient T cells compared to HC
    - Significantly reduced p-JNK signalling in patient T cells compared to HC
    - Patient T cells had reduced cytokine response compared to HC and a shift towards the Th2 cells

3.5 Discussion

The aims of this chapter were to confirm potential mutations and segregation in a patient with PID and to determine if these mutations were pathogenic and responsible for the patient phenotype, by looking at protein specific function in primary samples. The key findings summarised above show that these aims where mostly achieved. The CRACR2A mutations, R144G, E278D and E300*, and their segregation were confirmed in the patient. A significantly reduced function of p-JNK signalling and a mildly reduced calcium flux was found in patient primary T cells compared to healthy control. Both functional pathways have been linked to CRACR2A specific function previously in the literature (Srikanth, Jung, Kim, *et al.*, 2010; Srikanth *et al.*, 2016).

3.5.1 Whole Exome Sequencing

The importance and limitations of WES in identifying novel mutations is rare disease is heavily documented in literature (Richards *et al.*, 2015; Biesecker and Harrison, 2018) and is highlighted in this chapter. WES has expanded the field of PID and led to the discovery of many novel genes and mutations associated with this disease (Gallo *et al.*, 2016). WES was able to identify novel mutations in the patient discussed here and through filtration using databases and the patient phenotype this list of potential genes was filtered down to two candidates. These two genes are not currently on any NHS PID gene panels and the mild phenotype of the patient meant these mutations were unlikely to be discovered by methods other than WES. However, WES produces sequencing data for all coding regions of the genome but the coverage is not deep. This means that mistakes can arise. This is shown with the DHRS4 gene. The WES approach identified the gene to have a homozygous mutation, but when this exon was sequenced by Sanger sequencing the mutation was found to be heterozygous (Figure 3.3.1). This meant the mutation was unlikely to be pathogenic as there is still a WT copy of the gene present in the patient. This example highlights the importance of confirming WES results with sequencing techniques that provide deeper coverage.

3.5.2 CRACR2A mutations

In this case study, three heterozygous mutations were confirmed in CRACR2A. The mutations were found to be compound heterozygous through cloning of the patient cDNA and sequencing of the maternal genomic DNA. The maternal allele (R144G and E300*) and the potential paternal allele (E278D) can be seen in Figure 3.3.5.

The maternal allele is not likely to be expressed in the patient due to the lack of truncated protein seen in WB of patient T cells (Figure 3.3.8) and due to the low levels of this allele being present in patient cDNA observed during cloning. As a result only the E278D allele is expressed *in vivo* in the patient. Since CRACR2A is expressed at comparable levels, for the long isoform and reduced for the short isoform, compared to healthy control the mutation is unlikely to affect protein stability, but could affect protein function.

The compound heterozygous state may lead to a functional deficiency as no WT protein is present in the patient. This means that recessive mutations could now cause changes in function in cells. As the maternal allele is unlikely to be expressed this means that the mutations could also cause disease through haploinsufficiency, the second allele is unable to produce sufficient protein or activity to function properly.

3.5.3 Use of primary samples

Performing functional studies on primary samples is a very powerful way of looking at a patient phenotype, especially when the mutations are known so particular pathways of interest can be tested. However, using primary samples has a host of associated risks and limitations. The samples are rare and precious, so not many replicates are available, this can limit the confidence in the results. The primary blood samples contain multiple cell types as well as sub populations which can lead to natural variation between individuals before the mutations of interest comes into consideration. This variability cannot be controlled for, especially when few patients with the same mutation or affected protein are available. This is especially true here where the patient number n=1.

The final primary patient functional data presented in this chapter used cultured patient cells, instead of fresh patient sample. Fresh patient blood samples were not available when working with the Gwack lab and so isolated PBMCs were shipped to LA and then expanded prior to use in experiments. This meant that the calcium, cytokine, p-JNK and protein expression data (Figure 3.3.8, Figure 3.3.10, Figure 3.3.11, Figure 3.3.12 and Figure 3.3.13), was all generated using these expanded cells which is not the ideal representation of patient primary samples. This is especially true due to the patient phenotype, which showed that the CD8+ T population proliferated more than it did in the HC sample, and the already low C4+ cells did not expand as well as they did for the HC.

In order to test if the expanded cells were comparable to fresh samples an experiment was planned that tested three HC samples. The PBMCs were isolated and half were used in functional experiments, including JNK, calcium flux and cytokine studies. The other half were frozen and the culturing method and functional studies performed. Unfortunately, due to time constraints and equipment issues not all planned experiments could be completed. This experiment was expected to show minimal differences between the fresh and the frozen and expanded cells in regards to functional studies but with potentially reduced viability (Sadeghi *et al.*, 2013; Panch *et al.*, 2019).

Chapter 4 CRACR2A cell line work

4.1 Introduction

As seen in the previous chapter, there are many challenges in using primary patient cells to determine if the identified mutations are responsible for the phenotype observed in the patient. In this case, with confirmed compound heterozygous calcium release activated channel regulator 2A (CRACR2A) mutations (Allele 1: E278D and Allele 2: R144G and E300*), the patient T cells appeared to be the most affected. However, the low T cell numbers present in the patient blood samples and difficulties expanding this T cell population in the laboratory made it difficult to generate reproducible and reliable functional data. As a result, alternative methods were used to further explore if the mutations identified in this patient could be affecting the function of CRACR2A and, therefore, be causing the phenotype seen. There are several *in vitro* approaches available to do this, and in this chapter I will be focusing on the use of established cell lines.

4.1.1 Cell lines as a model for studying effects of mutations

The use of cell lines to investigate the effect of mutations on a cell type is well established. The two main avenues of investigation using cell lines are stopping the expression of a specific protein or expressing mutant proteins. Gene silencing can elude to the function of the protein and provide information about pathways the protein may affect. Knock out (KO) cell lines can also be used in combination with expression of mutant proteins, as the endogenous protein would not be present in the cells.

In vitro modifications to cell lines can be induced in a transient manner or permanently by creating stable cell lines. Transient changes by use of RNA interference (RNAi) or expression plasmids are a good tool for investigating the effect of mutations and proteins, in short term studies. However, transient modifications are not useful for long term functional studies as the DNA mutation changes are not incorporated into the cell line genome and therefore are not retained during cell culture and expansion

4.1.1.1 Gene silencing

Transient gene silencing is achieved by RNAi. The expression of a target gene is silenced or knocked down by the selective inactivation of its corresponding mRNA by double-stranded RNA (dsRNA), that is delivered to the cytoplasm of cells. Small interfering RNAs (siRNAs) lead to the degradation of a target mRNA, therefore stopping the production of the protein of interest, leading to a decrease in its levels within the cell and eventually knockdown (KD) (Keefe, 2013).

Stable gene silencing is induced by changing the cell genome, rather than the mRNA. Clustered regularly interspaced short palindromic repeats (CRISPR) and CRISPR associated protein 9 (cas9) are useful tools for causing specific genome editing. Guide RNA binds to a specific region important for the expression of a specific gene. The cas9 enzyme is then able to cleave the target DNA strand and DNA repair mechanisms in the cell repair the cleavage by removing the remaining complementary sequence in this region, therefore, allowing genome editing (Adli, 2018).

4.1.1.2 Expression of recombinant protein

Transient expression of recombinant protein in cell lines requires expression plasmid vectors, with the protein of interest encoded, to be transfected into the cell. The recombinant protein is normally overexpressed in these systems as the expression is not controlled by the genome. The recombinant protein can be designed to have a variety of modifications compared to the endogenous protein, depending on the experiment. Tags on the protein such as FLAG and His, allow for detection and capture of the protein. Fluorescent tags can allow for live cell imaging and mutations can be included into the protein to explore their effects.

Stable cell lines can also be made, which incorporate similar changes as mentioned above into the genome. This can be achieved by viral transduction or CRISPR. In stable cell lines the expression of the protein can be controlled and maintained. This means the expression of the protein can be made comparable to the endogenous levels and can therefore provide a better functional comparison to the wildtype protein.

4.1.2 Use of cell lines in CRACR2A research

The main cell type used for CRACR2A research is the Jurkat cell line, an immortal T cell. CRACR2A expression is shown to be high in lymphoid cells, especially basophils, NK cells and T cells, particularly memory T cells (Uhlen *et al.*, 2010; *The Human Protein Atlas*, 2020). In 2010, siRNA KD of CRAC2A were performed in Jurkat cells and HEK-293 cells (Srikanth, Jung, Kim, *et al.*, 2010). Both cell lines showed a decreased thapsigargin (TG)-induced store-operated calcium entry (SOCE) and reduced interleukin-2 (IL-2) synthesis. Jurkat cells also showed reduced the clustering of transfected stromal interaction molecule 1 (STIM1) and calcium release-activated calcium channel protein 1 (Orai1) in response to depletion of endoplasmic reticulum (ER) Ca^{2+} stores by TG treatment. Expression of CRACR2A increased SOCE and apoptosis in these KD cells. A $CRACR2A_{EFMUT}$ was expressed which was constitutively active and resulted in STIM1 clustering, increased SOCE and apoptosis. HeLa cells were also used in this paper for immunoprecipitation experiment and showed that CRACR2A was a binding partner of Orai1.

Jurkat cells in combination with mouse T cells have been used to identify the function of the CRACR2A long isoform (Srikanth *et al.*, 2016). The isoform was shown to localise to vesicles that translocate toward the immunological synapse and regulate JNK activation downstream of the T cell receptor (TCR). The role of CRACR2A in dynein transport was also demonstrated in Jurkat cells, though purified protein and HEK293 cells were also used (Wang *et al.*, 2019).

The other main cell line used is primary human umbilical vein endothelial cells (HUVEC). These have been used to identify CRACR2A role in endothelial tube formation and Weibel-Palade bodies (WPBs). In these cells, CRACR2A KD showed no effect on Ca^{2+}-release activated Ca^{2+} (CRAC) channels and SOCE (Wilson *et al.*, 2015).

4.1.3 Aims

The primary cell work presented in Chapter 3 strongly suggested that the CRACR2A mutations could be causing the patient's phenotype in this case study. However, the most compelling functional data was all performed in expanded T cell populations from the patient. The subtypes of the patient T cells were likely to be biased towards the CD8 population (Table 3.1.4) which have been shown to be less receptive to calcium flux stimuli (Arrol *et al.*, 2008). As a result any difference seen between patient and HC cell (Figure 3.3.8 tot Figure 3.3.13) could be a result of the T cell subtypes rather than the CRACR2A mutations directly. As a result, it was important to look at the patient alleles in isolation, using cell lines. The E278D mutation was of particular interest as the allele with the 300* mutation was shown to not be present in T cells (Figure 3.3.8).

The aims of the work presented in this chapter were:

- To make CRACR2A KO Jurkat cells
- Express patient mutations in KO cell lines
- Determine if these mutations affect the expression, location and function of CRACR2A

A collaboration was put in place with the Gwack lab at UCLA (Department of Physiology, UCLA, Los Angeles, USA). A three month secondment was organised with the aim to further explore the CRACR2A mutations identified in the patient presented in Chapter 3.This lab has been instrumental to CRACR2A research as they discovered this protein's role within the CRAC channel. Importantly, they had established protocols in place for the generation of KO CRACR2A Jurkat cells, retroviral transduction of mutated CRACR2A and single cell calcium imaging capabilities.

4.2 Method Strategies

In this chapter multiple methods and reagents were used in similar experiments, as they were performed in different laboratories. This is because not all the same reagents were available in all locations. During the secondment in LA, the Gwack Lab standard protocols and reagents were used rather than ones I had previously optimised. The protocol used is specified in the legends for all figures.

The simplified protocol for viral transfection is shown in Figure 4.2.1 and more details can be found in Chapter 2.

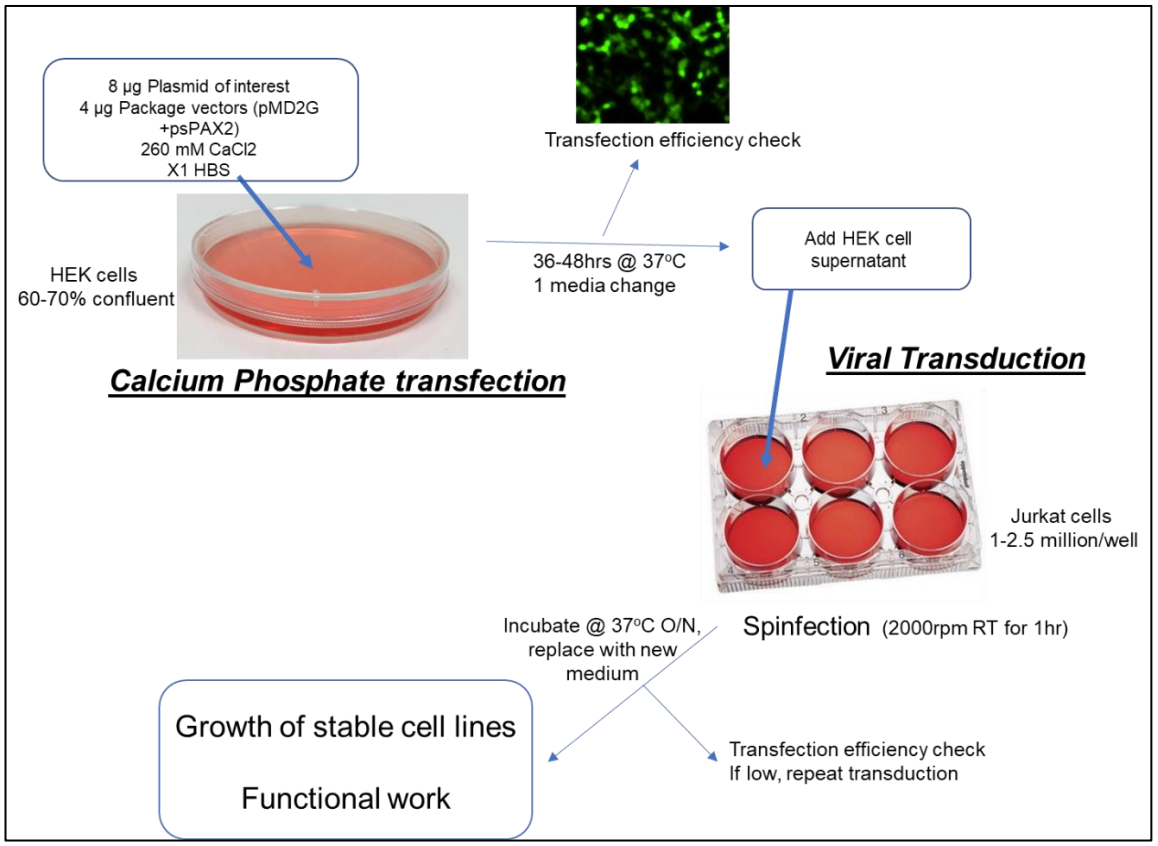

Figure 4.2.1 Simplified viral transduction method
Main steps of viral transfection shown, more detail can be found in the method Section 2.2.5.

4.3 Results

4.3.1 CRAC channel proteins expression in Jurkat cells

In order to explore the effect of the patient mutations, R144G, E278D and E300*, on the function of CRACR2A, the Jurkat cell line was used as a T cell model. The patient T cell related phenotype led to this selection due to the reduced T cells proliferation, cell number reduced calcium flux seen in the patient T cells. Jurkat cells express the main proteins of the CRAC channel, Orai1, STIM1 and CRACR2A, at detectable levels as can be seen in Figure 4.3.1. As a result, this cell line is a good model to study the effects of mutations on the function of the CRAC channel.

At the beginning of this project, the expression of CRAC channel related proteins was looked at in the following three cell lines that were planned to be used in future experiments: Jurkat cells as a T cell model, HEK293 to check transfection and transduction efficiency and HEK293T as donor cells in viral transduction. All three cells lines examined express the CRAC channel proteins at their expected sizes, although the level of expression differs (Figure 4.3.1). HEK293 and HEK293T cells have a higher level of STIM1 expression than Jurkat cells. The Jurkat cell line gives two bands for Orai1 compared to the single band at 50 kDa of the glycosylated protein seen in the two HEK derived lines (Cox *et al.*, 2013; Dörr *et al.*, 2016). CRACR2A is expressed in all three cell lines, although it is expressed at low levels in the HEK derived lines, especially HEK293.

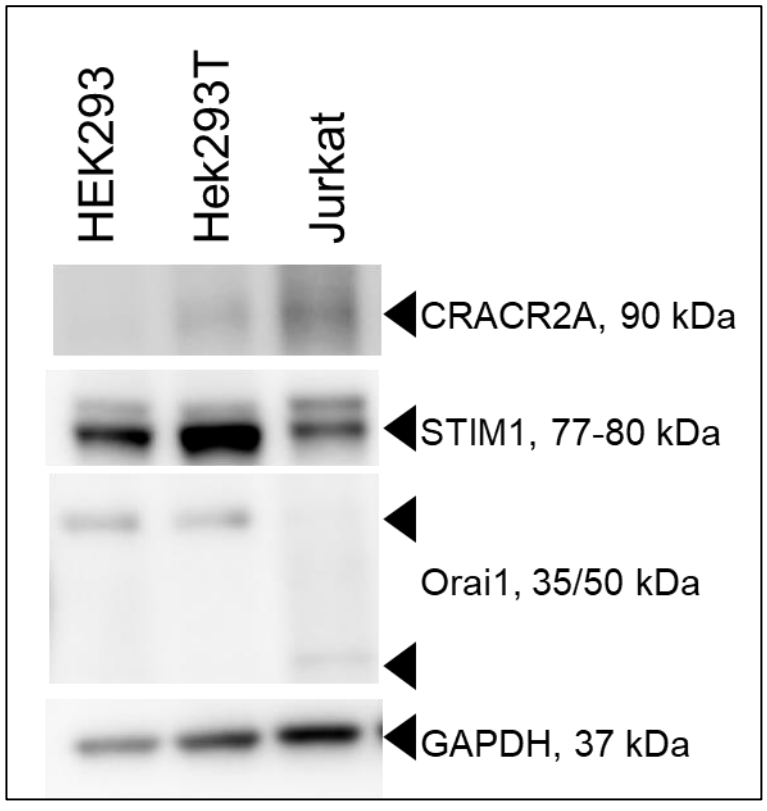

Figure 4.3.1 CRAC channel protein expression

Three cell lines were examined for the expression of the CRAC channel proteins. 20 µg total protein from each cell line/lane was resolved in 15-well gels and blotted as described in Section 2.2.6.1. Antibody details are given in Table 2.1.3 and dilutions used in this experiment were GAPDH (1.10000), Orai1 (1.100), STIM1 (1.250), CRACR2A (proteintech 1.700)

4.3.2 Immunofluorescence to examine CRAC channel proteins

IF was attempted to look at the interaction of CRACR2A in cells, with the CRAC channel components, STIM1 and Orai1. The aim was to explore potential differences between patient and HC T cells, and between cell lines expressing different patient mutations. This avenue of study was started due to the difference in the calcium flux response shown in patient and HC T cells using the Flex station (Figure 3.3.9), where the patient cells do not have a sustained calcium flux, but instead this dropped off after the initial peak. This lack of sustained calcium influx was hypothesised to be due to fast dissociation of the CRAC channel, possibly arising from the patient mutations altering the effect of CRACR2A which is known to have a role in stabilising the complex. However, because of issues with high background and non-specific staining with all rabbit primary antibodies, these experiments could not be completed.

The single cell calcium flux data gathered on patient and HC T cells showed this hypothesis to be unlikely, as the patient cells were observed to have sustained calcium flux using this more sensitive calcium sensing technique, as shown in Figure 3.3.11.

4.3.3 Transient expression models

Electroporation was used to perform transient transections in Jurkat cells to generate knock down CRACR2A using siRNA and to express CRACR2A mutants.

4.3.3.1 CRACR2A knock downs

siRNA is used to knock down genes of interest in a transient manner. As siRNA is small and the CRACR2A siRNA had previously been published (Srikanth, Jung, Kim, *et al.*, 2010; Wilson *et al.*, 2015; Miteva *et al.*, 2019), initial tests were run using the recommended nucleofection protocol, provided by the supplier. The siRNA knock down initial test was repeated twice. The initial test was performed after 24 hours. RNA was isolated and cDNA produced by reverse transcription. PCR was performed on the cDNA, with a range of primer pairs, including β-actin primers (Gertsch *et al.*, 2002) and CRACR2A var1 and 2 (Table 2.1.12, I+J, K+L). A positive control of fresh cDNA from the cell line showed visible PCR product with all primer sets. The transfected cells with and without siRNA resulted in PCR product that could not be visualised on a 3 % agarose gel and so the cDNA quality was determined to be poor.

The above test was repeated and cell lysate isolated after 36 hrs for protein analysis. The cell lysate did not contain much protein due to the low number of transfected cells, although some protein was detected by WB (Figure 4.3.2). The mock transfected cells showed less CRACR2A expression than the cells transfected with the siRNA. This was opposite to the expected result as siRNA transfection should have lowered the amount of CRACR2A protein produced in the cell. So further optimisation was needed to effectively reduce the amount of CRACR2A in Jurkat cells.

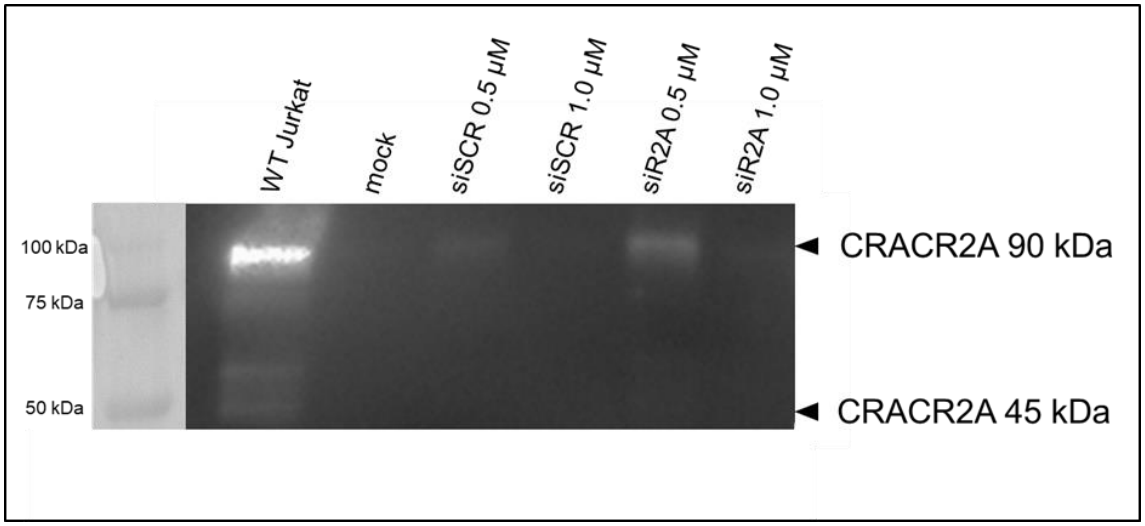

Figure 4.3.2 siRNA KD test

Amaxa® Cell Line Nucleofector® Kit V was used as per manufactures instructions, using the Jurkat specific protocol and siRNA CRACR2A (siR2A), siRNA scramble (siSCR) or no DNA (mock), as detailed in Section 2.2.4.1. Protein lysate was generated 36 hours post transfection, using NP40 lysis buffer, and loaded at 20 µg protein/lane as calculated using a BCA assay. WB was run using the protocol described in Section 2.2.6.1. CRACR2A Ab from Proteintech was used.

4.3.3.2 Monitoring the transfection

To optimise the nucleofection, a better way to measure transfection efficiency was needed. A plasmid containing EGFP was used, with an IRES2 linker connecting to CRACR2A cDNA in the same transcript. This allowed for the transfection efficiency to be monitored without the need for RNA or protein extraction, as the GFP expression could be seen using fluorescence, providing a more immediate readout of transfection efficiency, which made optimisation easier.

The transfection was performed and visualised after 24, 36 and 72 hours, and no GFP positive cells were found. This lack of expression could have been a result of a failed transfection. Flow cytometry was performed and this also showed no difference in GFP expression between mock and pIRES2_EGFP_empty transfected cells.

4.3.3.3 Testing other transfection protocols

Due to the lack of GFP expression in Jurkat cells with the recommended protocol, further tests were performed with HEK293 as a positive control, since this is an easily transfected cell line. The Jurkat protocol and the HEK293 protocol were performed on both cell lines using the pMAX GFP vector supplied by the manufacturer, which has a high transfection efficiency due to its small size (3.5 kb), compared to pIRES2_EGFP (5.3 kb).

The recommended protocol for Jurkat cells resulted in GFP expression in the HEK293 cells but not Jurkat cells (Figure 4.3.3). This explained the lack of response to siRNA and plasmid expression in the earlier experiments. However, the HEK293 protocol resulted in GFP visualisation in both cell types (Figure 4.3.4). The expression in Jurkat cells after 24 hrs in particular showed a large amount of GFP. The main differences between these two methods are in the machine programme (length and voltage of pulse). The HEK293 protocol also required a harder speed of centrifuge before transfer to cuvette (90 x g compared to 200 x g) and the Jurkat protocol left the cells incubating at room temperature in the cuvette for a further 10 minutes before being transferred to the cell culture plates. To identify the specific benefits of the HEK293 protocol, further experiments would need to be performed.

As shown, nucleofection is a viable way of transfecting Jurkat cells, though further optimisation would need to be performed with the CRACR2A plasmids and siRNA before use in further experiments. However, electroporation only results in transient expression, so only short term experiments could be performed using these reagents, as GPF expression was minimal after 48 hrs (images not shown here). Transient expression also results in low cell numbers, as daughter cells do not carry the modification. As a result, this methodology was halted and stable cell lines created.

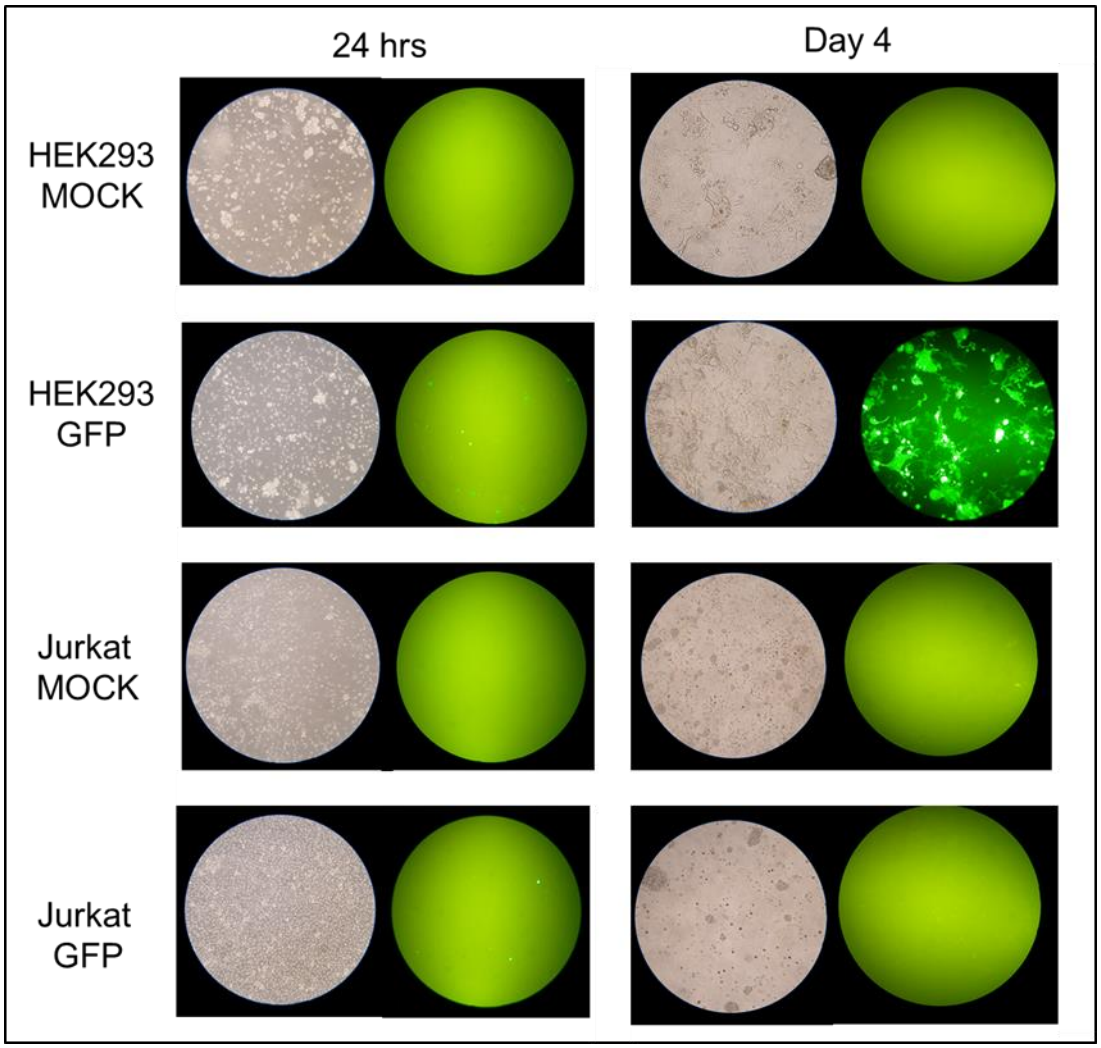

Figure 4.3.3 Recommended protocols for Jurkat cells

Nucleofection of 1000,000 cells with pMAX GFP vector (2 µg). Lonza recommended protocol for Jurkat cells was used, with the X-001 programme (Section 2.2.6.1). HEK293 p6 were transferred to a 6 well plate, while Jurkat p11 were transferred to a 12 well plate. The cells were imaged on a Zeiss, AxioImager.Z1 fluorescence microscope, with a x20 objective lens and exposure 120 ms.

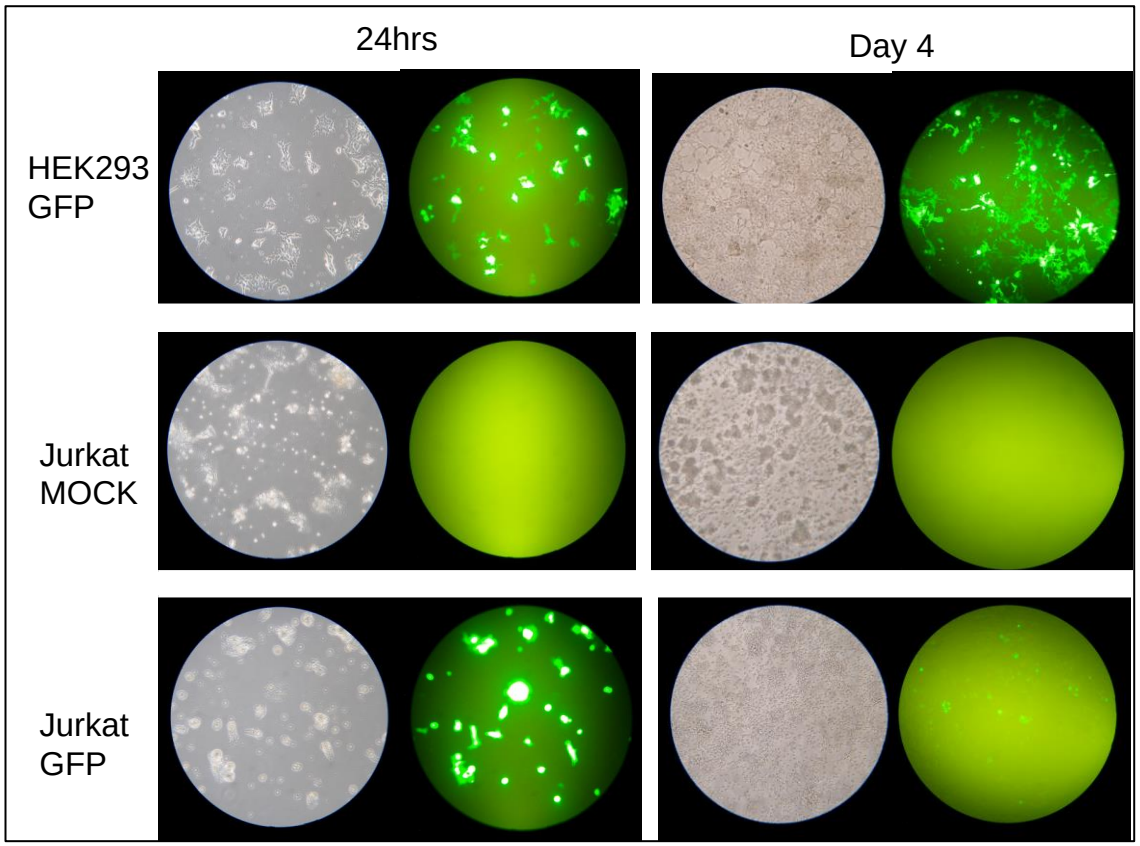

Figure 4.3.4 Recommended protocols for HEK293 cells

Nucleofection of 1000,000 cells with pMAX GFP vector (2 µg). Lonza recommended protocol for HEK293 cells was used, with the A-023 programme (Section 2.2.6.1). HEK293 p6 were transferred to a 6 well plate, while Jurkat p11 were transferred to a 12 well plate. The cells were imaged on a Zeiss, AxioImager.Z1 fluorescence microscope., with a x20 objective lens and exposure 120 ms.

4.3.3.4 Electroporation to test expression plasmids

As the project moved away from transient expression systems, due to the difficulties with measuring functional effects of mutated protein in these, stable cell lines were created. These cell lines were generated using viral transduction, which will be discussed in more detail in later sections. However, this methodology used FG11F expression plasmids containing CRACR2A. These vectors can be used in viral transduction and the sequence of interest incorporated into the cell genome, but they can also cause expression of protein of interest without the packaging vectors through transfection.

Electroporation tests were performed using the FG11F plasmids to check if the CRACR2A mutant proteins could be expressed in Jurkat cells. Electroporation is a good test for this as it is quick and the cells can be harvested after 24 hours, rather than after the two weeks of viral transduction. The method used for electroporation with FG11F plasmids differed from the nucleofection methods above, as the experiments were performed using the established Gwack lab protocol, as described in Section 2.2.4.2. The main disadvantage of this technique is the transient nature of the expression and the large cell numbers and high DNA amount needed. Between four and eight cuvettes were needed for each sample type to produce enough positively transfected cells to make a lysate containing sufficient protein for western blotting. This is due to the variability between the transfection efficiency which was determined by GFP expression visualised after 24 hours. Good transfection efficiency was defined as when more than 90 % of the cells had GFP expression, while poor efficiency was defined as when 50 % or less of the cells fluoresced.

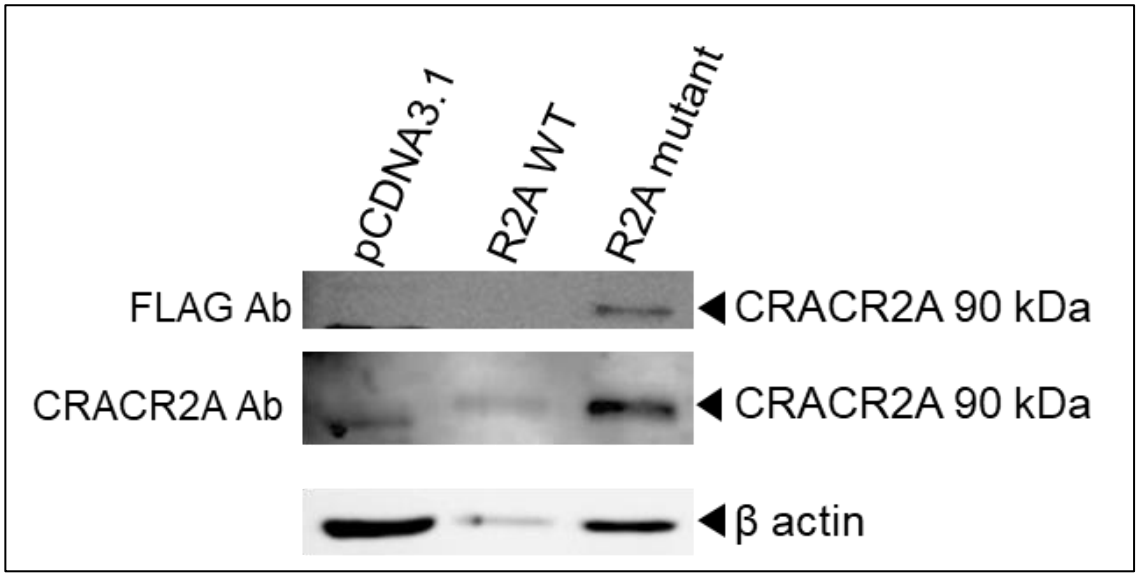

Figure 4.3.5 Electroporation test

300,000 Jurkat cells, 15 µg plasmid of interest and 5 µg FG11F empty for visualisation were used per transfection. The protocol for electroporation is given in Section 2.2.4.2. Cells were collected at 24 hrs after transfection. Samples are pooled from multiple transfections, 4 (pCDNA3.1 and mutant) or 8 (R2A WT) cuvettes, depending on transfection efficiency. WB protocol used is described in Section 2.2.6.2.

pCDNA3.1 was used as a control plasmid, containing unrelated DNA, to show endogenous CRACR2A expression after electroporation

The CRACR2A WT in particular had poor transfection efficiency, with < 50 % of the cells having GFP expression, so double the amount of cells were transfected. The lysate produced for the WT sample was less concentrated than that from the other two samples, as seen by the faint β-actin loading control band (Figure 4.3.5). It was less concentrated due to the high volume of loading dye used to resuspend the cells, which was more than double that of the other samples. When a comparable amount of loading dye was added to the WT cells, the lysate was too thick to pipette, so more loading dye and vortexing was performed on the sample, until it could be pipetted into the loading tips and loaded in the SDS-PAGE gel.

The aim of transient expression was to rapidly test the expression of different plasmids and mutant proteins in Jurkat cells lines. Electroporation was shown to be a good method for this, as confirmed by western blots. In order to determine if mutant proteins effect the function of the cell lines, stable expression had to be achieved.

4.3.4 Creating stable cell lines

The aim of making stable cell lines was to compare the function of mutant CRACR2A to WT protein, to see if the patient mutations affected the protein function. In order to achieve this, knockout (KO) cells were generated that lacked any endogenous CRACR2A protein.

4.3.4.1 KO CRACR2A Jurkat cells

KO CRACR2A Jurkat cells were generated using viral transduction and CRISPR reagents as described in Section 2.2.5 and Figure 4.2.1.

4.3.4.1.1 Puromycin Kill curve

Using the CRISPR system, puromycin was used to select for cells that take up the CRISPR-shR2A vector (Figure 2.2.11). In the literature, the recommended concentrations of puromycin is 1-10 µg/mL for eukaryotic cells and 4 µg/mL for Jurkat cells. In order to confirm that 4 µg/mL would work in this system, a puromycin kill curve was generated to find the lowest concentration possible that killed 100 % of untransduced cells in 48 hrs. MTT was used to measure the cell viability (Section 2.2.5.5). MTT is a yellow tetrazole that is reduced to purple formazan in living cells, and this colour change can be measured at 560 nm wavelength in a plate reader. In all MTT experiments, the controls were 50 % DMSO for complete death (<0.05 blank corrected Abs), media only wells and for the puromycin kill curve experiment the additional control of cells only was included.

Adherent cells are normally used in MTT assays so HEK293T were a control for the initial optimisation of Jurkat cell numbers required. The range of cell numbers tested for Jurkat cells (5,000 to 500,000 cells per well) was much higher than HEK 293T (2,500 to 5,000 cells per well) due to the smaller size and increased risk of losing cells when the supernatant was removed from spun down suspension cells. 50,000 Jurkat cells was selected as the optimal cell number per well.

A range of puromycin concentrations (0.25-20 µg/mL) were tested in triplicate, with 3 biological replicates. Puromycin at 4 µg/mL was found to be the lowest concentration of drug that killed the majority (<10 % viability) of the cells (Figure 4.3.7), as also recommended in the literature. This concentration was therefore, used to select for KO transduced cells.

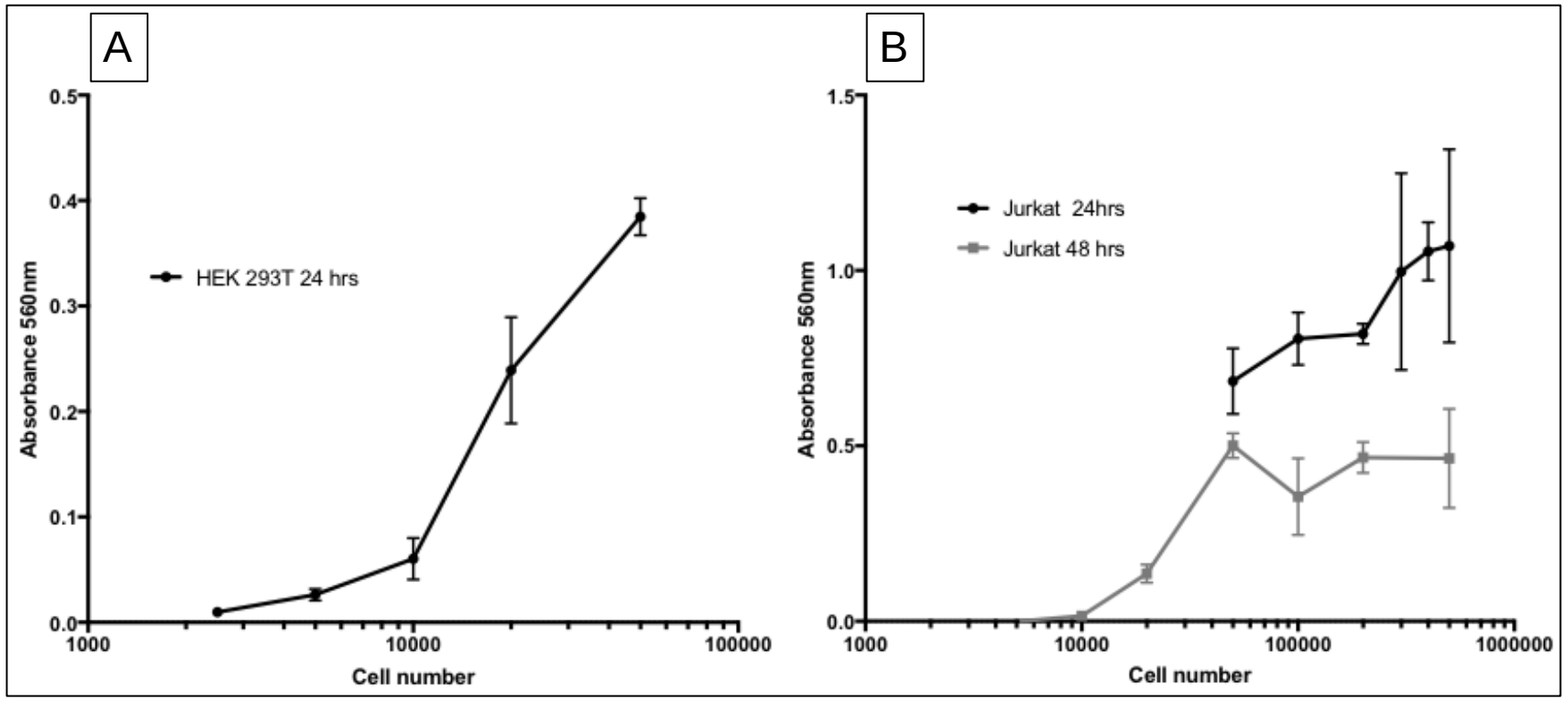

Figure 4.3.6 Optimising cell number per well for MTT assay

Cells were incubated at 37 ˚C for 24 or 48 hrs, in 200 µL of media. All absorbances are corrected against media only wells. All samples run in triplicate. A) HEK293T cells, B) Jurkat cell line.

Large standard deviations can be seen at each drug concentration, likely due to variability between wells of cell number at the initial loading. This has tried to be accounted for by the use of separate 'cells only' for each biological replicate to calculate % variability.

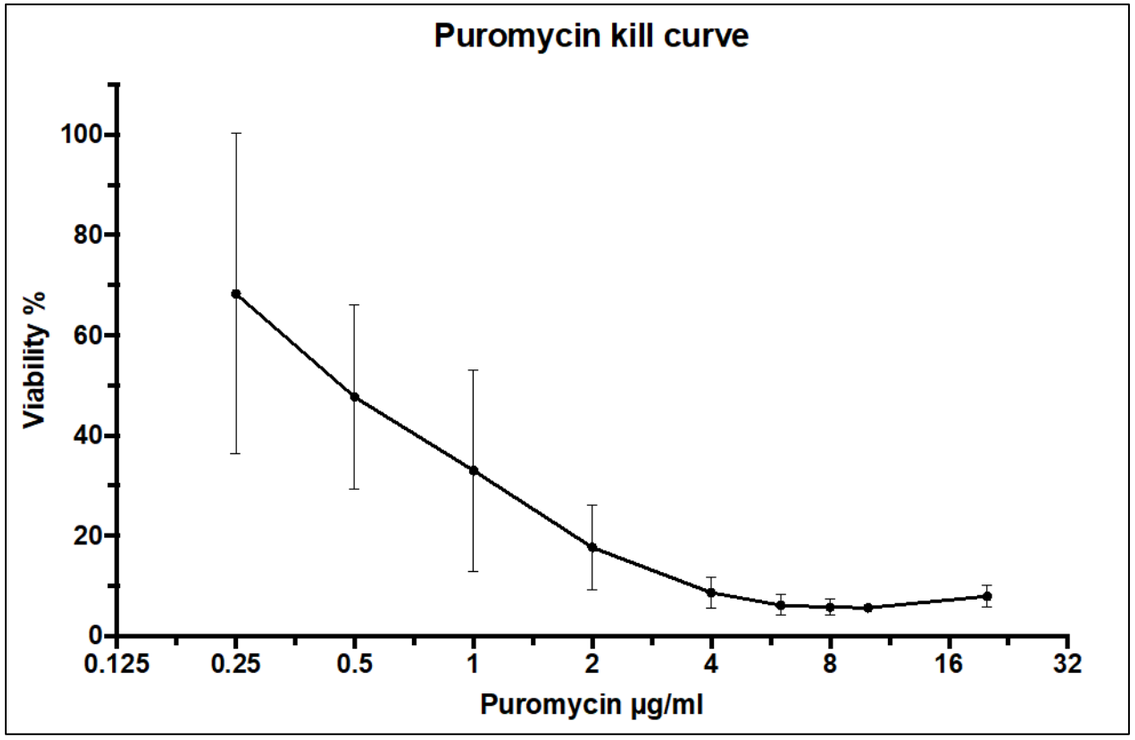

Figure 4.3.7 Puromycin kill curve

MTT assay performed as per Section 2.2.5.5. 50000 cells/well in 100 µL media were cultured overnight, then 100 µL of puromycin was added to a final concentration 0.25-20 µg/mL and left for 48 hrs. All samples were run in triplicate and data shown here is from 3 biological replicates. Every well was blank corrected using absorbance values for media only. Viability was normalised to cells only wells as 100 %, the % viability was calculated for samples as 100x (samples/cells only wells).

4.3.4.1.2 Production of donor cells

Published data by the Gwack lab used calcium phosphate transfections to introduce the CRACR2A KO plasmid and viral packaging vectors, specified in Table 2.1.2, into the HEK293T cell line, before the supernatant could be added to Jurkat cells for transduction (Srikanth *et al.*, 2016). An initial test was performed using the published method with CRISPR-shR2A KO plasmid, and CRACR2A visualised in Jurkat cells by western blot after puromycin selection at 4 µg/mL. The amount of CRACR2A in these KO cells was comparable to WT Jurkat cells, implying the transduction had poor efficiency. Due to the failure of the viral transduction to generate KO CRACR2A cells, the calcium phosphate transfection method was repeated with different plasmid reagents that could be more readily measured, namely N terminal FLAG tagged CRACR2A in FG11F plasmid. West blots showed the level of CRACR2A in these cells to be comparable to cells transfected with an empty FG11F plasmid, and FLAG antibodies detected very low levels of recombinant protein. Calcium phosphate transfections are known to have variable efficiency and to be sensitive to changes in pH (Guo *et al.*, 2017).

Due to the poor efficiency of the calcium phosphate transfection, a different method was tested to produce viral supernatant, as detailed below.

4.3.4.1.3 Alternate transfection method

The TransIT method was recommended by Dr Julie Burns (University of Leeds) as a more reliable and reproducible alternative to calcium phosphate transfection. The chemical transfection was performed on HEK293FT cells and then the supernatant transferred to Jurkat cells as before.

The efficiency of this method was tested with the CRISPR CRACR2A KO reagents and the FG11F R2A WT plasmid. A full transduction protocol was performed, as a fluorescent microscope was not available to visualise the Class 2 virus infected cells for a quick determination of transfection efficiency. Instead, the cell lysates were western blotted with CRACR2A Ab and a FLAG Ab to look at the expression, as seen in Figure 4.3.8.

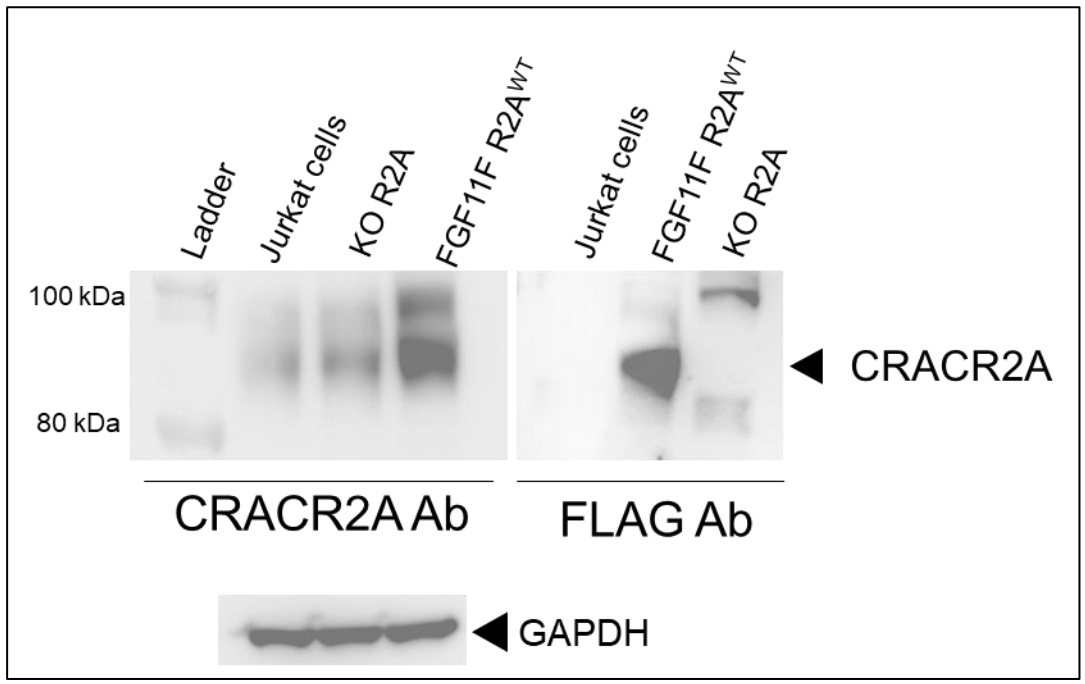

Figure 4.3.8 Trans-IT transfection test

Transduction of Jurkat cells using Trans-IT reagents and performed using methods detailed in Section 2.2.5.3. Puromycin selection was done for 48 hrs at 4 µg/mL on the KO cells. The WB was performed and visualised using the Method A (Section 2.2.6.1).

The KO reagents did not appear to have worked, due to the band present at the expected size of CRACR2A with the corresponding antibody. However, there was expression of the FG11F R2A^{WT}, due to the strong band detected with the FLAG antibody, which is not seen in the WT Jurkat or the KO cells, suggesting transfections had worked well. So, the KO cells underwent a second puromycin selection at a range of concentrations, to see if there were cells present that had incorporated the CRISPR reagents.

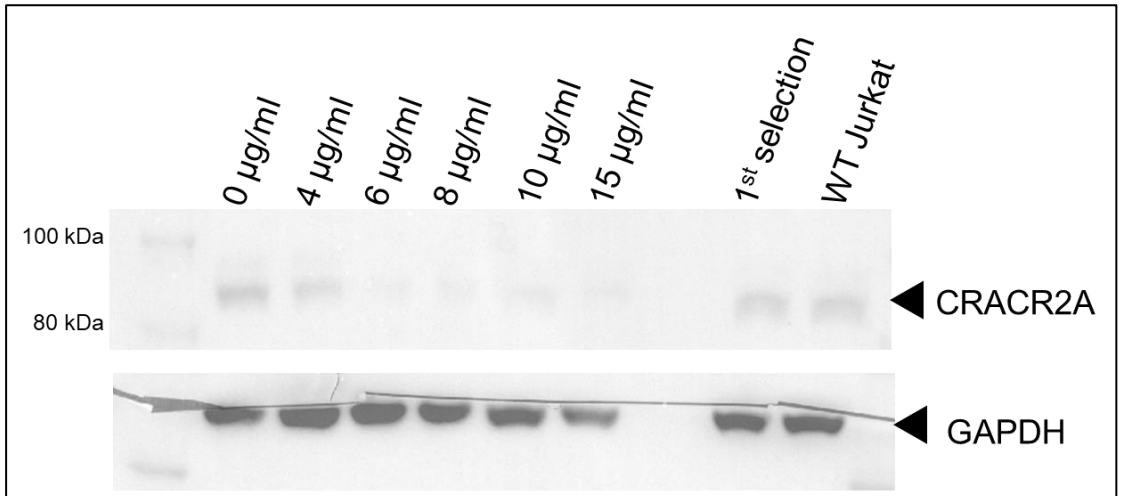

Puromycin µg/ml	R2A Area	R2A Percentage	Relative density	**% of WT R2A**	GAPDH Area	GAPDH Percentage	Relative density
WT older lysate	1941.569	11.590	0.131	**100.000**	14851.217	88.410	1.000
0	1522.305	14.230	0.166	**126.557**	9177.033	85.770	1.000
4	654.406	5.440	0.058	**43.884**	11366.296	94.560	1.000
6	218.142	1.750	0.018	**13.587**	12248.711	98.250	1.000
8	307.263	2.340	0.024	**18.278**	12822.175	97.660	1.000
10	294.920	2.200	0.022	**17.159**	13113.953	97.800	1.000
15	120.021	1.310	0.013	**10.125**	9009.104	98.690	1.000

Figure 4.3.9 Second puromycin selection treatment on KO CRACR2A Jurkat cells

KO CRACR2A Jurkat cells were incubated at a range of puromycin concentrations for 48 hrs, and left to rest for 24 hrs before NP40 lysate was generated and a WB performed with the CRACR2A Ab as per Section 2.2.6.1, with the additional step of washing the membrane overnight in 5 % Milk after the secondary incubation. The membrane images were analysed using Image J software, to calculate the area and percentage of the CRACR2A band and the loading control GAPDH. The relative density of GAPDH was set as 1.0 for each sample and the relative density of the CRACR2A was calculated in relation to the control band, to normalise the expression of each sample. The % of WT R2A was calculated by the WT Jurkat relative density being set as 100 % and the other samples being calculated in relation to it (Miller, 2010).

After the second selection with puromycin, the expression of CRACR2A had reduced in all samples (
Figure 4.3.9). The cells treated with 15 µg/mL of puromycin for 48 hrs had 10 % of CRACR2A expression compared to WT Jurkat cells. Thus, complete knock out was not seen in these cells after viral transduction with KO CRACR2A reagents. However, the level of CRACR2A was considered to have reduced sufficiently to test the calcium flux response in these cells, to see if an equivalent reduction was seen compared to WT Jurkat cells (Srikanth, Jung, Kim, *et al.*, 2010).

4.3.4.2 The function of CRACR2A KO cells

The function of the KO CARCR2A Jurkat cells was tested to determine if a large enough window was available in the response between KO and WT cells, so that subtle difference expected by the patient mutations could be observed.

4.3.4.2.1 Calcium flux

To compare the level of calcium flux response of KO CRACR2A and WT Jurkat cells, the Flex Station was used (Section 2.2.7.1.2). Minimal calcium flux was seen in both cell line when TG is added in calcium depleted conditions, but when calcium was added back into the system the calcium flux increased and the area under the curve could be measured (Figure 4.3.10). The area under the curve was significantly reduced in KO cells compared to WT cells, with or without TG. However, the peak response was comparable between the cell lines and so not shown here.

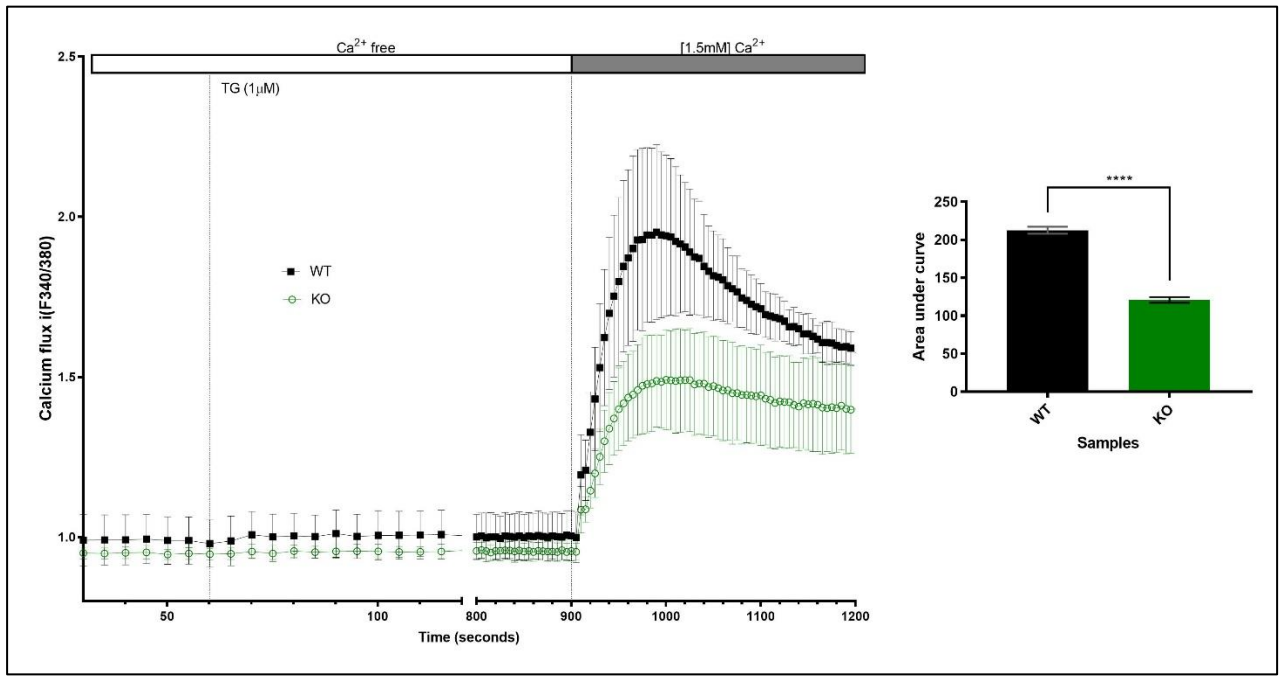

Figure 4.3.10 Calcium flux response to TG with Jurkat KO cells

Method was as described in Section 2.2.7.1.2. All samples were run in duplicate and performed to n=3. Data was analysed using Prism and significance was calculated using the ordinary one way ANOVA multiple comparisons. P values : ns P > 0.05 (ns), P ≤ 0.05 (*), P ≤ 0.01 (**),P ≤ 0.001 (***), P ≤ 0.0001 (****)

An experimental error occurred during data collection that lead to high responses from all DMSO samples. This data is still deemed to have a value as it allows for the comparison of calcium flux responses between the WT and KO cells. This could be due to the cells being kept in calcium free medium for an extended period of time, or TG being present in the DMSO controls. From this experiment the Flex Station was found to be not sensitive enough for subsequent experiments with CRACR2A variants.

The window between KO and WT cells measured using the Flex station was not large enough to observe potential differences expected from the mutants containing patient mutations. As a result a more sensitive and robust method of calcium flux was

needed, so a collaboration and secondment was initiated to gain access to more sensitive equipment in order to complete this aspect of the project.

4.3.4.3 Stable cells lines with CRACR2A mutants

The Gwack lab collaborators already had a KO CRACR2A Jurkat cell line, generated using calcium phosphate transfection and viral transduction (Srikanth *et al.*, 2016). This established KO CRACR2A cell line was used in all subsequent transductions. Viral transduction was used to generate stable cell lines that express mutant CRACR2A. Transfection efficiency was monitored using GFP expression in both the donor cell and Jurkat cell lines, transfected with FG11F an empty plasmid, and visualised using a fluorescent microscope. Stable cell lines were created when the virus produced by the donor HEK293 cells were used to infect the Jurkat cell lines, resulting in the plasmid of interest being incorporated into the genome and enabling the cell to express the CRACR2A mutant proteins.

Western blots were performed on the donor HEK293 cell lysates to check that the mutants expressed in the cells and in the final stable Jurkat cell lines. The expression of the recombinant protein was detected using CRACR2A Ab, which was also able to detect endogenous protein, and the FLAG Ab. The mutant vectors were all designed to have an N-terminal FLAG tag. The Western blot data are shown in Figure 4.3.11 and Figure 4.3.12 respectively.

The KO Jurkat cell lines had no full length CRACR2A in the FG11F transduced samples, confirming the complete KO of endogenous CRACR2A in these cells. The western blots confirmed expression of mutant CRACR2A in HEK293 and Jurkat KO cells. The double mutant cell lines had a truncated protein, as a result of the premature stop codon at amino acid 300.

A band can be seen in the HEK293 samples, in Figure 4.3.11, around 40 kDa for the cells expressing the full length CRACR2A (lysates WT, R144G and E278D). This is near the expected size of the short isoform of CRACR2A of 45 kDa. However, it is likely to be a degradant rather than the short isoform, due to the cDNA sequence used which encodes only for the full length protein.

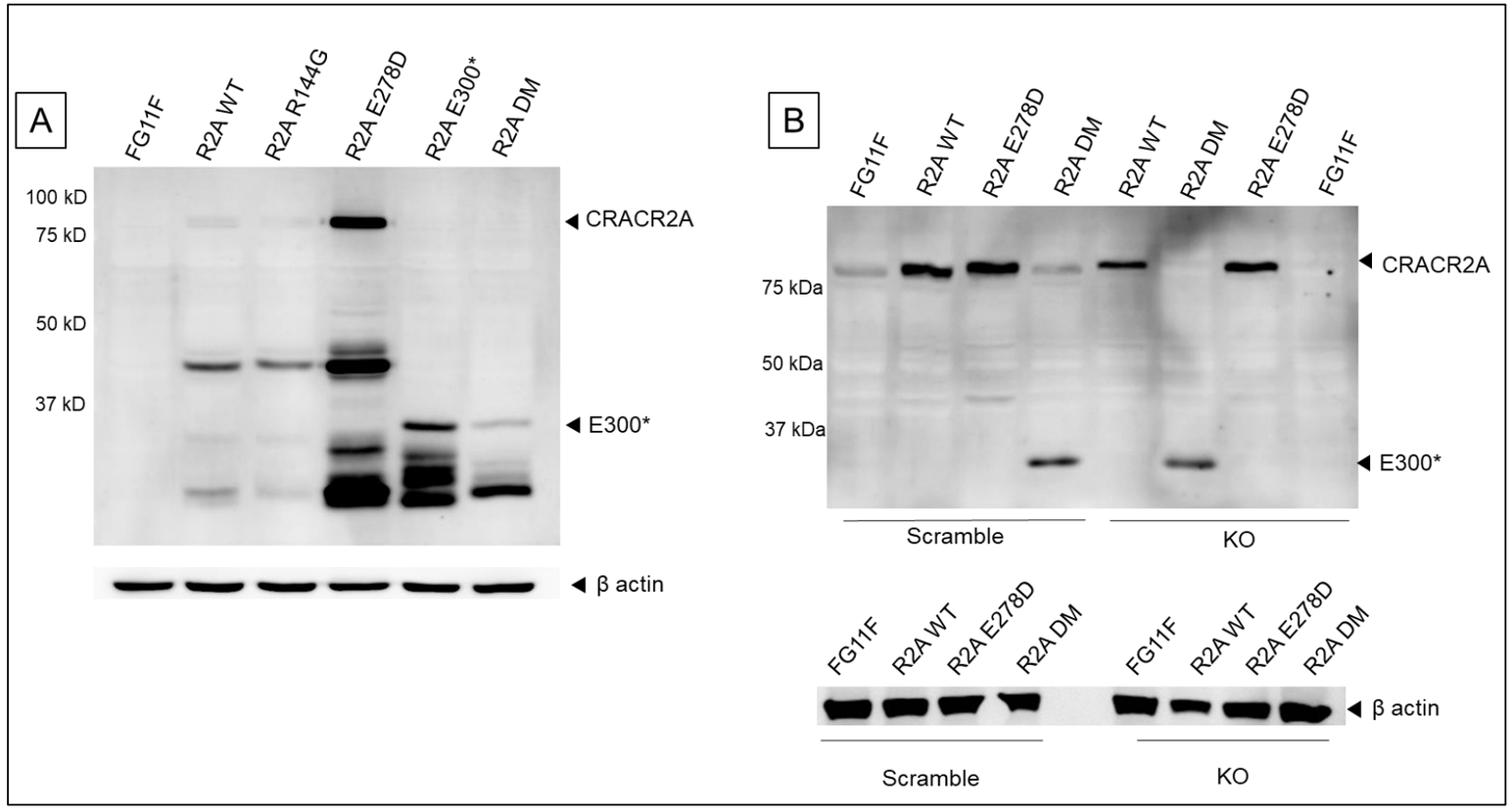

Figure 4.3.11 Stable cell line blotted with anti-CRACR2A Ab

Western blots performed using Method B (Section 2.2.6.2). A) HEK293 cells were collected 4 days post transfection, after supernatant used for viral transduction. B) Jurkat cells were collected 10 days post transduction Loading dye was added directly to cell pellet and sonicated

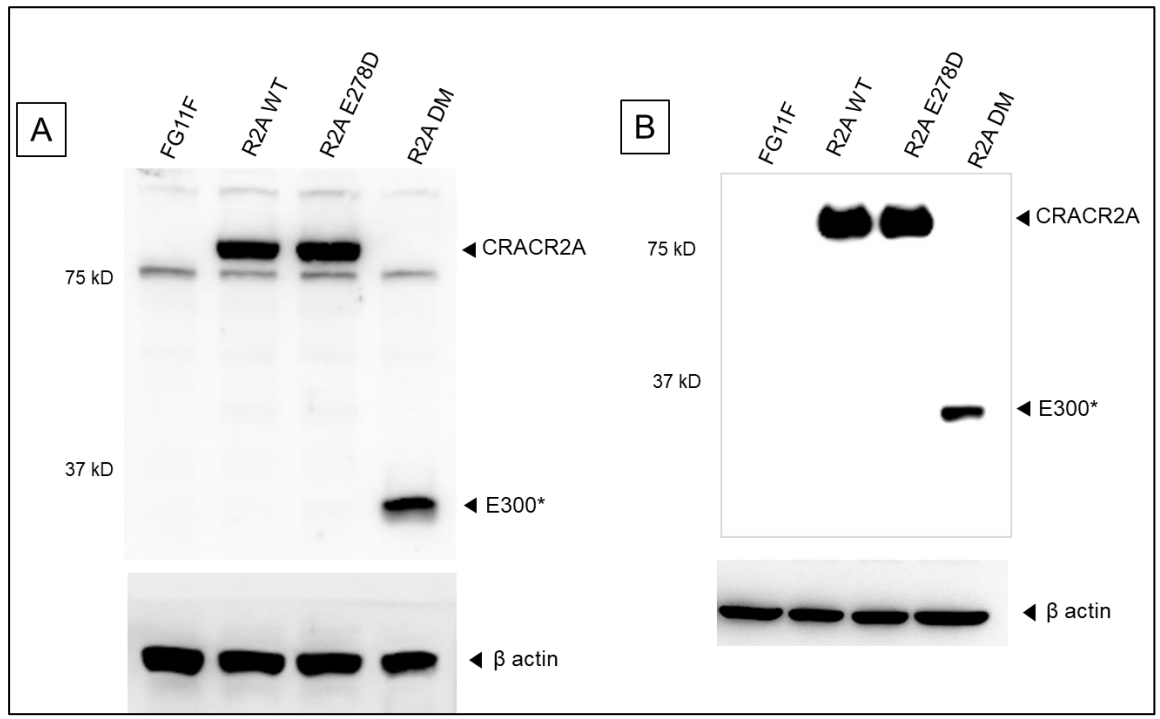

Figure 4.3.12 Stable cell lines blotted with anti-FLAG Ab

Data and figure generated in collaboration with the Gwack lab. The method details are found in Sections 2.2.5 and 2.2.6.2. A) HEK293 cells, B) Jurkat KO cells.

This experiment was initially performed by the author using the cell lines shown in Figure 4.3.11, and showed the same results. This figure represents the pooled data of n=3 which was generated by the Gwack lab for publication.

The patient mutations were expressed initially as single mutations R144G, E278D and E300* (Figure 4.3.11). Due to the high number of cell lines created with the additional controls of WT CRACR2A and empty FG11F cells, the functional experiments were performed on only the E278D cell line and a cell line generated with both the R144G and E300* (double mutant [DM]). These best represented the patient alleles determined in the previous chapter (Section 3.3.1.3).

4.3.5 CRACR2A function in stable transfected cell lines

The CRACR2A patient allele mutations, E278D and the DM (R144G and E300*), were expressed in the KO CRACR2A Jurkat cells to create stable cell lines, the expression was confirmed by western blot as described above. In order to further examine the function of these patient mutations, tests were performed to check the general function of the Jurkat cells, through IL-2 expression, and more specific CRACR2A related function, by calcium flux, JNK expression and protein localisation.

4.3.5.1 Localisation of mutant proteins

CRACR2A is known to localise to the Golgi and vesicles (Srikanth, Jung, Kim, *et al.*, 2010). The localisation of CRACR2A protein was tested in the stable cell lines using IF (Section 2.2.6.3) to check if the patient mutations affected protein localisation. The localisation was initially tested with Anti-FLAG antibody, which only binds to recombinant CRACR2A as shown in Figure 4.3.13. F-actin was stained in the cells using phalloidin, a molecule that binds F-actin with a conjugated fluorophore. F-actin was used do show the overall shape and structure of the cells. Localisation was comparable for WT protein and the E278D mutant, with the expected localisation to the Golgi and vesicles. However, the DM was not detected in the cells, even though the truncated protein was seen to be expressed in the cell by WB using the same anti-FLAG antibody for detection (Figure 4.3.12).

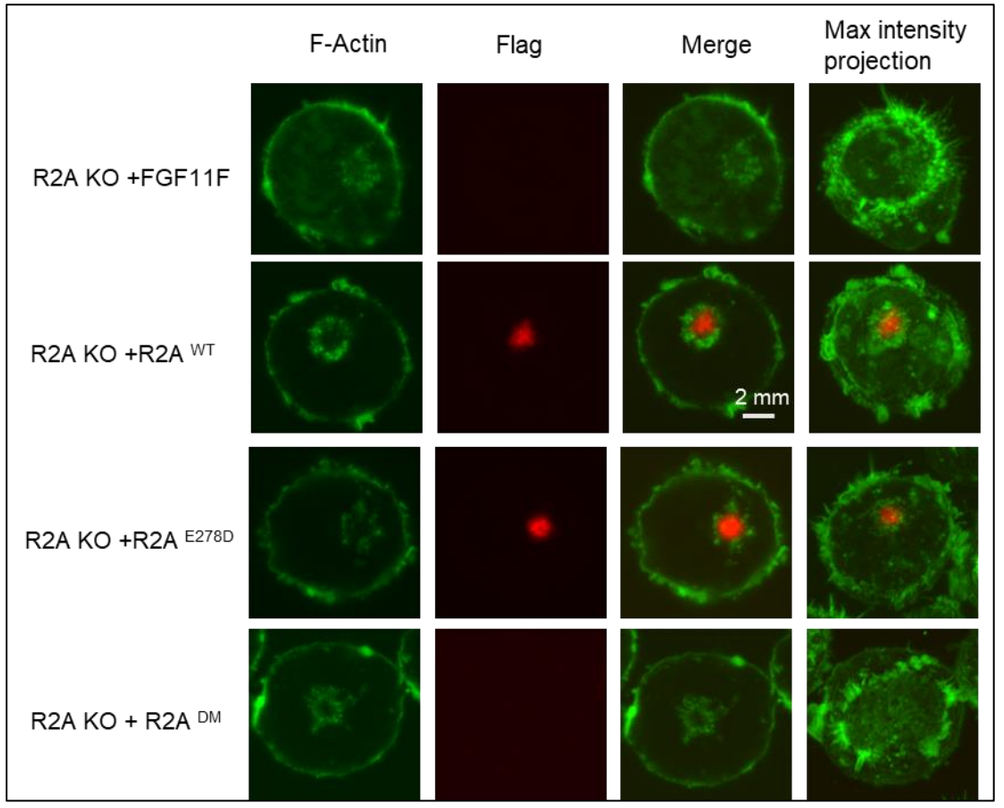

Figure 4.3.13 Localisation of mutants using FLAG Ab

z-stack microscope images were taken for each cell. For single channel images, the middle of the cell is shown. Stained with anti-FLAG. Images of between 8-12 cells were taken per cell line (Figure 4.3.11) and a single representative cell is displayed. For the max intensity projection of E278D, a different cell is imaged than the one shown in the single channel images.

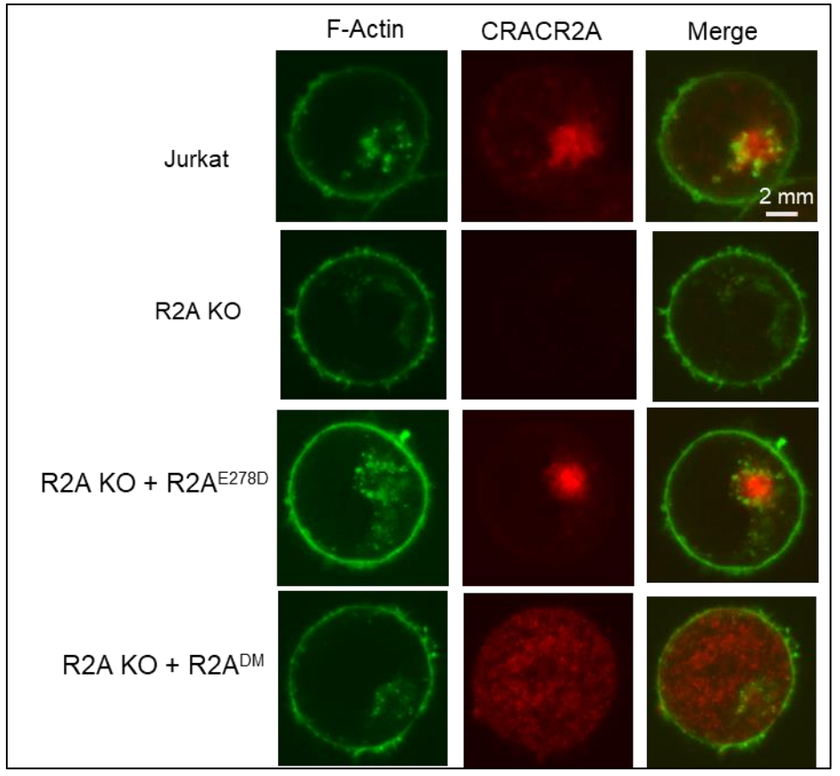

Figure 4.3.14 Localisation of mutants using CRACR2A Ab

z-stack microscope images were taken for each cell. For single channel images, the middle of the cell is shown. Stained with anti-FLAG. Images of between 8-12 cells were taken per cell line (Figure 4.3.11) and a single representative cell is displayed.

The absence of CRACR2A DM detection with the anti-FLAG Ab, meant further IF was performed with the Anti-CRACR2A Ab as shown in Figure 4.3.14. This Ab is able to bind to both endogenous and recombinant CRACR2A. As an additional control, normal Jurkat cells where stained, to show the endogenous localisation of CRACR2A protein. The localisation of endogenous CRACR2A seen was comparable to that detected with the anti-FLAG Ab in WT and E278D cell lines, although there was potentially additional vesicle staining in the normal Jurkat cells. The KO cell line was also stained and no protein was detected, confirming the absence of detectable CRACR2A as seen in the WB earlier (Figure 4.3.11 and Figure 4.3.12). The E278D cell line was stained with the anti-CRACR2A Ab, and showed the same localisation as with the anti-FLAG Ab to the Golgi and vesicles. The DM was detected with the anti-CRACR2A, but did not show the normal localisation seen for the other recombinant proteins. Instead, the DM protein was seen in the cytosol of the cells.

The localisation of CRACR2A was tested by IF, the E278D mutation did not appear to affect the localisation of the protein to the Golgi and vesicles. The DM did affect the localisation, which appeared as distributed throughout the cell. Interestingly, the DM was not detected by an anti-FLAG Ab, suggesting that something may have affected the N-terminal FLAG tag, even though the same Ab was able to detect the protein in a WB.

4.3.5.2 IL-2 expression

Interleukin 2 (IL-2) is a good functional test for Jurkat cells, comparable to the cytokine expression experiments done in patient primary T cells (Section 3.3.5). IL-2 is expressed in Jurkat cells in response to phorbol myristate acetate (PMA) and ionomycin (I) (Weiss A, Wiskocil RL, 1984; Held, 2018).

The stable cell lines were stimulated at two concentrations for 16 hrs (PMA [80 nM]+ ionomycin [1 µM] and PMA [20 nM]+ Ionomycin [0.5 µM]) or unstimulated. The higher stimulation conditions were chosen as they were in excess of the half maximal effective concentration (EC_{50}) of both drugs, in order to show the maximal response of the cells. The experimental EC_{50}, determined by the Gwack lab, with normal Jurkat cells was PMA [10 nM]+ ionomycin [0.2 µM]. The lower stimulation was double the EC_{50} of both ionomycin and PMA, and as such more subtle differences between the mutants response would be expected to occur. A lower stimulation at the EC_{50} was initially tested, but produced only low levels of detectable IL-2 expression in WT Jurkat cells, with a max response of 3 % expression when stimulated, compared to 0.8 % expression at rest, and so it was not continued in later experiments. The expression of the cytokine was measured by flow cytometry. BFA was added to

all cells two hours before processing, including those under resting conditions. BFA blocks transport of proteins out of the cell. This means that the cytokine can build up in each cell and so can be measured using internal staining techniques, such as cell fixation with PFA.

Jurkat cells transduced with CRACR2A KO and later CRACR2A mutants and Jurkat cells transduced with shRNA-Scramble (SCR), so express endogenous CRACR2A, were also tested here for IL-2 expression. However, no IL-2 expression was seen from any of the cells. The SCR transduced cells may have been of poor health prior due to the transduction, as all the cell lines gave minimal IL2 expression and the cell growth rate was slower than for KO cells. As a result further functional testing of these cells was not continued as the basic machinery of the cells was not responding. The SCR cell lines would have been a good control to include in experiments. It would have been a control for the initial CRACR2A KO transduction, as cells with endogenous CRACR2A expression levels and to see if the mutated CRACR2A had any effect on the endogenous protein.

The IL-2 expression could be measured successfully in the stable cells lines, as seen in Figure 4.3.15 Both E278D and the DM resulted in significantly lower expression compared to WT CRACR2A. This was observed at both high and low stimulation conditions. This showed that the mutant CRCAR2A studied herein were not able to rescue the reduced IL-2 phenotype in the KO line.

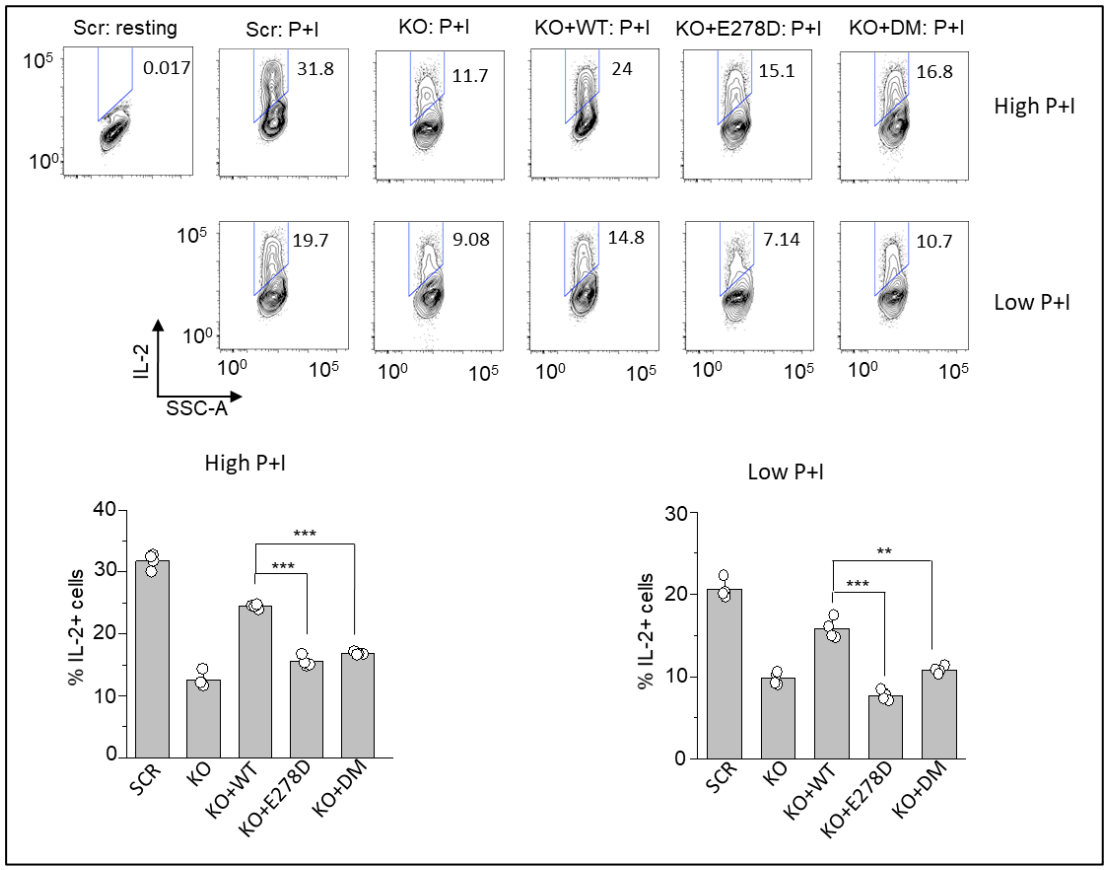

Figure 4.3.15 IL2 expression for stable cell lines

The data and this figure were generated in collaboration with the Gwack lab. n=3. Jurkat stable cells lines were cultured for 16 hrs with high, (PMA [80 nM]+ Ionomycin [1 µM]), low (PMA [20 nM]+ Ionomycin [0.5 µM]) stimulation or at rest in media, with BFA added at hour 14. Methods details are given in Section 2.2.8.5.
This experiment was initially performed by the author using the cell lines shown in Figure 4.3.11, and showed the same results. This figure represents the pooled data of n=3 which was generated by the Gwack lab for publication.

4.3.5.3 Calcium flux

Calcium flux was performed on the stable cell lines to see if the patient mutations affected the calcium flux response in Jurkat cells. Previously, KO of CRACR2A was shown to reduce calcium flux response in Jurkat cells by 50 % (Srikanth, Jung, Kim, *et al.*, 2010).

The calcium flux experiments were performed using a fluorescent microscope and fura-2 as the calcium sensor dye, using the same methodology as for the patient T cell experiments presented in Section 3.3.3.3.2. The cells are stationary with fluid being moved over the cells.

The calcium data, shown in Figure 4.3.16, illustrates the response to multiple challenges. In panel A, the physiological TCR activation response is modelled by the addition of CD3 Ab into calcium containing cells. Ionomycin is used to show the maximal response of the cells. In B, calcium add back is measured, the cells are first in a calcium free buffer, TG is then added which causes the calcium channels to be opened and the stores to the depleted. Calcium is then added back into the system, and the maximal calcium entry occurs.

The calcium flux response to all stimuli showed the same pattern. The KO Jurkat cell line had reduced flux compared to normal Jurkat cells (control). This defect was rescued in the KO cells with expression of WT CRACR2A. Both of the cell lines expressing the patient alleles were able to partially rescue the effect of knocking out the CRACR2A, but the response was not as high as for the WT protein. The calcium response was very similar with both patient alleles (E278D and the DM), however the DM showed slightly better calcium flux compared to the E278D mutated cells, although the difference was not statistically significant.

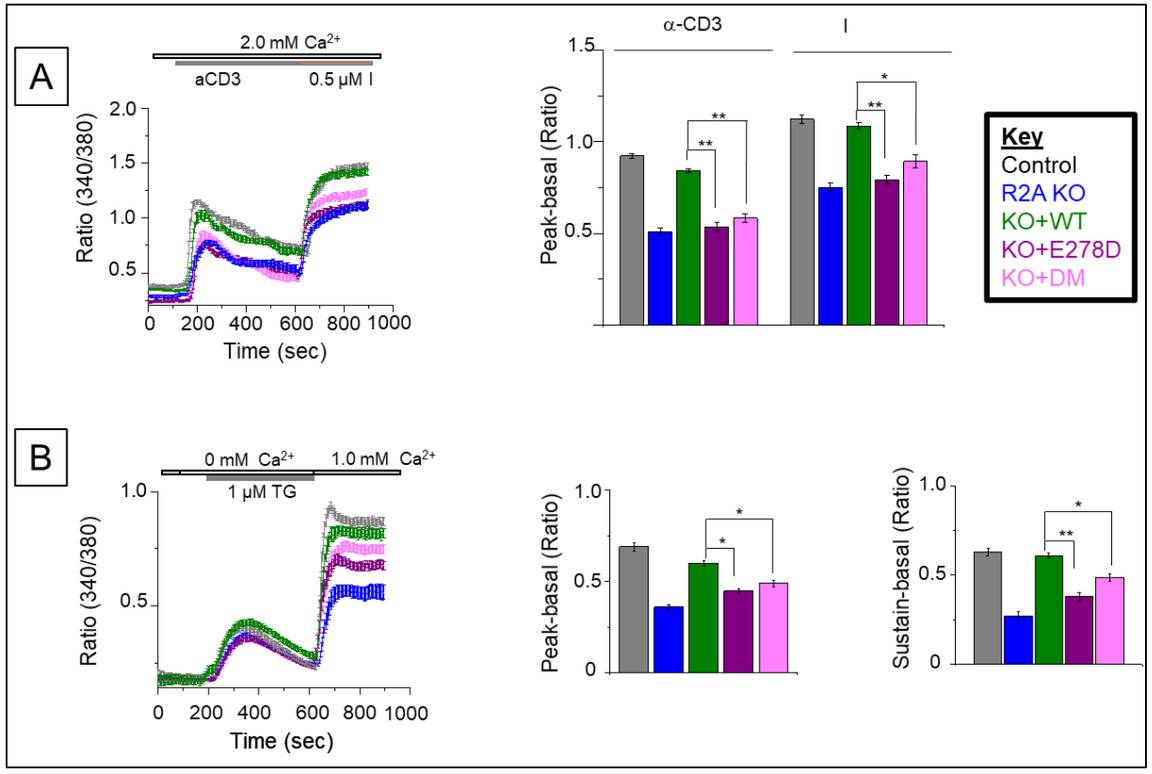

Figure 4.3.16 Calcium flux of stable cell lines

The data and this figure was generated in collabouration with the Gwack lab. There are 3 biological replicates for each sample, and each replicate is 50 cells. Some of the data was processed and analysed by the author. A) TCR activation and ionomycin response in calcium containing conditions. B) calcium add back response, as described in Section 2.2.7.1.3. P values : ns P > 0.05 (ns), P ≤ 0.05 (*), P ≤ 0.01 (**),P ≤ 0.001 (***), P ≤ 0.0001 (****)

The author observed the initial experiment with cell lines see in Figure 4.3.11 and performed the data analysis, including picking individual cells and statistics. The subsequent cell lines were performed by the Gwack lab due to the extensive equipment and training required for this technique.

4.3.5.4 pJNK

The pJNK expression was measured to look at the secondary function of CRACR2A. The JNK signalling was measured in the stable cell lines using a previously published method (Srikanth *et al.*, 2016) for primary cells but with tighter time points here, as the Gwack lab had determined Jurkat cells response occurs in the first 30 minutes of activation.

JNK signalling in the Jurkat stable cell lines expressing patient mutations was measured after TCR stimulation for 0, 10, 20 and 30 minutes, as seen in Figure 4.3.17. The normal Jurkat cells (control) showed the most expression of p-JNK under all stimulated conditions. The KO cells gave a reduced expression compared to normal Jurkat cells. Expression of the WT CRACR2A in KO cells rescued this defect at the 10 and 20 minute time points, but not at 30 minutes. The E278D mutant was also able rescue the phenotype at 10 and 20 minutes. The DM mutant was not able to rescue the KO phenotype, and the level of p-JNK was significantly reduced compared to WT CRACR2A at the 10 and 20 minute time points.

The results of this experiment suggest that the E278D mutation has no effect on the CRACR2A JNK related function, while the DM mutant does.

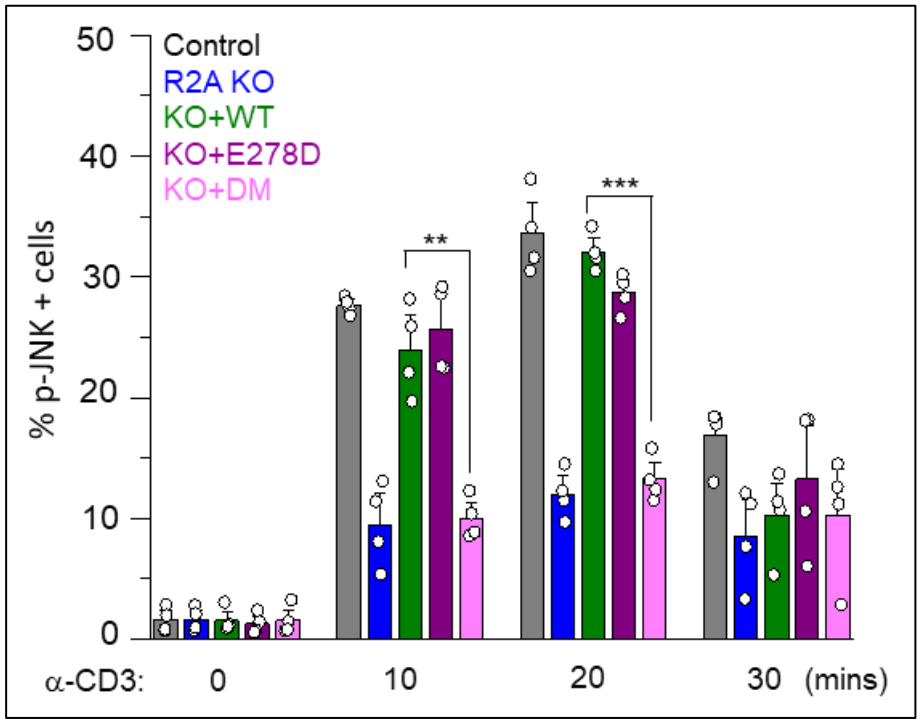

Figure 4.3.17 p-JNK response of stable cell lines to TCR stimulation

Data and figure were generated in collaboration by Gwack lab. The experiment was repeated to give an n=3. See Section 2.2.8.3 for method details.

The author performed the initial experiments on cell lines from Figure 4.3.11 alongside the Gwack lab.

4.3.5.5 Interaction with CRAC channel proteins

The binding efficiencies essential for CRACR2A function were tested using co-immunoprecipitation (co-IP), as shown in Figure 4.3.18. The interaction of CRACR2A mutants was observed with Orai1, STIM1 and vav guanine nucleotide exchange factor 1 (VAV1). This was done by transducing the binding proteins of interest into the cells, so they were present in abundance to allow for better visualisation. The CRACR2A mutants were captured by their FLAG tag and the binding partners visualised using primary antibodies. E278D mutation did not appear to affect binding to Orai1, STIM1 or VAV1, and gave comparable results to WT CRACR2A.

The DM was not able to bind to any of the proteins tested. As the pull down was performed with the anti-FLAG antibody, this result may be because of binding issues between the antibody and the DM rather than the protein binding partners tested.

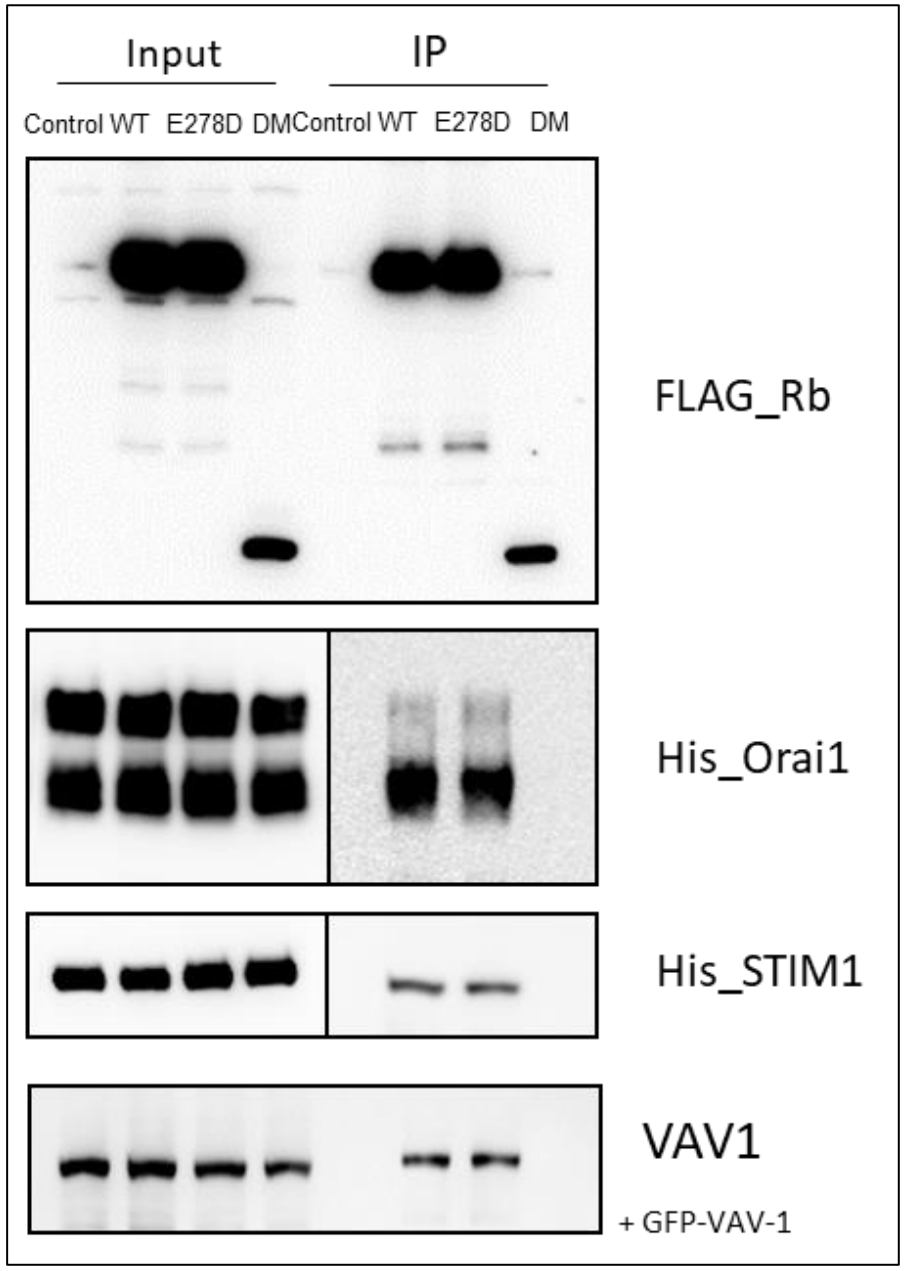

Figure 4.3.18 IP of stable cell lines

Data and figure were generated in collaboration with the Gwack lab, as described in (Section 2.2.6.5). CRACR2A was captured using anti-FLAG antibody as described in Srikanth *et al.*, 2016. Recombinant Orai1, Stim1 with a His tag, or VAV1 with GFP were transduced into HEK, and detected by western blot.

4.4 Key findings

- Generation of KO CRACR2A Jurkat cells, confirmed by WB, which gave reduced calcium flux response, pJNK signalling and IL2 expression. Expression of both patient mutant alleles E278D and DM (R144G and E300*) in HEK293T, FT cells and Jurkat cells, which was confirmed by WB.
- E278D mutant had normal CRACR2A localisation to the Golgi and vesicles. This mutant had significantly reduced IL2 expression and was able to only partially rescue calcium flux response seen in the KO cells. The JNK signalling was comparable to WT CRACR2A. The mutant was able to bind to Orai1, STIM1 and VAV1.
- DM resulted in a truncated protein at the predicted size for the E300* mutation, which was not visualised in patient primary T cells. This mutant had abnormal localisation, being present throughout the cytosol rather than only at the Golgi and vesicles. The IL2 expression, calcium flux and JNK signalling were all significantly reduced compared to WT CRACR2A protein, whereas, the E278D mutant had normal JNK signalling.

4.5 Discussion

The *in vitro* experiments described in this chapter allowed examination of the individual mutants and showed that the mutations E278D and the DM (R144G and E300*) were able to alter the function of CRACR2A as summarised in the key findings. These findings support the primary cell data discussed in Chapter 3, reinforcing that the CRACR2A mutations identified were causing the patient phenotype.

4.5.1 Cell lines as a model for CRACR2A mutations

Transient expression was performed in Jurkat and HEK293 cells using nucleofection and electroporation. These expression systems are good for having a quick look at the effect of KD or confirming the expression of mutant proteins, but don't allow for longer term functional experiments. As a result, all functional data was generated using stable cell lines, after the expression of the CRACR2A mutants was shown to be possible by electroporation and western blot.

There are many advantages of stables cell lines over primary cells, including high cell numbers, expression of a single selected allele, controllable cell populations and their expansion. These features were particularly beneficial to this project because of the low cell numbers and different expansion profiles of the T cell populations as seen for the patient primary cells in Chapter 3.

However, stable cell lines do have limitations when studying patient specific mutations. A range of proteins can be expressed *in vitro*, which may not occur in patient cells, so primary samples are needed to confirm expression *in vivo*. T cell subpopulations are not present in cell lines, so primary samples or mouse models are needed. The level of expression of the protein is often higher in stable cell lines and is not controlled between individual cells or cell lines, meaning potentially that the functional difference for mutations could also be a result of protein expression levels. The comparison between cell lines in this project was monitored by WB through loading controls, as well as by IF. The level of CRACR2A expression between the cell lines appeared similar in the IF images.

The use of mouse models can help overcome many of the limitations of using cell lines and primary samples when investigating the effects of mutation(s) in a single allele. These investigations in mouse models are currently in progress in the laboratory.

4.5.2 CRACR2A patient alleles

The functional data for the patient case study from primary cells (Chapter 3) and cell lines (Chapter 4) is summarised in Table 4.5.1.

In the patient primary T cells, the double mutant (DM, R144G and E300*) allele could not be detected by western blot (Figure 3.3.8) and it is likely that the transcript from this is sent for nonsense mediated decay. The DM was expressed in cell lines and a truncated protein was detected (Figure 4.3.11). The expression of mutant proteins not seen *in vivo* could be a result of altered nonsense mediated pathways in cell lines (Pereverzev *et al.*, 2015) or the particular expression system used to express the mutant. This difference was also observed in Chapter 5 for STIM1 P2, p.Leu74Pro mutation (Section 5.3.1.4.3). This discrepancy found between cell lines and patient cells highlights the need for both systems to be used to investigate the effects of disease causing mutations.

As the DM is not observed in patient cells, this implies that only the E278D mutant is likely to be expressed in the patient cells. In both primary cells and cell lines, this E278D mutant reduced the calcium flux response. However, in cell lines the JNK signalling is normal for this mutant but it is not so in primary cells.

Table 4.5.1 Primary and cell line functional data

Samples	Primary patient cells, compared to HC	Stable Jurkat cell lines, compared to WT CRACR2A		
Cells	**Expanded patient T cells**	**KO**	**E278D**	**DM**
CRACR2A protein expression	Both isoforms expressed Short isoform at low level No DM polypeptide seen	No	Yes Long isoform only	Yes Long isoform only
Calcium flux	Reduced with stimulation (TCR and ionomycin)	Reduced with all stimulations (TCR, I and TG)	Reduced with all stimulations	Reduced with all stimulations
Cytokine function	High IL-4 (Th2)	Reduced IL-2	Reduced IL-2	Reduced IL-2
p-JNK signalling	Reduced	Reduced	Normal	Reduced
Localisation to Golgi and vesicles	-	No protein	Normal	No localisation
Protein interaction	-	No protein	Normal with Orai1, STIM1 and VAV1	No interaction with Orai1, STIM1 and VAV1

4.5.2.1 Localisation of mutant proteins

CRACR2A is known to localise to the Golgi and vesicles (Srikanth, Jung, Kim, *et al.*, 2010). The localisation of CRACR2A was tested by IF. The E278D mutation did not appear to affect the localisation of the protein to the Golgi and vesicles (Figure 4.3.13).

The DM (R144G and E300*) was not able to localise to the Golgi and vesicles, and appeared to be distributed throughout the cell (Figure 4.3.14). Interestingly, the DM was not detected by an anti-FLAG Ab, suggesting that something may have affected the N-terminal FLAG tag, even though the same Ab was able to detect the protein in a WB (Figure 4.3.12). Potentially this could be due to changes in the 3D conformation of the protein, which could leave the FLAG tag unavailable for binding within the cells. During WB the samples are heated and the proteins denatured which would expose the tag and so allow for the protein to be detected. This inability of the DM to localise and potentially altered 3D structure could explain the reduced function

for this mutant in IL2 expression, calcium flux and JNK signalling. The DM may not be expressed in patient cells as it was not detected by WB (Figure 3.3.8).

Localisation of CRACR2A was not studied in patient samples due to the limited numbers of cells available. Functional tests such as calcium flux were prioritised over localisation. It would be beneficial to confirm that CRACR2A localises normally in the patient, which is expected due to the results for the E278D mutant in the cell lines. Use of IF in patient cells could also indicate the level of expression of CRACR2A and show if the mutant E278D affects polypeptide levels.

4.5.2.2 IL-2 expression

IL-2 expression can be used to monitor the cell's ability to produce cytokines, the T cell response and the general health of the cell line. In primary T cells, it causes the differentiation of T cells into effector T cells and memory T cells when stimulated by an antigen (Qiu *et al.*, 1999).

PMA and ionomycin can bypass the TCR complex and activate the T cell by activating protein kinase C (PKC) and increasing the calcium concentration (Kozak and Putney, 2017). T-cell activation occurs with the activation of the TCR and co-stimulatory molecules. This triggers the rapid hydrolysis of inositol phospholipids to diacylglycerol and inositol phosphates by PLC. Diacylglycerol is an allosteric activator of PKC activation and inositol phosphates, which trigger calcium release and mobilization, resulting in a cascade of additional cellular responses mediating T-cell activation. One of these cellular responses is the production and secretion of IL-2. This mechanism of action can be bypassed *in vivo* with PMA and ionomycin, which when used in combination strongly enhance IL-2 production. PMA is a small organic compound, with a structure analogous to diacylglycerol, that diffuses through the cell membrane into the cytoplasm where it directly activates PKC. Ionomycin is a calcium ionophore that triggers calcium release. Previously, siRNA-mediated depletion of CRACR2A in Jurkat cells have been shown to have reduced IL2 expression compared to control cells (Weiss A, Wiskocil RL, 1984; Srikanth, Jung, Kim, *et al.*, 2010; Held, 2018).

Both E278D and the DM cell lines showed significantly lower expression of IL-2 compared to WT CRACR2A. This was observed at both high and low stimulation conditions. This showed that both mutant CRCAR2A polypeptides studied were not able to rescue the reduced IL-2 phenotype in the KO cells. The cytokine analysis in patient CD4+ T cells also showed a change

compared to healthy control, due to a shift towards Th2 cells with the high expression of IL-4 cells. In order to understand what other cytokine pathways are affected by these mutations, further experiments are needed in patient cells or mouse models. Potentially, cytokine and pathways of interest include IL-10 due to the patient B cell phenotype and mitogen-activated protein kinase (MAPK), nuclear factor of activated T-cells (NFAT), nuclear factor-κB (NF-κB).

4.5.2.3 Calcium flux

Calcium flux was performed on the stable cell lines to see if the patient mutations affected the calcium flux response in Jurkat cells. Previously, KO of CRACR2A was shown to reduce calcium flux response in Jurkat cells by 50 % (Srikanth, Jung, Kim, *et al.*, 2010).

Using single cell imaging the calcium flux response was measured in the different cell lines, as shown in Figure 4.3.16. The KO Jurkat cell line had reduced flux compared to normal Jurkat cells (control), which was rescued in the KO cells with expression of WT CRACR2A. The cell lines expressing the patient alleles had significantly reduced calcium flux compared to WT protein. The mutants were able to, therefore, only partially rescue the effect of knocking out CRACR2A. The DM showed slightly better calcium flux compared to E278D, although the difference was not statistically significant. Patient T cells also showed reduced calcium flux results, so this is very likely to have been a direct result of the mutations.

Further investigations are needed to determine exactly how the mutation E278D could be altering the function of CRACR2A in regards to calcium flux , as the mutant has normal localisation and can interact with CRAC channel proteins. It may be that the reduced expression of the short isoform could be the cause as no data is available comparing the efficiencies of the long and short isoforms.

4.5.2.4 Calcium flux sensitivity

As discussed previously in Chapter 3, there are many challenges in measuring calcium flux in cells. In this chapter, data was collected using the plate reader methodology and single cell imaging. The main challenges of gathering calcium flux data from primary cells were overcome by using cell lines, as high cell numbers are available. Instead, sensitivity of the technique became the main limitation. The Flex Station methodology comparing KO CRACR2A and WT Jurkat cells showed very similar responses, as shown in Figure 4.3.10, with no significant difference seen. This meant that the smaller changes in calcium flux

expected in the mutant cell lines were unlikely to be detected using this method. As a result, single cell imaging was used. This method is sensitive and the calcium flux response measured between KO and WT cell lines showed a significant difference, which the mutant cell lines fell between. The smaller changes in calcium response between the different mutants was also detectable, although no significant difference was seen between the E278D and DM cell lines.

The single cell imaging method is not routinely available, and requires highly specialised expertise to run the experiments. As a result, single cell imaging was only performed during the secondment or by the Gwack group.

4.5.2.5 pJNK

The pJNK expression was measured to look at the secondary function of CRACR2A. Previously, JNK signalling was shown to be significantly reduced in mouse CRACR2A deficient $CD4^+$ T cells upon TCR activation (Srikanth *et al.*, 2016). The JNK signalling was measured in the stable cell lines using a similar method as that used on patient T cells. The E278D mutation has no effect on the CRACR2A JNK related function and was comparable to WT in the cell lines. The DM resulted in a reduced p-JNK response.

Only the E278D mutant is likely to be expressed in the patient cells. However, in cell lines the JNK signalling is normal for this mutant but not in primary cells. This suggests the reduced JNK signalling seen in the patient cells may not be directly due to the mutation in CRACR2A. However, this protein can affect this signalling pathway as seen in the KO cells herein and Srikanth *et al.*, 2019. JNK signalling is affected by cytokines expression, stress stimuli and has different roles in T cell subtypes (Conze *et al.*, 2002). As a result, the reduced JNK signalling seen in patient T cells compared to healthy control (HC) could be a result of different cytokine profiles (Figure 3.3.12) or subtype distributions (Table 3.1.2). This means further experiments would be needed to determine the cause of the reduced signalling, such as cell typing during flow cytometry experiments and looking at other pathways affected in the cells.

Examining other pathways affected by CRACR2A in addition to p-JNK was an avenue of the project which was not investigated due to time constraints. The plan was to perform PTMScan proteomics analysis using Cell Signalling Technology. No other functional pathways are known that are reduced by KO of CRACR2A, the GTPase domain could have multiple binding partners.

4.5.2.6 CRACR2A interaction with CRAC channel proteins

The binding efficiencies essential for CRACR2A function were tested using co-immunoprecipitation (co-IP), as shown in Figure 4.3.18. The E278D mutation did not appear to affect binding to Orai1, STIM1 or VAV1, and gave comparable results to WT CRACR2A.

The DM was not able to bind to any of the proteins tested. As the pull down was performed with the anti-FLAG antibody, this result may be because of binding issues between this antibody and the DM rather than the protein binding partners tested. Issues between anti-FLAG and CRACR2A DM were also seen during IF, where the DM was not detected (Figure 4.3.13), although interaction between the Ab and protein were seen in WBs (Figure 4.3.12). During WB the samples are heated and the proteins denatured which would expose the tag and so allow for the protein to be detected.

The observed lack of interaction between the DM and CRAC channel proteins may also be caused by the abnormal localisation seen in IF or due to the truncation of the protein at amino acid 300, though in published literature the interaction sites of CRACR2A with Orai1 and STIM1 appear to be contained in the C terminal region present in this mutant (Srikanth, Ribalet and Gwack, 2013). In order to confirm the ability of the DM to bind to Orai1, STIM1 or VAV1 a different pull down method is needed, such as using anti-CRACR2A. antibodies for the initial capture.

4.5.2.7 Other CRACR2A mutants

Stable cell lines expressing patient mutations in CRACR2A have not been previously published. As part of this project, other CRACR2A mutations were discovered and discussed in Chapter 3. Mutagenesis was performed on the FG11F CRACR2A plasmid, but there was not enough time to produce and test the function of these mutants in cell lines.

An additional plasmid was also made that only contained the short isoform of CRACR2A. This isoform contains the N terminal of CRACR2A with the EF hand domains and coiled coil needed for CRAC channel interaction and is 395 amino acids. The three mutations investigated in this chapter are located within the short isoform. It is only 95 amino acids longer than the DM that had reduced function in IL-2 expression, calcium flux and p-JNK. The aim was to produce a cell line expressing only the short form to see how it behaved in comparison to the long isoform and the truncated DM. No data is available in the published literature comparing the calcium flux contribution of the short and long isoform, though the short isoform has relatively low expression in all cell types apart from lymphocytes (www.proteinatlas.com).

Chapter 5 CRAC channel related protein mutations

5.1 Introduction

As described previously the Ca^{2+}-release activated Ca^{2+} (CRAC) channel contains two main proteins, calcium release-activated calcium channel protein 1 (Orai-1) and stromal interaction molecule 1 (STIM1), as well as a regulator protein called calcium release activated channel regulator 2A (CRACR2A), which was investigated in Chapters 3 and 4. The CRAC channel allows movement of calcium into the endoplasmic reticulum (ER) for storage, where it is used as a secondary massager. It is particularly important in the immune system and deficiency of STIM1 or Orai1 results in primary immunodeficiency (PID). Orai1 proteins form the pore of the channel in the plasma membrane, and STIM1 is located in the endoplasmic reticulum. When the intracellular calcium levels are low, STIM1 translocates from the ER and binds to Orai1 to activate the CRAC channel, as described in Section 1.3. STIM1 and Orai-1 are the focus of this chapter.

5.1.1 STIM1

The STIM1 protein has both an ER domain and a cytoplasmic domain as shown in Figure 5.1.1. The EF hands, located in the ER lumen detect changes in calcium concentration. The EF is structurally a helix-loop-helix motif with negatively charged residues (Asp and Glu) which bind calcium at high concentrations in the ER. A conformational change occurs in this region when the ER is depleted of calcium, because as the calcium dissociates from STIM1, the auto-inhibitory EF- sterile α motif (SAM) structure destabilises. STIM1 undergoes translocation to puncta at ER- plasma membrane (PM) junctions, oligomerization and cluster formation and subsequent calcium influx through the CRAC channel (Prakriya, 2009; Jairaman and Prakriya, 2013; Notarangelo *et al.*, 2013; Prakriya and Lewis, 2015).

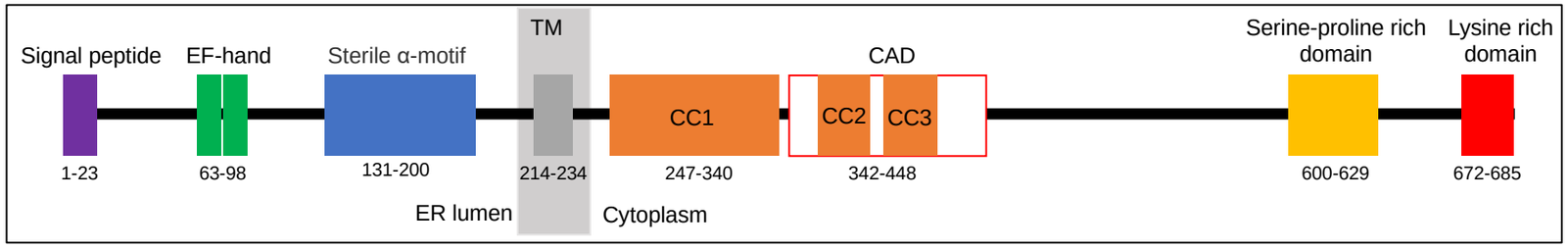

Figure 5.1.1 STIM1 protein functional domains

Figure compiled from databases (Ensembl, UniProt) and Kozak and Putney 2017. STIM1 is a ubiquitously expressed, 77 kDa single-pass ER membrane protein as shown by the transmembrane (TM) region.

The EF-hand domain is a Ca^{2+} sensor. Sterile α motif (SAM) is a protein interaction domain, During high Ca^{2+} in the ER it maintains the folded conformation of the protein and facilitates oligomerisation during ER store depletion. The coiled-coil (CC) domains are involved in ER retention and stability. The region annotated as CAD (CRAC activation domain, p.342–448) is required for the activation of CRAC channels, alternative names include SOAR (STIM1-Orai1 activating region, residues 345–444), or Ccb9 (residues 339–446). Mutations in this region inhibit the activation of Orai1, if the SOAR dimer cannot form. In the CC1 regions is an inhibitory helix (p.310-337) which interacts with SOAR and keeps STIM1 in an inactive conformation (Kozak and Putney, 2017; Nelson and Roe, 2018; Nelson *et al.*, 2018).

5.1.1.1 STIM2

Humans also express STIM2 which has complementary, and nonredundant, functions in Ca^{2+} signalling (Collins and Meyer, 2011). STIM1 and STIM2 share many core functional domains shown in Figure 5.1.1, so are likely to use the similar mechanisms of sensing and communicating Ca^{2+} store depletion, such as EF hand domains and translocation to puncta.

However, there are differences between the two homologs. The N-terminal of STIM2, including the EF hand and SAM domains are more structurally stable, which allows for faster reactions to smaller decreases in [Ca^{2+}] ER (Zheng *et al.*, 2011).

5.1.1.2 PID associated with STIM1

Loss of function or null mutations of STIM1 are known to cause early-onset combined immunodeficiency (CID) disease with recurrent and chronic infections, autoimmunity, haemolytic anaemia, ectodermal dysplasia, muscular weakness and myalgia (Feske, Picard and Fischer, 2010; Feske, 2011; Jairaman and Prakriya, 2013). STIM1 deficiency is described in more detail in Section 1.3.3 and Table 1.3.1.

STIM1-deficient patients have impaired T cells and natural killer (NK) cell function, a normal distribution of the major immune cell types, including T cells, B cells and NK cells and with a T cell repertoire that is normally comparable to healthy individuals (Jairaman and Prakriya, 2013). STIM1 deficiency results in no store-operated calcium entry (SOCE) in T cells and as a result the patient cells cannot respond appropriately to T cell receptor (TCR) activation or pharmacological agents such as ionomycin, thapsigargin, which typically trigger Ca^{2+} influx (Feske, Picard and Fischer, 2010).

The CRAC channel is essential for normal T cell function. STIM1 deficient patient T cells lack SOCE and so have impaired proliferation and cytokine production such as IL-2, IFNy, and IL-17, regardless of naïve or effector T cells (Oh-hora *et al.*, 2008; Beyersdorf *et al.*, 2009; McCarl *et al.*, 2010). However, SOCE is not essential for T cell development, through positive selection of TCRαβ^{+}T cells, so patients with STIM1 deficiency often have a normal number of T cells in their peripheral blood (Kozak and Putney, 2017).

5.1.1.3 CANT1 mutations

Calcium activated nucleotidase 1 (CANT1) mutation identified in STIM1 P1 has previously been linked to disease. CANT1 preferentially hydrolyses uridine diphosphate (UDP) followed by guanosine diphosphate (GDP), uridine triphosphate (UTP) and adenosine diphosphate (ADP) in the ER and golgi (Furuichi *et al.*, 2011; Nizon *et al.*, 2012; Rice *et al.*, 2019).

CANT1 gene mutations have been linked to chondrodysplasia, a disease that is related to human stature. Desbuquois dysplasia (DBQD) type 1, is a rare autosomal recessive chondrodysplasia, characterized by short stature, joint laxity, short extremities and round face; the radiological features include “Swedish key” appearance of the proximal femur, advanced carpal and tarsal bone age and progressive scoliosis. Type 1 DBQD differs from type 2 by hand anomalies (extra ossification centre distal to the second metacarpal, delta phalanx, bifid distal phalanx of the thumb and phalangeal dislocations) (Furuichi *et al.*, 2011; Paganini *et al.*, 2019; Rice *et al.*, 2019).

5.1.2 STING

Stimulator of interferon genes (STING) is involved in the innate immune response, through the production of type I IFNs. STING or transmembrane protein 173 (TMEM173), is a 379 amino acid protein, and the functional domains in this protein are shown in Figure 5.1.2. Under resting conditions STING is localised in the ER and is expressed mainly in hematopoietic cells (macrophages, natural killer cells, and T cells), endothelial and epithelial cells, which are all exposed to the environment and thus susceptible to infectious agents (Uhlen *et al.*, 2010; Shang *et al.*, 2012; *The Human Protein Atlas*, 2020).

STING is an ER sensor that is activated directly by cyclic dinucleotides (CDNs) which are secreted by intracellular bacteria, like *Listeria monocytogenes*. It is also activated by non-canonical cyclic-GMP-AMP generated by cyclic GMP-AMP synthase (cGAS). The cGAS pathway is a viral immune response, which is activated by double stranded DNA in the cytosol. Activation of STING leads to a conformational change and triggers the trafficking of STING complexed with TANK-binding kinase 1 (TBK1) from the ER to endosomal/lysosomal perinuclear regions. TBK1 phosphorylates transcription factors interferon regulatory factor 3 (IRF3) and NF-κB, which translocate to the nucleus and initiate innate immune gene transcription. STING is suppressed and

rapidly degraded after activation, to avoid sustained cytokine and autoinflammatory disease (Ishikawa and Barber, 2008; Ishikawa, Ma and Barber, 2009; Pokatayev and Yan, 2017; Ahn and Barber, 2019; Zhang *et al.*, 2019).

The importance of STING function is highlighted by the growing evidence that a variety of microorganisms have attempted to evolve strategies to inhibit STING-dependent signalling and autoimmune diseases resulting from STING mutations (Ahn and Barber, 2019; Motwani, Pesiridis and Fitzgerald, 2019).

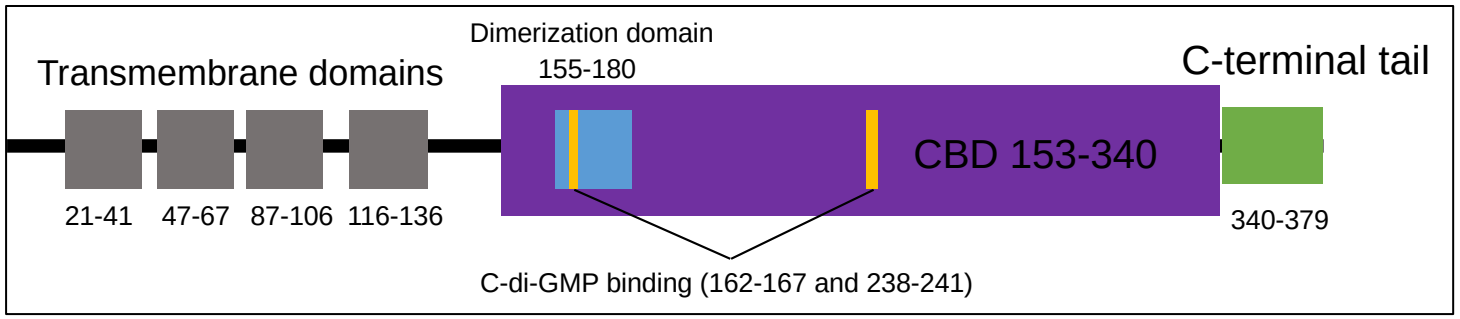

Figure 5.1.2 STING protein functional domains
Image compiled from Xiaomei Wu et al. 2014) and Uniprot.org. Cyclic dinucleotide-binding domain (CBD).

5.1.2.1 Disease association

Deficiency of STING leads to a type of systemic autoinflammatory disease (SAID), which comprises disorders of the innate immune system. This autoinflammatory autosomal dominant condition is called STING-associated vasculopathy with onset in infancy (SAVI). This is an autoinflammatory vasculopathy causing severe skin lesions, particularly affecting the face, ears, nose, and hands, and resulting in ulceration, eschar formation, necrosis, and, in some cases, amputation. Patients often have interstitial lung disease and increased β-interferon signalling (Liu *et al.*, 2014; Kacar, Pathak and Savic, 2019).

STING-deficient cell lines are defective in IFN-I induction. STING-deficient mice are more sensitive to DNA and RNA viruses compared to controls, such as HSV-1, suggesting an important role in maintaining immune homeostasis (Ishikawa, Ma and Barber, 2009; Ahn and Barber, 2019).

5.1.2.2 Association with STIM1

STIM1 was found to act as a negative regulator for STING. STIM1 was shown to inhibit STING trafficking by physically interacting with STING and retaining it at the ER membrane. This interaction is important in maintaining STING in an inactive state. High STING expression results in decreased SOCE, due to the decrease of STIM at puncta sites. In SAVI, the interaction between STIM1 and STING is weakened (Rice *et al.*, 2019; Srikanth *et al.*, 2019).

5.1.3 Aims

The work in this chapter focuses on smaller case studies than that shown in Chapters 3 and 4. The three patients discussed in this chapter were all identified to have mutations in genes which had previously been linked to disease. This meant less evidence was needed to show that the mutations were pathogenic as literature was available on previous cases. However, the phenotypes for some of these patients were not in line with current classical symptoms so these new case studies can still add to the field of PID.

All the genes identified containing mutations in this chapter have previously been associated with the CRAC channel and so can further our understanding of this pathway.

The aims of the work presented in this chapter were to:

- Identify CRAC channel related mutations in patients with PID
- Confirm lack of STIM1 function in primary patient samples
- Determine if IGS expression is affected in a patient with a STING mutation

5.2 Method strategies

5.2.1 Sequencing strategies

WES and filtering for the STIM1 P2 and STING patient was done using the same strategy as described in Section 2.2.1.1 and 2.2.1.2 for the CRACR2A case. For STIM1 P1, STIM1 deficiency was suspected due to their classical phenotype, so a modified exome sequencing approach was performed using the Agilent SureSelectXT with All Exon v5 capture library and sequenced on Illumina HiSeq 3000 for 2× 150-bp paired-end sequencing.

5.2.2 Publications about these specific patients

In this chapter, two cases of STIM1 deficiency are presented, which have been published. The case study of P1 has been published in two articles: Rice *et al.*, 2019 and Srikanth *et al.*, 2019. The case study of P2 has been published in two articles: Parry *et al.*, 2016 and Rice *et al.*, 2019.

5.2.2.1 Immunoglobulin gene expression data

Immunoglobulin related gene expression was measured using the protocol detailed in Section 2.2.1.9.1. This was performed on STIM1 P1 and STIM1 P2 and published in Srikanth *et al.*, 2019 and Rice *et al.*, 2019 respectively. The same method was performed on the STING 1 patient.

The data for each experiment was analysed separately. The relative abundance of each transcript was normalized to the expression level of *HPRT* to obtain ΔC_T and further normalized to the values obtained for healthy controls to obtain $\Delta\Delta C_T$. To compare the data generated for the STIM1 P1 and STING patient, the HC normalised data $\Delta\Delta C_T$ was taken. This means the patients are normalised to different HCs but any assay variation was accounted for. Prism software was used to determine statistical significance, using Holm-Sidak multiple T tests.

5.3 Results

5.3.1 STIM1 patients

In this section, results from two STIM1 deficient patients are described. Different mutations can present with different phenotypes and so the functional and immunological profiles have been compared to try and gain a better understanding of the breadth of STIM1 related deficiency with PID.

5.3.1.1 STIM1 mutations

5.3.1.1.1 Patient 1

This is a 5-year-old male of consanguineous Pakistani background. For P1, two mutations were identified on the clinical exome, described in Section 5.2.1. The clinical exome sequences only genes known to cause disease. For P1 a homozygous mutation was identified in the *STIM1* gene and another in the *CANT1* gene.

Sanger sequencing confirmed the homozygous deletion in *STIM1*: c.478del, p.(Ser160ValfsTer15). This was performed as part of the clinical diagnosis by the hospital, and so no genomic DNA was available for this project. Parental DNA was sequenced in-house by Sanger sequencing to look at the segregation of the of the STIM1 mutation. Both parents were found to have a deletion at the same position as the proband, though in a heterozygous form, which confirms the segregation of the mutant allele in this family, as can be seen in Figure 5.3.1. The single base deletion in codon 160, occurs in the SAM domain of the corresponding polypeptide (Figure 5.1.1). The single base deletion results in a reading frameshift that creates a premature stop codon 15 amino acids downstream of the deletion, which will produce a truncated STIM1 protein that lacks essential functional domains, including the TM domain.

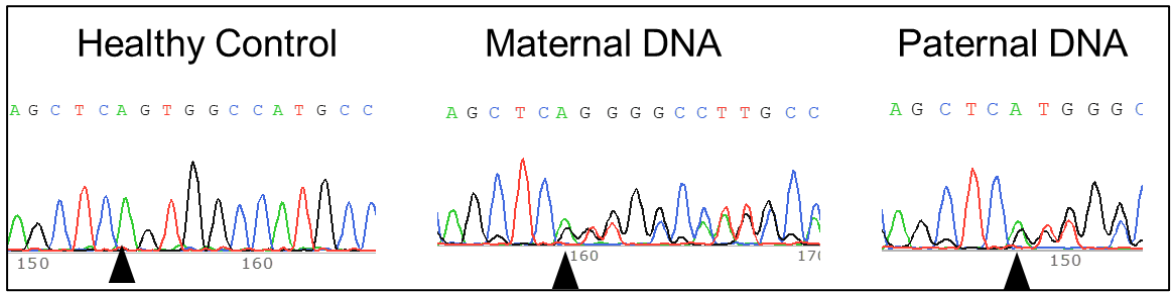

Figure 5.3.1 *STIM1* Sanger sequencing of P1 family

STIM1 gene is located at Chromosome 11: 3,854,527-4,093,210, on the forward strand. Genomic DNA isolation from patient whole blood, PCR and Sanger sequencing were performed as per Section 2.2.1.4 . Primer pairs Z and A1 were used to generate PCR products (Table 2.1.1). The PCR products was amplified in duplicate and run on a 1.5 % agarose gel, to confirm the predicted sizes. They were then directly sequenced using both the forward and reverse primers defined above.

The arrow indicates where the deletion of the A base occurred. In the parents, before the deletion a single trace is present, meaning the two alleles have the same sequence, after the deletion two traces can be seen, indicating that only one allele has the mutation.

The *CANT1* homozygous missense mutation c.676 G>A, p.(Val226Met), codon Gtg>Atg was also confirmed as part of the clinical diagnosis and segregation was confirmed in parental DNA. The pedigree of the patient containing both mutations is shown in Figure 5.3.2.

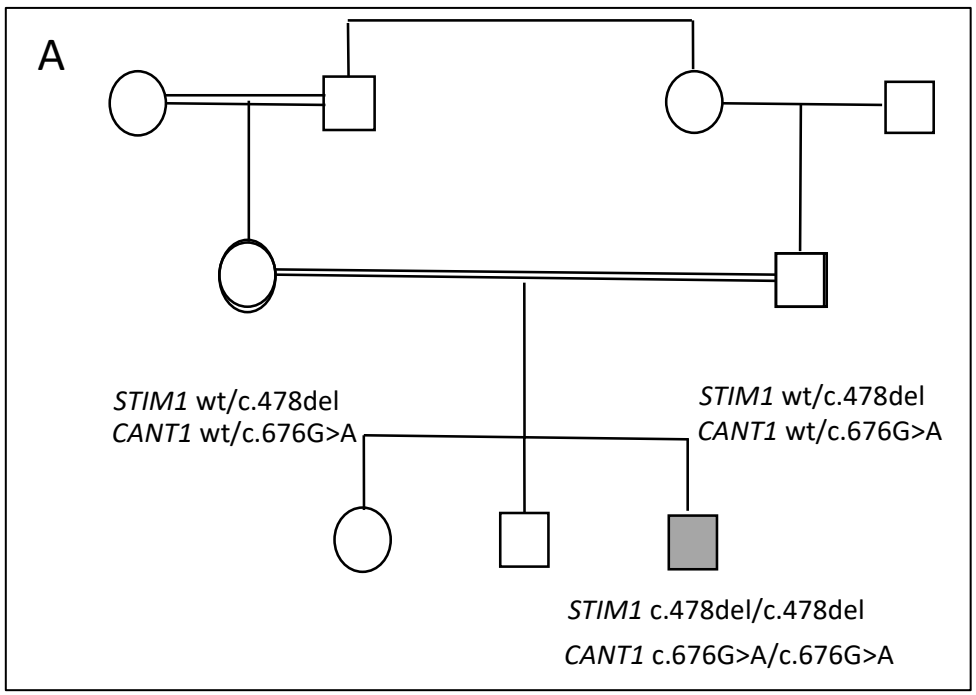

Figure 5.3.2 P1 family pedigree.

Only the genomic DNA from parents and the patient was sequenced. The two siblings are fit and healthy, they were not analysed as part of this project and so their genotype is unknown. The double lines indicate a consanguineous union. Patient genotype was confirmed by the clinical department and Sanger sequencing of parental genomic DNA performed by the author.

5.3.1.1.2 Patient 2

Patient 2 is a male case aged 17years from a consanguineous family. The *STIM1* mutation was identified via WES by Parry *et al.*, 2016 and Sanger sequencing confirmed the presence and segregation of the homozygous *STIM1* c.221T>C. This mutation results in the p.Leu74Pro amino acid change in the EF-hand domain of the protein.

5.3.1.2 P1 *CANT* mutation

As stated above the *CANT1* homozygous missense mutation c.676 G>A, p.Val226Met. Gtg>Atg was confirmed by the hospital and segregated by Sanger sequencing of paternal DNA, with primer pair B1 and C1 in Table 2.1.1 using the same method as used to confirm the STIM1 mutation. None of the *CANT1* sequencing is shown here. The known pathogenic *CANT1* mutation has previously been described in multiple patients with BKim-variant Desbuquois dysplasia, usually in compound heterozygosity with another mutation (Kim *et al.*, 2010; Furuichi *et al.*, 2011).

The overall small stature observed in P1 was consistent with previous reports regarding the effects of this *CANT1* variant. A skeletal survey was performed. The skeletal survey showed an abnormal early maturation of carpal bones and a gentle curve scoliosis of the cervicothoracic spine, both of which have previously been seen in *CANT1*-related disorders (Nizon *et al.*, 2012; Bui *et al.*, 2014). Though the monkey wrench deformity of the femoral necks, shortened metacarpal bones, and other abnormalities was not seen in this patient. Images of this can be seen in Figure 3 of Rice *et al.*, 2019.

The homozygous mutation of CANT1 c.676G>A has previously been shown to affect the protein function. This missense mutation significantly reduces, but does not eliminate, the nucleotidase activity of *CANT1* (Furuichi *et al.*, 2011). In patients with disease, a second mutation is also normally present which results in a premature stop codon or more significantly reduced *CANT1* nucleotidase activity. No such second mutation was identified in P1. As such, this single homozygous mutation in *CANT1* causes a less severe phenotype than the “Kim-variant” Desbuquois dysplasia, which occurs when a more damaging mutation is present on the other allele (Balasubramanian *et al.*, 2017; Rice *et al.*, 2019).

5.3.1.3 Patient immunological profiles

5.3.1.3.1 Patient 1 (P1)

The patient was suspected of having CRAC channel deficiencies early in life due to their recurrent tooth infections and tooth enamel deficiency. A full dental clearance was needed. Other symptoms include; reduced muscle bulk, hypermobile joints, proximal weakness, fixed dilated pupils, recurrent sinopulmonary infections, ichthyosis, anhidrosis, severe eczema mainly affected the palms and soles of the feet and cheeks and nail dystrophy.

P1 had normal numbers of T, B, and NK cells, which is typical for STIM1 deficiency, as seen in Table 5.3.1. The immunoglobulins (IgG, IgA, IgM, and IgG subclasses) were normal with marginally elevated total IgE. The levels of specific antibodies to tetanus and Haemophilus influenza type b (Hib) were adequate. The total anti-pneumococcal antibody levels were reduced. However, following a challenge vaccination with pneumovax, the levels increased well above the protective titre (from 6.2 to 120.7 µg/mL). The T cell proliferation response to PHA was overall comparable to HC, though one measurement at the highest stimulation was reduced. This latter result was not seen the next year, as seen in Table 5.3.2.

Table 5.3.1 Lymphocyte and immunoglobulin counts and challenge response of P1

	cells/µL		
	May 2017	Nov-2018	Normal range
Total Lymphocyte	4609	6285	1700 - 6900
CD3	3581	5329	900 - 4500
CD19	749	1001	200 - 2100
CD4	2120	3467	500 - 2400
CD8	1141	1636	300 - 1600
NK	273	132	100 - 1000
Ratio (CD4/CD8)	1.86	2.11	1.07 - 1.87
	g/L		
IgG	8.8	-	4.9 - 16.1
IgA	1.41	-	0.40 - 2.00
IgM	0.62	-	0.50 - 2.00
IgG1	6.47	-	3.62 - 12.28
IgG2	1.98	-	0.57 - 2.90
IgG3	0.475	-	0.129 - 0.789
IgG4	0.044	-	0.013 - 1.446
Total IgE	60.8 ku/L	-	<52 ku/L
	Antibody Response (see normal ranges for units)		
Haemophilus Ab	3.259	5.776	(µg/mL): Inadequate <0.1, Suboptimal 0.1-1, Adequate >1
Pneumococcal Ab	120.7	6.2	(µg/mL): Inadequate <10, Suboptimal 10-30, Adequate >30
Tetanus Ab	0.804	1.099	(IU/mL): Inadequate <0.01, Suboptimal 0.01-0.15, Adequate >0.15

Data was generated by Leeds Clinical Department and supplied by Clive Carter (SJUH). Results from patient whole blood. Values outside the normal ranges are highlighted in red.

Table 5.3.2 T cell proliferation

	11.11.2017	14.05.2018
PHA at 100 µg/mL	Counts per minute (cpm)	
P1	13956	46630
HC	65335	55285
PHA at 10 µg/mL	Counts per minute (cpm)	
P1	73322	69595
HC	118453	98104

Data generated by Leeds Clinical Department and supplied by Clive Carter (SJUH). Results below (blue) the HC values are colour coded. For PHA the dose was increased and the number of initial cells per condition stayed the same.

5.3.1.3.2 Patient 2 (P2)

Patient 2 has recurrent infections, mild muscles weakness, normal reflexes, hypermobile, diminished sweating and generalised hypomineralised amelogenesis imperfecta (AI) (Parry *et al.*, 2016; Rice *et al.*, 2019). The initial patient tests, in 2011 and 2013, showed an immunological profile within normal ranges for bacterial and viral antibodies, lymphocyte counts, T cell proliferation and immunoglobulins. The CD4/CD8 ratio was elevated to 1.9 in 2013 (normal 1.07-1.87). In 2018, additional tests showed normal cell counts of T cell subsets, B cells and NK cells and normal T cell spectratyping of the β chain of the TCR. The only result out of normal ranges was for the reduced CD4+ DR+ count of effector memory T cells.

5.3.1.4 STIM1 expression

5.3.1.4.1 Patient 1 mutation

The homozygous deletion in *STIM1* NM_003156.3:c.478del, p.(Ser160ValfsTer15) creates a frameshift that results in a premature stop codon. It is likely that this transcript is sent for nonsense mediated decay. The stop codon occurs in the SAM domain and the predicted truncated protein would not contain important functional domains of STIM1, such as the CRAC activation domai

n (CAD p.342-448) needed for Orai1 interaction, as seen in Figure 5.3.3.

A

> 791amino acid (84 kDa)

MDVCVRLALWLLWGLLLHQGQSLSHSHSEKATGTSSGANSEESTAAEFCRIDKPLCHSEDE
KLSFEAVRNIHKLMDDDANGDVDVEESDEFLREDLNYHDPTVKHSTFHGEDKLISVEDLWKA
WKSSEVYNWTVDEVVQWLITYVELPQYEETFRKLQL**S**GHAMPRLAVTNTTMTGTVLKMTDR
SHRQKLQLKALDTVLFGPPLLTRHNHLKDFMLVVSIVIGVGGCWFAYIQNRYSKEHMKKMMK
DLEGLHRAEQSLHDLQERLHKAQEEHRTVEVEKVHLEKKLRDEINLAKQEAQRLKELREGTE
NERSRQKYAEEELEQVREALRKAEKELESHSSWYAPEALQKWLQLTHEVEVQYYNIKKQNA
EKQLLVAKEGAEKIKKKRNTLFGTFHVAHSSSLDDVDHKILTAKQALSEVTAALRERLHRWQQ
IEILCGFQIVNNPGIHSLVAALNIDPSWMGSTRPNPAHFIMTDDVDDMDEEIVSPLSMQSPSLQ
SSVRQRLTEPQHGLGSQRLVEGEAGHFLTSRVSLRRMRSLSSGQSFSSEGYGTSSPSASA
AASCSSSITTITTTTTTTTTFTTVHVHPVYYHHSTSYFLQMEPYPDTPPSDSTAVMPGHSESL
GDLTHSDSESSLHMSDRQRVAPKPPQMSRAADEALNAMTSNGSHRLIEGVHPGSLVEKLPD
SPALAKKALLALNHGLDKAHSLMELSPSAPPGGSPHLDSSRSHSPSSPDPDTPSPVGDSRA
LQASRNTRIPHLAGKKAVAEEDNGSIGEETDSSPGRKKFPLKIFKKPLKK*

B

>173 amino acids (20 kDa)

MDVCVRLALWLLWGLLLHQGQSLSHSHSEKATGTSSGANSEESTAAEFCRIDKPLCHSEDE
KLSFEAVRNIHKLMDDDANGDVDVEESDEFLREDLNYHDPTVKHSTFHGEDKLISVEDLWKA
WKSSEVYNWTVDEVVQWLITYVELPQYEETFRKLQL**MAMPCQGWLSPTPP***

Figure 5.3.3 Amino acid sequence of STIM1.

A) WT STIM1 sequence (Transcript ENST00000616714.4). This shows the amino acid (S) directly affected by the deletion as underlined and the grey amino acids are absent in the patient STIM1 polypeptide. B) Predicted patient sequence, highlighted is the alternate polypeptide sequence p.Ser160ValfsTer15.

5.3.1.4.2 STIM1 mRNA

To see if any STIM1 transcripts were present in P1 despite the frameshift pS160fs, qPCR of the patient cDNA was performed. The levels of mRNA for STIM1 in the patient PBMCs was comparable to that for HC, as shown in Figure 5.3.4. In order to determine if any STIM1 protein was expressed from the mutant transcript, western blots were performed (Section 5.3.1.4.3).

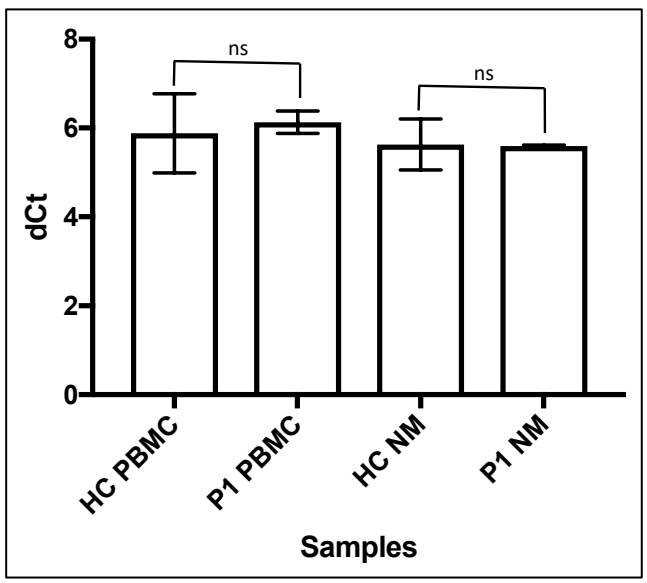

Figure 5.3.4 qPCR of STIM1 in Patient 1

PBMCs and non-monocytes (NM) were isolated by gradient separation and negative selection of monocytes (Sections 2.2.3.4). RNA was isolated and cDNA produced using high capacity reverse transcription (Section 2.2.1.6). SYBR green qPCR was performed (2.2.1.9). The melt curves indicate a single band was produced with both primer pairs.
qPCR data comparing cDNA for 2 HC with P1. H36B4 was used to normalise each sample, which were run in triplicate. 2 separate HC were used. There were 2 types of cells for each individual, total PBMCs and non-monocytes (NM). There was no significant difference <0.05 using a Two-Tailed unpaired student T test.
P1 vs HC(pooled) PBMC P=0.6597, P1 vs HC(pooled) non-monocytes P=0.9215

5.3.1.4.3 Protein expression in primary patients samples

To confirm the predicted premature codon in P1 western blots were performed with the patient PBMCs to look for full length STIM1 and the truncated STIM1 at 20 kDa.

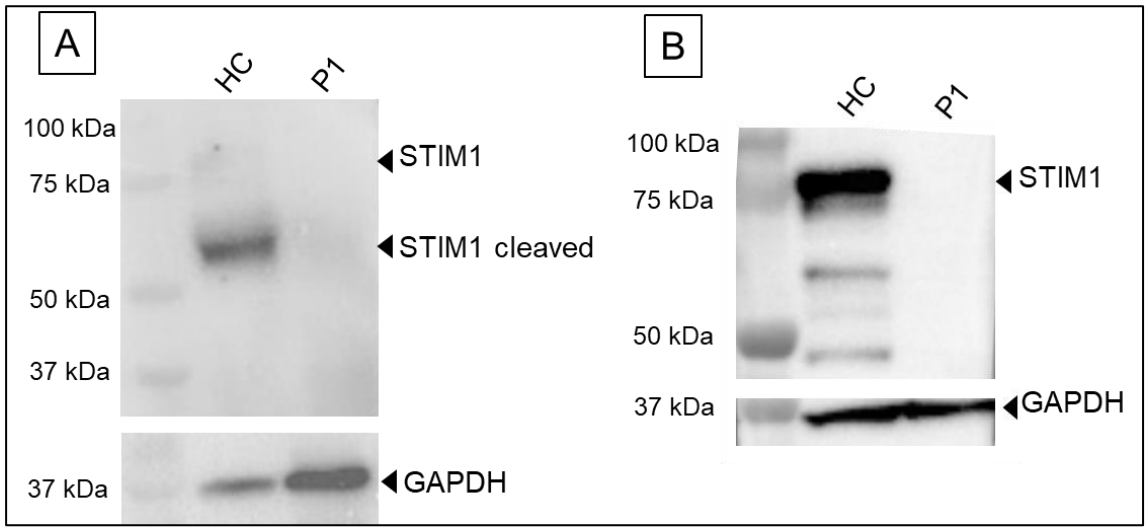

Figure 5.3.5 STIM1 WB with P1 sample

Both western blots were performed using the WB Method A (Section 2.2.6.1) with 20 µg/lane loaded and visualised with anti-STIM1 and anti-GAPDH antibodies, for details see Table 2.1.3. A) The lysate was made from P1 and HC PBMC's that had undergone negative T cell selection (Section 2.2.3.3.2), before NP40 lysis. B) The lysate used fresh PBMCs including T cells using the same NP40 lysis method as for (A).

The WB in Figure 5.3.5 of patient PBMCs without T cells (A) and fresh PBMCs (B) used the same STIM1 Ab, which was a mouse monoclonal, raised against full length STIM1. In both primary patient sample types, no full length STIM1 can be seen in the patient. However, the PBMCs without T cell samples did not give an intense band in the HC at the expected size for full length STIM1 (84 kDa) that can be seen in Figure 1.3.5 B). Instead, the darkest band can be seen at approximately 60 kDA, and a band of this size is also present in the fresh PBMCs but to a lesser extent. This band may be a result of calpain cleavage, a Ca^{2+} -dependent protease (Prins and Michalak, 2015) that results in a 60 kDa product. The lysates in panel A) underwent the additional step of negative selection, so they were more heavily manipulated and at room temperature for longer than those cells lysed in B), which could have increase the amount of calpain cleaved protein.

The antibody used in Figure 5.3.5 was a mouse monoclonal, raised against recombinant full length STIM1, with an unspecified epitope, which reduces the possibility of detecting truncated forms of STIM1, so a range of STIM1 antibodies were used to try and visualise the predicted 20 kDa protein in P1. Figure 5.3.6.A) used a C-terminal specific monoclonal antibody raised against a synthetic peptide corresponding to residues surrounding Pro622 of human STIM1 protein. This meant it is unlikely to detect the truncated form of STIM1 in P1. Figure 5.3.6.B) used a N-terminal specific antibody raised against amino acid 25-139 of STIM1, which lies before the patient frameshift at p.S160. This was the antibody most likely to detect the truncated form, but

no band could be seen. Figure 5.3.6.C) used a rabbit bleed, so contained many possible antibodies raised against STIM1, no bands were seen at the predicted size of the truncated protein.

Three different purified antibodies and an un-purified rabbit bleed where not able to detect any STIM1 protein in the P1 PBMCs as shown in Figure 5.3.5 and Figure 5.3.6. This suggests that the patient mutation may result in a transcript that is sent for nonsense mediated decay, or produces a very unstable protein. A lack of protein was also seen in P2 which was unexpected as the mutation resulted in an amino acid change and not a premature stop codon. When this patient was previously published (Parry *et al.*, 2016), no WBs were performed on patient samples and as a result normal protein expression was assumed. In this paper, the mutation was expressed in HEK293 cell lines and expression was comparable to WT protein. The discrepancy seen between expression of this mutant STIM1 protein in cell lines and patient PBMCs may be due to the vector used for lentiviral transduction. The publication used YFP-STIM1 plasmids (Addgene, plasmid 18857) which contains a human cytomegalovirus (CMV) immediate-early enhancer, to cause a multiple-log increase in expression (Gruh *et al.*, 2008).

5.3.1.5 STIM2 expression

STIM2 is a homolog of STIM1, and shares 62.42 % identity at the protein level. STIM2 has been shown to interact with STIM1 in T cells (Beyersdorf *et al.*, 2009). In some cell types STIM2 has been shown to have a direct effect on SOCE, but its main function in T cell is in regulating the resting calcium level in the ER and calcium leakage (Gruszczynska-Biegala *et al.*, 2011). Over expression of STIM2 was seen in PBMCs from both patients when compared to HC by WB, though the protein band appears darker in P1 (Figure 5.3.7). To quantify expression, the full length protein of STIM2 at 100 kDa and the loading control were compared in ImageJ, where the pixel density of the bands was given as an area, the percentage of each band was relative to both the loading control and the protein of interest. The relative density was calculated using the relative percentages of STIM2 compared to ß actin. For example, when there is no STIM2 band present, the area would be 0 %, and the relative density compared to ß actin would be 0. The highest relative density of the full length STIM2 protein band was found in P1, at 0.54 (Figure 1.3.7).

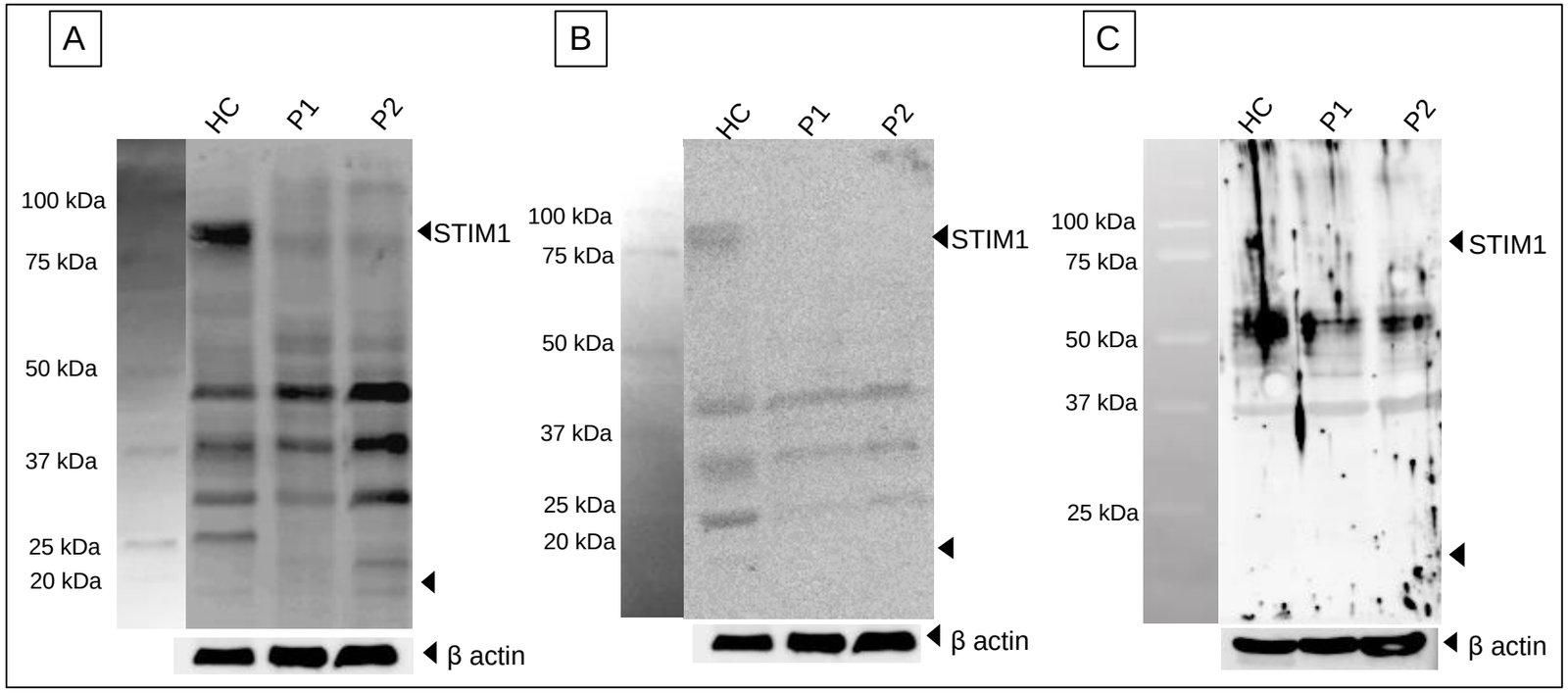

Figure 5.3.6 Range of STIM1 Antibodies with P1 and P2

All WB seen here were performed using WB Method B (Section 2.2.6.2). Lysate made from frozen PBMCs by sonication. Maximal loading was used of these lysates rather than a specific amount of total protein. The blots used different antibodies, more details can be found in Table 2.1.3. A) C-terminal STIM1 D88E10 , B) N-terminal specific antibody Anti-GOK/Stim1 and C) used an unpurified rabbit bleed (sera). Full length STIM1 at 84 kDa is indicated by an arrow, the unlabelled arrow indicates where the truncated patient mutation is predicted to occur, at 20 kDa.

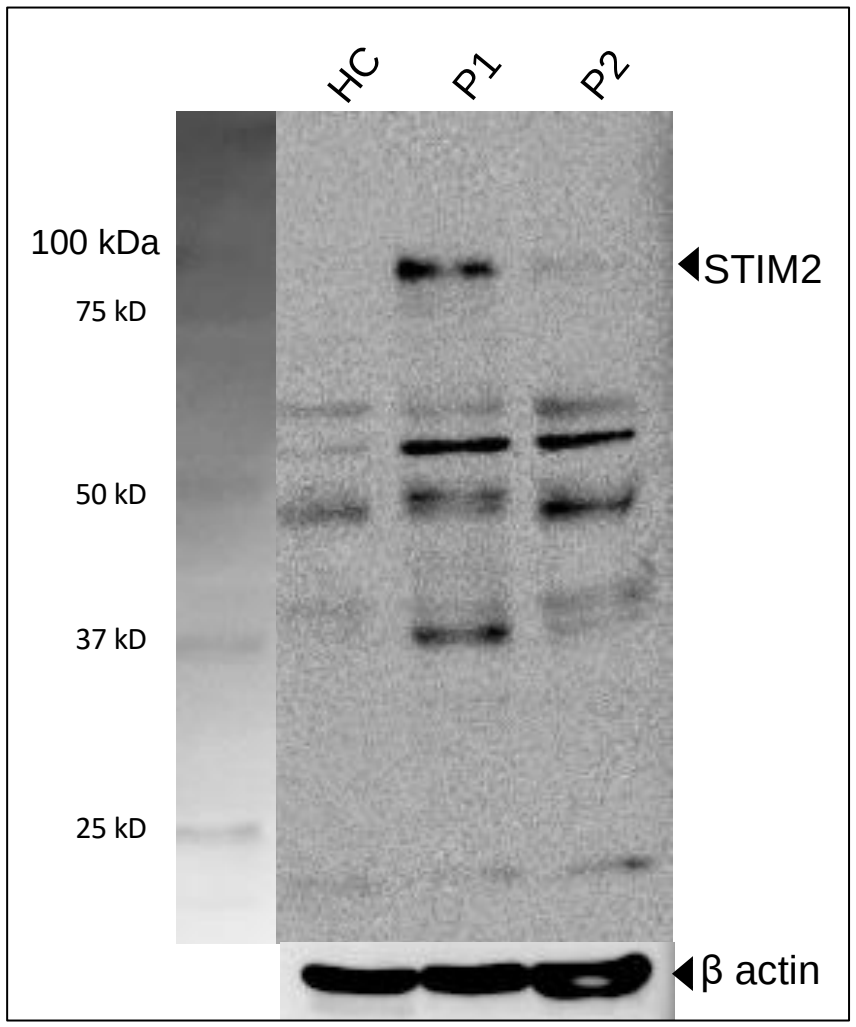

Lane	Area of STIM2	% of STIM2	Relative density of STIM2	Area of β actin	% of β actin	Relative density of β actin
HC	0.00	0.00	0.00	15564.69	100.00	1.00
P1	9411.30	35.00	0.54	17499.45	65.00	1.12
P2	600.51	2.58	0.03	22672.92	97.42	1.46

Figure 5.3.7 STIM2 WB

WB was run using the same lysate and method as detailed for Figure 5.3.6, with maximal loading and blotted with STIM2 Ab, full length protein can be seen at 100 kDa. ImageJ was used to calculate the relative density of the ß actin and full length STIM2 band using the same protocol (Miller, 2010).

β actin is overexposed and more protein may have been loaded for P2.

5.3.1.6 Calcium flux of patient T cells

STIM1 deficient T cells, have been shown to have no SOCE when stimulated with TG, TCR activation and Ionomycin. P2 T cells and NK cells were previously shown to have no SOCE, though additional samples were not available to reconfirm this result using the plate reader method. In Figure 5.3.8, this same lack of response was observed when using T cells from the STIM1 patient. (Feske, Picard and Fischer, 2010; Feske, 2011; Jairaman and Prakriya, 2013; Parry *et al.*, 2016)

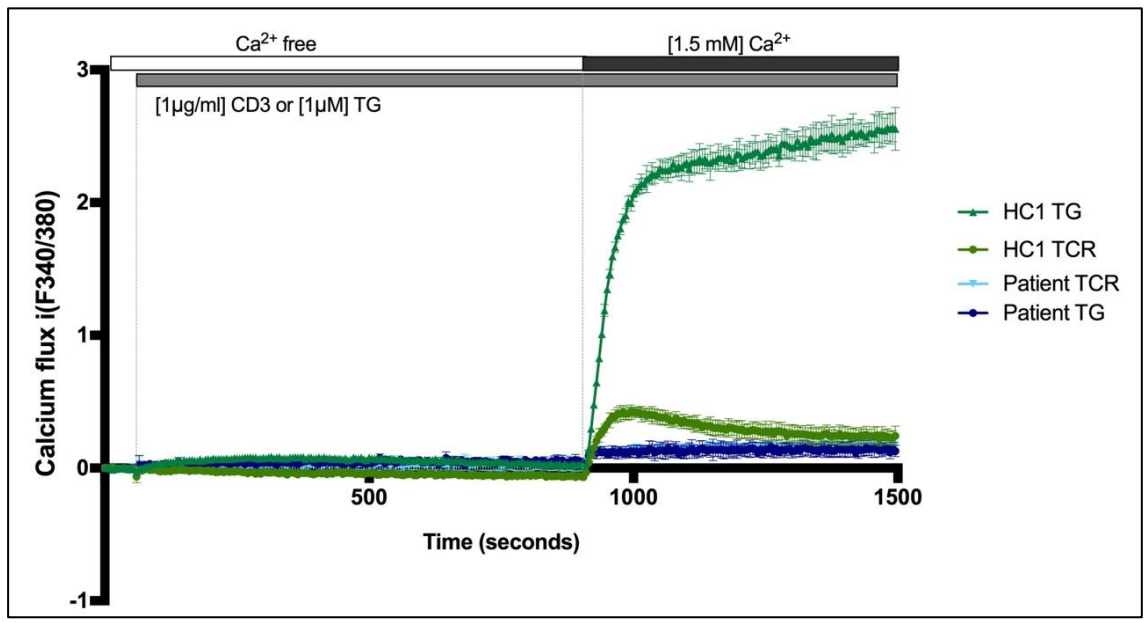

Figure 5.3.8 Calcium flux of P1 T cells

Calcium flux was run using the Flex Station protocol described in Section 2.2.7.1.2. For a system check Jurkat cell were run on the same day, and on both occurrences the cell line responded as seen previously. Calcium flux of STIM1 patient showed no response to either TG or TCR stimulation, each condition was run in duplicate. Patient cells were run on 2 separate occasions and neither showed any response to stimulation. No SOCE was observed in the patient cells.

5.3.1.7 Interferon levels in patients

In (Srikanth *et al.*, 2019), P1 was shown to have increased expression of type 1 interferons under resting conditions using cDNA and increased IFNß cytokine in the serum of the patient compared to HC using an ELISA. The paper also showed an increased IFNß protein in STIM1 deficient MEF supernatant.

The plasma IFN in the two STIM1 patients described in this project could not be compared via protein analysis as no plasma sample were available from P2. Therefore, quantitative RT-PCR was used to look at the levels of mRNA of IFN alpha and beta.

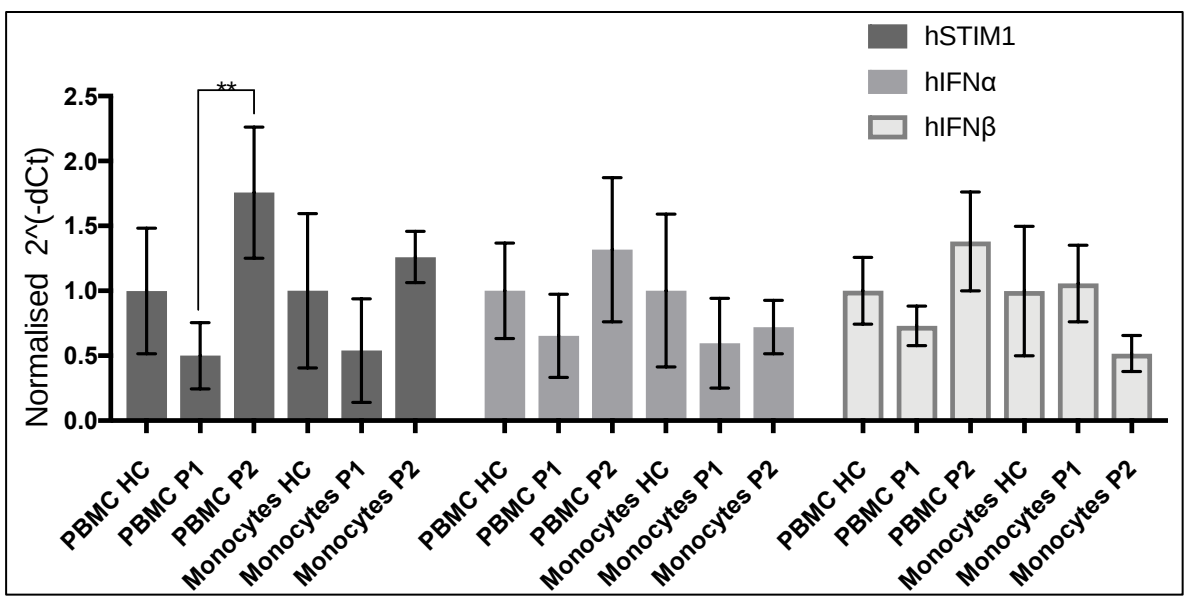

Figure 5.3.9 qPCR of STIM1 patients basal Interferon levels
Method described in 2.2.1.9. All samples were run in triplicate and normalised to H36B4 before further processing. The data was all normalised to the mean of 2 HC samples, so HC=1. 2 way ANOVA multiple comparisons shows the only significant difference ($p<0.05$) found was between hSTIM1 of P1 and P2 PBMCs ($p=0.0076$)

The increased IFNß protein previously reported in P1 was not reflected in the mRNA levels of the patient, as shown in Figure 5.3.9, where no significant difference was seen between the HCs and P1 for IFN α and ß. There was also no difference seen in P2 compared to HC for these two IFNs.

5.3.2 STING patient

STIM1 and STING functions were recently found to be linked (Srikanth *et al.*, 2019). and increased IFN protein levels and IFN gene transcription was shown in STIM1 deficient human and mice. WES identified a patient with a homozygous STING mutation and so functional tests were performed to see if their IFN expression levels were comparable to HC and ultimately to STIM1 patients detailed in section 1.3.1. The STING patient is a female from Czechoslovakia.

5.3.2.1 Patient Phenotype

The patient was diagnosed with systemic autoinflammatory diseases (SAID). They had periodic fever and the classical SAVI phenotype, recurrent fevers, abdominal pain and arthralgia. The phenotype displayed many characteristics typical of STING mutation carriage. Only minimal immunological data was available. They were found to have significantly elevated inflammatory markers, inflammation in the gut and active lymph nodes.

No improvement was seen with anakinra (anti-IL-1 therapy). The patient is currently responding to tocilizulab (anti-IL-6). IL-6 neutralizing antibodies promote the degradation of STING as part of the downstream molecule of STING along the DNA sensor pathway (Liu *et al.*, 2014; Wu *et al.*, 2017). IL-6 serves as a negative feedback mechanism to limit innate immune response induced by dsDNA. Another treatment for SAVI is JAK inhibition (Kacar, Pathak and Savic, 2019) .

5.3.2.2 Genetics

The homozygous missense mutation was identified by WES in the gene TMEM173 which encodes for the protein STING. The mutation found was c.992 G>A, p.Arg331Gln in the C-terminal tail (CTT). This change could affect autoinhibitory interaction with c-di-GMP-binding domain (CBD), constitutively mimicking activation by cGAMP (Huang *et al.*, 2012; Ouyang *et al.*, 2012; Shu *et al.*, 2012).

This mutation is present in the normal population in heterozygous form with a frequency of 0.0000955 (gnomAD, URL, accession date), which makes it a rare mutation and therefore increases the likelihood of the mutation being pathogenic. Arg331 is a highly conserved amino acid in the STING protein throughout evolution. This Arg131 conservation is seen in 100 vertebrates (http://genome.ucsc.edu), except in elephants who have tryptophan at this position instead.

Sanger sequencing was used to confirm the c.992G>A homozygous point mutation, as shown in Figure 5.3.10. Unfortunately any family members were not available for DNA sequence analysis and so no pedigree or segregation information could be obtained. No history of disease was mentioned in the patient's family, so the parents could potentially be heterozygous carriers as seen in the normal population.

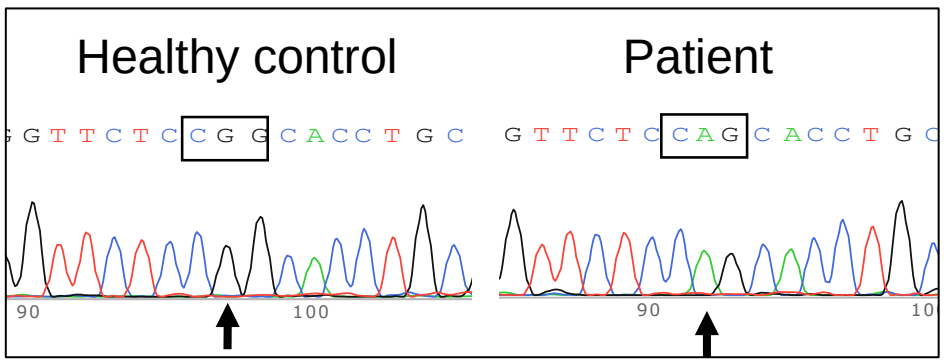

Figure 5.3.10 Sanger sequencing of *TMEM173* from patient genomic DNA
STING gene (*TMEM173*) is located on Chromosome 5: 139,475,533-139,482,935, reverse strand. Genomic DNA isolation was from patient whole blood and PCR and Sanger sequencing were performed as per Section 2.2.1.2. Primer pairs D1and E1 were used to generate PCR products (Table 2.1.1). The PCR products were amplified in duplicate and run on a 1.5 % agarose gel, to confirm the predicted sizes. They were then directly sequenced using both the forward and reverse primers defined above, but only the forward traces are shown here. The box indicates the codon and the arrow shows the codon where the point mutation occurs (cGg> cAg).

5.3.2.3 Predicted change in STING protein

The missense p.Arg331Gln mutation occurs in the C-terminal tail of the protein, as shown in Figure 5.3.11.The amino acid change from arginine to glutamine is quite a significant change in the side change, from a large basic charged side chain to a smaller polar side group. This change could potentially affect the function of the protein by altering the tertiary structure or its interaction with other proteins, especially as it is located on the exterior of the protein.

Comprehensive prediction software was used to look at the changes in atom potentials and torsion angle potentials. The mutation was found to be potentially disabling due to unfavourable torsion angles (Huang *et al.*, 2012; Ouyang *et al.*, 2012).

The C-terminal tail domain is important due to its autoinhibitory interaction with c-di-GMP-binding domain. This means a mutation in this region could result in a constitutive activation of STING by mimicking of cGAMP binding (Huang *et al.*, 2012; Ouyang *et al.*, 2012; Shu *et al.*, 2012).

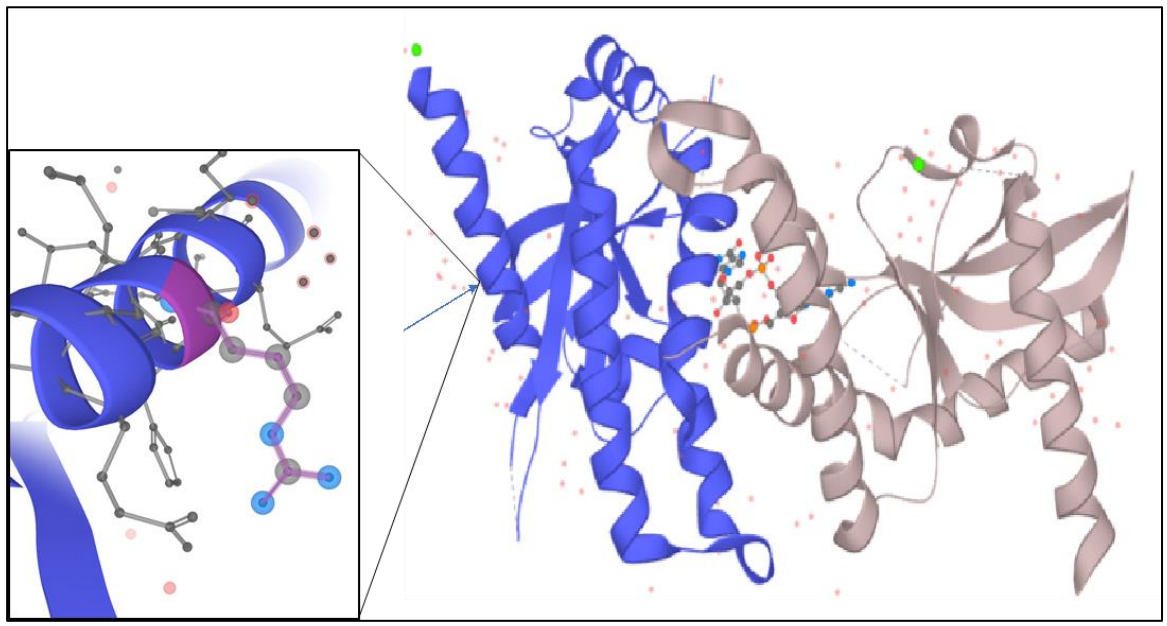

Figure 5.3.11 Structure of STING and pArg331
Crystal structure of ligand free human STING (4EMU) (Shu *et al.*, 2012), with amino acid of interest highlighted in purple. This figure was produced using https://www.uniprot.org/uniprot/ (accession data 14Sep2018).

5.3.2.4 Interferon levels in STING patient

STING has an important role in activating innate immune gene transcription and the interferon response. Preliminary IFN response experiments were performed using an established TaqMan assay to look at the effect of the STING mutations on gene expression profiles. A range of genes well known to be involved in the interferon response were measured (York *et al.*, 2015; Shrivastava *et al.*, 2016). A brief description of the genes are provided in Table 5.3.3.

In this experiment, HC and STING patient cells were compared. Three cell types were isolated, monocytes, non-monocytes and PBMC, and the IFN gene transcription levels quantified at baseline and after stimulation with IFNα. Of the three cells types monocytes had the higher overall ISGs expression and can be seen in Figure 5.3.12. This expression was abolished with IFN stimulation, except for in *CXCL10*, for which levels remained high.

Overall not much difference was seen between patient and HC for any cell type. In particular no significant trends were seen in non-monocytes or PBMCs at baseline or stimulated cells. These cell types are less sensitive to IFNα stimulation and produce less IFN than monocytes, and so the result was not unexpected. Therefore, all graphs for these cell types are not shown, but the statistically significant results from all cell types are presented in Table 5.3.4.

Table 5.3.3 Gene panel for TaqMan experiment

Gene	Function
HPRT	Name - Hypoxanthine Phosphoribosyltransferase gene Transferase enzyme, Housekeeping gene
IFI44	Name - Interferon Induced Protein 44 Associated with hepatitis C virus (HCV) infection (Power *et al.*, 2015)
CXCL10	Name - C-X-C Motif Chemokine Ligand 10 Ligand for the receptor CXCR3. Binding results in pleiotropic effects, including stimulation of monocytes, natural killer and T-cell migration, and modulation of adhesion molecule expression. (Vazirinejad *et al.*, 2014)
IFIT1	Name - Interferon Induced Protein with Tetratricopeptide (IFIT1) Inhibiting viral replication and translational initiation. Sensor of viral single-stranded RNAs. Inhibiting expression of viral messenger RNAs. (Fensterl and Sen, 2015)
MX1	Name - MX Dynamin Like GTPase 1 Encodes for GTP-metabolizing *protein* that participates in the cellular antiviral response
OASL	Name - 2'-5'-Oligoadenylate Synthetase Like Binds double-stranded RNA. Antiviral activity and enhances retinoic acid-inducible gene 1 (RIG-1) signalling to activate cellular innate immunity. (J. Zhu *et al.*, 2014)
IF16	Name - Interferon Gamma Inducible *Protein* 16 Antiviral & pathogen detection activity. Encodes for a nuclear *protein* that functions as a transcriptional repressor
IF127	Name - Interferon Alpha Inducible Protein 2 RNA polymerase II activating transcription factor binding and lamin binding. Diseases associated with IFI27 include Hepatitis C Virus and Hepatitis C.
ISG15	Name - Interferon-stimulated gene 15 Ubiquitin-Like Modifier conjugated to intracellular target proteins upon activation. Antiviral activity
IL6 FAM	Name - Interleukin 6 Cytokine that functions in inflammation and the maturation of B cells
IFI44L	Name - Interferon Induced Protein 44 Like Antiviral activity against HCV (Huang *et al.*, 2018)
PPIA	Name - Peptidylprolyl Isomerase A Accelerates the folding of proteins. The encoded protein is a cyclosporin binding-protein and may play a role in cyclosporin A-mediated immunosuppression.
m1 RSAD2	Name - Radical S-Adenosyl Methionine Domain Containing 2 Major role in the cell antiviral state induced by type I and type II interferon

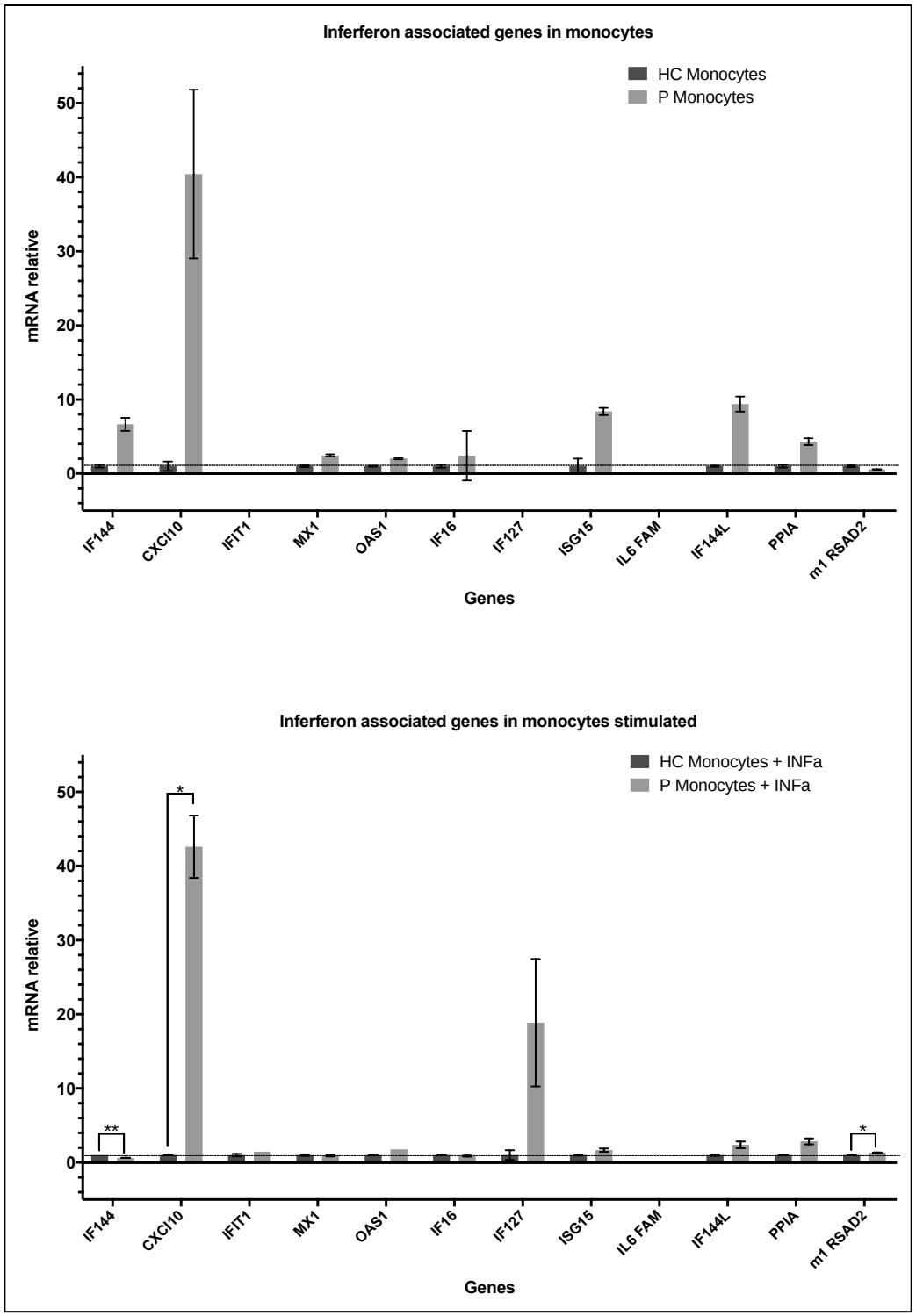

Figure 5.3.12 Interferon related gene expression in monocytes

TaqMan qPCR protocol described in Section 2.2.1.9.1 was used for this experiment, which was established by Srikanth *et al.*, 2019. All expression was normalised to HC which was made as 1. A large standard deviation was seen for each gene in both the HC and patient data. For more conclusive data this experiment needed to be repeated, but unfortunately no patient sample was available. Multiple T tests used to analyse data. P values : ns $P > 0.05$ (ns), $P \leq 0.05$ (*), $P \leq 0.01$ (**),$P \leq 0.001$ (***), $P \leq 0.0001$ (****)

Table 5.3.4 Significant results from ISGs experiment of STING patient

Cell type	Gene	P value	Patient Mean	SE of difference	Adjusted P Value
PBMC	CXCI10	0.0005	6.8	0.1302	0.0045
PBMC	m1 RSAD2	0.0047	0.1169	0.06074	0.037
Stimulated PBMCs	IF127	0.0002	8.153	0.09076	0.0019
Stimulated PBMCs	ISG15	0.0015	2	0.03896	0.0165
Stimulated monocytes	IF144	0.0004	0.6313	0.007155	0.0038
Stimulated monocytes	CXCI10	0.0051	42.61	2.974	0.0419
Stimulated monocytes	m1 RSAD2	0.0047	1.335	0.02318	0.0419

This table highlights all statistically significant results ($p < 0.05$) from qPCR experiment, shown in Figure 5.3.12. Statically significance was calculated using multiple T tests. Mean HC for all samples was normalised to 1. SE = Standard Error.

5.3.2.5 Interferon response compared to STIM1 deficient patient

The interferon response was compared between STIM1 P1 and the STING patient, as seen in Figure 5.3.13, in stimulated PBMCs and monocytes. The STIM1 patient had significantly elevated levels of expression compared to the STING patient, in both cell types. *CXCL10* expression, however, was significantly higher in the STING patient. This gene was comparable to HC in both STIM1 P1 and P2 (Rice *et al.*, 2019).

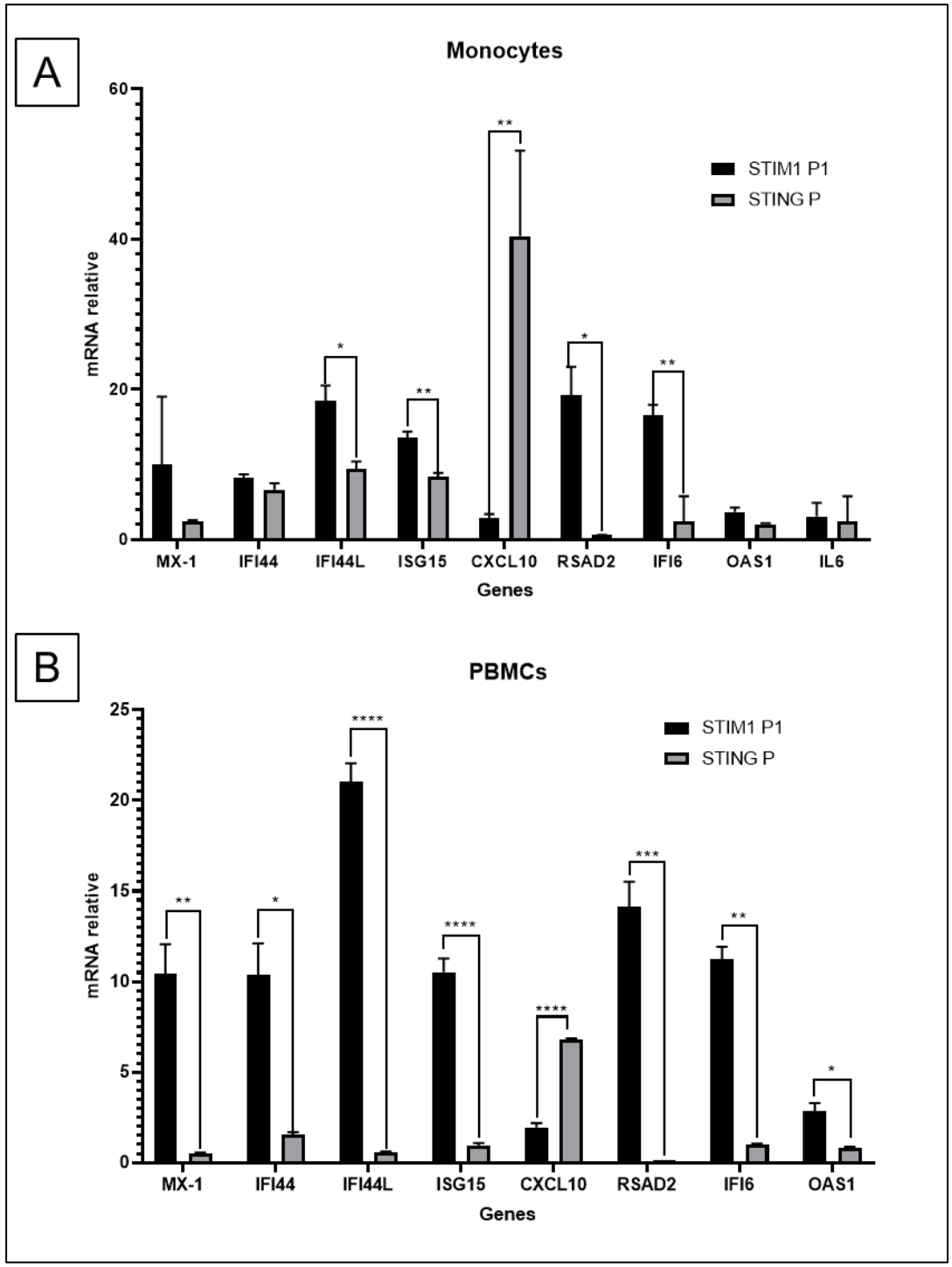

Figure 5.3.13 IFN response of patient cells

Stimulated cell data for both patients was normalised to the HC run in the same experiment, as originally reported (Section 5.3.2.4 and Srikanth *et al.*, 2019). This was done to eliminate differences between the experiments, but could incorporate bias as the HC were not the same. The STIM1 P1 data was produced by Dr Yasser M. El-Sherbiny (Srikanth *et al.*, 2019) and the raw data provided for analysis. Statically significance was calculated using multiple T tests. P values : ns $P > 0.05$ (ns), $P \leq 0.05$ (*), $P \leq 0.01$ (**),$P \leq 0.001$ (***), $P \leq 0.0001$ (****)

5.4 Key findings

In this chapter, experiments were performed on primary samples from three patients with PID to further understand the cause of their disease.

- Segregation of the homozygous STIM1 mutation c.478del, p.Ser160ValfsTer15 was confirmed in P1, by Sanger sequencing of parental DNA.
- Mutations c.478del (p.Ser160ValfsTer15) and c.221T>C (p.Leu74Pro) in *STIM1* in P1 and P2 respectively, resulted in no protein expression of STIM1.
- STIM1 deficiency and subsequent lack of calcium flux in patient T cells can present with a mild immunological phenotype.
- Sanger sequencing confirmed the homozygous STING mutation, c.992 G>A, p.Arg331Gln.
- A patient with the STING mutation above had comparable IGS expression to HC at baseline, as well as following IFNα stimulation.

5.5 Discussion

The aims of this chapter were to confirm potential mutations in patients with PID, show the functional effects of STIM1 mutations in patient cells and to determine the IGS expression of a patient with a STING mutation. The key findings summarised above show that these aims where achieved.

5.5.1 STIM1 phenotype

Two patients with STIM1 mutations were investigated in this chapter. P1 was newly identified and the mutation was confirmed (c.478del, p.Ser160ValfsTer15), segregation shown in their pedigree, no protein expression shown in PBMCs and no SOCE shown in patient T cells. This patient showed classical STIM1 deficiency traits, such as tooth enamel deficiency, recurrent infection and anhidrosis. Outside of the classical phenotype they presented with eczema ichthyosis and a normal T cell proliferation and normal cell numbers. The most recent cell numbers were slightly above the normal range for some T cell populations but this was not seen in the previous testing so could have been a result of infection (Table 5.3.1). The autoinflammatory features of the fever and rash were novel for patients with this deficiency (Picard *et al.*, 2009; Byun *et al.*, 2010; Wang *et al.*, 2014; Rice *et al.*, 2019).

P2 had been previously confirmed to have a *STIM1* mutation (c.221T>C, p.L74P). In this project, this mutations was shown to cause STIM1 deficiency rather than the lack of function previously reported as no protein was detected in patient PBMCs (Parry *et al.*, 2016). P2 phenotype also showed mild immunodeficiency, normal cell numbers, enamel deficiency and anhidrosis. This patient had not developed any overt immunological problems during their 6 year follow up.

Both P1 and P2 had significantly increased interferon gene expression after stimulation compared to HC (Rice *et al.*, 2019; Srikanth *et al.*, 2019). P2 had a milder increase in gene expression compared to P1. This may offer some protection against viral pathogens (Bourdon, Manet and Montagutelli, 2020). Mutations in Orai1 and STIM1 that abolish SOCE were recently reported to cause a new form of anhidrotic ectodermal dysplasia with immunodeficiency (EDA-ID) (Lian *et al.*, 2018). This differs from EDA-ID caused by defects in NF-κB signalling. Classical EDA-ID is linked to mutations in inhibitor of nuclear factor

kappa-B kinase regulatory subunit gamma (*IKBKG*) and nuclear factor kappa-B inhibitor alpha (*NFKBIA*) genes (Picard, Casanova and Puel, 2011; Kawai, Nishikomori and Heike, 2012). It presents with hypotrichosis, hypodontia, hypohidrosis, and recurrent bacterial, viral, and fungal infections. These conditions are seen in patients with STIM1 deficiency and share overlapping susceptibility to pathogens. Patients with *IKBKG* mutations have presented with inflammatory bowel disease, whereas in STIM1 patients autoimmune presentations are normally thrombocytopenia (Kawai, Nishikomori and Heike, 2012). In contrast, P1 presented with the additional phenotype of rashes. The data presented here supports this new form of anhidrotic ectodermal dysplasia with immunodeficiency for patients with STIM1 deficiency. However, the immunodeficiency can vary in severity, and P2 in particular had very mild immunodeficiency.

5.5.2 STIM2 overexpression

STIM2 has been shown to interact with STIM1 and is thought to play a role in regulating SOCE. In alphaT3 cells STIM2 is thought to play a role in translocation of STIM1, Orai1 interaction and SOCE activation (Berna-Erro *et al.*, 2017). However, overexpression of STIM2 appeared to inhibit STIM1 function downstream of puncta formation in HEK293, PC12, A7r5 and Jurkat T cells (Soboloff *et al.*, 2006).

The western blot of patient PBMCs (Figure 5.3.7) showed that both patients had an overexpression of STIM2 compared to HC, with P1 showing the highest relative density compared to the no visible protein seen in HC. The loading control of P2 showed a more intense band , which suggested more protein was loaded for this sample. Potentially, STIM2 expression would have been seen in HC if similar amounts of protein were loaded and so this experiment would need to be repeated to confirm the overexpression of STIM2 in P2. However, the overexpression of STIM2 in P1 is a valid conclusion from this blot. It is interesting to note that this potential compensatory mechanism for STIM1 deficiency (Figure 5.3.6) was not seen in both patients.

For both compensation mechanisms, STIM2 expression and interferon gene expression, for STIM1 deficiency P1 showed significantly more expression than P2. This could potentially be due to the milder immunodeficiency displayed by P2 or the younger age of P1. The difference in cytokine and protein expression between children and adults is still not completely understood (Decker, Grobusch and Ritz, 2017).

5.5.3 Measuring IFN levels

As shown in Section 5.3.1.7, there is a discrepancy between the mRNA and protein levels for IFN expression. The increased IFNß protein previously reported in P1 (Srikanth *et al.*, 2019) could not be seen at the mRNA levels in the patient (Figure 5.3.9), where no significant difference was seen between the HCs and P1 for IFN alpha and ß.

This discrepancy between mRNA and protein levels for cytokines is well documented due to regulation at a translational (IL4 and 10) and post-translational (IL1 and 18) level (Le *et al.*, 1997; Petrilli, Papin and Tschopp, 2005; Scheu *et al.*, 2006; Amsen, Visser and Town, 2009). Therefore, where possible it is best to test both the mRNA and protein of cytokines of interest. Data at the protein level was not available for STIM1 P2 or the STING patient, which both showed less interferon stimulated gene elevation than P1 by qPCR. If time and patient sample was available it would have been beneficial to look at the levels of protein for important cytokine and interferons by ELISA or WB.

5.5.4 ISGs

Expression of ISGs are induced by type I interferon via the JAK-STAT signalling pathway. ISGs are involved in a wide spectrum of cellular activities including apoptosis, immune modulation, cell migration and adhesion, and antiviral responses. Some ISGs have multiple roles in immune regulation (Fensterl and Sen, 2015).

Interferon stimulated genes were measured in all three patients discussed in this chapter. For the two STIM1 patients the results were generated by Dr Yasser El-Sherbiny at the University of Leeds and are now published (Rice *et al.*, 2019; Srikanth *et al.*, 2019).

Both patients with STIM1 deficiency showed significantly elevated ISGs when stimulated IFNα in PBMCs and monocytes compared to HC. IGS was measured in these patients due to the recent link between STING and STIM1. STIM1 acts as a negative regulator for STING and can inhibit STING trafficking by physically interacting with STING and retaining it at the ER membrane. Therefore, retaining STING in an inactive state. STIM1 deficiency causes elevated ISG expression as STING is no longer inhibited by this mechanism (Srikanth *et al.*, 2019).

STIM1 P1 results showed unstimulated PBMCS and monocytes with all ISG genes significantly increased compared to HC (Srikanth *et al.*, 2019), except for CXCL10, which showed comparable levels to that seen in HC for both cell types. STIM1 P2 also showed increased expression of ISG genes in PBMCs and monocytes (baseline data only) (Rice *et al.*, 2019). However, P1 showed higher expression than P2. All genes showed increased expression in monocytes, apart from CXCL10 and OAS1 which were comparable to HC, and MX-1 which was significantly reduced. In P2 PBMCs, all genes showed significant increase in expression, apart from CXCL10 which showed a slight decrease in expression and OAS1 which was significantly reduced.

The same experiment was performed using patient cells with a confirmed STING mutation (c.992 G>A, p.Arg331Gln). This mutation occurs in the C-terminal tail domain which has an autoinhibitory function, due to interaction with c-di-GMP-binding domain. This means a mutation in this region could result in a constitutively active STING by mimicking of cGAMP binding (Huang *et al.*, 2012; Ouyang *et al.*, 2012; Shu *et al.*, 2012). The ISG profile for this patient was comparable to HC for most genes and suggests that the patient mutation does not affect the protein function. This would need to be confirmed by more vigorous functional testing, such as binding studies, additional ISG experiments with different stimuli and protein modelling.

A gene of interest, C-X-C Motif Chemokine Ligand 10 (CXCL10), was identified by comparing the gene expression profiles of the STING patient to HC and STIM1 P1. This gene was significantly elevated in the STING patient under both baseline and stimulated conditions. The expression of this gene was comparable to HC in both STIM1 patients.

CXCL10 encodes for interferon-γ-inducible protein 10, a chemokine which is induced by IFN-γ and is produced by a wide range of cell types, including monocytes and neutrophils. CXCL10 binds to CXCR3. Both CXCL10 and CXCR3 are essential for leukocyte trafficking and homing and perpetuation of inflamed tissues. CXCR3 is preferentially expressed on activated Th1 cells. These proteins have been linked to multiple sclerosis and autoimmune disease (Vazirinejad *et al.*, 2014). In the literature, recent studies have shown links between STING and CXCL10 in mice, CXCL10 signalling promotes viral persistence and knock outs show a moderate decrease in immune cell numbers (Tao Lin, Tingting Geng, Andrew Harrison, Duomeng Yang, Anthony T. Vella, Erol Fikrig, 2021). Due to time limitations no further work was done on these two genes. However, looking at their protein expression and pathways may provide insights into a new link between them and STING

The data generated for the STING patient would need to be repeated before additional experiments can be performed. The standard deviation showed high variation and some data was missing for multiple genes. Different stimulations, such as cGAS, might provide additional information about the effect of the mutation, as IFNα does not activate the STING pathway directly.

Chapter 6 General discussion

For a more in depth discussion of the data and results of this thesis please see the discussion section at the end of each results chapter.

6.1 Aims

The two overall aims of this project are summarised below.

6.1.1 Confirm potential mutations and their segregation in patients with PID.

Sanger sequencing was used to confirm the presence of mutations identified by whole exome sequencing (WES) and gene panels (Chapter 3 and 5). This is also essential for mutations identified by next generation sequencing (NGS) as all of these approaches can result in false mutations due to the large data and filtering approach needed for its analysis. This is highlighted by the identification of the dehydrogenase/ reductase 4 (*DHRS4*) mutation as homozygous rather than heterozygous (Chapter 3).

Where possible the segregation of these mutations was found by sequencing of parental DNA or by cloning which isolated the patient alleles. This can improve the likelihood of mutations being pathogenic if only the proband has no WT allele due to homozygous or compound heterozygous mutations and the rest of the family are carriers or wildtype homozygous (Section 5.3.1.1.1, stromal interaction molecule 1 [STIM1] P1).

6.1.2 Use primary samples and *in vitro models* to determine if mutations identified are pathogenic and causing of the patient's phenotype

For patients with confirmed STIM1 and calcium release activated channel regulator 2A (CRACR2A) mutations, the protein expression in peripheral blood mononuclear cell (PBMC) was examined. This was done to determine if the mutations affected the expression of the protein, such as protein deficiency (Chapter 5, STIM1 P1 and P2) or truncated forms (The section on 'Protein expression in patient cells' showed no truncated CRACR2A).

Functional experiments were developed to look at the overall function of patient primary cells (cytokine expression and proliferation) and specific function related to the mutated protein (Calcium flux, Jun N-terminal kinase [JNK] signalling and ISG expression). Where further information was required for the effect of mutations cell lines were produced, that had the protein knocked-out (KO) and the patient alleles expressed. Functional experiments were then performed on these cell lines.

STIM1 deficiency was confirmed in two patients (Chapter 5). For STIM1 P2 this contrasted the previously published *in vitro* data (Parry *et al.*, 2016), which had assumed it was a loss of function mutant due to its ability to be expressed in cell lines. The main functional experiments performed in this study were for calcium flux. A range of methodologies were used to show the effect of confirmed mutations in patient T cells and cell lines by plate reader (Chapter 5, STIM1 P1) and single cell imaging (Chapter 3 and 4, CRACR2A).

The important overall conclusion from this work is that both primary samples from the patient and cell lines are needed to fully understand the functional effects of mutations identified in the CRAC channel components.

6.2 Impact of work

6.2.1 Effect on patient treatment

PIDs are rare diseases (O'Shea, 2018). The number of patients being diagnosed with PID is increasing. However, as at 2018 less than 22 % of patients had a proven genetic defect underlying their PID (Shillitoe *et al.*, 2018). Being able to identify the genetic cause of PID disease can improve the diagnosis and treatment options available to the patients. Personalized medicine or gene therapies may be available depending on the genetic cause. Furthermore, family members at risk can also be identified.

Personalised treatments are sometimes available when genes or mutations have already been identified as pathogenic. In this project, the confirmation of a stimulator of interferon genes (STING) mutation allowed for patient treatment by tocilizulab (Chapter 5), which is an anti-IL-6 neutralizing antibody that promotes the degradation of STING.

Currently no changes in treatment have been implemented as a result of this case study into the patient with CRACR2A mutations. This is because there is no specific CRACR2A drug and the patient's main phenotype of low immunoglobulins is managed by immunoglobulin replacement therapy. Their quality of life is considered good and so no further treatments are needed. If over time the phenotype progresses and further treatment is needed, the identification of T cells being the cell type affected, rather than B cells, may impact treatment. The identification of patients with CRACR2A mutations with heart conditions means this may be monitored more closely in the Leeds patient in the future.

6.2.2 Primary immunodeficiency field

This project supports previous studies that highlight the benefits of NGS in identifying pathogenic variants in patients (Y. Yang *et al.*, 2013; Rae *et al.*, 2018). It has also led to the identification of a potential novel gene, CRACR2A, causing PID. The case study in Chapters 3 and 4 strongly suggest that mutations in this gene could cause PID, though recessive inheritance, such as haploinsufficiency or in a compound heterozygous state. This was demonstrate by the lack of maternal allele (R144G, E300*) expression in patient T cells (Figure 3.3.8), which had reduced calcium flux, JNK expression and abnormal cytokine profiles (Figure 3.3.11, Figure 3.3.12 and Figure 3.3.13). These CRACR2A alleles also showed altered function in cell lines (Figure 4.3.15, Figure 4.3.16 and Figure 4.3.17), which supported the primary cell data as shown in Table 4.5.1

The data in Chapter 5 supports the new form of anhidrotic ectodermal dysplasia with immunodeficiency (EDA-ID) for patients with STIM1 deficiency. Which was previously reported in patients with Orai1 deficiency (Lian *et al.*, 2018).

6.2.3 The pathogenic effect of CRACR2A mutations

CRACR2A mutations have been identified in only a few patients to date, and these cases have very varied phenotypes, as shown in Table 6.2.1. As a result it is hard to determine if the mutations or lack of CRACR2A protein will cause disease. The main patient presented in this chapter displayed a T cell specific immunodeficiency, as seen by the reduced calcium flux, proliferation and cytokine response. To better understand if the identified mutations were causing the immunological profile in the patient in vitro studies will need to be developed in Jurkat cells, which is a human T cell derived line.

The cardiac related phenotypes observed in the other CRACR2A patients is something not seen in patients with confirmed STIM1 or Orai1 deficiency or mutations. It is difficult to determine if this phenotype is related to CRACR2A mutations, especially as it is not seen in the main patient presented here, which was the only patient available for further study.

In vitro studies were started on all other patient mutations in Table 6.2.1, by performing mutagenesis in vectors used to express CRACR2A in Jurkat cell lines. Primer information is given Table 2.1.1. However, due to time constraints no cell work was performed with the mutant plasmid constructs

Table 6.2.1 CRACR2A Phenotypes

		CRACR2A cases			
Deficiency	**Orai1 and STIM1**	**Leeds**	**Cambridge**	**USA**	**Italy**
Mutation	**Multiple**	p. R144G, E300*, E279D,	p.Q131*	p.Thr355Argfs X18	p. D230A
Immune dysfunction	Infections T cell activation defect Mitochondria-mediated cell death pathways ↓ Treg numbers ↓	Recurrent sinopulmonary infections Bronchiectasis Immunoglobulins ↓ CD4 ↓ T cell activation defect	-	Bacterial and viral susceptibility Mast cell disorder	-
Autoimmunity	Neutropenia Thrombocytopenia Splenomegaly Lymphadenopathy AIHA	Normal	-	Rashes Hysterectomy endometriosis	-
Muscular dysfunction	Congenital, global Respiratory muscle insufficiency Atrophy of type II muscle fibres	Normal	-	Ehlers-Danlos syndrome	-
Ectodermal dysplasia	Dental enamel defect (amelogenesis imperfecta type III) Anhidrosis	Normal	-	Bone pain	-
Thrombocyte function	No bleeding diathesis Thrombocytopenia (autoimmune)	Normal	-	Anaemia	-
Cardiac function	Normal	Normal	Heart defect	POTS	Pulmonary arterial hypertension
Additional details	N/A	Compound heterozygous. See Chapter 3 for details.	Homozygous (https://bioresource.nihr.ac.uk).	Germline heterozygous. Gwack lab investigating ongoing	Homozygous (Barozzi *et al.*, 2019)

STIM1 and Orai1 phenotypes were taken from Table 1.3.1. For the CRACR2A cases other than Leeds patient, the clinical and immunological information was limited.

6.2.4 CRAC channel inhibitors as drug targets

The CRAC channel as previously discussed has a role in many tissue types as shown by the SCID like disease that deficiency of STIM1 or Orai1 can cause. As a result CRAC channel inhibitors have been identified as useful therapeutics for autoimmune, inflammatory and other conditions, as shown in Table 6.2.2. As a result the more information that is known about these proteins and the effects of STIM1 and Orai1 deficiency and mutations in particular can lead to a better understanding of possible off target effects.

CRAC channel inhibitors stabilise the pulmonary endothelium and block proinflammatory cytokine release, potentially mitigating respiratory complications observed in patients with COVID-19. Clinical trials are ongoing (Table 6.2.2) but initial data on the safety and efficacy of Auxora was promising and improved the outcome in patients with severe COVID-19 pneumonia (Miller *et al.*, 2020).

Previously CRAC channel inhibitors have been researched as possible therapies in cancer. Calcium signals and CRAC channels are known to influence the development, growth, and metastasis of cancer, including cervical, breast, prostate, glioblastoma, esophageal cell carcinoma, hepatocellular carcinoma and pancreatic ductal adenocarcinoma (Yang, Zhang and Huang, 2009; Flourakis *et al.*, 2010; Chen *et al.*, 2011; Liu *et al.*, 2011; N. Yang *et al.*, 2013; H. Zhu *et al.*, 2014; Khan *et al.*, 2020). STIM1 and Orai1 have been seen to be overexpressed in cancer cells and so inhibition of the CRAC channel and its associated signalling pathways has been used as a potential therapy (Khan *et al.*, 2020).

CRAC channel mediated SOCE plays a key role in airway smooth muscle cell (ASMC) proliferation and as such, STIM1 or Orai1 represent targets that reduce airway remodelling in chronic asthma. Hyperplasia of ASMC is a characteristic of chronic asthma patients. SOCE plays an important role in regulating Ca^{2+} signalling and cellular responses of ASMCs. SOCE is upregulated during ASMC proliferation, which results in a mild increase of STIM1 and a significant increase of Orai1 mRNA expression, which is partially inhibited by CRAC channel blockers (Zou *et al.*, 2011).

Different T cell subsets require different levels of SOCE for their function. Th1 and Th17 cell function is inhibited by changes in calcium influx, whereas Treg, and CD8+ T cells are not as affected by the suppression of CRAC channel function. This

difference between T cell subsets could allow for the suppression of proinflammatory Th1 and Th17 cells, while maintaining immune tolerance in other T cell subsets (Vaeth, Kahlfuss and Feske, 2020).

Inhibition of the main proteins of the CRAC channel, Orai1 and STIM1, may result in off target effects due to their role in enamel, heart and muscle tissues (Stauderman, 2018) . CRACR2A has been shown in this project to potentially be more specific to T cells, so could provide a more specific target for autoimmune and autoinflammatory diseases..

Table 6.2.2 CRAC channel inhibitor or modulator clinical trials

Drug	Company	Phase	Treatment	Result	NTC identifier	Publication
CM4620-IE	CalciMedica	2 Safety and efficacy	Acute pancreatitis and systemic inflammatory response syndrome	Awaiting results, completed April 2019	NCT03401190	None
Auxora CM4620	CalciMedica	1	COVID-19 Pneumonia	Initial results promising Completion predicted April 2021	NCT04345614	(Miller *et al.*, 2020)
Auxora CM4620-IE	CalciMedica	2	COVID-19 Pneumonia	Starting Dec 2020	NCT04661540	None
RP3128	Rhizen Pharmaceuticals SA	I/Iia Safety, tolerability and pharmacokinetics	Asthma	Well tolerated. Lower plasma levels of tumour necrosis factor-alpha (TNFα) and interleukin-4 (IL-4) seen. Completed Oct 2019.	NCT02958982	(Barde *et al.*, 2020)
RP4010	Rhizen Pharmaceuticals SA	I/Ib Safety and efficacy	Relapsed or Refractory Lymphomas	Awaiting results Completed Dec 2019	NCT03119467	None
PRCL-02	PRCL Research Inc.	1	Plaque Psoriasis	No results reported Completed Feb 2018,	NCT03062618	None

6.3 Limitations

The main limitation in this project is the low number of mutations and patients available for study. This means data is potentially biased to the single patient and may not be directly applicable to a wider population. This is a recurring issue with rare diseases such as PID, which highlights the use of cell lines and mouse models for further study of the protein function and effect of mutations.

Low cell numbers from patient primary samples was a limiting factor in many experiments (Chapter 3 and 5). Alternative methodologies were used where possible that required less cells. Expansion of the CRACR2A patient cells was also used, though the patient phenotype caused issues because the cells were difficult to expand and had a preference for CD8 T cell expansion over CD4, which is the opposite of that seen in healthy controls. The CD8 T cells are also known to be less responsive to calcium flux changes, which may be a reason for the reduced response seen when comparing HC to patient in the expanded populations. Other limitations of the different calcium flux methods used were discussed in more detail in Chapters 3 and 4.

6.4 Future work

Future work and outstanding experiments are discussed in the results chapters. The main avenues to explore would be:

1. Identification of more patients with mutations in CRAC channel related proteins
2. Mouse studies
    - CRACR2A deficiency and mutant expression. These experiments are currently being undertaken by collaborators (Gwack lab)
3. Identification of additional pathways affected by CRACR2A
    - mRNA or proteomic studies using stable cell lines

References

1000 Genomes Project Consortium, {fname} *et al.* (2015) 'A global reference for human genetic variation.', *Nature*, 526(7571), pp. 68–74. doi: 10.1038/nature15393.

Adli, M. (2018) 'The CRISPR tool kit for genome editing and beyond', *Nature Communications*, 9(1), p. 1911. doi: 10.1038/s41467-018-04252-2.

Ahn, J. and Barber, G. N. (2019) 'STING signaling and host defense against microbial infection', *Experimental & Molecular Medicine*, 51(12), pp. 1–10. doi: 10.1038/s12276-019-0333-0.

Al-Herz, W. and Notarangelo, L. D. (2012) 'Classification of primary immunodeficiency disorders: One-fits-all does not help anymore', *Clinical Immunology*, pp. 24–25. doi: 10.1016/j.clim.2012.05.003.

Allenspach, E., Rawlings, D. J. and Scharenberg, A. M. (1993) *X-Linked Severe Combined Immunodeficiency*, *GeneReviews(®)*. Available at: http://www.ncbi.nlm.nih.gov/pubmed/20301584 (Accessed: 9 January 2017).

Alsharief, A. N. *et al.* (2020) 'Monogenic autoinflammatory diseases in children: single center experience with clinical, genetic, and imaging review', *Insights into Imaging*, 11(1), p. 87. doi: 10.1186/s13244-020-00889-0.

Ameratunga, R. *et al.* (2014) 'Comparison of Diagnostic Criteria for Common Variable Immunodeficiency Disorder', *Frontiers in Immunology*, 5. doi: 10.3389/fimmu.2014.00415.

Amsen, D., Visser, K. E. and Town, T. (2009) 'Approaches to Determine Expression of Inflammatory Cytokines', in, pp. 107–142. doi: 10.1007/978-1-59745-447-6_5.

Andrä, I. *et al.* (2020) 'An Evaluation of T-Cell Functionality After Flow Cytometry Sorting Revealed p38 MAPK Activation', *Cytometry Part A*, 97(2), pp. 171–183. doi: 10.1002/cyto.a.23964.

Arrol, H. P. *et al.* (2008) 'Intracellular calcium signalling patterns reflect the differentiation status of human T cells', *Clinical & Experimental Immunology*, 153(1), pp. 86–95. doi: 10.1111/j.1365-2249.2008.03677.x.

Baba, Y. *et al.* (2008) 'Essential function for the calcium sensor STIM1 in mast cell activation and anaphylactic responses', *Nature Immunology*, 9(1), pp. 81–88. doi: 10.1038/ni1546.

Balasubramanian, K. *et al.* (2017) 'MED resulting from recessively inherited mutations in the gene encoding calcium-activated nucleotidase CANT1', *American Journal of Medical Genetics Part A*, 173(9), pp. 2415–2421. doi: 10.1002/ajmg.a.38349.

Barde, P. J. *et al.* (2020) 'A first-in-human study to evaluate the safety, tolerability and pharmacokinetics of RP3128, an oral calcium release-activated calcium (CRAC) channel modulator in healthy volunteers', *Journal of Clinical Pharmacy and Therapeutics*, p. jcpt.13322. doi: 10.1111/jcpt.13322.

Barozzi, C. *et al.* (2019) 'A Combined Targeted and Whole Exome Sequencing Approach Identified Novel Candidate Genes Involved in Heritable Pulmonary Arterial Hypertension', *Scientific Reports*, 9(1), pp. 1–9. doi: 10.1038/s41598-018-37277-0.

Barr, V. A. *et al.* (2008) 'Dynamic Movement of the Calcium Sensor STIM1 and the Calcium Channel Orai1 in Activated T-Cells: Puncta and Distal Caps', *Molecular Biology of the Cell*. Edited by C.-H. Heldin, 19(7), pp. 2802–2817. doi: 10.1091/mbc.e08-02-0146.

Barr, V. A. *et al.* (2009) 'Formation of STIM and Orai complexes: puncta and distal caps', *Immunological Reviews*, 231(1), pp. 148–159. doi: 10.1111/j.1600-065X.2009.00812.x.

Beriault, D. R. and Werstuck, G. H. (2013) 'Detection and quantification of endoplasmic reticulum stress in living cells using the fluorescent compound, Thioflavin T', *Biochimica et Biophysica Acta (BBA) - Molecular Cell Research*, 1833(10), pp. 2293–2301. doi: 10.1016/j.bbamcr.2013.05.020.

Berna-Erro, A. *et al.* (2017) 'Role of STIM2 in cell function and physiopathology', *The Journal of Physiology*, 595(10), pp. 3111–3128. doi: 10.1113/JP273889.

Beyersdorf, N. *et al.* (2009) 'STIM1-Independent T Cell Development and Effector Function In Vivo', *The Journal of Immunology*, 182(6), pp. 3390–3397. doi: 10.4049/jimmunol.0802888.

Biesecker, L. G. and Harrison, S. M. (2018) 'The ACMG/AMP reputable source criteria for the interpretation of sequence variants', *Genetics in Medicine*, 20(12), pp. 1687–1688. doi: 10.1038/gim.2018.42.

Bittremieux, M. *et al.* (2017) 'DPB162-AE, an inhibitor of store-operated Ca2+ entry, can deplete the endoplasmic reticulum Ca2+ store', *Cell Calcium*, 62, pp. 60–70. doi: 10.1016/j.ceca.2017.01.015.

Blank, U. and Rivera, J. (2004) 'The ins and outs of IgE-dependent mast-cell exocytosis', *Trends in Immunology*, 25(5), pp. 266–273. doi: 10.1016/j.it.2004.03.005.

Boisson, B., Quartier, P. and Casanova, J.-L. (2015) 'Immunological loss-of-function due to genetic gain-of-function in humans: autosomal dominance of the third kind.', *Current opinion in immunology*. NIH Public Access, 32, pp. 90–105. doi: 10.1016/j.coi.2015.01.005.

Bollimuntha, S., Pani, B. and Singh, B. B. (2017) 'Neurological and Motor Disorders: Neuronal Store-Operated Ca2+ Signaling: An Overview and Its Function', in, pp. 535–556. doi: 10.1007/978-3-319-57732-6_27.

Bompard, G. and Caron, E. (2004) 'Regulation of WASP/WAVE proteins: making a long story short', *Journal of Cell Biology*, 166(7), pp. 957–962. doi: 10.1083/jcb.200403127.

Bourdon, M., Manet, C. and Montagutelli, X. (2020) 'Host genetic susceptibility to viral infections: the role of type I interferon induction', *Genes & Immunity*. doi: 10.1038/s41435-020-00116-2.

Bousfiha, A. *et al.* (2015) 'The 2015 IUIS Phenotypic Classification for Primary Immunodeficiencies', *Journal of Clinical Immunology*, 35(8), pp. 727–738. doi: 10.1007/s10875-015-0198-5.

Bousfiha, A. *et al.* (2018) 'The 2017 IUIS Phenotypic Classification for Primary Immunodeficiencies', *Journal of Clinical Immunology*, 38(1), pp. 129–143. doi: 10.1007/s10875-017-0465-8.

Bousfiha, A. *et al.* (2020) 'Human Inborn Errors of Immunity: 2019 Update of the IUIS Phenotypical Classification', *Journal of Clinical Immunology*, 40(1), pp. 66–81. doi: 10.1007/s10875-020-00758-x.

Bousfiha, A. A. *et al.* (2013) 'Primary Immunodeficiency Diseases Worldwide: More Common than Generally Thought', *Journal of Clinical Immunology*, 33(1), pp. 1–7. doi: 10.1007/s10875-012-9751-7.

Bucciol, G. and Meyts, I. (2020) 'Recent advances in primary immunodeficiency: from molecular diagnosis to treatment', *F1000Research*, 9, p. 194. doi: 10.12688/f1000research.21553.1.

Bui, C. *et al.* (2014) 'XYLT1 Mutations in Desbuquois Dysplasia Type 2', *The American Journal of Human Genetics*, 94(3), pp. 405–414. doi: 10.1016/j.ajhg.2014.01.020.

Bulent Arman Aksoy, Pinar Aksoy, Megan Wyatt, Chrystal Paulos, J. H. (2018) 'Human primary T cells: A practical guide', *PeerJ Preprints*, 6(26993). doi: 10.7287/peerj.preprints.26993v1.

Byun, M. *et al.* (2010) ‘Whole-exome sequencing-based discovery of STIM1 deficiency in a child with fatal classic Kaposi sarcoma’, *Journal of Experimental Medicine*, 207(11), pp. 2307–2312. doi: 10.1084/jem.20101597.

Carrasco, S. and Meyer, T. (2010) ‘Cracking CRAC’, *Nature Cell Biology*. Nature Publishing Group, 12(5), pp. 416–418. doi: 10.1038/ncb0510-416.

Casanova, J. L. *et al.* (2014) ‘Guidelines for genetic studies in single patients: lessons from primary immunodeficiencies’, *Journal of Experimental Medicine*, 211(11), pp. 2137–2149. doi: 10.1084/jem.20140520.

Chen, X., Welner, R. S. and Kincade, P. W. (2009) ‘A possible contribution of retinoids to regulation of fetal B lymphopoiesis’, *European Journal of Immunology*. WILEY-VCH Verlag, 39(9), pp. 2515–2524. doi: 10.1002/eji.200939374.

Chen, Y.-F. *et al.* (2011) ‘Calcium store sensor stromal-interaction molecule 1-dependent signaling plays an important role in cervical cancer growth, migration, and angiogenesis’, *Proceedings of the National Academy of Sciences*, 108(37), pp. 15225–15230. doi: 10.1073/pnas.1103315108.

Chinn, I. K. *et al.* (2020) ‘Diagnostic interpretation of genetic studies in patients with primary immunodeficiency diseases: A working group report of the Primary Immunodeficiency Diseases Committee of the American Academy of Allergy, Asthma & Immunology’, *Journal of Allergy and Clinical Immunology*, 145(1), pp. 46–69. doi: 10.1016/j.jaci.2019.09.009.

Chiu, S. and Bharat, A. (2016) ‘Role of monocytes and macrophages in regulating immune response following lung transplantation’, *Current Opinion in Organ Transplantation*, 21(3), pp. 239–245. doi: 10.1097/MOT.0000000000000313.

Choi, M. *et al.* (2009) ‘Genetic diagnosis by whole exome capture and massively parallel DNA sequencing’, *Proceedings of the National Academy of Sciences*, 106(45), pp. 19096–19101. doi: 10.1073/pnas.0910672106.

Christo, S. N. *et al.* (2015) ‘Scrutinizing calcium flux oscillations in T lymphocytes to deduce the strength of stimulus’, *Scientific Reports*, 5(1), p. 7760. doi: 10.1038/srep07760.

Collins, S. R. and Meyer, T. (2011) ‘Evolutionary origins of STIM1 and STIM2 within ancient Ca2+ signaling systems’, *Trends in Cell Biology*, 21(4), pp. 202–211. doi: 10.1016/j.tcb.2011.01.002.

Concepcion, A. R. *et al.* (2016) ‘Store-operated Ca2+ entry regulates Ca2+-activated chloride channels and eccrine sweat gland function’, *Journal of Clinical Investigation*. American Society for Clinical Investigation, 126(11), pp. 4303–4318. doi: 10.1172/JCI89056.

Conze, D. *et al.* (2002) ‘c-Jun NH2-Terminal Kinase (JNK)1 and JNK2 Have Distinct Roles in CD8+ T Cell Activation’, *Journal of Experimental Medicine*, 195(7), pp. 811–823. doi: 10.1084/jem.20011508.

Cox, J. H. *et al.* (2013) ‘Antibody-Mediated Targeting of the Orai1 Calcium Channel Inhibits T Cell Function’, *PLoS ONE*. Edited by M. Pietropaolo, 8(12), p. e82944. doi: 10.1371/journal.pone.0082944.

Dadak, M. *et al.* (2017) ‘Gain-of-function STAT1 mutations are associated with intracranial aneurysms’, *Clinical Immunology*, 178, pp. 79–85. doi: 10.1016/j.clim.2017.01.012.

Decker, M.-L., Grobusch, M. P. and Ritz, N. (2017) ‘Influence of Age and Other Factors on Cytokine Expression Profiles in Healthy Children—A Systematic Review’, *Frontiers in Pediatrics*, 5. doi: 10.3389/fped.2017.00255.

Dhanasekaran, D. N. and Reddy, E. P. (2017) ‘JNK-signaling: A multiplexing hub in programmed cell death’, *Genes & Cancer*, 8(9–10), pp. 682–694. doi: 10.18632/genesandcancer.155.

Dominguez, R., Lee, I. G. (2020) ‘Complex of CRACR2a with a Dynein Light Intermediate Chain Peptide’. doi:

10.2210/pdb6psd/pdb.

Dörr, K. *et al.* (2016) 'Cell type–specific glycosylation of Orai1 modulates store-operated Ca 2+ entry', *Science Signaling*, 9(418), pp. ra25–ra25. doi: 10.1126/scisignal.aaa9913.

Eckstein, M. and Lacruz, R. S. (2018) 'CRAC channels in dental enamel cells', *Cell Calcium*, 75, pp. 14–20. doi: 10.1016/j.ceca.2018.07.012.

Ensembl genome browser 89 (no date). Available at: http://www.ensembl.org/index.html (Accessed: 4 August 2017).

Fensterl, V. and Sen, G. C. (2015) 'Interferon-Induced Ifit Proteins: Their Role in Viral Pathogenesis', *Journal of Virology*. Edited by S. P. Goff, 89(5), pp. 2462–2468. doi: 10.1128/JVI.02744-14.

Feske, S. (2010) 'CRAC channelopathies', *Pflügers Archiv - European Journal of Physiology*, 460(2), pp. 417–435. doi: 10.1007/s00424-009-0777-5.

Feske, S. (2011) 'Immunodeficiency due to defects in store-operated calcium entry.', *Annals of the New York Academy of Sciences*. NIH Public Access, 1238, pp. 74–90. doi: 10.1111/j.1749-6632.2011.06240.x.

Feske, S., Picard, C. and Fischer, A. (2010) 'Immunodeficiency due to mutations in ORAI1 and STIM1.', *Clinical immunology (Orlando, Fla.)*. NIH Public Access, 135(2), pp. 169–82. doi: 10.1016/j.clim.2010.01.011.

Flourakis, M. *et al.* (2010) 'Orai1 contributes to the establishment of an apoptosis-resistant phenotype in prostate cancer cells', *Cell Death & Disease*, 1(9), pp. e75–e75. doi: 10.1038/cddis.2010.52.

Furuichi, T. *et al.* (2011) 'CANT1 mutation is also responsible for Desbuquois dysplasia, type 2 and Kim variant', *Journal of Medical Genetics*, 48(1), pp. 32–37. doi: 10.1136/jmg.2010.080226.

Gallo, V. *et al.* (2016) 'Diagnostics of Primary Immunodeficiencies through Next-Generation Sequencing', *Frontiers in Immunology*, 7. doi: 10.3389/fimmu.2016.00466.

Geginat, J., Lanzavecchia, A. and Sallusto, F. (2003) 'Proliferation and differentiation potential of human CD8+ memory T-cell subsets in response to antigen or homeostatic cytokines', *Blood*, 101(11), pp. 4260–4266. doi: 10.1182/blood-2002-11-3577.

Gertsch, J. *et al.* (2002) 'Relative quantification of mRNA levels in Jurkat T cells with RT-real time-PCR (RT-rt-PCR): new possibilities for the screening of anti-inflammatory and cytotoxic compounds', *Pharmaceutical research*. United States, 19(8), pp. 1236–1243. doi: 10.1023/a:1019818814336.

Giardino, G. *et al.* (2016) 'Unbalanced Immune System: Immunodeficiencies and Autoimmunity.', *Frontiers in pediatrics*. Frontiers Media SA, 4, p. 107. doi: 10.3389/fped.2016.00107.

Golubovskaya, V. and Wu, L. (2016) 'Different Subsets of T Cells, Memory, Effector Functions, and CAR-T Immunotherapy', *Cancers*, 8(3), p. 36. doi: 10.3390/cancers8030036.

Goyal, R. *et al.* (2009) 'Rheumatologic and autoimmune manifestations of primary immunodeficiency disorders', *Current Opinion in Rheumatology*, 21(1), pp. 78–84. doi: 10.1097/BOR.0b013e32831cb939.

Gruh, I. *et al.* (2008) 'Human CMV immediate-early enhancer: a useful tool to enhance cell-type-specific expression from lentiviral vectors', *The Journal of Gene Medicine*, 10(1), pp. 21–32. doi: 10.1002/jgm.1122.

Gruszczynska-Biegala, J. *et al.* (2011) 'Differential Roles for STIM1 and STIM2 in Store-Operated Calcium Entry in Rat Neurons', *PLoS ONE*. Edited by D. Holowka, 6(4), p. e19285. doi: 10.1371/journal.pone.0019285.

Guo, L. *et al.* (2017) 'Optimizing conditions for calcium phosphate mediated transient transfection', *Saudi Journal of Biological Sciences*, 24(3), pp. 622–629. doi: 10.1016/j.sjbs.2017.01.034.

Gwack, Y. *et al.* (2008) 'Hair Loss and Defective T- and B-Cell Function in Mice Lacking ORAI1', *Molecular and Cellular Biology*, 28(17), pp. 5209–5222. doi: 10.1128/MCB.00360-08.

Held, P. (2018) 'Stimulation of IL-2 Secretion in Human Lymphocytes'. BioTek. Available at: https://www.biotek.com/assets/tech_resources/ELISPOT App_Note.pdf.

Hendron, E. *et al.* (2014) 'Potent functional uncoupling between STIM1 and Orai1 by dimeric 2-aminodiphenyl borinate analogs', *Cell Calcium*, 56(6), pp. 482–492. doi: 10.1016/j.ceca.2014.10.005.

Henke, N. *et al.* (2012) 'Stromal interaction molecule 1 (STIM1) is involved in the regulation of mitochondrial shape and bioenergetics and plays a role in oxidative stress.', *The Journal of biological chemistry*, 287(50), pp. 42042–52. doi: 10.1074/jbc.M112.417212.

Hoffman, W., Lakkis, F. G. and Chalasani, G. (2016) 'B Cells, Antibodies, and More', *Clinical Journal of the American Society of Nephrology*, 11(1), pp. 137–154. doi: 10.2215/CJN.09430915.

Hoover, P. J., Lewis, R. S. and Aldrich, R. W. (no date) 'Stoichiometric requirements for trapping and gating of Ca 2+ release-activated Ca 2+ (CRAC) channels by stromal interaction molecule 1 (STIM1)'. doi: 10.1073/pnas.1101664108.

Hoth, M. and Penner, R. (1992) 'Depletion of intracellular calcium stores activates a calcium current in mast cells', *Nature*, 355(6358), pp. 353–356. doi: 10.1038/355353a0.

Huang, W.-C. *et al.* (2018) 'IFI44L is a novel tumor suppressor in human hepatocellular carcinoma affecting cancer stemness, metastasis, and drug resistance via regulating met/Src signaling pathway', *BMC Cancer*, 18(1), p. 609. doi: 10.1186/s12885-018-4529-9.

Huang, Y.-H. *et al.* (2012) 'The structural basis for the sensing and binding of cyclic di-GMP by STING', *Nature Structural & Molecular Biology*, 19(7), pp. 728–730. doi: 10.1038/nsmb.2333.

IPOPI (2016) 'HOW ARE PRIMARY IMMUNODEFICIENCIES CLASSIFIED?' International Patient Organisation for Primary Immunode ciencies (IPOPI), p. 12. Available at: http://www.ipopi.org/uploads/WEB_IPOPI_Classification.pdf (Accessed: 3 January 2017).

Ishikawa, H. and Barber, G. N. (2008) 'STING is an endoplasmic reticulum adaptor that facilitates innate immune signalling', *Nature*, 455(7213), pp. 674–678. doi: 10.1038/nature07317.

Ishikawa, H., Ma, Z. and Barber, G. N. (2009) 'STING regulates intracellular DNA-mediated, type I interferon-dependent innate immunity', *Nature*, 461(7265), pp. 788–792. doi: 10.1038/nature08476.

Ivashkiv, L. B. and Donlin, L. T. (2014) 'Regulation of type I interferon responses', *Nature Reviews Immunology*, 14(1), pp. 36–49. doi: 10.1038/nri3581.

Jairaman, A. and Prakriya, M. (2013) 'Molecular pharmacology of store-operated CRAC channels', *Channels*. doi: 10.4161/chan.25292.

Janeway CA Jr, Travers P, Walport M, et al. (2001) *Immunobiology: The Immune System in Health and Disease. 5th edition.* Available at: https://www.ncbi.nlm.nih.gov/books/NBK27092/.

Joseph, N., Reicher, B. and Barda-Saad, M. (2014) 'The calcium feedback loop and T cell activation: How cytoskeleton

networks control intracellular calcium flux', *Biochimica et Biophysica Acta (BBA) - Biomembranes*, 1838(2), pp. 557–568. doi: 10.1016/j.bbamem.2013.07.009.

Kacar, M., Pathak, S. and Savic, S. (2019) 'Hereditary systemic autoinflammatory diseases and Schnitzler's syndrome', *Rheumatology*, 58(Supplement_6), pp. vi31–vi43. doi: 10.1093/rheumatology/kez448.

Kawai, T., Nishikomori, R. and Heike, T. (2012) 'Diagnosis and Treatment in Anhidrotic Ectodermal Dysplasia with Immunodeficiency', *Allergology International*, 61(2), pp. 207–217. doi: 10.2332/allergolint.12-RAI-0446.

Keefe, E. P. O. (2013) 'siRNAs and shRNAs: Tools for Protein Knockdown by Gene Silencing', *Materials and Methods [ISSN : 2329-5139]*, 3(197). doi: //dx.doi.org/10.13070/mm.en.3.197.

Khan, H. Y. *et al.* (2020) 'Calcium Release-Activated Calcium (CRAC) Channel Inhibition Suppresses Pancreatic Ductal Adenocarcinoma Cell Proliferation and Patient-Derived Tumor Growth', *Cancers*, 12(3), p. 750. doi: 10.3390/cancers12030750.

Kim, K.-D. *et al.* (2011) 'ORAI1 Deficiency Impairs Activated T Cell Death and Enhances T Cell Survival', *The Journal of Immunology*, 187(7), pp. 3620–3630. doi: 10.4049/jimmunol.1100847.

Kim, O.-H. *et al.* (2010) 'A variant of Desbuquois dysplasia characterized by advanced carpal bone age, short metacarpals, and elongated phalanges: Report of seven cases', *American Journal of Medical Genetics Part A*, 152A(4), pp. 875–885. doi: 10.1002/ajmg.a.33347.

Kiviluoto, S. *et al.* (2011) 'STIM1 as a key regulator for Ca2+ homeostasis in skeletal-muscle development and function', *Skeletal Muscle*, 1(1), p. 16. doi: 10.1186/2044-5040-1-16.

Klein, L. *et al.* (2014) 'Positive and negative selection of the T cell repertoire: what thymocytes see (and don't see)', *Nature Reviews Immunology*, 14(6), pp. 377–391. doi: 10.1038/nri3667.

Kozak, J. A. and Putney, J. W. (eds) (2017) *Calcium Entry Channels in Non-Excitable Cells*. Boca Raton : Taylor & Francis, 2017. | Series: Methods in signal transduction series: CRC Press. doi: 10.1201/9781315152592.

Kwun, J. *et al.* (2017) 'Crosstalk Between T and B Cells in the Germinal Center After Transplantation', *Transplantation*, 101(4), pp. 704–712. doi: 10.1097/TP.0000000000001588.

LaRosa, D. F. and Orange, J. S. (2008) . 'Lymphocytes', *J Allergy Clin Immunol*, 121, pp. 364–9. doi: 10.1016/j.jaci.2007.06.016.

Lawrence, T. *et al.* (2005) 'Autosomal-dominant primary immunodeficiencies.', *Current opinion in hematology*, 12(1), pp. 22–30. Available at: http://www.ncbi.nlm.nih.gov/pubmed/15604887 (Accessed: 20 February 2017).

Le, T. *et al.* (1997) 'Regulation of interleukin-10 gene expression: possible mechanisms accounting for its upregulation and for maturational differences in its expression by blood mononuclear cells.', *Blood*, 89(11), pp. 4112–9. Available at: http://www.ncbi.nlm.nih.gov/pubmed/9166853.

Lewis, R. S. (2001) 'CALCIUM SIGNALING MECHANISMS IN T LYMPHOCYTES', *Annu. Rev. Immunol*, 19, pp. 497–521. Available at: http://www.annualreviews.org/doi/pdf/10.1146/annurev.immunol.19.1.497 (Accessed: 16 May 2017).

Li, T. *et al.* (2012) 'STIM1-Ca2+ Signaling Is Required for the Hypertrophic Growth of Skeletal Muscle in Mice', *Molecular and Cellular Biology*, 32(15), pp. 3009–3017. doi: 10.1128/MCB.06599-11.

Lian, J. *et al.* (2018) 'ORAI1 mutations abolishing store-operated Ca2+ entry cause anhidrotic ectodermal dysplasia with immunodeficiency', *Journal of Allergy and Clinical Immunology*, 142(4), pp. 1297-1310.e11. doi: 10.1016/j.jaci.2017.10.031.

Liu, H. *et al.* (2011) 'Calcium entry via ORAI1 regulates glioblastoma cell proliferation and apoptosis', *Experimental and Molecular Pathology*, 91(3), pp. 753–760. doi: 10.1016/j.yexmp.2011.09.005.

Liu, Y. *et al.* (2014) 'Activated STING in a Vascular and Pulmonary Syndrome', *New England Journal of Medicine*, 371(6), pp. 507–518. doi: 10.1056/NEJMoa1312625.

Ma, J. *et al.* (2010) 'T-cell-specific deletion of STIM1 and STIM2 protects mice from EAE by impairing the effector functions of Th1 and Th17 cells', *European Journal of Immunology*, 40(11), pp. 3028–3042. doi: 10.1002/eji.201040614.

Matsumoto, M. *et al.* (2011) 'The Calcium Sensors STIM1 and STIM2 Control B Cell Regulatory Function through Interleukin-10 Production', *Immunity*, 34(5), pp. 703–714. doi: 10.1016/j.immuni.2011.03.016.

McCarl, C.-A. *et al.* (2009) 'ORAI1 deficiency and lack of store-operated Ca2+ entry cause immunodeficiency, myopathy, and ectodermal dysplasia', *Journal of Allergy and Clinical Immunology*, 124(6), pp. 1311-1318.e7. doi: 10.1016/j.jaci.2009.10.007.

McCarl, C.-A. *et al.* (2010) 'Store-Operated Ca 2+ Entry through ORAI1 Is Critical for T Cell-Mediated Autoimmunity and Allograft Rejection', *The Journal of Immunology*, 185(10), pp. 5845–5858. doi: 10.4049/jimmunol.1001796.

Mcnally, B. A. *et al.* (2012) 'Gated regulation of CRAC channel ion selectivity by STIM1', *Nature*, 482. doi: 10.1038/nature10752.

Meyts, I. *et al.* (2016) 'Exome and genome sequencing for inborn errors of immunity', *Journal of Allergy and Clinical Immunology*, 138(4), pp. 957–969. doi: 10.1016/j.jaci.2016.08.003.

Miller, J. *et al.* (2020) 'Auxora versus standard of care for the treatment of severe or critical COVID-19 pneumonia: results from a randomized controlled trial', *Critical Care*, 24(1), p. 502. doi: 10.1186/s13054-020-03220-x.

Miller, L. (2010) *Analyzing gels and western blots with ImageJ*, *lukemiller.org*. Available at: https://lukemiller.org/index.php/2010/11/analyzing-gels-and-western-blots-with-image-j/.

Miteva, K. T. *et al.* (2019) 'Rab46 integrates Ca2+ and histamine signaling to regulate selective cargo release from Weibel-Palade bodies', *Journal of Cell Biology*, 218(7), pp. 2232–2246. doi: 10.1083/jcb.201810118.

Motwani, M., Pesiridis, S. and Fitzgerald, K. A. (2019) 'DNA sensing by the cGAS–STING pathway in health and disease', *Nature Reviews Genetics*. doi: 10.1038/s41576-019-0151-1.

Nelson, H. A. *et al.* (2018) 'Interplay between ER Ca2+ binding proteins, STIM1 and STIM2, is required for store-operated Ca2+ entry', *International Journal of Molecular Sciences*, 19(5). doi: 10.3390/ijms19051522.

Nelson, H. A. and Roe, M. W. (2018) 'Molecular physiology and pathophysiology of stromal interaction molecules', *Experimental Biology and Medicine*, 243(5), pp. 451–472. doi: 10.1177/1535370218754524.

Nizon, M. *et al.* (2012) 'Further delineation of CANT1 phenotypic spectrum and demonstration of its role in proteoglycan synthesis', *Human Mutation*, 33(8), pp. 1261–1266. doi: 10.1002/humu.22104.

Notarangelo, L. D. *et al.* (2013) 'Partial defects of T-cell development associated with poor T-cell function.', *The Journal of allergy and clinical immunology*. Elsevier, 131(5), pp. 1297–305. doi: 10.1016/j.jaci.2013.01.020.

O'Shea, D. (2018) *Primary immunodeficiency: the latest UK prevalence estimates*. Available at: https://www.univadis.co.uk/viewarticle/primary-immunodeficiency-the-latest-uk-prevalence-estimates-608261#:~:text=The latest report from the,stands at 5.90%2F100%2C000 population.

Oh-hora, M. *et al.* (2008) 'Dual functions for the endoplasmic reticulum calcium sensors STIM1 and STIM2 in T cell activation

and tolerance', *Nature Immunology*, 9(4), pp. 432–443. doi: 10.1038/ni1574.

Oh-hora, M. and Rao, A. (2008) 'Calcium signaling in lymphocytes', *Current Opinion in Immunology*, 20(3), pp. 250–258. doi: 10.1016/j.coi.2008.04.004.

Ohga, K. *et al.* (2008) 'Characterization of YM-58483/BTP2, a novel store-operated Ca2+ entry blocker, on T cell-mediated immune responses in vivo', *International Immunopharmacology*, 8(13–14), pp. 1787–1792. doi: 10.1016/j.intimp.2008.08.016.

Ouyang, S. *et al.* (2012) 'Structural Analysis of the STING Adaptor Protein Reveals a Hydrophobic Dimer Interface and Mode of Cyclic di-GMP Binding', *Immunity*, 36(6), pp. 1073–1086. doi: 10.1016/j.immuni.2012.03.019.

Paganini, C. *et al.* (2019) 'Calcium activated nucleotidase 1 (CANT1) is critical for glycosaminoglycan biosynthesis in cartilage and endochondral ossification', *Matrix Biology*, 81, pp. 70–90. doi: 10.1016/j.matbio.2018.11.002.

Pai, S.-Y. (2019) 'Treatment of primary immunodeficiency with allogeneic transplant and gene therapy.', *Hematology. American Society of Hematology. Education Program*, 2019(1), pp. 457–465. doi: 10.1182/hematology.2019000052.

Panch, S. R. *et al.* (2019) 'Effect of Cryopreservation on Autologous Chimeric Antigen Receptor T Cell Characteristics', *Molecular Therapy*, 27(7), pp. 1275–1285. doi: 10.1016/j.ymthe.2019.05.015.

Parekh, A. B. (2017) 'Regulation of CRAC channels by Ca2+-dependent inactivation', *Cell Calcium*, 63, pp. 20–23. doi: 10.1016/j.ceca.2016.12.003.

Parry, D. A. *et al.* (2016) 'A homozygous STIM1 mutation impairs store-operated calcium entry and natural killer cell effector function without clinical immunodeficiency.', *The Journal of allergy and clinical immunology*. Elsevier, 137(3), pp. 955–7.e8. doi: 10.1016/j.jaci.2015.08.051.

Pennock, N. D. *et al.* (2013) 'T cell responses: naïve to memory and everything in between', *Advances in Physiology Education*, 37(4), pp. 273–283. doi: 10.1152/advan.00066.2013.

Pereverzev, A. P. *et al.* (2015) 'Differences in nonsense-mediated mRNA decay activity in mammalian cell lines revealed by a fluorescence reporter', *Russian Journal of Bioorganic Chemistry*, 41(5), pp. 525–528. doi: 10.1134/S1068162015050118.

Petersone, L. *et al.* (2018) 'T Cell/B Cell Collaboration and Autoimmunity: An Intimate Relationship', *Frontiers in Immunology*, 9. doi: 10.3389/fimmu.2018.01941.

Petrilli, V., Papin, S. and Tschopp, J. (2005) 'The inflammasome', *Current Biology*, 15(15), p. R581. doi: 10.1016/j.cub.2005.07.049.

Picard, C. *et al.* (2009) 'STIM1 Mutation Associated with a Syndrome of Immunodeficiency and Autoimmunity', *New England Journal of Medicine*, 360(19), pp. 1971–1980. doi: 10.1056/NEJMoa0900082.

Picard, C. *et al.* (2015) 'Primary Immunodeficiency Diseases: an Update on the Classification from the International Union of Immunological Societies Expert Committee for Primary Immunodeficiency 2015', *Journal of Clinical Immunology*. Springer US, 35(8), pp. 696–726. doi: 10.1007/s10875-015-0201-1.

Picard, C. *et al.* (2018) 'International Union of Immunological Societies: 2017 Primary Immunodeficiency Diseases Committee Report on Inborn Errors of Immunity', *Journal of Clinical Immunology*, 38(1), pp. 96–128. doi: 10.1007/s10875-017-0464-9.

Picard, C., Casanova, J.-L. J.-L. and Puel, A. (2011) 'Infectious Diseases in Patients with IRAK-4, MyD88, NEMO, or I B Deficiency', *Clinical Microbiology Reviews*. American Society for Microbiology, 24(3), pp. 490–497. doi: 10.1128/CMR.00001-11.

Pokatayev, V. and Yan, N. (2017) ‘Methods of Assessing STING Activation and Trafficking’, in, pp. 167–174. doi: 10.1007/978-1-4939-7237-1_10.

Power, D. *et al.* (2015) ‘IFI44 suppresses HIV-1 LTR promoter activity and facilitates its latency’, *Virology*, 481, pp. 142–150. doi: 10.1016/j.virol.2015.02.046.

Prakriya, M. (2009) ‘The molecular physiology of CRAC channels’, *Immunological Reviews*. NIH Public Access, 231(1), pp. 88–98. doi: 10.1111/j.1600-065X.2009.00820.x.

Prakriya, M. and Lewis, R. S. (2015) ‘Store-Operated Calcium Channels.’, *Physiological reviews*. American Physiological Society, 95(4), pp. 1383–436. doi: 10.1152/physrev.00020.2014.

Prins, D. and Michalak, M. (2015) ‘STIM1 is cleaved by calpain’, *FEBS Letters*, 589(21), pp. 3294–3301. doi: https://doi.org/10.1016/j.febslet.2015.09.015.

Qiu, D. *et al.* (1999) ‘Immunosuppressant PG490 (triptolide) inhibits T-cell interleukin-2 expression at the level of purine-box/nuclear factor of activated T-cells and NF-kappaB transcriptional activation.’, *The Journal of biological chemistry*, 274(19), pp. 13443–50. doi: 10.1074/jbc.274.19.13443.

Rae, W. *et al.* (2018) ‘Clinical efficacy of a next-generation sequencing gene panel for primary immunodeficiency diagnostics’, *Clinical Genetics*, 93(3), pp. 647–655. doi: 10.1111/cge.13163.

Rahit, K. M. T. H. and Tarailo-Graovac, M. (2020) ‘Genetic Modifiers and Rare Mendelian Disease’, *Genes*, 11(3), p. 239. doi: 10.3390/genes11030239.

Raphael, I. *et al.* (2015) ‘T cell subsets and their signature cytokines in autoimmune and inflammatory diseases’, *Cytokine*, 74(1), pp. 5–17. doi: 10.1016/j.cyto.2014.09.011.

Raverdeau, M. and Mills, K. H. G. (2014) ‘Modulation of T Cell and Innate Immune Responses by Retinoic Acid’, *The Journal of Immunology*, 192(7). Available at: http://www.jimmunol.org/content/192/7/2953.long (Accessed: 11 July 2017).

Rice, L. *et al.* (2019) ‘A Report of Novel STIM1 Deficiency and 6-Year Follow-Up of Two Previous Cases Associated with Mild Immunological Phenotype’, *Journal of Clinical Immunology*, 39(3), pp. 249–256. doi: 10.1007/s10875-019-00618-3.

Richards, S. *et al.* (2015) ‘Standards and guidelines for the interpretation of sequence variants: a joint consensus recommendation of the American College of Medical Genetics and Genomics and the Association for Molecular Pathology.’, *Genetics in medicine : official journal of the American College of Medical Genetics*, 17(5), pp. 405–24. doi: 10.1038/gim.2015.30.

Robert, C. (2020) ‘A decade of immune-checkpoint inhibitors in cancer therapy’, *Nature Communications*, 11(1), p. 3801. doi: 10.1038/s41467-020-17670-y.

Romagnani, S. (2000) ‘T-cell subsets (Th1 versus Th2)’, *Annals of Allergy, Asthma & Immunology*, 85(1), pp. 9–21. doi: 10.1016/S1081-1206(10)62426-X.

Rosenberg, S. A., Yang, J. C. and Restifo, N. P. (2004) ‘Cancer immunotherapy: moving beyond current vaccines’, *Nature Medicine*, 10(9), pp. 909–915. doi: 10.1038/nm1100.

Sadeghi, A. *et al.* (2013) ‘Rapid expansion of T cells: Effects of culture and cryopreservation and importance of short-term cell recovery’, *Acta Oncologica*, 52(5), pp. 978–986. doi: 10.3109/0284186X.2012.737020.

Scharenberg, A. M., Humphries, L. A. and Rawlings, D. J. (2007) ‘Calcium signalling and cell-fate choice in B cells.’, *Nature*

reviews. Immunology. NIH Public Access, 7(10), pp. 778–89. doi: 10.1038/nri2172.

Scheu, S. *et al.* (2006) 'Activation of the integrated stress response during T helper cell differentiation', *Nature Immunology*, 7(6), pp. 644–651. doi: 10.1038/ni1338.

Shang, G. *et al.* (2012) 'Crystal structures of STING protein reveal basis for recognition of cyclic di-GMP.', *Nature structural & molecular biology*, 19(7), pp. 725–7. doi: 10.1038/nsmb.2332.

Shillitoe, B. *et al.* (2018) 'The United Kingdom Primary Immune Deficiency (UKPID) registry 2012 to 2017', *Clinical & Experimental Immunology*, 192(3), pp. 284–291. doi: 10.1111/cei.13125.

Shrivastava, S. *et al.* (2016) 'Elevated hepatic lipid and interferon stimulated gene expression in HCV GT3 patients relative to non-alcoholic steatohepatitis', *Hepatology International*, 10(6), pp. 937–946. doi: 10.1007/s12072-016-9733-6.

Shu, C. *et al.* (2012) 'Structure of STING bound to cyclic di-GMP reveals the mechanism of cyclic dinucleotide recognition by the immune system.', *Nature structural & molecular biology*, 19(7), pp. 722–4. doi: 10.1038/nsmb.2331.

Soboloff, J. *et al.* (2006) 'STIM2 Is an Inhibitor of STIM1-Mediated Store-Operated Ca2+ Entry', *Current Biology*, 16(14), pp. 1465–1470. doi: 10.1016/j.cub.2006.05.051.

Srikanth, S., Jung, H.-J., Kim, K.-D., *et al.* (2010) 'A novel EF-hand protein, CRACR2A, is a cytosolic Ca2+ sensor that stabilizes CRAC channels in T cells.', *Nature cell biology*. NIH Public Access, 12(5), pp. 436–46. doi: 10.1038/ncb2045.

Srikanth, S., Jung, H.-J., Ribalet, B., *et al.* (2010) 'The intracellular loop of Orai1 plays a central role in fast inactivation of Ca2+ release-activated Ca2+ channels.', *The Journal of biological chemistry*. American Society for Biochemistry and Molecular Biology, 285(7), pp. 5066–75. doi: 10.1074/jbc.M109.072736.

Srikanth, S. *et al.* (2016) 'A large Rab GTPase encoded by CRACR2A is a component of subsynaptic vesicles that transmit T cell activation signals', *Science Signaling*, 9(420).

Srikanth, S. *et al.* (2019) 'The Ca2+ sensor STIM1 regulates the type I interferon response by retaining the signaling adaptor STING at the endoplasmic reticulum', *Nature Immunology*, 20(2), pp. 152–162. doi: 10.1038/s41590-018-0287-8.

Srikanth, S. and Gwack, Y. (2012) 'Orai1, STIM1, and their associating partners.', *The Journal of physiology*. Wiley-Blackwell, 590(17), pp. 4169–77. doi: 10.1113/jphysiol.2012.231522.

Srikanth, S., Ribalet, B. and Gwack, Y. (2013) 'Regulation of CRAC channels by protein interactions and post-translational modification', *Channels*, 7(5), pp. 354–363. doi: 10.4161/chan.23801.

Stauderman, K. A. (2018) 'CRAC channels as targets for drug discovery and development', *Cell Calcium*, 74, pp. 147–159. doi: 10.1016/j.ceca.2018.07.005.

StemCell (2019) *WA10006-Frequencies_Cell_Types_Human_Peripheral_Blood*, *STEMCELL technology*. Available at: https://www.stemcell.com/media/files/wallchart/WA10006-Frequencies_Cell_Types_Human_Peripheral_Blood.pdf.

Takeuchi, O. and Akira, S. (2010) 'Pattern Recognition Receptors and Inflammation', *Cell*, 140(6), pp. 805–820. doi: 10.1016/j.cell.2010.01.022.

Tangye, S. G. *et al.* (2020) 'Human Inborn Errors of Immunity: 2019 Update on the Classification from the International Union of Immunological Societies Expert Committee', *Journal of Clinical Immunology*, 40(1), pp. 24–64. doi: 10.1007/s10875-019-00737-x.

Tao Lin, Tingting Geng, Andrew Harrison, Duomeng Yang, Anthony T. Vella, Erol Fikrig, P. W. (2021) 'STING deficiency-associated aberrant CXCL10 expression contributes to pathogenesis of arthritogenic alphaviruses', *bioRxiv Preprint*. doi: https://doi.org/10.1101/2020.05.13.095083.

The Human Protein Atlas (2020). Available at: https://www.proteinatlas.org/.

Tian, C. *et al.* (2016) 'Store-operated CRAC channel inhibitors: opportunities and challenges', *Future Medicinal Chemistry*, 8(7), pp. 817–832. doi: 10.4155/fmc-2016-0024.

Todoric, K. *et al.* (2013) 'Autoimmunity in Immunodeficiency', *Current Allergy and Asthma Reports*, 13(4), pp. 361–370. doi: 10.1007/s11882-013-0350-3.

Torres, K. C. L., Dutra, W. O. and Gollob, K. J. (2004) 'Endogenous IL-4 and IFN-γ are essential for expression of Th2, but not Th1 cytokine message during the early differentiation of human CD4+ T helper cells', *Human Immunology*, 65(11), pp. 1328–1335. doi: 10.1016/j.humimm.2004.06.007.

Trebak, M. and Kinet, J.-P. (2019) 'Calcium signalling in T cells', *Nature Reviews Immunology*, 19(3), pp. 154–169. doi: 10.1038/s41577-018-0110-7.

Trinchieri, G. (2010) 'Type I interferon: friend or foe?', *Journal of Experimental Medicine*, 207(10), pp. 2053–2063. doi: 10.1084/jem.20101664.

Truedsson, L., Bengtsson, A. A. and Sturfelt, G. (2007) 'Complement deficiencies and systemic lupus erythematosus', *Autoimmunity*. Taylor & Francis, 40(8), pp. 560–566. doi: 10.1080/08916930701510673.

Uhlen, M. *et al.* (2010) 'Towards a knowledge-based Human Protein Atlas', *Nature Biotechnology*, 28(12), pp. 1248–1250. doi: 10.1038/nbt1210-1248.

UniProt (no date). Available at: http://www.uniprot.org/ (Accessed: 4 August 2017).

Vaeth, M., Kahlfuss, S. and Feske, S. (2020) 'CRAC Channels and Calcium Signaling in T Cell-Mediated Immunity', *Trends in Immunology*, 41(10), pp. 878–901. doi: 10.1016/j.it.2020.06.012.

Varga, G. and Foell, D. (2018) 'Anti-inflammatory monocytes—interplay of innate and adaptive immunity', *Molecular and Cellular Pediatrics*, 5(1), p. 5. doi: 10.1186/s40348-018-0083-4.

Vazirinejad, R. *et al.* (2014) 'The Biological Functions, Structure and Sources of CXCL10 and Its Outstanding Part in the Pathophysiology of Multiple Sclerosis', *Neuroimmunomodulation*, 21(6), pp. 322–330. doi: 10.1159/000357780.

Wandinger-Ness, A. and Zerial, M. (2014) 'Rab Proteins and the Compartmentalization of the Endosomal System', *Cold Spring Harbor Perspectives in Biology*, 6(11), pp. a022616–a022616. doi: 10.1101/cshperspect.a022616.

Wang, S. *et al.* (2014) 'STIM1 and SLC24A4 Are Critical for Enamel Maturation', *Journal of Dental Research*, 93(7_suppl), pp. 94S-100S. doi: 10.1177/0022034514527971.

Wang, Y. *et al.* (2019) 'CRACR2a is a calcium-activated dynein adaptor protein that regulates endocytic traffic', *Journal of Cell Biology*, 218(5), pp. 1619–1633. doi: 10.1083/jcb.201806097.

Warr, A. *et al.* (2015) 'Exome Sequencing: Current and Future Perspectives', *G3: Genes|Genomes|Genetics*. Genetics Society of America, 5(8), pp. 1543–1550. doi: 10.1534/g3.115.018564.

Weiss A, Wiskocil RL, S. J. (1984) 'The role of T3 surface molecules in the activation of human T cells: a two-stimulus

requirement for IL 2 production reflects events occurring at a pre-translational level.', *J Immunol.*, 133, pp. 123–8.

Wilson, L. A. *et al.* (2015) 'Expression of a long variant of CRACR2A that belongs to the Rab GTPase protein family in endothelial cells', *Biochemical and Biophysical Research Communications*, 456(1), pp. 398–402. doi: 10.1016/j.bbrc.2014.11.095.

Wong, G. K. and Huissoon, A. P. (2016) 'T-cell abnormalities in common variable immunodeficiency: the hidden defect', *Journal of Clinical Pathology*, 69(8), pp. 672–676. doi: 10.1136/jclinpath-2015-203351.

Woo, J. S. *et al.* (2018) 'CRACR2A-Mediated TCR Signaling Promotes Local Effector Th1 and Th17 Responses', *The Journal of Immunology*, 201(4), pp. 1174–1185. doi: 10.4049/jimmunol.1800659.

Wright, C. F., FitzPatrick, D. R. and Firth, H. V. (2018) 'Paediatric genomics: diagnosing rare disease in children', *Nature Reviews Genetics*, 19(5), pp. 253–268. doi: 10.1038/nrg.2017.116.

Wu, X. *et al.* (2014) 'Molecular evolutionary and structural analysis of the cytosolic DNA sensor cGAS and STING', *Nucleic Acids Research*, 42(13), pp. 8243–8257. doi: 10.1093/nar/gku569.

Wu, X. *et al.* (2017) 'RIG-I and IL-6 are negative-feedback regulators of STING induced by double-stranded DNA', *PLOS ONE*. Edited by K. Li, 12(8), p. e0182961. doi: 10.1371/journal.pone.0182961.

Yang, N. *et al.* (2013) 'Blockade of store-operated Ca2+ entry inhibits hepatocarcinoma cell migration and invasion by regulating focal adhesion turnover', *Cancer Letters*, 330(2), pp. 163–169. doi: 10.1016/j.canlet.2012.11.040.

Yang, S., Zhang, J. J. and Huang, X.-Y. (2009) 'Orai1 and STIM1 Are Critical for Breast Tumor Cell Migration and Metastasis', *Cancer Cell*, 15(2), pp. 124–134. doi: 10.1016/j.ccr.2008.12.019.

Yang, Y. *et al.* (2013) 'Clinical Whole-Exome Sequencing for the Diagnosis of Mendelian Disorders', *New England Journal of Medicine*, 369(16), pp. 1502–1511. doi: 10.1056/NEJMoa1306555.

York, A. G. *et al.* (2015) 'Limiting Cholesterol Biosynthetic Flux Spontaneously Engages Type I IFN Signaling', *Cell*, 163(7), pp. 1716–1729. doi: 10.1016/j.cell.2015.11.045.

Yoshino, T. *et al.* (2007) 'YM-58483, a selective CRAC channel inhibitor, prevents antigen-induced airway eosinophilia and late phase asthmatic responses via Th2 cytokine inhibition in animal models', *European Journal of Pharmacology*, 560(2), pp. 225–233. doi: 10.1016/j.ejphar.2007.01.012.

Zhang, C. *et al.* (2019) 'Structural basis of STING binding with and phosphorylation by TBK1', *Nature*, 567(7748), pp. 394–398. doi: 10.1038/s41586-019-1000-2.

Zheng, L. *et al.* (2011) 'Auto-inhibitory role of the EF-SAM domain of STIM proteins in store-operated calcium entry', *Proceedings of the National Academy of Sciences*, 108(4), pp. 1337–1342. doi: 10.1073/pnas.1015125108.

Zhou, Y. *et al.* (2015) 'STIM1 dimers undergo unimolecular coupling to activate Orai1 channels', *Nature Communications*. The Author(s), 6, p. 8395. Available at: http://dx.doi.org/10.1038/ncomms9395.

Zhu, H. *et al.* (2014) 'Elevated Orai1 expression mediates tumor-promoting intracellular Ca2+ oscillations in human esophageal squamous cell carcinoma', *Oncotarget*, 5(11), pp. 3455–3471. doi: 10.18632/oncotarget.1903.

Zhu, J. *et al.* (2014) 'Antiviral Activity of Human OASL Protein Is Mediated by Enhancing Signaling of the RIG-I RNA Sensor', *Immunity*, 40(6), pp. 936–948. doi: 10.1016/j.immuni.2014.05.007.

Zitt, C. *et al.* (2004) ‘Potent Inhibition of Ca $^{2+}$ Release-activated Ca $^{2+}$ Channels and T-lymphocyte Activation by the Pyrazole Derivative BTP2’, *Journal of Biological Chemistry*, 279(13), pp. 12427–12437. doi: 10.1074/jbc.M309297200.

Zou, J. *et al.* (2011) ‘Role of STIM1/Orai1-mediated store-operated Ca 2+ entry in airway smooth muscle cell proliferation’, *Journal of Applied Physiology*, 110(5), pp. 1256–1263. doi: 10.1152/japplphysiol.01124.2010.

Zweifach, A. and Lewis, R. S. (1993) ‘Mitogen-regulated Ca2+ current of T lymphocytes is activated by depletion of intracellular Ca2+ stores.’, *Proceedings of the National Academy of Sciences*, 90(13), pp. 6295–6299. doi: 10.1073/pnas.90.13.6295.